

Aus dem Institut für Biomechanik und Orthopädie
der Deutschen Sporthochschule Köln
Geschäftsführender Leiter: Universitätsprofessor Dr. Gert-Peter Brüggemann

Relation of muscular contractions to mechanical deformation in the human tibia
during different locomotive activities

von der Deutschen Sporthochschule Köln zur
Erlangung des akademischen Grades

Doktor der Sportwissenschaft
genehmigte Dissertation

vorgelegt von

Pengfei Yang

Köln 2013

Referees

First Referee:

Univ.-Prof. Dr. Gert-Peter Brüggemann
Institute of Biomechanics and Orthopaedics
German Sport University Cologne

Second Referee:

Prof. Dr. Jörn Rittweger
Institute of Aerospace Medicine
German Aerospace Center

Chair of doctorate committee:

Univ.-Prof. Dr. Wilhelm Bloch
Department of Molecular and Cellular Sport Medicine
German Sport University Cologne

Date of Ph.D defense:

Thursday, 04th July, 2013

Declaration/Eidesstattliche Erklärung

Hierdurch erkläre ich, dass ich die Leitlinien guter wissenschaftlicher Praxis der Deutschen Sporthochschule Köln eingehalten habe.

Köln, den 05.06.2013

Pengfei Yang

Hierdurch versichere ich: Ich habe diese Arbeit selbstständig und nur unter Benutzung der angegebenen Quellen und technischen Hilfen angefertigt; sie hat noch keiner anderen Stelle zur Prüfung vorgelegen. Wörtlich übernommene Textstellen, auch Einzelsätze oder Teile davon, sind als Zitate kenntlich gemacht worden.

Köln, den 05.06.2013

Pengfei Yang

„This thesis is dedicated to my dear grandfather in heaven“

Contents

Chapter 1.....	1
General introduction and outline of the thesis	
Chapter 2.....	13
Literature review on <i>in vivo</i> bone deformation measurements in humans	
Chapter 3.....	45
Establishment of a novel optical segment tracking (OST) approach for <i>in vivo</i> bone deformation measurements	
Chapter 4.....	67
Tibia deformations induced by simulated muscle forces: <i>ex vivo</i> validation of the OST approach in human tibia	
Chapter 5.....	85
<i>In vivo</i> application of the OST approach for bone deformation recording in humans: a reliability study	
Chapter 6.....	109
Bending and torsion predominate the <i>in vivo</i> human tibia deformation regimes during walking and running	
Chapter 7.....	137
On the relationship between the <i>in vivo</i> tibia torsional deformation in humans and the muscle contractions	
Chapter 8.....	169
General discussion and conclusions	
Publications.....	187
Acknowledgements.....	189
Appendix.....	193

CHAPTER 1

General introduction and outline of the thesis

General introduction

1. Bones adapt to the mechanical environment

As one of the major hard tissue in humans and most vertebrates, the skeleton, generally referring to bone, provides the essential frame to support the body and to thus permit locomotion. Considering the functional requirements of bones across different species, *e.g.* from rats to dinosaurs, or during different growth periods, *e.g.* from embryo to old age, it is not difficult to conceive that bones adapt to the experienced mechanical environment. In fact, mechanically regulated bone modeling and remodeling is one of the major means to maintain regular bone metabolism. The findings on the bone adaptation to the mechanical environment have been well theorized by Julius Wolff in 1890s [1] as ‘Wolff’s law’ and refined later by Harold Frost as ‘mechanostat’ [2-4]. Evidence from numerous animal studies in the past revealed the adaptation process of the bones to the well-defined artificial mechanical environment and suggested certain relationship between the adaptation in relation to the types of loading, *e.g.* loading amplitude, loading cycle, loading frequency and so on [5-8]. Conversely, bone degradation was generally observed during disuse, *e.g.* prolonged bed rest [9], or in the microgravity environment during space flight [10]. Indeed, the best way to further our understanding in this adaptation process is to quantitatively study the mechanical loading on bone during daily locomotor activities. However, this is still rather challenging due to technical difficulties. More importantly, the mechanical load on bones can vary greatly across individuals or species, as the variance between the body size, locomotor pattern and speed.

2. Mechanical load on bone and mechanical strains

Mechanical deformation in bone, also frequently referred to as bone strain, which is based on its capability of withstanding bone loading, has attracted much attention in the context of studies aiming at understanding bone adaptation. To a certain extent, it is more essential to discover the mechanical deformation in bone than exploring the mechanical load on bone itself. The early work of the 1970s

and 1980s also pointed out that the skeletal stress and bone strains during gait are almost invariant across different species despite enormous differences in body weight [11-13]. Solid evidence also suggested that mechanical strains in bone play a decisive role in its mechanical adaptation [2], and that it is linearly related to the bone response, *i.e.* low and high strain levels lead to removal or to new bone formation, respectively [6].

A comprehensive assessment of bone strains during daily activities seems essential to lead a better understanding about how bones adapted themselves to the current structure. With the development of the methodology of the *in vivo* bone strain measurements, in particular the so called strain gauge techniques, quantitative assessment of bone strains *in vivo* has been possible. *In vivo* bone strains on different sites or different bones have been extensively studied in the animals in the past. Typical peak principal compressive strain amplitude is approximately 1500-3000 μ strain in most animals [14-16]. Nevertheless, the bone strain levels in humans still remain largely unknown. Today, only few *in vivo* bone strain measurements in humans have been conducted since the first pioneering study from 1975 [17]. From 1996 onwards, there are approximately 40 subjects of whom *in vivo* bone strains have been investigated [18]. Evidence from these human studies suggested that the peak principal tibial strains in humans range between 1300 μ strain and 3200 μ strain [18, 19]. However, there are still several open questions which have not been addressed on both the technical and the scientific issues.

3. Methodological considerations for bone strain measurements

Our present understanding of *in vivo* bone strains in humans are based upon the surgical implanted strain gauge approaches. The inherent shortcomings with these approaches have been discussed in details in Chapter 2 in this thesis [20]. Firstly, it can be quite invasive during the direct affixation of strain gauges onto bone surface whilst the periosteum has to be removed. Secondly, quantitatively assessing the bonding quality of the strain gauges on the moist and greasy bone surface is rather challenging. Thirdly, only local strain from the area covered by

the gauges can be yield, it thus failed to provide the deformation regimes across the bone segment. Fourthly, and most importantly, it is difficult for the strain gauge techniques to assess the composition of the bone strains, *e.g.* the strain distribution across the bone and the components of bending and torsion, without influencing the regular muscle function in human bones. This is because that at least pair of strain gauges which are attached on the opposite sites of the bone are needed to compute bending deformation, but most of the long bone surface is covered by muscles. Of note, the bending strain is normally referred as one of the key factors in bone fracture. Taking the limitations of the traditional strain gauge approaches together, new and informative approaches would certainly be helpful for further our understanding about the *in vivo* bone deformations. Developing a novel approach to measure *in vivo* bone deformation in humans is one of the objectives in this thesis.

4. Open questions in muscle-bone interactions

One of the open questions relates to the origin of the mechanical load on bones. The contribution of the gravity-derived forces and muscle forces to the mechanical loading on bone is still under debate [21-24], although the ‘mechanostat theory’ has proposed that muscles are the one which generate the largest force on bone and the concept of muscle-bone unit is becoming more and more appreciated [25, 26].

The perception of muscle forces predominating bone loading is initially from the biomechanical analysis. Considering that most of the muscles work against shorter level arm than the external forces, larger forces must be generated by muscles to counterbalance the external forces or accelerate the body.

Nevertheless, due to the apparent difficulties of accurately assessing muscle forces and mechanical loading of bone *in vivo*, the indirect parameters of muscles and bones, *e.g.* muscle mass, muscle cross section area, bone area and bone mass, were employed to test the muscle-bone hypothesis.

Although muscle-bone relationships vary between genders, strong correlation between muscle area and bone area in puberty populations did provide evidence to

support the muscle-bone hypothesis [27]. Upon these first observations, another study focusing on the timing of the peak lean body mass accrual and peak bone mineral content accretion in the puberty populations indicated that muscle development precedes bone development, meaning that the latter is very likely driven by the former [28]. Furthermore, the strong influence of local muscle activities on bone has been found in youth tennis players, namely the dramatic side-side strength difference of ulna and humerus between the racquet side and the non-racquet side [29].

However, the bone responses to the exercises before and after puberty suggested that the muscle-bone relationship seems to be different after puberty. Even so, the close relationship between muscle and bone cross section area in the lower leg of the adults still holds true [30]. During the recovery phase from bed-rest induced bone loss, corresponding to the timing of the muscle and bone development during puberty, muscle recovery seems to precede the bone recovery again [31].

Taking all of this evidence together, it seems that the muscle activities are indeed regulating bone modeling and remodeling by generating forces acting on bones. If this holds true, muscle contractions are supposed to initiate or considerably contribute to a reasonable amount of bone deformation to maintain the regular bone structure. An early study on long bone curvature speculated that the muscle contractions may contribute to the bending of the bone on the basis of the bone curvature itself [32]. However, more and more evidence available from computer modeling lately starts to oppose this opinion and suggests that muscle groups work in a coordinated manner to minimize the bending moment on bone and prevent potential bending fracture [18, 33, 34].

Moreover, on the other hand, those who argue the importance of the gravity-derived force rather than the muscle forces mostly because of the observations under weightlessness during space flight about the site-specific bone loss from the lower extremities and upper body. The former experiences both of the gravity-derived forces and local muscle forces on the ground, but the latter primarily experiences local muscle forces. The significant bone losses in astronauts after 4-6

6 Chapter 1

month space flight were found only in the lower extremities, the so called weight-bearing bones, but not in the upper body [35]. To be fair, it is difficult, not to say impossible, to distinguish the influence of the gravity-derived force and the muscle force on bone during the locomotor activities, especially for the lower extremities.

However, due to the lack of direct quantitative evidence, the open questions arising from this argument are: 1) How much bone deformation can be induced by muscle contractions? 2) How much bone deformation can be contributed by the gravity-derived force, for the lower extremities? 3) Which type of bone deformation can be contributed by the muscle contractions? 4) What is the temporal and spatial relationship between the muscle activities and bone deformation? 5) Are bone deformations always a mere function of muscle activities, or are muscles in some cases more effective in deforming the bones than the other cases? If the latter is the case, one might be able to develop certain training protocols to benefit our bones.

In this thesis, the human tibia was taken as the study object to further address the above proposed questions. The detailed objectives and the outline of this thesis are described as follows.

Objectives and outline of the thesis

The general purposes of the presented thesis were to investigate 1) the character of the *in vivo* tibia deformation regimes in humans during different locomotor activities, including walking, running, stair-case negotiation, isometric muscle contraction, *etc.*, 2) the role of related muscle contractions in the generation of those tibia deformations during the locomotor activities.

Chapter 2 described the in-depth literature research on the *in vivo* bone deformation measurements in humans in the past [20]. More specifically, the basic components of the *in vivo* bone deformation, *i.e.* axial strain, shear strain, bending

and torsion strain, were summarized and demonstrated. The techniques developed and adopted in the past *in vivo* bone deformation studies in humans, mostly based on strain gauges, were reviewed in details. The advantages and inherent shortcomings of the strain gauge approaches were pointed out. The knowledge we have gained from the past *in vivo* human bone deformation studies was summarized. Finally and most importantly, the open questions which have been left from previous studies and the necessities to develop new approaches to further our understanding in *in vivo* bone deformation were elucidated.

Chapter 3 proposed a concept of novel optical segment tracking (OST) approach for bone deformation measurements based on a commercial motion capture system [36]. In this chapter, the performance of the motion capture system for capturing minute movement of specific retro-reflective markers within certain 3D volume was evaluated. Aiming at capturing 20 μm 's movement within $400 \times 300 \times 300 \text{ mm}^3$, which typically covers the range of the tibia motion during the stance phase of one gait cycle, the accuracy and repeatability of the optical system were assessed. Of note, the target of 20 μm 's movement was approximately equal to the situation of 100 μstrain tibia axial deformation. The results provided several insights into optimizing the configurations of the optical system, *e.g.* camera distance and retro-reflective marker size, to achieve high and balanced resolution, accuracy and precision during the minute movement recording. In addition, the possible way to apply the OST approach *in vivo* in humans was discussed.

Chapter 4 demonstrated an application of the OST approach in tibia deformation recording in cadaveric specimens. After the custom-made retro-reflective marker clusters were affixed into the tibia cortex by bone screws, cadaveric tibia was loaded under different artificial loading conditions in a custom-made Lower Extremity Loading Device (LELD) to simulate physiological muscle contractions. The tibia deformations, *i.e.* antero-posterior, medio-lateral bending angles and internal-external torsion angles, under different muscle group contractions were

further analyzed. The repeatable deformation results between the repetitions thus further demonstrated the potential feasibility of the OST approach in the application of tibia deformation recording.

Chapter 5 described a reliability study on the *in vivo* application of the OST approach for tibia deformation recording. In this chapter, the details of the surgical procedures and the *in vivo* application of the OST technique were described. Above all, the stability of the bone screws and marker clusters in the tibia cortex were tested by assessing the resonance frequency of the screw-cluster structure and comparing the relative position between the tibia-affixed mark clusters prior to and after the intense exercises. Tibia deformation angles during squatting exercises were presented to further demonstrate the repeatability of the OST approach.

Chapter 6 presented the tibia deformation results, *i.e.* tibia antero-posterior bending angle, medio-lateral bending angle and internal-external torsion angle, during the daily exercises, *i.e.* walking and running. Firstly, the tibia deformation regimes during walking and running were presented. The relationships between the tibia deformation angles and the moving speed were assessed. To further investigate the possible force origin to induce tibia deformation, the responses of the tibia deformation to the vertical ground reaction forces or vertical free moments during overground walking were also evaluated.

Chapter 7 primarily presented one of the most interesting findings in this thesis: the character of the related muscle contractions in the generation of the tibia torsional deformation. It is difficult, if not impossible, to distinguish the role of muscle activities and the impact loading due to the body acceleration in tibia deformation during exercises, as that the muscles are needed to remain active to maintain the normal motion. In this chapter, tibia deformations were recorded under the low and high calf muscle activities, which were achieved by performing

different functional exercises, *e.g.* stair ascent with forefoot and full foot contact, forefoot and rear foot running, respectively. Isometric plantar flexion was carried out to isolate the effect of plantar flexor contractions on tibia deformation from the impact loading caused by body acceleration. Moreover, the time course of the deformation angles during the stance phase of gait cycle and its relation to muscle activities were further analyzed.

Chapter 8 finally discussed and summarized the main and the other noteworthy findings during the literature review, proposing and establishment of the OST approach for *in vivo* bone deformation measurements, validation study in the cadaveric specimens, the reliability study of the *in vivo* application of the OST approach and the *in vivo* study in humans. The advantages, as well as shortcomings which should be improved, and future potential application of the presented OST technique were discussed. Likewise, the discussion about the knowledge on bone deformation regimes and its relation to the related muscle activities which has been gained from the presented study, and its potential meaning in the scientific research field of muscle-bone interaction, recovery and treatment of bone-related diseases in the clinical terms were presented in this thesis.

References

1. Wolff J (1986) Concept of the Law of Bone Remodelling. *The Law of Bone Remodelling*: Springer Berlin Heidelberg. pp. 1-1.
2. Frost HM (1987) The mechanostat: a proposed pathogenic mechanism of osteoporoses and the bone mass effects of mechanical and nonmechanical agents. *Bone Miner* 2: 73-85.
3. Frost HM (1987) Bone "mass" and the "mechanostat": a proposal. *Anat Rec* 219: 1-9.
4. Frost HM (2003) Bone's mechanostat: a 2003 update. *Anat Rec A Discov Mol Cell Evol Biol* 275: 1081-1101.
5. Hsieh YF, Robling AG, Ambrosius WT, Burr DB, Turner CH (2001) Mechanical loading of diaphyseal bone *in vivo*: the strain threshold for an osteogenic response varies with location. *J Bone Miner Res* 16: 2291-2297.

10 Chapter 1

6. Sugiyama T, Meakin LB, Browne WJ, Galea GL, Price JS, et al. (2012) Bones' adaptive response to mechanical loading is essentially linear between the low strains associated with disuse and the high strains associated with the lamellar/woven bone transition. *J Bone Miner Res* 27: 1784-1793.
7. Warden SJ, Turner CH (2004) Mechanotransduction in cortical bone is most efficient at loading frequencies of 5-10 Hz. *Bone* 34: 261-270.
8. Zhang P, Tanaka SM, Jiang H, Su M, Yokota H (2006) Diaphyseal bone formation in murine tibiae in response to knee loading. *J Appl Physiol* 100: 1452-1459.
9. Donaldson CL, Hulley SB, Vogel JM, Hattner RS, Bayers JH, et al. (1970) Effect of prolonged bed rest on bone mineral. *Metabolism* 19: 1071-1084.
10. Lang T, LeBlanc A, Evans H, Lu Y, Genant H, et al. (2004) Cortical and trabecular bone mineral loss from the spine and hip in long-duration spaceflight. *J Bone Miner Res* 19: 1006-1012.
11. Alexander RM, Jayes AS, Maloiy GMO, Wathuta EM (1979) Allometry of the Limb Bones of Mammals from Shrews (*Sorex*) to Elephant (*Loxodonta*). *J Zool* 189: 305-314.
12. Biewener AA, Taylor CR (1986) Bone strain: a determinant of gait and speed? *J Exp Biol* 123: 383-400.
13. Rubin CT, Lanyon LE (1984) Dynamic Strain Similarity in Vertebrates - an Alternative to Allometric Limb Bone Scaling. *J Theor Biol* 107: 321-327.
14. de Jong WC, Koolstra JH, Korfage JA, van Ruijven LJ, Langenbach GE (2010) The daily habitual in vivo strain history of a non-weight-bearing bone. *Bone* 46: 196-202.
15. Rubin CT, Lanyon LE (1982) Limb Mechanics as a Function of Speed and Gait - a Study of Functional Strains in the Radius and Tibia of Horse and Dog. *J Exp Biol* 101: 187-211.
16. Swartz SM, Bennett MB, Carrier DR (1992) Wing bone stresses in free flying bats and the evolution of skeletal design for flight. *Nature* 359: 726-729.
17. Lanyon LE, Hampson WG, Goodship AE, Shah JS (1975) Bone deformation recorded in vivo from strain gauges attached to the human tibial shaft. *Acta Orthop Scand* 46: 256-268.
18. Burr DB, Milgrom C, Fyhrie D, Forwood M, Nyska M, et al. (1996) In vivo measurement of human tibial strains during vigorous activity. *Bone* 18: 405-410.
19. Milgrom C, Finestone A, Simkin A, Ekenman I, Mendelson S, et al. (2000) In-vivo strain measurements to evaluate the strengthening potential of exercises on the tibial bone. *J Bone Joint Surg Br* 82: 591-594.
20. Yang PF, Bruggemann GP, Rittweger J (2011) What do we currently know from in vivo bone strain measurements in humans? *J Musculoskeletal Neuronal Interact* 11: 8-20.
21. Beck BR (2009) Muscle forces or gravity--what predominates mechanical loading on bone? Introduction. *Med Sci Sports Exerc* 41: 2033-2036.
22. Judex S, Carlson KJ (2009) Is Bone's Response to Mechanical Signals

- Dominated by Gravitational Loading? *Med Sci Sports Exerc* 41: 2037-2043.
- 23. Kohrt WM, Barry DW, Schwartz RS (2009) Muscle forces or gravity: what predominates mechanical loading on bone? *Med Sci Sports Exerc* 41: 2050-2055.
 - 24. Robling AG (2009) Is Bone's Response to Mechanical Signals Dominated by Muscle Forces? *Med Sci Sports Exerc* 41: 2044-2049.
 - 25. Rittweger J (2008) Ten years muscle-bone hypothesis: what have we learned so far?--almost a festschrift. *J Musculoskelet Neuronal Interact* 8: 174-178.
 - 26. Schiessl H, Frost HM, Jee WS (1998) Estrogen and bone-muscle strength and mass relationships. *Bone* 22: 1-6.
 - 27. Schoenau E, Neu CM, Mokov E, Wassmer G, Manz F (2000) Influence of puberty on muscle area and cortical bone area of the forearm in boys and girls. *J Clin Endocrinol Metab* 85: 1095-1098.
 - 28. Rauch F, Bailey DA, Baxter-Jones A, Mirwald R, Faulkner R (2004) The 'muscle-bone unit' during the pubertal growth spurt. *Bone* 34: 771-775.
 - 29. Ireland A, Maden-Wilkinson T, McPhee J, Cooke K, Narici M, et al. (2013) Upper Limb Muscle-Bone Asymmetries and Bone Adaptation in Elite Youth Tennis Players. *Med Sci Sports Exerc*.
 - 30. Rittweger J, Beller G, Ehrig J, Jung C, Koch U, et al. (2000) Bone-muscle strength indices for the human lower leg. *Bone* 27: 319-326.
 - 31. Rittweger J, Felsenberg D (2009) Recovery of muscle atrophy and bone loss from 90 days bed rest: results from a one-year follow-up. *Bone* 44: 214-224.
 - 32. Bertram JE, Biewener AA (1988) Bone curvature: sacrificing strength for load predictability? *J Theor Biol* 131: 75-92.
 - 33. Munih M, Kralj A (1997) Modelling muscle activity in standing with considerations for bone safety. *J Biomech* 30: 49-56.
 - 34. Sverdlova NS, Witzel U (2010) Principles of determination and verification of muscle forces in the human musculoskeletal system: Muscle forces to minimise bending stress. *J Biomech* 43: 387-396.
 - 35. LeBlanc A, Schneider V, Shackelford L, West S, Oganov V, et al. (2000) Bone mineral and lean tissue loss after long duration space flight. *J Musculoskelet Neuronal Interact* 1: 157-160.
 - 36. Yang PF, Sanno M, Bruggemann GP, Rittweger J (2012) Evaluation of the performance of a motion capture system for small displacement recording and a discussion for its application potential in bone deformation in vivo measurements. *Proc Inst Mech Eng H* 226: 838-847.

CHAPTER 2

**Literature review on *in vivo* bone deformation measurements in
humans**

What do we currently know from *in vivo* bone strain measurements in humans?

Peng-Fei Yang, Gert-Peter Brüggemann, Jörn Rittweger

J Musculoskelet Neuronal Interact, 2011; 11(1): 8-20.

Abstract

Bone strains are the most important factors for osteogenic adaptive responses. During past decades, scientists have been trying to describe the relationship between bone strain and bone osteogenic responses quantitatively. However, only a few studies have examined bone strains under physiological condition in humans, owing to technical difficulty and ethical restrictions. The present paper reviewed previous work on *in vivo* bone strain measurements in humans, and the various methodologies adopted in these measurements were discussed. Several proposals were made for future work to improve our understanding of the human musculoskeletal system. Literature suggested that strains and strain patterns vary systematically in response to different locomotive activities, foot wear, and even different venues. The principal compressive, tension and engineering shear strain, compressive strain rate and shear strain rate in the tibia during running seemed to be larger than those during walking. The high impact exercises, such as zig-zag hopping and basketball rebounding induced greater principal strains and strain rates in the tibia than normal activities. Also, evidence suggested an increase of tibia strain and strain rate after muscle fatigue, which strongly supports the opinion that muscle contractions play a role on the alteration of bone strain patterns.

Keywords: Bone strain; *In vivo*; Bending; Strain gauge; Muscle fatigue

Introduction

It is well accepted that bones adapt to different types of loading, *e.g.* by various exercises or by disuse, the former being followed by anabolic responses and the latter by bone losses. Literature suggested that specific exercises or training can improve people's bone mass and strength [1]. On the other hand, disuse during space flight was shown to induce a loss of more than 2% in hip trabecular volumetric bone mineral density (vBMD) per month [2]. Inevitably, bone deformation will be induced by dynamic loading (because the static bone loading rarely happens *in vivo*, it is not included in this discussion). The effects of the various factors involved in bone loading, which include strain magnitude, strain rate, and the number of loading cycles were well documented [3, 4]. Strain magnitude (symbol: ϵ or $\mu\epsilon$) which refers to the extent of bone deformation is easy to understand. Strain rate (symbol: ϵ/s or $\mu\epsilon/s$) is the rate of strain change per unit of time, or more simply, the rapidity with which strain alterations occur. Evidence from animal studies indicated that strain rate can constitute an osteogenic stimulus independent of strain magnitude [5, 6].

It is commonly thought that both ground reaction force (so called weight-bearing) as well as forces arising from muscular contraction contribute to the loading of the leg bones. Importantly, biomechanical analyses suggest that, of the two, the larger forces are caused by muscular contractions [7]. Moreover, there are co-contractions of agonist-antagonistic muscle systems in virtually all motion patterns. Therefore, mere estimations of bone deformation by assessment of external loading and inverse dynamics approach cannot provide a full account of the relationship between bone strains and osteogenic bone response. Even though the importance of bone strain for bone metabolism has been realized, knowledge of *in vivo* bone strains during habitual physical activities and specific exercises is very limited.

With development of the methodology of *in vivo* bone strain measurements, it has become possible to record bone deformation under physiological conditions. A

number of *in vivo* animal studies provide compelling quantitative evidence for the relationship between bone strain and osteogenic response. In these studies, different methods for *in vivo* bone strain measurement have been applied.

It has to be considered, though, that *in vivo* bone strain measurements are invasive and technically challenging. Nevertheless, the first pioneering study in humans stems from 1975 [8] and the bulk of the currently available studies starts from 1996 onwards. Today, there are a total of approximately 40 subjects of whom *in vivo* bone strain data have been published. However, there are a couple of important questions that have still not been addressed, which is the subject of the following appraisal.

Type of bone deformation

Strain is the geometric deformation within the material. One way to measure it is by strain gauges. Strain is expressed as the ratio between the length change and original length, and it is therefore given as a dimensionless number. According to the following equations:

$$\text{Compressive strain: } \varepsilon_{compressive} = \frac{L - L_o}{L_o} = \frac{-|\Delta L|}{L_o};$$

$$\text{Tensile strain: } \varepsilon_{tensional} = \frac{L - L_o}{L_o} = \frac{|\Delta L|}{L_o};$$

Where L_o : original length; L : current length; $|\Delta L|$: length change. According to above equations, compressive strain and tensile strain are negative and positive values, respectively.

Strain can be simply tensile or compressive (axial strain, Fig.1A). More complex strains are generated by *e.g.* two planes sliding over each other (shear strain, Fig.1B), by bending (bending strain, Fig.1C) or by rotation (torsion strain, Fig.1D).

Axial strain

Axial strain is, by definition, a strain in the same direction as the applied load. Both compressive strain and tensile strain are axial strains. For long bones, axial

strain under physiological conditions is mostly along the long axis of the bone. It is generally thought that compressive and tensile strains are the main component of the entire bone strain during most kind of activities.

Shear strain

When loading a solid material, there will always be both compressive and tensile strains, with a certain angle between them. In any direction within this angle, shear strain exists along the surface of the structure.

Generally, the distortion in shear can be described as the combination of two ideal types of strain: simple shear (Fig. 2A) and pure shear (Fig. 2B). The sum of these two shears is equal to the so called engineering shear strain which is defined as the angle change between two lines initially perpendicular to each other in the non-deformed or initial configuration. Because the engineering shear strain is equal to the difference between two principal strain values, it can conveniently be calculated and has frequently been reported in literature [9-12]. As expected, shear strain was found during almost all activities, such as walking, running.

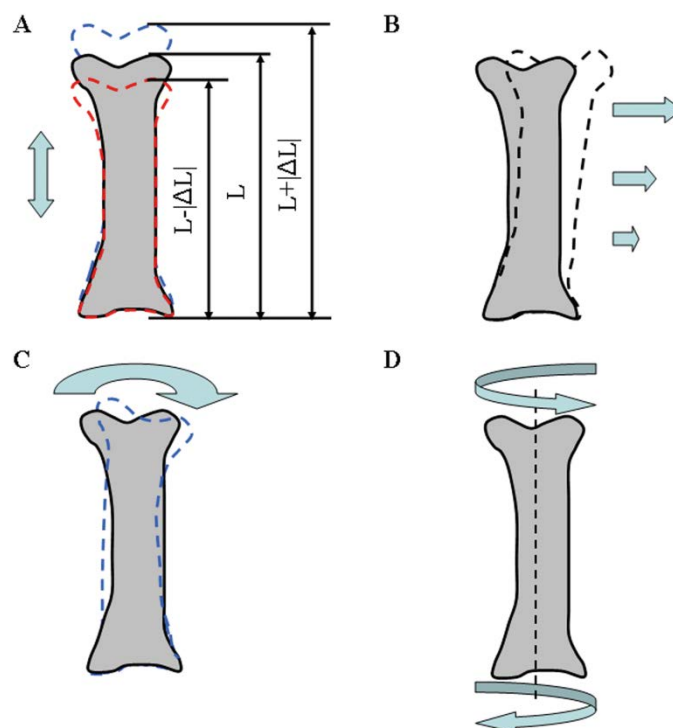


Fig.1. Different types of bone strain. A: axial strain; B: shear strain; C: bending strain; D: torsion strain.

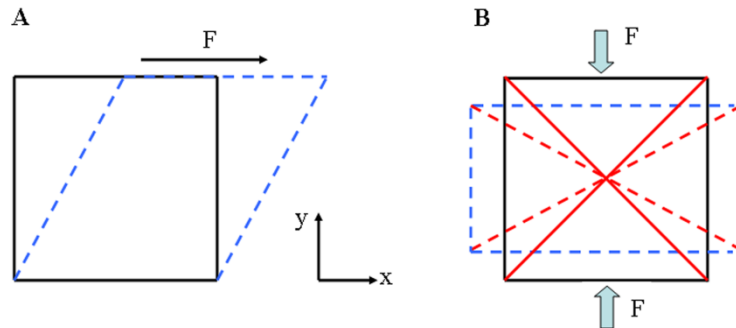


Fig. 2. Shear strains. These are due to a two-dimensional geometric deformation of an infinitesimal material element (plain black line: original geometry, dashed blue line: sheared geometry). A: simple shear. F: shear force exerted on the infinitesimal material element; B: pure shear. There is pure shear along the diagonals of the element (plain red lines: original diagonals, dashed red lines: sheared diagonals). F: compression force exerted on the element.

Bending strain

Bone bending strain is induced by the external force or force component which is applied perpendicular to the longitudinal axis of the bone. The external force can be due to eccentric (off-axis) loading, and also due to axial force acting about a bone's longitudinal curvature [13]. The bending strain may cause tension in one part (*e.g.* anterior aspect) of the bone and compression in the opposite part (*e.g.* posterior aspect) of the bone (Fig. 3A). Normally, the bending strain is superimposed with axial compressive strain (Fig. 3A), and the question arises how bending and principle strain magnitude compare to each other.

Some evidence, however, does exist to account for the presence and magnitude of *in vivo* bending strains in the human body. For example, it has been observed during zig-zag hopping that the angle of maximum principal compression to the long axis of tibia varies considerably, much more than during walking and jogging [12]. The most likely explanation for that angle change seems to be variation induced by bending moments during intense exercise, such as zig-zag hopping. However, no direct or quantitative *in vivo* bending strain data are as yet available in humans.

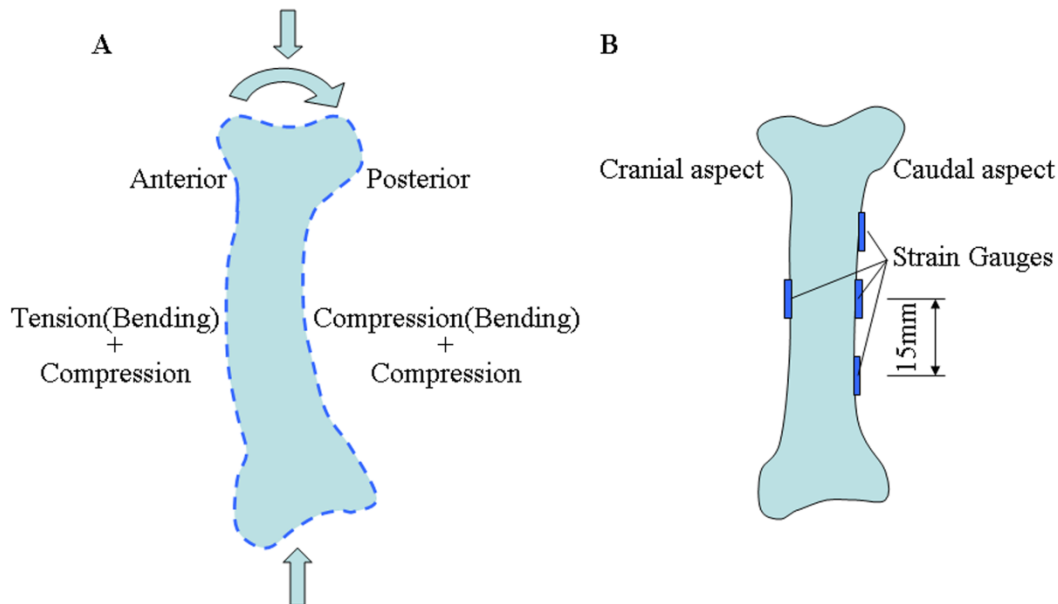


Fig. 3. A: Bending superimposed with axial compression; B: As a demonstration of bending strains in previous study, strain gauges were attached on both side of the radius in a goat [14].

Torsion

Finally, there is a possibility of torsional loading on bone if the long axis of bone is twisted (Fig. 1D). Assuming the long axis of the bone as 0° , the orientations of torsion strain in relation to the long bone axis will be at 45° or -45° , respectively, depending on the twisted direction of the long axis. For example, torsion of tibia is produced by the combination of ground frictional force relative to the foot and the resulting moment. Bones are generally weak in shear, and shear is typically induced by torsion or bending. In an *ex vivo* testing, the fatigue strength of bovine compact bone under torsion loading was about half of the compressive fatigue strain for the same material [15]. According to Taylor *et al.* [15], the largest part of shear strain arose from torsion, whilst transverse tensile stress *in vivo* was rare. Shear strain induced by torsion might therefore play an important role in bone fatigue fracture.

The methodology adopted for *in vivo* bone strain measurements

The development of appropriate bonding and recording methods made it possible to assess bone strain *in vivo* in animals and humans. Since the 1940s, scientists

have started to establish and apply different methods for measuring bone strain *in vivo* [16]. Although several methods have been developed during the past few decades, only two of them (strain gauges and bone staples) have been successfully applied in the human body as so far. The development of these methods will be discussed in the following.

The first generation: Strain gauge methods

The principle and the procedure of strain gauge measurements

As the gold standard of material strain and stress analysis, electric resistance wire strain gauges have been used in most *in vivo* bone strain measurement studies.

Their principle is based on the fact that the electrical resistance of a specially designed wire increases with increasing strain, and that it decreases with decreasing strain. When strain gauges are firmly attached on a material, they are assumed to undergo the same deformation as the material, and measurement of the electrical resistance, then allows the assessment of strain. However, a single wire strain gauge can measure strain in one direction only. In order to measure the strain with unknown directions, rosette strain gauges (Fig. 4) have to be used. In that case, the principal strain and the angle between the grids of strain gauge can be calculated. The details about the rosette strain gauges can be referred to the technical notes from the manufacturers [17].

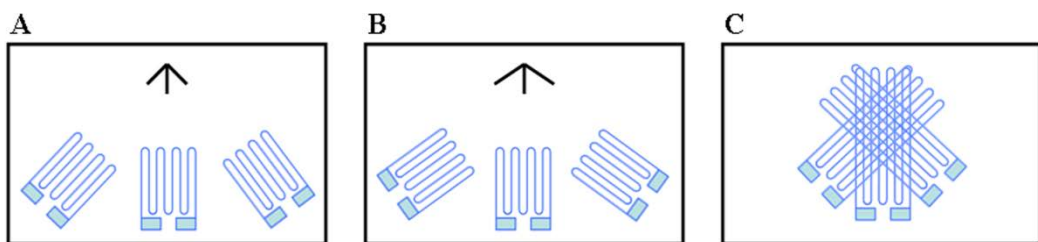


Fig. 4. Basic types of rosette strain gauges. A: 45° rectangular rosette strain gauges; B: 60° delta rosette strain gauges; C: Stacked construction rosette strain gauges. Three strain gauges are placed together in a “rosette”-like layout with each gage oriented in a different direction. When the strain direction is unknown, the principal strains and their direction can be calculated by the signal from three strain gauges of rosette strain gauge.

A series of original investigations and review papers in the 1970s have described how the strain gauges should be prepared and correctly used in bone strain

measurements *in vivo* [18-20]. Some modifications were also made for improving the bonding quality *in vivo* at a later stage [21]. So far, most *in vivo* bone strain measurement approaches have used such strain gauges, even though some modifications have been made (refer to the discussion of bone staple methods). With rosette strain gauges bonded directly to the bone surface, Lanyon LE *et al.* and Burr *et al.* performed the first and second *in vivo* bone strain recording in humans, respectively [8, 9]. The general procedure for implanting strain gauges during that study is described as following: The tissue overlying the proposed gauges site of the leg was anaesthetized first, and then a 5-10cm long skin incision down to the periosteum was made. Part of the periosteum was removed and the bone surface was cleaned. Next, the strain gauges were glued on the prepared bone surface with adhesive (isobutyl 2-cyanoacrylate monomer or polymethyl methacrylate). Then the wire of strain gauges was passed out of the wound and sutured to the periosteum. Importantly, the operation in that study took 1 hour, but the strain gauge could stay thereafter for 3 days for data collection.

In Burr's and Milgrom's paper, degreasing of bone surface with alcohol and scoring with a bone punch were reported, as additional measures to improve strain gauge bonding [9, 22]. The strain gauge signal was recorded with a portable analog tape recorder in that study, which allowed the subjects a greater degree of mobility. No pain or discomfort was reported.

Disadvantages of strain gauges

Bonding problems: Technically, the surface for bonding strain gauges should be chemically clean (*i.e.* free of oil, greases, organic contaminants and soluble chemical residues), water proof and sufficiently rough. However, it is almost impossible to reach these harsh conditions by preparation *in vivo*, especially during long term recordings. In the study of Burr *et al.*, strain gauges from one of two subjects were not firmly attached when they were checked after recording, and the data from this subject had to be abandoned [9]. Even without significant debonding, there is no way to evaluate the bonding stability *in vivo*. The bonding

quality is the key point for the accuracy of foil strain gauges. Insecure bonding is likely to result in under-estimation of strain values.

Bending strain: Assessing bending strains with strain gauges is feasible only with a set of two rosette strain gauges attached on two opposing aspects of bone [23]. In a study by Biewener *et al.* [14], for example, the strain gauges were bonded on the cranial and caudal aspect of the radial and tibial diaphysis of goats (Fig. 3B). Then, the ratio between the compressive strain due to bending and axial compression in three goats during gait at a constant speed (up to 5 m/s) was calculated, as 8.1 for the radius and 11.6 for the tibia. Furthermore, this ratio did not change significantly throughout the speed range. This suggests that bending is the predominant strain in bone during gait. Unfortunately, such an approach is hardly feasible for the human body, in particular for the tibia, as it is by virtue of the human anatomy quite impossible to attach a pair of strain gauges on two opposite sides of a bone, without destroying muscles. However, the axial and bending strain of bone cannot be distinguished with strain gauge attached on one side of a bone only. Accordingly, there are as yet no measurements in human body to provide *in vivo* bone 3D deformation.

Temperature drift: temperature related effects are the most common cause of error in the application of strain gauges. This is because the electrical resistance is dependent on temperature. For obvious reasons, using two or more strain gauges *in vivo* in order to compensate the effect of temperature, as one would do in an engineering scenario, is not feasible.

Calibration: For the strain gauges, the purpose of calibration is to develop an accurate relationship between the output voltage and bone strain. The calibration procedure is a cumbersome business, because of the potential effects of the implantation procedure [24], the linearity of strain gauges and the length of lead wire required for strain gauges (the wire cables which connect the strain gauges to the Wheatstone bridge. When the strain gauges are remote from the recording instrument, the resistance of wire cable has to be taken into account) [25].

The second generation: Extensometers and bone staples with strain gauges

Obviously, there was a desire to reduce the invasiveness of direct bonding of strain gauges to bone. To do this, the extensometers have been developed that can be externally mounted on two K-wires placed percutaneously into the bone cortex. The underlying idea was to isolate the deformation in a measurement device that was stably mounted on the bone. Before inserting the K-wires, local anesthesia was administered. Next, two K-wires were affixed into the predrilled holes to a depth of 4mm, so that the extensometer can be mounted on the K-wires. The extensometer was composed of a bronze beam with two pairs of strain gauges bonding to the top and the bottom surface of the beam, respectively (Fig.5A). Bone strains were then transmitted to the beam' strain gauges through the K-wires. Again, strain gauges were connected to the recording device via cable connection. Unfortunately, however, this approach seemed to generate artifacts induced by the heel strike, and generate smaller strain value readings than the classical strain gauge approach [26-28].

Based upon the same principle, commercial bone staples with instrumented strain gauges have also been used [29]. Subsequently, Milgrom C. *et al.* modified this method and included three strain gauges into one bone staple in a 30° rosette pattern (Fig.5B) [30]. Obviously, this requires additional holes in the tibia, which caused a practical problem related to increased invasiveness, as well as a theoretical problem related to possible effects of the holes upon structural rigidity of the instrumented bone. On the other hand, principal compressive and tensile strain, as well as engineering shear strain, can be conveniently calculated with this set up.

Compared to the strain gauges glued directly onto the bone, the application of bone staples resolved the bonding problem. Moreover, this technique required less invasive surgery for the subjects because the periosteum was mostly left intact. However, gauge failure or damage due to the surgery occurred very often [10].

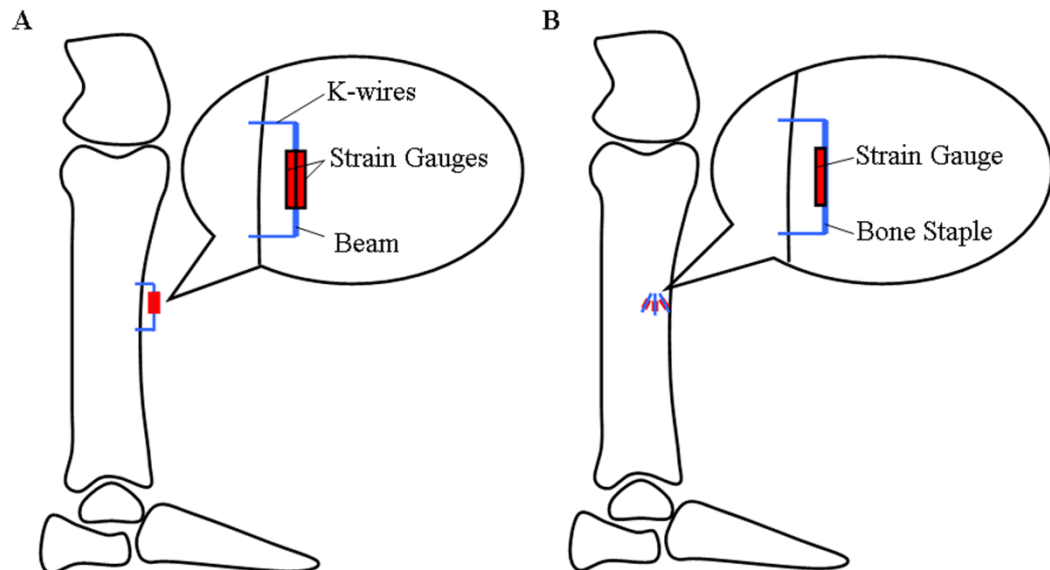


Fig. 5. Diagram of extensometer and strain gauged bone staples in bone. The principle idea was to create a mechanically stable link between the bone and the extensometer to isolate strains in the extensometer. A: extensometer which was only able to record axial strain; B: strain gauged bone staples in 30° rosette pattern which was able to record axial and shear strain. Blue line: bone staples. The strain gauges were glued on the undersurface of the staples [12].

Results from *in vivo* bone strain measurements in humans

Results from *in vivo* bone strain measurements in humans have been summarized in Table 1.

Table 1 Overview of *in vivo* bone strain (tibia, metatarsal and radius) results in humans

Study	Type of exercises	Peak Strain ($\mu\epsilon$)			Peak Strain Rate ($\mu\epsilon/\text{s}$)		
		Com. (-)	Tension (+)	Shear (+)	Com.	Tension	Shear
Tibia							
Lanyon LE <i>et al.</i> 1975	Walking	30-850	30-580	-	-	-	-
Burr DB <i>et al.</i> 1996	Walking, Jogging, Sprinting, Zigzag running	400-1300	380-750	700-2000	7000-30000	7000-20000	13500-50000
Milgrom C <i>et al.</i> 1996	Walking and running with different shoes	400-1000	540-680	760-1500	2200-14000	-	-
Rolf C <i>et al.</i> 1997	Forward jump with forefoot and heel landing	-	-	-	-	-	-
Fyhrie DP <i>et al.</i> 1998	Walking before and after exhaustion	-	-	-	-	-	-
Mendelson S <i>et al.</i> 1998	Walking with and without cane	Axial peak to peak strain: 65-230	270-2500	-	-	-	-
Milgrom C <i>et al.</i> 1998	Walking and running with different shoes	-	-	-	-	-	-
Milgrom C <i>et al.</i> 2000	Running, Drop jump	1900-2100	900-1000	5300-7400	9600-13000	4800-7600	28500-50900
Milgrom C <i>et al.</i> 2000	Running, Cycling, leg press	290-1700	270-1400	630-5000	1500-1000	1300-8200	4500-38000
Milgrom C <i>et al.</i> 2000	Walking, Running, Basketball rebound	560-3200	700-1600	1200-9000	4300-19000	3700-7400	12500-58000
Milgrom C <i>et al.</i> 2001	Walking, Jumping, Hopping	250-2200	500-2200	400-4100	2000-8000	2500-16000	5000-25000
Milgrom C <i>et al.</i> 2001	Walking with four different shoes	700-1200	460-720	1250-2600	6200-6500	2800-4000	12700-16000
Ekenman I <i>et al.</i> 2002	Walking and running with different shoes	Axial peak to peak strain: 1000-2400	3000-15000	4200-15600	-	-	-
Milgrom C <i>et al.</i> 2002	Walking, Jogging, broad jump, Vertical jump	360-700	160-1250	-	2500-8300	2100-14000	-
Milgrom C <i>et al.</i> 2003	Running at treadmill and on asphalt	400-2500	650-1250	-	3200-15000	3200-17000	-
Milgrom C <i>et al.</i> 2007	Before and after fatigue (2km run, 30km march)	470-720	340-610	-	3700-4700	4400-5600	-
Metatarsal							
Milgrom C <i>et al.</i> 2002	Walking, Jogging, Jumping	2600-2700	230-1100	-	9800-46000	3400-12000	-
Arndt A <i>et al.</i> 2002	Walking before and after fatigue	1500-2200	140-440	-	4200-5500	-	-
Radius							
Földházy Z <i>et al.</i> 2005	Arm curl, Chin up, Fall, Push up, Stirring, type writing, vacuuming carpet and wrist curl	0-6000	0-1500	-	0-85000	-	-

Bone strain induced by different activities

To date, most *in vivo* bone strain measurements focus on the human tibia. Pioneering work was done by Lanyon and co-workers as early as in 1975 [8]. With a rosette strain gauge attached to the anteromedial aspect of tibia midshaft, tibia strains were recorded during walking on a treadmill and on the floor. The principal strain and strain angle relative to the tibia's long axis were calculated. The strain magnitude when walking was found to be approximately $-430 \mu\epsilon$ ('-': compression strain) during heel off to toe off, but up to $850 \mu\epsilon$ ('+': tensile strain) when running during heel strike to toe off. As commented by Burr *et al.* [9], that work demonstrated the general possibility of such strain recording in humans.

Almost 20 years later, after the development of a portable strain measurement system, Burr *et al.* performed the second *in vivo* human tibia strain measurements during vigorous activities [9]. Data from this investigation indicated that the greatest principal strains and engineering shear strain during most vigorous activities (jogging, sprinting, running, zig-zag running) were significantly higher than those during walking. The greatest strain was engineering shear strain which occurred during zigzag uphill and downhill running (approximately $2000 \mu\epsilon$). For strain rate, the greatest compressive, tensile and engineering shear strain rate was recorded during sprinting on a level surface. By contrast, the strain rate during walking was much smaller than those of running (see also Table 1 and 2). Burr's study gave us the first comprehensive impression about the *in vivo* tibia strain in human during vigorous activities.

Moreover, the principal compressive, tension and engineering shear strain, compressive strain rate and shear strain rate in the tibia during running on a cinder track were found to be significantly higher than those during walking, which was seen as baseline due to its minimal bone remodeling [11]. Surprisingly, during running, the principal strains were comparable to those during high impact exercise (drop jump), and the strain rate seems to be even higher in running than during the drop jump exercises [10]. All of the above running data were based on running on cinder track. Much lower axial principal strains and strain rates were

reported in literature during treadmill running [31].

However, compared to running, walking, vertical jump and hopping, larger principal strains and strain rates in the tibia were found during other kinds of high impact exercises, such as zig-zag hopping [12], and even more so during basketball rebounding, where the greatest values of principal compression, tension and shear strain during rebounding were about 2 to 7 times greater than those during walking. The strain rates were approximately 2 to 5 times larger than during walking [30].

As mentioned in the ‘methodology’ section, three methods were adopted in the previous studies in tibia strain recording: strain gauges directly bonded onto the tibia, the extensometer method and the approach with bone staples. With the extensometer method, the range of tibial strains observed during walking was approximately one third of the strains recorded with strain gauge directly bonded to the tibia [26]. The discrepancy between methods can arise in several ways. Firstly, the stability of the K-wire inside the tibia was not checked during the measurements. Second, there was a possibility of artifacts induced by K-wires bending during the measurements. On the other hand, the two approaches (directly bonded strain gauges and staples) yielded very similar results during walking. This suggests that the bone staple may be a quite efficient substitute for the method of direct bonding to bone surface under certain circumstances [9, 32].

Besides the tibia, the metatarsal was another common site of study. It is of specific interest because it is a common site for fatigue fractures. Few studies have recorded the human metatarsal strain during different locomotive activities. The results indicated that peak axial metatarsal compressive and tensile strains, as well as strain rate were significantly higher than those in the tibia during treadmill walking. Moreover, high strains seemed to also occur when subjects were jogging barefoot (Table 2). During jumping on one and two legs, the tensile and compressive strains exceeded $3000 \mu\epsilon$ [33]. These data may indicate that the metatarsals have a much higher fatigue fracture incidence than the tibia because of the greater strains that they are typically exposed to.

To the best of our knowledge, there was only one *in vivo* strain recording available in the human upper extremity, namely in the distal radial metaphysis. Ten different activities, mainly with upper extremity, were studied, including arm curl, chin up, fall forward from standing and kneeling, push up, wrist curl in extension and flexion with 2 kg weight. Results indicated that the largest radius tensile strain occurred during chin up. Conversely, there was no tensile strain in the radius observed during arm curl, fall or push up exercise. Among all those activities, falling and push up exercises resulted in the largest compressive strain, which amounted to up to -6000 $\mu\epsilon$ and -4300 $\mu\epsilon$, respectively [34].

External factors influencing bone strain and strain rate

As often advertised for running shoes, the soft soles or embedded air cells in shoes are supposed to absorb the impulse energy from the ground reaction force. To some extent, this point of view was supported by scientific literature. As previous studies have shown, the compression and engineering shear strains were significantly attenuated with heel air cell embedded in the shoe during walking (from ~900 to ~700 $\mu\epsilon$ and from ~1800 to ~1250 $\mu\epsilon$, respectively). Shear strain rate also was significantly reduced by the heel air cell [32]. Similarly, results in another study suggested that soft orthoses have potential to lower the tibia tension and compressive strain rate during walking [35].

Finally, one study has investigated the effects of ipsilateral and contralateral cane use upon tibia axial strains and strain rate. Interestingly, cane usage generally failed to reduce tibial strains, but decreases in strain rate were observed [26]. .

From geometric evidence, close functional relationship between muscle function and bone anabolism exists [36]. Besides the ground reaction force, agonistic muscles also exert force on bone through tendons to realize the specific movement of human body. Accordingly, muscular contraction forces also seem to be a source of mechanical stimulation. Also, as the counterpart of agonistic muscles, antagonistic muscle can increase the loading on bone during ‘ballistic’ or ‘open-loop’ motor actions.

So far, only few data related muscle activities to *in vivo* bone strain. Arndt *et al.*

[37] reported the alteration of human second metatarsal (MTII) dorsal strain before and after M. flexor digitorum longus (FDL) fatigue. FDL contractions induced dorsal tensile strains and reduced compressive deformation of MTII which was induced by ground reaction force and dorsiflexors during the stand phase. Part of this inference was tested in the study under discussion. Tensile strain of dorsal MTII surface was in close temporal relationship to activation of FDL. The peak activation of FDL occurred during the transition from MTII tensile strain to compressive strain during mid-stance phase. After the FDL muscle was fatigued the average peak compressive strain increased 42% and the peak tensile strain decreased 55% [37]. It seems, therefore, that the bone strain protecting capacity of FDL was attenuated after the muscle had been fatigued. Similarly, in another study, after whole body fatigue (2km running and 30km march), tibia strain during walking was measured. Compared to the initial conditions, the tensile strain increased and the compressive strain decreased following the run and the march, respectively (The quantitative data was shown in Table 2). The tensile and compressive strain rates also increased after fatigue (Peak gastrocnemius torque was measured in this study to assess muscle fatigue) [38]. Thus, muscular fatigue can be assumed to cause high bone strains and may therefore contribute to the development of stress fracture. In the study of Fyhrie *et al.*, the tibia strains were assessed after the fatigue exercise. Results suggested that high strain rates were induced after fatigue in younger subjects which means that bone strain rate, in addition to strain magnitude might contribute more to the stress fracture [28]. Moreover, a study by Milgrom *et al.* has also reported that tibia strain was significantly enhanced by fatigue, and that higher strains are to be recorded during vigorous physical activities in a fatigued state, which again underlines a possible causative role of muscle fatigue in the development of stress fracture [38].

Table 2 Overview of *in vivo* bone strain studies in humans

Study	N	t	Aim	Methods and site	Type of exercises	Output
Lanyon LE <i>et al.</i> 1975	1	3d	Tibia recording	strain Foil 45° rosette SG Anteromedial aspect of tibial midshaft	Walking on treadmill or the floor, with or without shoes, with 0, 21, 45, or 71kg weights	<p>1. Walking: The end of swing period, prior to 'heel strike', principal CS > principle TS, in line with long axis;</p> <p>2. Swing forward: strain pattern reversed;</p> <p>3. Wearing shoes (swing phase): deformation increased and decreased when foot was on the ground;</p> <p>4. Walking on a concrete floor with increasing loading: angle pattern keep constant,</p> <p>5. Between 'full foot' and 'heel off', strain increased greatly.</p> <p>6. Running without shoes: larger deformation during stance phase of running than when compared to walking.</p>
Burr DB <i>et al.</i> 1996	2	<1d	Tibia during vigorous activities	strain 45° rosette SG Medial midshaft	Walking (5km/h) Jogging (10.15km/h) Sprinting (13.38km/h) Walking with 17kg load Walking or running, zigzag running uphill, downhill	<p>1. Principal CS: -414 $\mu\epsilon$ (downhill walk) ~-1226 $\mu\epsilon$(zigzag-run uphill)</p> <p>2. Principal TS: 381(walking + 17kg) ~743 $\mu\epsilon$ (zigzag run uphill)</p> <p>3. SS: 1583 $\mu\epsilon$ (sprinting) ~871 $\mu\epsilon$(walking)</p> <p>4. Highest CSR and TSR: sprinting and downhill zigzag run and smallest when walking</p> <p>5. Highest SSR: sprinting, downhill running</p>

Milgrom C <i>et al.</i> 1996	2	<1d	Compare tibia strain when subjects wearing different shoes	the 45° rosette SG	Walking at 3miles/h with shoes:	During walking	
					1. Rockport prowalker 7580 tibial midshaft	1. Zohar infantry boots had lowest principal CS and CSR;	
					2. New balance running shoes	2. New balance running shoes had lowest SS;	
					3. Light Israeli infantry boots	3. no single shoe lowered all the strain and SR;	
					4. 2 layer sole infantry boots	During running, zohar boot had lowest strain and SR.	
					5. Zohar infantry boots		
Fyhrie DP <i>et al.</i> 1998	7(6)	<1d	Fatigue, strain and age	tibia extensometer (SG) 5km/h Anteromedial tibial midshaft	Running on the track	before and after	
					exhaustion exercise		
Mendelson S, <i>et al.</i> 1998	7(6)	<1d	Tibia strain and cane usage	extensometer (SG) Anteromedial tibial midshaft	Walking without cane	1. Tibia strain depicts a increase after muscle fatigue in old people, but have no change in young people;	
					Walking with cane in right hand	2. Heel strike impact is increased in young people, but decreased in old people after muscle fatigue;	
					Walking with cane in left hand	1. Cane did not reduce the peak to peak tibial axial strain: 170, 169 vs. 148 $\mu\epsilon$	
						2. However, cane usage reduced the max. tibial tibial CSR: 1048, 794 vs. 757 $\mu\epsilon/s$	
Milgrom C <i>et al.</i> 1998	7(6)	<1d	Compare tibia strain effect on tibia strain	the extensometer (SG) on Anteromedial tibial midshaft	Walking (5km/h), run (16.3km/h):	1. Walking: Zohar shoe had lowest CS, TS and CSR, TSR;	
						2. Running: No differences on CS, TS and SR between these shoes;	
						3. No difference on CS, TS and SR between walking on corridor and on treadmill;	
Milgrom C <i>et al.</i> 2000	6(4)	1d	Tibia during	strain high rosette pattern (SG)	Running at 17km/h Drop jump (26, 39 and 52cm)	1. No difference in CS, TS and SS with increasing jump heights, but CSR decreased;	

impact exercise and running	Medial aspect of midtibial diaphysis	2. No relation between max. principal CS and jump potential energy;
		3. No difference between the principal strain during running and jumping from 52cm (up to ~5500 $\mu\epsilon$), but TSR higher during running.
Milgrom C <i>et al.</i> 2000	1d Evaluation of bone staples in rosette pattern (SG) potential strengthening exercise with Medial aspect of mid tibial diaphysis	1. No difference in principal TS, CS and SS between walking, leg press or stepmaster; 2. Higher strain during running than walking; 3. TSR and SSR are lower in cycling than walking; 4. Max. TSR during walking were higher than leg press, stepmaster and cycling; 5. Highest max. CS and SS during running, during walking were higher than cycling and leg press.
Milgrom C <i>et al.</i> 2000	1d Assess bone strain developed during sporting activities	6. From the view of bone strain, only running is effective strengthening for tibia. 1. The principal CS, TS and SS during running were 2 to 4.5 times those of walking, but those during basketball rebounding were 2.25 to 7.41 times greater than during walking. 2. The TSR, CSR and SSR during rebounding and running were 2.16 to 4.60 times higher than during walking.
Milgrom C <i>et al.</i> 2001	1d Assess the bone strain induced by lower limb	Male: 1. Highest CS; jogging, hopping 50cm and zig-zag hopping;
		Free walking; Jogging at 17km/h; Vertical jump on two legs to 5cm;

indoor exercise compared with those of walking	Medial aspect of midtibial diaphysis	Standing broad jump to 20cm; Hopping 50cm on right leg;	Zig-zag hopping on the right leg.	2. Highest TS: jogging, vertical jump on right leg to 5cm, hopping 50cm and zig-zag hopping;	3. Highest SS: hopping 50cm and zig-zag hopping;	4. Highest SSR: jogging;	2. Highest TS: jogging, vertical jump on right leg to 5cm, hopping 50cm and zig-zag hopping;
Milgrom C et al. 2001	1d Test influences of rosette pattern (SG) shoe sole	the Bone staples in Walking at 5km/h with shoes:	1. 65 shore A polyurethane (SAP) 2. 65 SAP with heel air cell	CS, SS and shear SR is lower with air cells embedded shoes;	Lower TS and CSR with 75 SAP shoes;	Lower SS rate with air cells embedded shoes;	Before running: Walking: higher peak to peak axial (p-p) strain with boots than running shoes; lower p-p strain with orthoses; soft orthoses with boot lowered the TSR
Ekenman I et al. 2002	9 Access influence running shoes and military	the Bone staples in rosette pattern (SG)	Walking 5 km/h before and after run; Running shoes and army boots with and without semirigid and soft orthoses;	Walking 5 km/h before and after run; Running shoes and army boots with and without semirigid and soft orthoses;			

boots with shoe orthoses on bone strain	middle and tibial diaphysis	distal	walking 5km/h;	and CSR; Running: P-p strain with boots was not higher than running shoes; semirigid orthoses with boots increased TSR and CSR;	
	Run 2km (13 km/h) + running shoes Run 1km +army boots;			walking again after running. No increase in TSR and CSR compared with before running; Shoe orthoses may be warranted for fracture during mostly walking exercise, but not mostly running exercise.	
Milgrom C <i>et al.</i> 2002	1d	Compare strain in second metatarsal with the tibia and access the effect of shoe gear on these strain	Bone staples with two perpendicular SG • Medial aspect midtibial diaphysis • Dorsal surface of mid 2 nd metatarsal diaphysis	Walking at 5 km/h 2. Logging at 11 km/h One subject: 1. 50cm broad jump 2. Vertical jump to 10cm (one leg) 3. Vertical jump to 10cm (two legs)	Barefoot walking: 1. Peak axial metatarsal CS, TS, SR >those of tibia 2. Barefoot jogging: 3. Peak metatarsal CS and SR > those of tibia; 4. Peak axial CS reach 5677 $\mu\epsilon$; Wearing running shoes: 1. Metatarsal strain lower, but not tibia compression strain; 2. Tension strain increased; 3. Metatarsal CS, TS and SR > those of tibia; 4. Broad jumping, vertical jumping: strain>3000 $\mu\epsilon$;
Arndt A <i>et al.</i> 2002	8	<3h	Evaluate effect of muscle fatigue on	Walking barefoot (3km/h) until Fatigue: Pre-fatigue without 20kg backpack; Pre-fatigue with 20kg backpack; Pre-fatigue, no backpack: 1. Toe down was followed by peak tension (8±7%), followed by max. compression (65±15%),	

metatarsal strain	Dorsal surface of mid 2 nd metatarsal diaphysis	Post-fatigue without 20kg backpack; Post-fatigue with 20kg backpack;	immediately after, compression decreased to about zero;			
			2. Mean peak CS: -1534±636 $\mu\epsilon$, TS: 346±359 $\mu\epsilon$, SR: 4165±1233 $\mu\epsilon/s$;			
			3. Peak compression during baseline without backpack less than other condition;			
			4. SR increased with backpack but not post-fatigue; Post-fatigue:			
			1. Peak tension decreased with backpack;			
			2. Time of peak CS was later for post fatigue without backpack;			
			3. Peak TS occurred earlier without backpack;			
Milgrom C <i>et al.</i> 2003	3	1d	Determine the difference during treadmill and overground running	Bone staples with one SG Medial aspect of the mid tibial diaphysis	With Nike Air Max shoes: Running at 11km/h at treadmill Free running on asphalt at 11km/h;	Peak mean axial CS and TS, peal mean TSR and CSR were higher during running on overground than on treadmill:
Földhazy Z <i>et al.</i> 2005	10	<2h	Evaluate the different type of exercises	Bone staples with two perpendicular SG distal metaphysis radial metaphysis	Arm curl with 7kg Chin up; Fall, standing and kneeling; Push up on knee; Stirring; Type writing;	1. Max. CS for falling and push up > for the others (except falling on knee vs. arm-curl and wrist-curl); 2. Max. TS for chin-up > for arm-curl, fall kneeling, push up, stirring and typing;

Vacuuming carpet;
Wrist curl in extension with 2kg;
Wrist curl in flexion with 2kg;

3. For push-up: there is no any tension, p-p strain around 2300 $\mu\epsilon$;
4. Median value of strain rate: for falling (from standing: 45954 $\mu\epsilon/s$, on kneeling: 18582 $\mu\epsilon/s$) > for the other activities;

Milgrom C et al. 2007	4	Evaluate the effect of muscle fatigue on tibia strain	Bone staples in rosette pattern (SG)	Before and after fatigue:	Max. right GM isokinetic torque, Tibia strain, force plate measure;	Fatigue procedure:	After the march:
			Medial aspect of midtibial diaphysis	1. 2km run (>12km/h) 2. 30km march (6km/h)			

- The peak GM isokinetic torque was reduced by 37%, 31%, 21% and 23% respectively;
- TS: 26% increased post run and 29% increased after march;
- TSR: 13% increased post run and 11% increased after march
- CS: 15% decreased post run and 24% decreased after march;
- CSR: 9% increased post run and 17% increased after march;

Risk evaluation (Pain and Infection)

Most *in vivo* studies have reported swelling and tenderness at the surgical site in some subjects. These complaints did generally recover well, so that subjects were able to return to their normal activities within few weeks, except for one or two exceptions that required longer recovery (less than a few months). Another problem which has to be considered seriously is the risk of infection, especially during the application of bone staples. In previous studies, bone staples were inserted into cortical bone to a depth of approximately 4 mm to avoid penetration of the cortex, thereby reducing the infection risk. Despite this, the risk is still one of the obvious problems in bone strain *in vivo* measurement.

What should be done in the future?

As discussed above, the few *in vivo* bone strain measurements that have been done in the past decade have greatly contributed to musculoskeletal science [8-12, 22, 26-35, 37, 38]. On the other hand, these studies have given us only an incomplete impression about *in vivo* bone strain, and they were mainly limited to the tibia and metatarsal. Accordingly, there are many open questions which we cannot answer.

First, there are serious limitations imposed by the current methodological approach. As mentioned above, the goal must be to improve our understanding of bone strain within the human body, and to do so in a way that is less invasive and more accurate at the same time, to ideally reveal also 3-dimensional strain information. Of interest, accurate and less invasive approaches have been proposed, although no data from human *in vivo* application are available as yet. One of such approaches is based upon an optical technique for non-contact, 3-dimensional deformation measurement, namely the digital image correlation (DIC). This has been employed to measure the strain distribution of animals' bone *ex vivo*. In this method, a high contrast speckle pattern (normally with painting or spraying) was applied onto the bone surface. The speckle pattern changed during loading was then optically tracked. Compared with strain gauges, this method was

more informative for anisotropic materials, such as bone. Although some *in vivo* bone strain recordings have been done in animals [39, 40], further improvements are needed to avoid exposing and painting bone surface for *in vivo* bone strain measurements in human. To overcome the limitations of invasiveness in the methods mentioned above, ultrasound wave assessment was introduced to measure bone deformation [41]. Again, no *in vivo* data are available as yet. Summarizing the above discussion, from the available methods so far, there are not too many choices to assess *in vivo* bone strains in the human body. With the exception of strain gauges and bone staples which have been used in previous *in vivo* studies, a few new methods are conceivable, none of which is easy to apply. However, these new methods could have the potential to give more strain information and thus may constitute a new step in the field of bone research.

Second, the strain pattern of bone *in vivo* is not clear during locomotive activities, even in tibia and metatarsal. Besides compressive and tensile strain, torsion and bending strain are very important composition of bone strain pattern as well, the latter one was even believed to be the key factors in bone fracture. However, with the available techniques, no reliable data can be obtained to understand bending and torsion strains.

Third, strain gauges, as frequently used in bone surface strain measurement *in vivo* and *ex vivo*, do not provide global strain distribution and 3D components of strain. From literature, almost all the strain data were recorded in one or two sites of bone which cannot represent that in other bone sites. In addition, the mechanical properties of cortical and trabecular bone are different, and previous data have shown that the bone periosteal and endocortical region have different responses to the non-invasive loading [42]. This implies that the strain gradient in the radial direction of long bone should not be ignored. How to measure the inner bone strain *in vivo* is still a big challenge. Future work could yield more information about strain distribution and 3D strain, which would certainly help to improve our understanding about the relationship between bone strain and bone modeling, remodeling process.

Fourth, according the theory of ‘Wolff’s law’, bone will optimize its structure in response to the way it is loaded. Accordingly, the strain distribution might vary between subjects with different bone architecture. For example, with micro CT scanning and finite element analyses, Rietbergen and his co-workers have suggested that differences in strain magnitude and distribution may exist between osteoporotic and healthy femurs [43]. If *in vivo* bone strain data were available from different populations with healthy and unhealthy bones, in combination with information on their bone structure, there will be more evidence to evaluate ‘Wolff’s law’ quantitatively.

Fifth, close functional relationships between the musculature and bone were observed in many studies [43-46]. Muscle has been proposed as a primary source of mechanical stimulation for bone metabolism. If this hypothesis is true, bone strain, as an indicator of mechanical stimulation in bone, should have strong relationship with muscle activities. However, muscle activities, especially in lower leg, are also linked to ground reaction force which is also recognized as one of the sources of bone deformation. So, how much bone strain is contributed by ground reaction force and muscle activities, respectively? Some *in vivo* study suggested that more than 70% of the forces in femur during gait were resulted from muscle forces, only less than 30% derived from body weight [47]. However, there is no quantitative data available in tibia so far. Another question arising in this context is whether there are spatial and temporal relationships between muscle activities and bone strain patterns. The answer will be yes if the muscle forces do indeed play a decisive role in the loading of bone.

Conclusions

The pioneering works of Evans, Lanyon and other scientists mark the beginning of the *in vivo* bone strain research field, and extensive data have been recorded in animal studies since then. The unique data from these studies has helped to expand our understanding of the bone adaption to bone strain induced by muscle contraction and external force. However, the measurements in human body are

limited by the invasiveness and complexity.

Due to the restriction of externally available specific zones of bone *in vivo*, strain measurements were limited to few locations only, for example the antero-medial aspect in the human tibia and dorsal surface in the metatarsal. According to these data, the strain magnitude in the tibia is within the range of 0-5000 $\mu\epsilon$, and in some vigorous activities, such as jumping, basketball rebounding, the tibia strain magnitude can reach approximately 9000 $\mu\epsilon$. Relative to strain magnitude, high rate strain is another potential stimuli factor to stimulate osteogenic responses. Depending on the specific kinds of exercise, bone strain rate is normally in the range of 1500-20000 $\mu\epsilon/s$ and could reach up to 58000 $\mu\epsilon/s$ during vigorous activities (Table 1).

Acknowledgments

We would like to thank Thomas Förster in the Institute of Biomechanics and Orthopaedics, German Sport University Cologne for numerous discussions about the application of strain gauges. Special thanks go to Alex Ireland for linguistic scrutiny. Pengfei Yang acknowledges his scholarship by the China Scholarship Council (CSC No.: 2009629013).

References

1. Suominen H (2006) Muscle training for bone strength. *Aging Clin Exp Res* 18: 85-93.
2. Lang T, LeBlanc A, Evans H, Lu Y, Genant H, et al. (2004) Cortical and trabecular bone mineral loss from the spine and hip in long-duration spaceflight. *J Bone Miner Res* 19: 1006-1012.
3. Forwood MR, Turner CH (1995) Skeletal adaptations to mechanical usage: results from tibial loading studies in rats. *Bone* 17: 197S-205S.
4. Duncan RL, Turner CH (1995) Mechanotransduction and the functional response of bone to mechanical strain. *Calcif Tissue Int* 57: 344-358.
5. Mosley JR, Lanyon LE (1998) Strain rate as a controlling influence on adaptive modeling in response to dynamic loading of the ulna in growing male rats. *Bone* 23: 313-318.
6. Turner CH, Owan I, Takano Y (1995) Mechanotransduction in bone: role of

- strain rate. *Am J Physiol* 269: E438-442.
7. Rittweger J (2007) Physiological targets of artificial gravity: adaptive processes in bone. In: Clement G, Buckley A, editors. *Artificial Gravity*. Berlin: Springer. pp. 191-231.
 8. Lanyon LE, Hampson WG, Goodship AE, Shah JS (1975) Bone deformation recorded in vivo from strain gauges attached to the human tibial shaft. *Acta Orthop Scand* 46: 256-268.
 9. Burr DB, Milgrom C, Fyhrie D, Forwood M, Nyska M, et al. (1996) In vivo measurement of human tibial strains during vigorous activity. *Bone* 18: 405-410.
 10. Milgrom C, Finestone A, Levi Y, Simkin A, Ekenman I, et al. (2000) Do high impact exercises produce higher tibial strains than running? *Br J Sports Med* 34: 195-199.
 11. Milgrom C, Finestone A, Simkin A, Ekenman I, Mendelson S, et al. (2000) In vivo strain measurements to evaluate the strengthening potential of exercises on the tibial bone. *J Bone Joint Surg Br* 82-B: 591-594.
 12. Milgrom C, Miligram M, Simkin A, Burr D, Ekenman I, et al. (2001) A home exercise program for tibial bone strengthening based on in vivo strain measurements. *Am J Phys Med Rehabil* 80: 433-438.
 13. Biewener AA (1991) Musculoskeletal design in relation to body size. *J Biomech* 24 Suppl 1: 19-29.
 14. Biewener A, Taylor C (1986) Bone strain: a determinant of gait and speed? *J Exp Biol* 123: 383-400.
 15. Taylor D, O'Reilly P, Vallet L, Lee TC (2003) The fatigue strength of compact bone in torsion. *J Biomech* 36: 1103-1109.
 16. Caler WE, Carter DR, Harris WH (1981) Techniques for implementing an in vivo bone strain gage system. *Journal of biomechanics* 14: 503-505, 507.
 17. TN-515 VM-MTN (2010) Strain gage rosettes: selection, application and data reduction Measurements Group, Inc.
 18. Van Cochran GB (1974) A method for direct recording of electromechanical data from skeletal bone in living animals. *J Biomech* 7: 563-565.
 19. Cochran GV (1972) Implantation of strain gages on bone in vivo. *J Biomech* 5: 119-123.
 20. Wright TM, Hayes WC (1979) Strain gage application on compact bone. *J Biomech* 12: 471-473, 475.
 21. Hoshaw SJ, Fyhrie DP, Takano Y, Burr DB, Milgrom C (1997) A method suitable for in vivo measurement of bone strain in humans. *J Biomech* 30: 521-524.
 22. Milgrom C, Burr D, Fyhrie D, Forwood M, Finestone A, et al. (1996) The effect of shoe gear on human tibial strains recorded during dynamic loading: a pilot study. *Foot Ankle Int* 17: 667-671.
 23. Rubin C, Lanyon L (1982) Limb mechanics as a function of speed and gait: a study of functional strains in the radius and tibia of horse and dog. *J Exp Biol* 101: 187-211.

24. TN-509 VM-MTN (2005) Error due to transverse sensitivity in strain gages. Measurements Group, Inc.
25. TN-514 VM-MTN (2007) Shunt calibration of strain gage instrumentation. Vishay Measurements Group, Inc.
26. Mendelson S, Milgrom C, Finestone A, Lewis J, Ronen M, et al. (1998) Effect of cane use on tibial strain and strain rates. *Am J Phys Med Rehabil* 77: 333-338.
27. Milgrom C, Burr D, Fyhrie D, Hoshaw S, Finestone A, et al. (1998) A comparison of the effect of shoes on human tibial axial strains recorded during dynamic loading. *Foot Ankle Int* 19: 85-90.
28. Fyhrie DP, Milgrom C, Hoshaw SJ, Simkin A, Dar S, et al. (1998) Effect of fatiguing exercise on longitudinal bone strain as related to stress fracture in humans. *Ann Biomed Eng* 26: 660-665.
29. Rolf C, Westblad P, Ekenman I, Lundberg A, Murphy N, et al. (1997) An experimental in vivo method for analysis of local deformation on tibia, with simultaneous measures of ground reaction forces, lower extremity muscle activity and joint motion. *Scand J Med Sci Sports* 7: 144-151.
30. Milgrom C, Simkin A, Eldad A, Nyska M, Finestone A (2000) Using bone's adaptation ability to lower the incidence of stress fractures. *Am J Sports Med* 28: 245-251.
31. Milgrom C, Finestone A, Segev S, Olin C, Arndt T, et al. (2003) Are overground or treadmill runners more likely to sustain tibial stress fracture? *Br J Sports Med* 37: 160-163.
32. Milgrom C, Finestone A, Ekenman I, Simkin A, Nyska M (2001) The effect of shoe sole composition on in vivo tibial strains during walking. *Foot Ankle Int* 22: 598-602.
33. Milgrom C, Finestone A, Sharkey N, Hamel A, Mandes V, et al. (2002) Metatarsal strains are sufficient to cause fatigue fracture during cyclic overloading. *Foot Ankle Int* 23: 230-235.
34. Foldhazi Z, Arndt A, Milgrom C, Finestone A, Ekenman I (2005) Exercise-induced strain and strain rate in the distal radius. *J Bone Joint Surg Br* 87: 261-266.
35. Ekenman I, Milgrom C, Finestone A, Begin M, Olin C, et al. (2002) The role of biomechanical shoe orthoses in tibial stress fracture prevention. *Am J Sports Med* 30: 866-870.
36. Fricke O, Beccard R, Semler O, Schoenau E (2010) Analyses of muscular mass and function: the impact on bone mineral density and peak muscle mass. *Pediatr Nephrol* 25: 2393-2400.
37. Arndt A, Ekenman I, Westblad P, Lundberg A (2002) Effects of fatigue and load variation on metatarsal deformation measured in vivo during barefoot walking. *J Biomech* 35: 621-628.
38. Milgrom C, Radeva-Petrova DR, Finestone A, Nyska M, Mendelson S, et al. (2007) The effect of muscle fatigue on in vivo tibial strains. *J Biomech* 40: 845-850.

39. Yang L, Zhang P, Liu S, Samala PR, Su M, et al. (2007) Measurement of strain distributions in mouse femora with 3D-digital speckle pattern interferometry. *Opt Lasers Eng* 45: 843-851.
40. Sztefek P, Vanleene M, Olsson R, Collinson R, Pitsillides AA, et al. (2010) Using digital image correlation to determine bone surface strains during loading and after adaptation of the mouse tibia. *J Biomech* 43: 599-605.
41. Matsuyama J, Ohnishi I, Sakai R, Suzuki H, Harada A, et al. (2006) A new method for measurement of bone deformation by echo tracking. *Med Eng Phys* 28: 588-595.
42. LaMothe JM, Zernicke RF (2008) The relation between loading rate, strain gradients, and bone adaptation. *J Bone Joint Surg Br* 90-B: 78-c-.
43. Van Rietbergen B, Huiskes R, Eckstein F, Ruegsegger P (2003) Trabecular bone tissue strains in the healthy and osteoporotic human femur. *J Bone Miner Res* 18: 1781-1788.
44. Manske SL, Boyd SK, Zernicke RF (2010) Muscle and bone follow similar temporal patterns of recovery from muscle-induced disuse due to botulinum toxin injection. *Bone* 46: 24-31.
45. Rittweger J, Felsenberg D (2009) Recovery of muscle atrophy and bone loss from 90 days bed rest: results from a one-year follow-up. *Bone* 44: 214-224.
46. Fricke O, Beccard R, Semler O, Schoenau E (2010) Analyses of muscular mass and function: the impact on bone mineral density and peak muscle mass. *Pediatr Nephrol*.
47. Lu TW, Taylor SJ, O'Connor JJ, Walker PS (1997) Influence of muscle activity on the forces in the femur: an in vivo study. *J Biomech* 30: 1101-1106.

CHAPTER 3

Establishment of a novel optical segment tracking (OST) approach for *in vivo* bone deformation measurements

Evaluation of the performance of a motion capture system for small displacement recording and a discussion for its application potential in bone deformation *in vivo* measurements

Peng-Fei Yang, Maximilian Sanno, Gert-Peter Brüggemann, Jörn Rittweger

Proc IME H J Eng Med, 2012; 226(11): 838-47.

Abstract

The aim of this study is to evaluate the performance of a motion capture system and discuss the application potential of proposed system in *in vivo* bone-segment deformation measurements. In this study, the effects of calibration procedure, camera distance and marker size on the accuracy and precision of the motion capture system were investigated by comparing the captured movement of the markers with reference movement. The results indicated that the system resolution is at least 20 μm in a capture volume of $400 \times 300 \times 300 \text{ mm}^3$, which mostly cover the range of motion of the tibia during stance phase of one gait cycle. Within this volume, the system accuracy and precision decreased following the increase of camera distance along the optical axis of the cameras. With the best configuration, the absolute error and precision for the range of 20 μm displacement were 1.2-1.8 μm and 1.5-2.5 μm , respectively. Small markers ($\varnothing 3\text{-}8 \text{ mm}$) yielded better accuracy and repeatability than the larger marker ($\varnothing 10.5 \text{ mm}$). We conclude that the proposed system is capable to record minute displacement in a relatively large volume.

Keywords: Motion capture system; Bone strain; *in vivo*; Accuracy; Precision

Introduction

Bone strain is widely accepted as one of the most important factors in bone adaptation. The exploration made by scientists over the past few decades provides reliable and quantitative evidence to suggest a relationship between bone strain and osteogenic responses [1-4]. Nevertheless, *in vivo* bone strains measurement is still technically challenging, especially in humans. Despite the invasiveness, in previous studies, the inherent shortcomings of the methodologies based on strain gauges during the application of *in vivo* bone strain recording are likely to result in under-estimating the real strain values due to the low bonding quality [5-8]. On the other hand, strain gauges can reflect strains in specific areas only that are covered by the gauges, but yield no information regarding the bone-segment deformation on a large scale. Even more importantly, it is difficult, not to say impossible, to assess bending and torsional strains with strain gauges in humans [5].

In order to overcome the drawbacks of this traditional method, several new methods have been developed to assess bone strain. such as a non-contact optical technique, referred to as digital image correlation (DIC) [9-11], as well as ultrasound wave propagation [12]. However, the potential of these methods for *in vivo* application is still highly debatable.

Camera based motion capture systems are nowadays widely used in the field of biomechanics. These systems work with markers that are attached to the landmark positions of the human body and then captured by cameras. The data processing then involves a) location of the markers in the 2D-space of each camera, and b) reconstruction of each marker in the real-world 3D-space by convergence of the information from the set of cameras [13]. Although the performance of motion capture system varies with the specific system set-up [14], it is theoretically possible to achieve very high accuracy. The prerequisites are a proper calibration procedure, choice of markers and the positioning of the cameras. Liu *et al.* evaluated the accuracy and precision of the Qualisys motion capture system

(Qualisys, Inc., Gothenberg, Sweden) in the measurements of small displacements in a small field of view [15]. Results indicated that, in a $68 \times 51 \text{ mm}^2$ field of view, the system resolution was $10 \mu\text{m}$. In the range of $20\text{-}200 \mu\text{m}$, the absolute displacement errors were from ± 2.1 to $\pm 3.0 \mu\text{m}$ for diamond markers, and from ± 2.5 to $\pm 4.25 \mu\text{m}$ when sphere markers were used. The standard deviation of the repetitions was $1.7\text{-}2.3 \mu\text{m}$ for diamond markers, and $1.9\text{-}3.9 \mu\text{m}$ for sphere markers, respectively [15]. With the Vicon-460 motion capture system (Vicon Motion System Ltd., LA, USA), accuracy of $63 \mu\text{m}$ and precision of $15 \mu\text{m}$ can be achieved in a volume of $180 \times 180 \times 150 \text{ mm}^3$ [14]. Overall, the previous studies have demonstrated that, with proper parameters and setup, commercially available motion capture systems are able to provide sufficient accuracy and precision (also called repeatability or reproducibility) to measure small movement of the markers in relative small 3D volume. If these markers are affixed to the bone, *e.g.* human tibia, theoretically, the tibia deformation should be able to be measured by recording the relative movement between the markers, and then the tibia-segment deformation will be able to be calculated. By doing so, the complex measurements of different type of tibia-segment deformation essentially turn to be the simple measurements of markers' coordinate in 3D volume. During the stance phase of one human gait cycle, the range of motion of the tibia is almost constant and within certain 3D volume. In another words, the movement of the markers which affixed to the tibia during the stance phase of one gait cycle also stay within certain 3D volume. As long as the markers' coordinates in this 3D volume is able to be recorded with high accuracy and repeatability, axial, shear and torsion bone-segment deformation should be able to be calculated. However, despite this high level of accuracy, the very limited volume covered in the aforementioned studies seems to impede the application of motion capture camera systems for *in vivo* bone-segment deformation measurements. To our knowledge, neither the performance of motion capture systems in relatively large volume nor the potential of applying motion capture system in bone deformation (most commonly refer to tibia) *in vivo* measurements has been reported and discussed before.

Taking the human tibia as an example, assuming the distance between the markers affixed in the tibia as $L = 20\text{cm}$ and the detection limit of the optical method as $100 \mu\epsilon$ (Compared with approximately $2000 \mu\epsilon$ *in vivo* tibia strain [6, 16], the detection limit of $100 \mu\epsilon$ is acceptable), respectively, the required resolution of the optical method, ΔL , can be calculated as following: $\Delta L = L \times 100 \mu\epsilon = 20 \mu\text{m}$.

Although this is only a rough figure, it can inform us about the required resolution of an optical method to assess the tibia deformation. We therefore ventured to evaluate the optical system, thus using an optical method for measuring small displacement ($20 \mu\text{m}$) in relative large volume. More specifically we are addressing, firstly, whether $20 \mu\text{m}$ of resolution is able to be achieved with proposed system configuration in this study was assessed. Secondly, the accuracy and precision during the measurement of $20 \mu\text{m}$ movement in large volume were evaluated. In addition, the application potential of this system in bone deformation *in vivo* measurements is discussed.

Materials and Methods

The Vicon MX motion capture system (Vicon Motion System Ltd., LA, USA), including Vicon F40 cameras (4 Megapixel, 370 fps full frame top speed), MX Giganet controlling hardware module and Vicon Nexus 1.6.1 software, was adopted to capture the motion of the retro-reflective markers. The performance (accuracy and precision) of this system was evaluated to further establish the proposed method.

As mentioned above, the motion of human tibia and the markers affixed to the tibia during the stance phase of one gait cycle stays within certain volume, which is able to be assumed by the length of tibia. Typically, the length of the tibia is approximately 400 mm. Accordingly, the volume of interest during a tibia's stance phase has dimensions of $400 \times 300 \times 300 \text{ mm}^3$. In this volume, the performance of this optical system was assessed. Assuming an inter-marker distance of 20 cm, one has to resolve marker displacement by $20 \mu\text{m}$ in order to assess strains of $100 \mu\epsilon$ – goal that seems worthwhile to achieve. Several previous *in vivo* bone strains

studies with strain gauges suggested that more than $2000 \mu\epsilon$ of bone deformation can be reached during the exercises [5]. Comparably, the detection limit of $100 \mu\epsilon$ in the proposed method would be acceptable for *in vivo* bone strains recording.

Within the selected volume, the minute movement of the markers was carried out by a universal milling machine (DMU 50M, DMG Vertriebs und Service GmbH, Bielefeld, Germany) with the ability to position its spindle in three dimensions accurately (resolution in all axes: $1 \mu\text{m}$). After being affixed on the spindle of the milling machine, the markers were moved along three orthogonal directions within the volume of $400 \times 300 \times 300 \text{ mm}^3$ (Fig. 1).

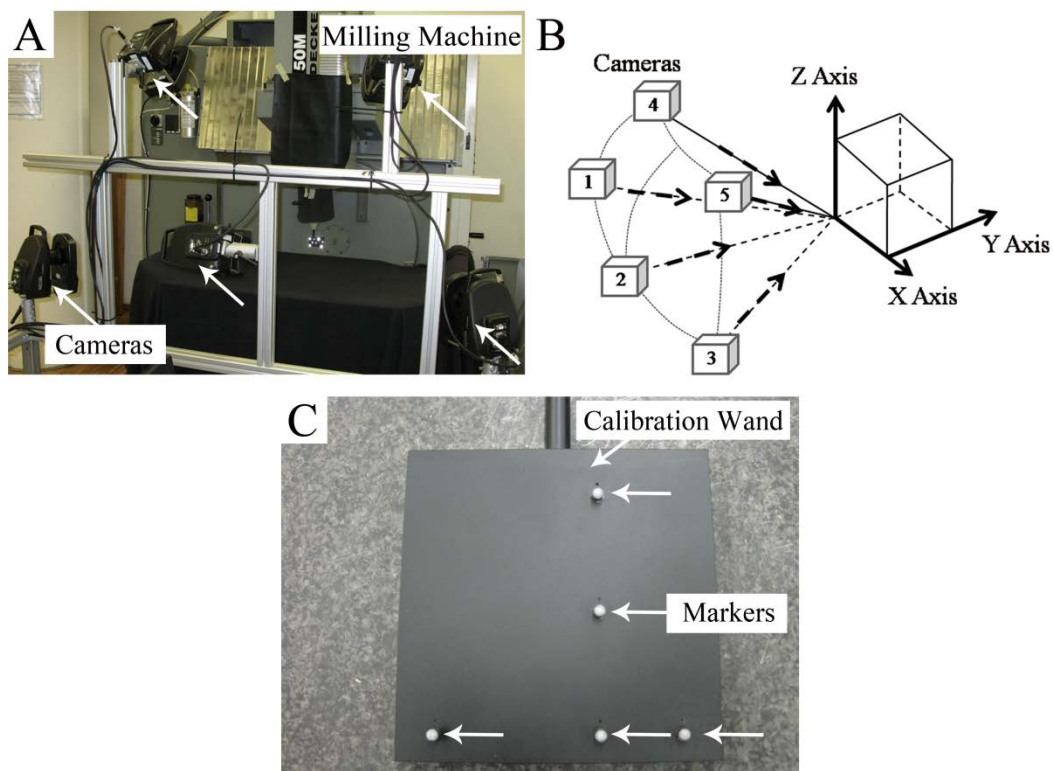


Fig. 1. The configuration of optical system and calibration procedure. A: Configuration of the cameras and the milling machine. B: The sketch of camera distribution and the volume. Box 1-5 refers to different cameras; Dashed arrow: optical axes of cameras; X, Y and Z axes are the three orthogonal directions along which the markers were moved. C: Custom mad calibration wand that was used in this study.

Parameters in the optical system configuration

Cameras setup: Five Vicon F40 cameras with 16 mm focal length lenses were used in this study. Custom-made aluminum frames were used to position the

cameras. The cameras were placed as close as possible to the milling machine in order to maximize the resolution of the system. The distance between the cameras and the center of the volume ranged between 100 and 120 cm.

The cameras were set up in near umbrella configuration according to the recommendations by the manufacturer [17]. The optical axis and location of each camera were adjusted to involve the volume of $400 \times 300 \times 300$ mm³ into the overlap field of view. The sampling frequency of the system was set at 100 Hz.

System calibration: A custom-made calibration wand (Fig. 1C) with Ø4 mm sphere markers was used to calibrate the system before the measurements. In the selected volume, manual and automatic calibrations were carried out respectively to assess the effects of the calibration procedure on the performance of this optical system. The manual calibration was performed by hand according to the manufacturers' recommendations. During the automatic full volume calibration, the calibration wand was moved (speed: 5 m/min) along the programmed motion path through the entire volume.

Camera distance and axis: The sphere markers were driven to a total of 80 positions which uniformly distributed in the selected volume (Fig. 2).

At each position, the markers were driven for a distance of 20 µm along the positive direction of three orthogonal axes respectively and back (Fig. 2, X, Y and Z axis). For the distance of 20 µm, the starting position, movement path and the final position of the markers have been recorded. Measurements were repeated three times for each condition. The increase of camera distance relative to camera position (Fig. 2, D1: the closest distance, D2, D3 and D4: the furthest distance) mostly aligned with y axis. Twenty positions were located at each distance.

Marker size: In order to assess the effects of marker size on the performance of the proposed optical method, sphere markers in four different sizes (diameter: Ø3 mm, Ø4 mm, Ø8 mm and Ø10.5 mm) were used in this study. The sphere markers were manufactured as copper balls coated with standard Vicon retro-reflective tape (Vicon Motion System Ltd., LA, USA). Smallest markers which are possibly manufactured with smooth surface (Ø3 mm and Ø4 mm markers) were selected to

evaluate the effects of small markers on the performance of the system. Reasonable large markers ($\varnothing 8$ mm and $\varnothing 10.8$ mm) which are suitable for the future *in vivo* tibia deformation measurements and low opportunities of markers overlap were selected as well.

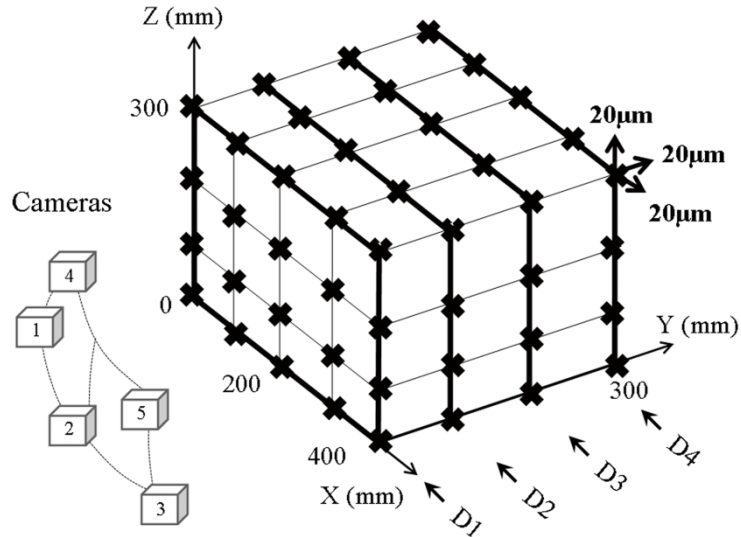


Fig. 2. Demonstration of the 80 positions within the sampling volume ($400 \times 300 \times 300$ mm 3). ‘x’ denotes the different positions. D₁, D₂, D₃ and D₄ are the different camera distance at 0, 100 mm, 200 mm and 300 mm of y axis, respectively. Bold lines: the vertical planes at different camera distances.

Random noise: Random noise of the system induced by ambient factors has to be considered during very accurate measurements. A previous study has indicated that the resolution and system repeatability were affected by the random noise level [15]. So, the coordinates’ data of markers under static condition was recorded to evaluate the random noise level in the proposed system.

Data Processing

Raw trajectory data of the markers were further processed with Matlab (The MathWorks, Inc. Version 7.9.0 R2009b).

Coordinate transformation: The Cartesian dimensions of the milling machine could deviate from the Cartesian dimensions of the optical system. Coordinate transformation was performed to compensate such mis-alignment.

System accuracy: In order to minimize the effect of noise, position data was averaged over 1s (100 frames). The system accuracy describes the closeness of the

recorded value to the reference value from the milling machine ($20 \mu\text{m}$). In order to assess the effects of different parameters (calibration procedure, cameras distance, marker size and axis) on the performance of the optical system, the absolute error between recorded movement and the reference movement of each measurement was calculated. The measurement accuracy was then expressed as the percent error, which is given by

$$\text{Percentage error} = \frac{\text{absolute error}}{\text{reference value}} \times 100$$

System precision: The precision describes the repeatability of the recorded value with the same setup of system. With the repetitions of the measurements at each camera distance (Fig. 2: D1, D2, D3 and D4), the standard deviation (S.D.) of the recorded value was calculated as the system precision.

Random noise: Noise level along different axis was expressed as the root mean square (RMS) amplitude about the mean under static capturing at 100 Hz.

Statistics

Statistical analyses were performed using R statistic software (version 2.12.2, R Development Core Team, 2011) and Graphpad Prism statistical software (version 5.00, GraphPad software, Inc., La Jolla, CA). Three-way ANOVA was employed to examine the main and interaction effects of four parameters mentioned above (calibration procedure: manual and automatic calibration; marker size: Ø3 mm, Ø4 mm, Ø8 mm and Ø10.5 mm; camera distance: D1, D2, D3 and D4; axis: X, Y and Z) on the accuracy. Data regarding to the accuracy of the system are presented as mean ($\pm\text{S.D.}$) of the absolute error.

As the reflection of the system precision (the S.D. of the repeated measurements), the homogeneity of the variances of the recorded movement (reference movement is $20 \mu\text{m}$) were the assessed by Fligner-Killeen's test. Main and interaction effects of system factors on the precision were reported. Data regarding to the precision are presented as the $\pm\text{S.D.}$ value. Statistical significance was accepted at $p \leq 0.05$.

Results

System accuracy

Calibration Procedure: For the displacement of 20 μm , the effects of calibration procedures were assessed at all 80 positions. Statistical analysis showed no significant ($p = 0.37$) main effect of calibration procedure on system accuracy (Fig. 3). However, significant main effects of camera distance ($p < 0.001$) and axis ($p < 0.001$) were found for the system accuracy. Moreover, an interaction effect ($p < 0.001$) between camera distance and axis was indicated. A greater error in the Y axis was encountered for camera distance D3 and D4 than for D1 ($p < 0.001$).

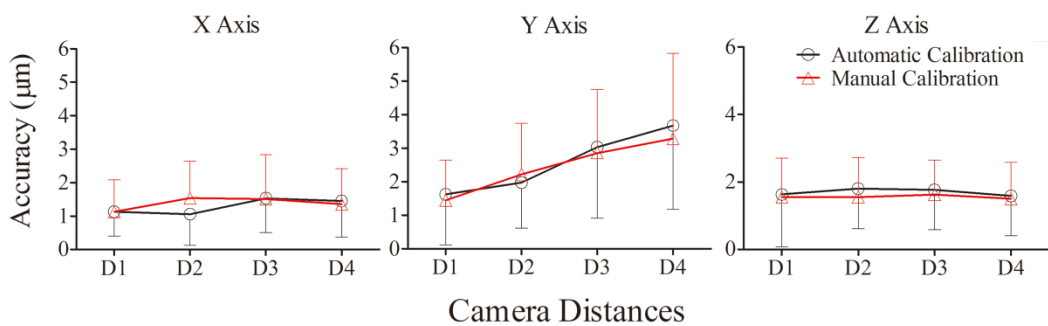


Fig. 3. The system accuracy in X, Y and Z axis with the automatic and manual calibration procedures, respectively. No significant difference on absolute error was found with two calibration procedures ($p = 0.37$). With both of the calibration procedures, the absolute error in Y axis increased with the increase of camera distance, especially in camera distance D3 and D4 ($p < 0.001$).

Camera distance, marker size and axis: Statistical analysis of the data showed significant ($p < 0.001$) main effects of camera distance and axis on system accuracy, respectively. System accuracy reduced (the absolute error increased) significantly along the Y axis ($p = 0.04$). Furthermore, two-way interactions were found between camera distance and axis ($p < 0.001$), marker size and axis ($p = 0.03$), respectively. At camera distance D3, larger absolute errors in the Y axis was associated with the usage of larger markers ($\varnothing 10.5 \text{ mm}$) as compared to smaller markers ($\varnothing 3 \text{ mm}$, $\varnothing 4 \text{ mm}$ and $\varnothing 8 \text{ mm}$) ($p = 0.02$, Fig. 4). For all the markers, larger absolute errors in the Y axis than the other axes were found at camera distance D2, D3 and D4 ($p < 0.001$ vs. $p = 0.17$ at D1).

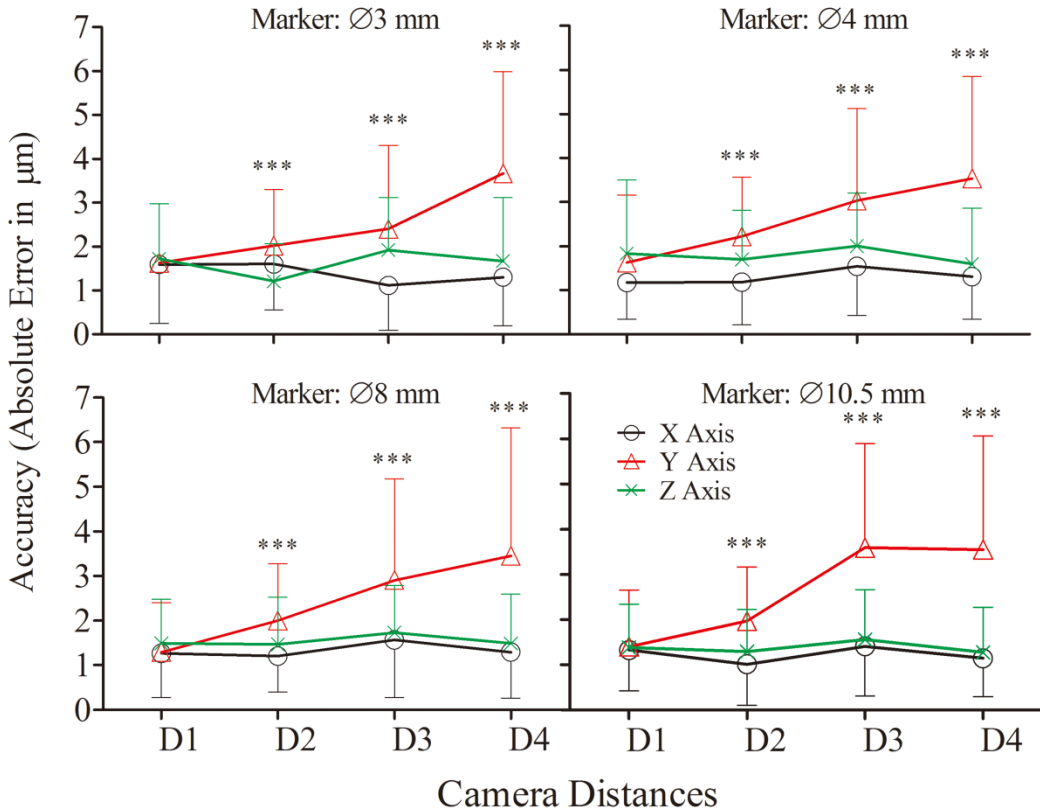


Fig. 4. The effect of different parameters on the accuracy of the optical system. For all the markers, larger absolute error was induced with the increase of the camera distance in Y axis at camera distance D2, D3 and D4 (***: $p < 0.001$). At the cameras distance D3, larger marker ($\varnothing 10.5$ mm) brought more absolute error than the other markers ($p = 0.02$).

By contrast, no significant main effect of marker size was found ($p = 0.22$). The statistical results indicated no other significant interaction effects, including three-way interactions among camera distance, marker size and axis ($p = 0.16$).

When averaged over all axes, the accuracy ranged from 1.2-1.8 μm (from 6% to 9%) at D1, 1.0-2.2 μm (from 5% to 11%) at D2, 1.1-3.6 μm (from 5.5% to 18%) at D3 and 1.2-3.7 μm (from 6% to 18.5%) at D4, respectively.

System Precision

Calibration Procedure: Both calibration procedures yielded comparable results with regards to system precision ($p = 0.65$, Fig. 5). There were, however, main effects of camera distance at D2, D3 and D4 and axis in Y axis, demonstrating larger (worse) precision as compared the other distances ($p < 0.001$) and axes ($p < 0.001$).

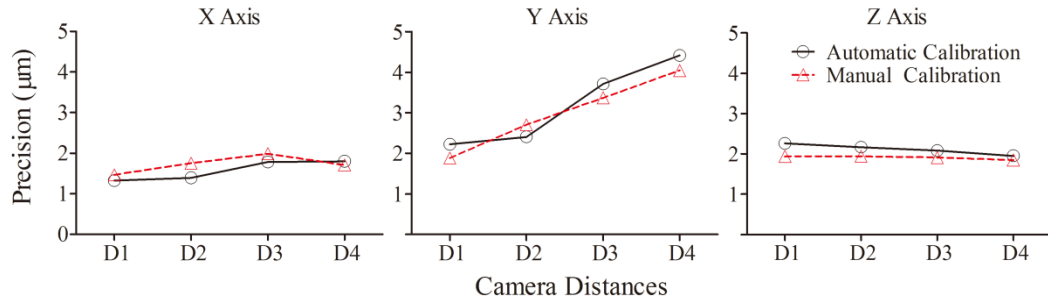


Fig. 5. The precision at all 80 positions along X, Y and Z axis with both calibration procedures. Similar to the results of absolute error, no significant difference in precision was found between the two calibration procedures ($p = 0.65$). With both the calibration procedures, the precision in Y axis increased with increasing camera distance ($p < 0.001$).

Camera distance, marker size and axis: Main effects of the three parameters (camera distance, marker size and axis) on system precision indicated the major differences in axes ($p < 0.001$) and camera distance ($p < 0.001$), but only minor differences in marker size ($p = 0.18$, Fig. 6).

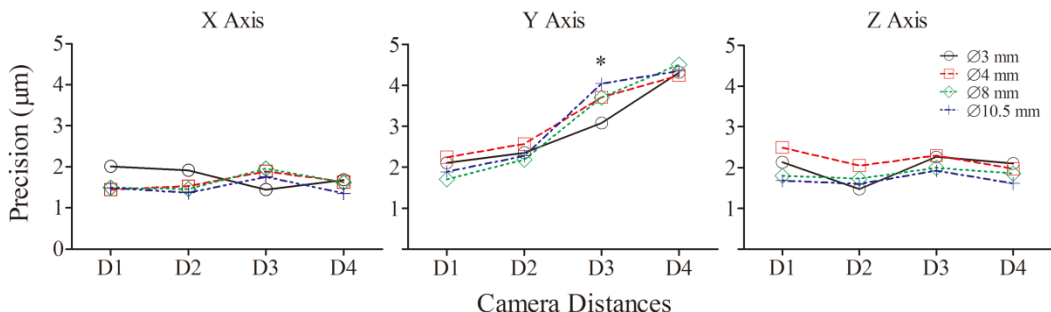


Fig. 6. The effects of different camera distances, marker size and axis on the precision of the optical system. The precision value increased with the increase of the camera distance in Y axis. In the other axes, no effects of camera distance and marker size on the system precision were found. *: comparison of precision between 3 mm marker and 10.5 mm marker in Y axis at distance D3. *: $p < 0.05$.

All the different camera distances, except D1, were associated with larger precision error along the Y axis ($p < 0.001$, $p = 0.96$ at D1). At camera distance D3, the marker with Ø10.5 mm induced larger precision values than Ø3 mm marker in the Y axis ($p = 0.02$, Fig. 6). No other interactions were found among camera distance, marker size and axis. For all the axes, precision ranged between 1.5-2.5 μm at camera distance D1, 1.4-2.6 μm at D2, 1.4-4.0 μm at D3 and 1.4-4.5 μm at D4, respectively.

Random Noise

The system random noise (RMS amplitude) was 1.9 μm , 4.0 μm and 3.0 μm in X, Y and Z axis, respectively.

Discussion and Conclusions

This study assessed the performance of an optical system for measuring small amplitude movements in a relative large volume. The effects of calibration procedure, retro-reflective marker size, camera distance and axis upon system accuracy and precision have been evaluated by comparing with the reference movement. From the results of this study, it seems prudent to suggest that 20 μm movements could be measured with acceptable accuracy and precision within a volume of $400 \times 300 \times 300 \text{ mm}^3$, which means the system resolution was at least 20 μm in this volume.

Large volume

Previous studies have tracked motion with high resolution, accuracy and precision, but only in a relatively small volume [14, 15, 18, 19]. The system information and results from previous studies are summarized in table 1. Thus, compared to most previous studies, a better resolution (at least 20 μm), accuracy and precision have been achieved by the presented approach, despite that fact that a larger volume has been used. It is evident that this improvement in system performance is mostly attributable to the higher resolution of the cameras (4 Megapixel), even though some parameters in the system configuration will probably also have a contribution. More importantly, for most of cases, the volume evaluated in this study covers the motion of the tibia during a stance phase of gait. Based on the results, the trajectory of the markers is able to be recorded in this volume with high accuracy and precision. Accordingly, the tibia deformation is able to be calculated with the same accuracy and precision if the markers are affixed to tibia.

Table 1. Summary of the optical system information and results from previous and this study.

Studies	Parameters of System Optical System	Volume, Field of View or Camera Distance	Markers	Results Resolution	Accuracy	Precision
[15]	Qualisys ProReflex-MCU120 ^a	Field of view: $68.18 \times 51.14 \text{ mm}^2$	$\varnothing 2.5 \text{ mm}$, Sphere, Retro-reflective	$10 \mu\text{m}$	1.39% to 2.37%	1.9 to $3.9 \mu\text{m}$
[18]	Optotrak 3020 ^b	Camera distance: 1.75 m to 4 m	Active marker ^c	-	$\geq 3\%$	0.29 mm
[14]	Vicon-460 ^d	Volume: $180 \times 180 \times 150 \text{ mm}^3$	$\varnothing 25 \text{ mm}$, Sphere, Retro-reflective	-	$63 \pm 5 \mu\text{m}$	15 to $21 \mu\text{m}$
[19]	Optorak ^b	Camera distance: 1.5 m to 4.5 m	Active marker	<10 μm	In-plane: <0.53% out-of-plane: <1.56%	0.6 to $29.2 \mu\text{m}$
In this study	Vicon MX ^d	Volume: $400 \times 300 \times 300 \text{ mm}^3$ Camera distance to the centre of the volume: 100-120 cm	$\varnothing 3, 4, 8, 10.5 \text{ mm}$, Sphere, Retro-reflective	$\leq 20 \mu\text{m}$	6% to 9%	1.5 to $2.5 \mu\text{m}$

^a Qualisys motion capture system (Qualisys, Inc., Gothenberg, Sweden).^b Optotrak motion capture system (Northern Digital Inc., Waterloo, Ontario).^c infrared light-emitting diodes.^d Vicon motion capture system (Vicon Motion System Ltd., LA, USA).

Calibration procedure, camera distance and marker size

Unlike the observations in the study of Windolf *et al.* [14], differences in calibration procedure did not affect the system performance in our study. Our results therefore imply that systematic error of this optical system, which mostly induced by the calibration procedure, was very low and did not go to such an extent as to affect the system accuracy. In keeping with Maletsky's study [18], increasing the camera distance increased the measured error and decreased the precision of the system along the main Y axis. In some contrast with the findings from Windolf *et al.* [14], greater marker size did not improve accuracy and precision over smaller markers, in this study, especially in Y axis. This finding might also be explained by the above reason. Although more pixels are available with larger markers, that does imply an improvement for marker location precision, as more artifacts during the calculation of the marker center might be introduced while the marker move further from cameras or the surface of the markers is not perfectly smooth. The other factors, such as different camera setup, cameras numbers, marker quality (roundness and reflective quality) and surrounding environment condition, might also affect the performance of the optical system, as has been partly demonstrated in the past [14, 17].

Why is the error enhanced in the Y axis?

At 80 positions of the measured volume, accuracy and precision have been evaluated in three orthogonal directions (X, Y and Z axis). The results suggested that the accuracy and precision was greater in the X and Z axis than that in the Y axis at two greatest camera distances (D3 and D4). A similar tendency was found when different sizes of markers were used. Interestingly, similar observations have been made in the study of Liu *et al.* and Windolf *et al.* as well [14, 15]. The likely explanation for these two effects is that the number of pixels available from each marker diminishes when the markers are remote from the cameras. A reduction in pixel number is bound to enhance the error when calculating the central points of marker with the gray scale reconstruction and circle fitting techniques. Oppositely, movement in the X and Z axis does not affect the pixel number, and it did

accordingly not induce as large an error as in the Y axis.

Is the proposed optical system good enough to serve its purpose?

Due to the irregular shape of long bones, axial deformation, shear, bending, torsion and their combination will occur on them under different loading condition. The traditional methods for measuring strains, *e.g.* strain gauges, are not suitable for describing bone-segment deformation in three dimensions [5].

As mentioned above, the purpose of this study was to establish an optical method and explore its potential for *in vivo* bone-segment deformation measurements. For humans, the feasible anatomical sites for such measurements are limited. To date, most *in vivo* bone strain studies in humans have focused on the tibia. Results from these studies have shown that peak principal tibia strain is approximately 1200 $\mu\epsilon$ under the conditions of daily normal activity [5, 6, 20], and that peak principal strains $>3000 \mu\epsilon$ can be observed during more vigorous activities [21]. However, in these studies, bone strains were measured by either attaching strain gauges onto the bone surface, or by inserting strain gauged bone staples into bone. With these technical setups, strains were available over a very limited surface area, typically few square millimeters. To our knowledge, no methods are available to record the tibia-segment deformation *in vivo* as so far, owing to the invasiveness and technical issues during the measurements [5].

Based on rough calculation mentioned in the ‘Introduction’ section and the results from this study, at least 20 μm resolution (100 $\mu\epsilon$ for original length of 20 cm), high accuracy and precision in the defined volume demonstrates that the optical system has the ability to record *in vivo* tibia deformation in humans. Moreover, as indicated in a recent review article about *in vivo* bone strain measurements [5], no information is available in humans regarding the possible bending and torsion deformation *in vivo*.

During the past decades, intracortical pins or screws with marker clusters were used in numerous studies to measure three-dimensional kinematics of the tibiofemoral [22] and the patellofemoral joint [23] as well as the foot bones [24]. The relative bone motion in 6 degrees of freedom (three rotations and three

translations) can be clearly described, most commonly, in the anatomical coordinate systems [25]. For example, based on Cardan/Eular angle, the flexion/extension, ab/adduction, internal/external knee rotation and the translation can be calculated in the knee joint.

During kinematics studies, the bone segments usually were considered to be rigid, thus totally neglecting any bone deformation. However, the methodology to describe the flexion/extension, ab/adduction, internal/external rotation and the translation still can be adopted to refer to the bending, torsion and axial deformation of bone. So, the following setup (Fig. 7) is recommended to be used in tibia-segment deformation recording *in vivo*. Few bone pins or screws with retro-reflective marker clusters (Three marker clusters with non-collinear markers on each cluster in Fig. 7) could be inserted into anterior-medial aspect of proximal, mid-shaft and distal tibia. An optical motion capture system could then be set up according the configuration recommended in this study. The coordinates of the markers will be available during one step of different locomotive activities, such as gait. Whatever the type of bone deformation is, axial, shear or torsion, all of them are able to be expressed by the relative movement between marker clusters and calculated as long as the accurate and repeatable marker trajectories are available.

Recommendation for the application of proposed method in bone-segment deformation in vivo measurements

According to the results from this study and the proposed setup of markers in human tibia in Fig. 7, close camera positioning (camera distance: D1, <90 cm) and reducing marker size (diameter: Ø3-Ø8 mm) seems to be the best choice to improve the performance of this optical system and realize *in vivo* tibia-segment deformation recording with high accuracy and precision. Furthermore, the movement of the markers in the direction of cameras distance should be avoided as possible as the subjects can, which means the subjects should not move towards the cameras, but pass by the cameras to try to keep almost constant and close cameras distance.

Concerning the detailed technically issues of applying proposed method in tibia-segment deformation *in vivo* measurements, the pain induced by the screw insertion should be minimized using thin bone screws. The invasiveness inflicted upon the subjects will be reduced with bone pins, as the periosteum will almost not be severed. In addition, skin incision with appropriate length at the site of bone screws insertion should be made to avoid the contact between soft tissues with bone screws during gait.

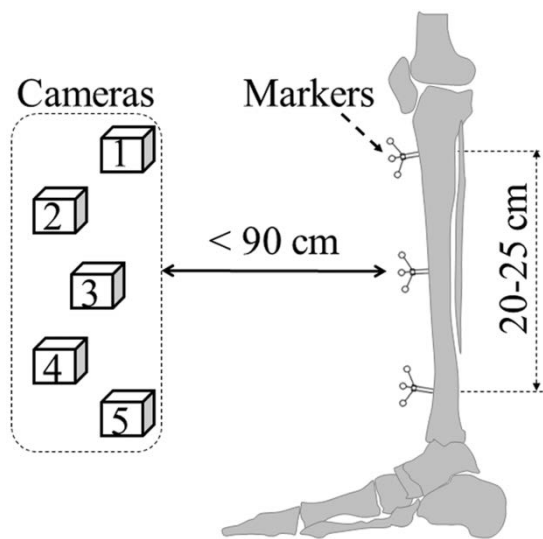


Fig. 7. The recommended configuration for *in vivo* tibia deformation recording in humans. Firstly, the marker clusters (at least 3 markers in one cluster) with small markers ($\varnothing 3\text{-}\varnothing 8$ mm) and close camera distance (< 90 cm) should be used. In addition, the movement of the tibia along the optical axis of camera lens (Y axis in this study) should be minimized as less as possible.

Comparison between the proposed method with existed methods

As the gold standard for measuring mechanical strain in the engineering applications, strain gauge methods have been often used in the *in vivo* bone strain measurements in the past. However, the credibility of recorded strain data with bonding strain gauges is under debate due to the uncontrollable of the bonding quality between the strain gauges and the bone surface. This means that the so call ‘gold standard’ method might not suit bone strain measurements perfectly because of the difficulties of bone surface preparation to fulfill the requirement of bonding strain gauges. Comparatively, the proposed method overcomes several drawbacks of the traditional strain gauges method. First, it will provide the tibia-segment

deformation information which never has been observed *in vivo* before. Integrating with anatomical coordinate system or more advanced method, such as finite element model, 3D *in vivo* tibia strain information will then be able to be estimated; second, it will make it possible to explore to which extent bending and torsion are occurring in the human tibia. For this reason, the optical method proposed in this study is assessed and compared with an accurate reference movement produced by milling machine rather than strain gauge methods. On top of above novel possibilities by our proposed method, the strain detection limit of the method is acceptable for the *in vivo* bone-segment deformation recording. Taking 20 μm , resolution for example, the detection limit will be 100 $\mu\epsilon$ for 20 cm bone. However, compared to maximum 1500-2000 $\mu\epsilon$ during normal locomotive activities, 100 $\mu\epsilon$ of detection limit will be acceptable. Based on different principals with proposed method, several other optical methods, such as digital image corrections (DIC) [9-11] and machine vision photogrammetry (DISMAP) [26] have been explored to measure bone strains as well. Unquestionably, these methods have the ability of obtaining high resolution strain distribution on certain area of bone surface. However, so far, it is apparently difficult for these optical methods to measure the *in vivo* bone strains due to its requirement of bone surface preparation and exposure to the cameras. This probably will be the main limitation for the application of above two optical methods in the future bone strains *in vivo* measurements.

Conclusion

To conclude, the performance of the proposed method based on a motion capture system is capable of recording the displacement of 20 μm with high accuracy and precision in a relatively large volume of $400 \times 300 \times 300 \text{ mm}^3$. Therefore, the results suggest that the proposed method has great application potential in the future for *in vivo* tibia segment deformation measurements recording.

Acknowledgments

The authors have no conflict of interest. We would like to thank Hans-Martin Küsel-Feldker and Thomas Förster in the Institute of Biomechanics and Orthopaedics, German Sport University Cologne for operating the milling machine and numerous discussions about the ideas in this study. Thanks also to Michel Ducos for the discussion regarding to statistics. Peng-Fei Yang acknowledges his scholarship by the China Scholarship Council (CSC No.: 2009629013).

Funding

This research received no specific grant from any funding agency in the public, commercial, or not-for-profit sectors.

Declaration of Conflicting Interests

The Authors declare that there is no conflict of interest.

References

1. Duncan RL, Turner CH (1995) Mechanotransduction and the functional response of bone to mechanical strain. *Calcif Tissue Int* 57: 344-358.
2. Forwood MR, Turner CH (1995) Skeletal adaptations to mechanical usage: results from tibial loading studies in rats. *Bone* 17: 197S-205S.
3. Turner CH, Owan I, Takano Y (1995) Mechanotransduction in bone: role of strain rate. *Am J Physiol* 269: E438-442.
4. Mosley JR, Lanyon LE (1998) Strain rate as a controlling influence on adaptive modeling in response to dynamic loading of the ulna in growing male rats. *Bone* 23: 313-318.
5. Yang PF, Bruggemann GP, Rittweger J (2011) What do we currently know from in vivo bone strain measurements in humans? *J Musculoskelet Neuronal Interact* 11: 8-20.
6. Burr DB, Milgrom C, Fyhrie D, Forwood M, Nyska M, et al. (1996) In vivo measurement of human tibial strains during vigorous activity. *Bone* 18: 405-410.
7. Ekenman I, Halvorsen K, Westblad P, Fellander-Tsai L, Rolf C (1998) The reliability and validity of an instrumented staple system for in vivo

- measurement of local bone deformation. An in vitro study. *Scand J Med Sci Sports* 8: 172-176.
8. Milgrom C, Finestone A, Hamel A, Mandes V, Burr D, et al. (2004) A comparison of bone strain measurements at anatomically relevant sites using surface gauges versus strain gauged bone staples. *J Biomech* 37: 947-952.
 9. Yang L, Zhang P, Liu S, Samala PR, Su M, et al. (2007) Measurement of Strain Distributions in Mouse Femora with 3D-Digital Speckle Pattern Interferometry. *Opt Lasers Eng* 45: 843-851.
 10. Sztefek P, Vanleene M, Olsson R, Collinson R, Pitsillides AA, et al. (2010) Using digital image correlation to determine bone surface strains during loading and after adaptation of the mouse tibia. *J Biomech* 43: 599-605.
 11. Zauel R, Yeni YN, Bay BK, Dong XN, Fyhrie DP (2006) Comparison of the linear finite element prediction of deformation and strain of human cancellous bone to 3D digital volume correlation measurements. *J Biomech Eng* 128: 1-6.
 12. Matsuyama J, Ohnishi I, Sakai R, Suzuki H, Harada A, et al. (2006) A new method for measurement of bone deformation by echo tracking. *Med Eng & Phys* 28: 588-595.
 13. Abdel-Aziz YI, Karara HM (1971) Direct Linear Transformation from comparator coordinates into object space coordinates in close range photogrammetry. In: Proceedings of the symposium on close-range photogrammetry Falls Church, VA: American Society of Photogrammetry.
 14. Windolf M, Gotzen N, Morlock M (2008) Systematic accuracy and precision analysis of video motion capturing systems--exemplified on the Vicon-460 system. *J Biomech* 41: 2776-2780.
 15. Liu H, Holt C, Evans S (2007) Accuracy and repeatability of an optical motion analysis system for measuring small deformations of biological tissues. *J Biomech* 40: 210-214.
 16. Milgrom C, Finestone A, Levi Y, Simkin A, Ekenman I, et al. (2000) Do high impact exercises produce higher tibial strains than running? *Br J Sports Med* 34: 195-199.
 17. Nigg BM, Herzog W, editors (2007) Biomechanics of the Musculo-skeletal System. 3rd ed. West Sussex: Wiley and Sons Ltd. 362-391 p.
 18. Maletsky LP, Sun J, Morton NA (2007) Accuracy of an optical active-marker system to track the relative motion of rigid bodies. *J Biomech* 40: 682-685.
 19. Schmidt J, Berg DR, Ploeg H-L (2009) Precision, repeatability and accuracy of Optotrak optical motion tracking systems. *Int J Exp Comp Biomech* 1: 114-127.
 20. Milgrom C, Miligram M, Simkin A, Burr D, Ekenman I, et al. (2001) A home exercise program for tibial bone strengthening based on in vivo strain measurements. *Am J Phys Med Rehabil* 80: 433-438.
 21. Milgrom C, Simkin A, Eldad A, Nyska M, Finestone A (2000) Using bone's adaptation ability to lower the incidence of stress fractures. *Am J Sports*

- Med 28: 245-251.
- 22. Ramsey DK, Wretenberg PF, Benoit DL, Lamontagne M, Németh G (2003) Methodological concerns using intra-cortical pins to measure tibiofemoral kinematics. *Knee Surg Sports Traumatol Arthrosc* 11: 344-349.
 - 23. Ramsey DK, Wretenberg PF (1999) Biomechanics of the knee: methodological considerations in the in vivo kinematic analysis of the tibiofemoral and patellofemoral joint. *Clin Biomech (Bristol, Avon)* 14: 595-611.
 - 24. Nester C, Jones RK, Liu A, Howard D, Lundberg A, et al. (2007) Foot kinematics during walking measured using bone and surface mounted markers. *J Biomech* 40: 3412-3423.
 - 25. Grood ES, Suntay WJ (1983) A joint coordinate system for the clinical description of three-dimensional motions: application to the knee. *J Biomech Eng* 105: 136-144.
 - 26. Kim DG, Brunski IB, Nicolella DP (2005) Microstrain fields for cortical bone in uniaxial tension: optical analysis method. *Proc Inst Mech Eng H* 219: 119-128.

CHAPTER 4

**Tibia deformation induced by simulated muscle forces: *ex vivo*
validation of the OST approach in human tibia**

Tibia segment deformation under simulated muscle force: a human cadaveric study with a novel optical segment tracking (OST) approach

Peng-Fei Yang, Karsten Engel, Maximilian Sanno, Jens Dargel, Kilian Wegmann, Gert-Peter Brüggemann, Jörn Rittweger

In Preparation

Abstract

Bone deformation is accepted as a crucial factor in bone mechanical adaptation. However, our current understanding of *in vivo* bone deformation is limited due to the intrinsic shortcomings of the widely adopted strain gauge methods in the past. To overcome the drawbacks of the strain gauge approaches, a novel optical segment tracking (OST) approach on the basis of a motion capture system was proposed in our previous study. However, the OST approach has not been validated in a well-defined scenario in humans before. Furthermore, the contribution of muscular contractions to the bone loading remained largely unexplored. Therefore, in the presented study, custom-made Lower Extremity Loading Device (LELD) was developed to simulate physiological muscle contractions in six human cadaveric lower extremities. Tibia segment deformation was measured by tracking the relative movement between two marker clusters (three non-collinear retro-reflective markers on each cluster) which were affixed into the proximal and distal tibia, respectively. Comparing to the physiological situation, the simulated muscle forces for all cadaveric specimens remained at a low level, from 68 N to 505 N. When quadriceps muscle was loaded with forces from 198 N to 505 N, the proximal tibia bent to posterior aspect by 0.12°-0.25° for all specimens and bent to lateral aspect by 0.06°-0.21° for five of all specimens

with respect to the distal tibia, respectively. The relatively large tibia bending angles were found when simulating the co-contraction of upper leg muscles and plantar flexors, and of all leg muscles, respectively. The variance between the repetitions remained very low, ranging between 0° and 0.04° for the bending and torsion angles. We therefore conclude that the OST approach has the potential to be applied *in vivo* and pick up muscle-induced bone deformations.

Keywords: Tibia segment deformation; Simulated muscle contractions; Optical approach; *Ex vivo*

Introduction

Numerous animal studies suggested that bone strain, or deformation, plays a crucial role in the mechano-adaption of bones [1, 2]. However, as outlined in the previous chapters, our current understanding of such bone strains in humans is still limited due to technical difficulties. The bipedal locomotion of humans enforces the bones in lower extremity to bear the body weight during the locomotor activities, whilst the muscles provide the main driven forces to move the body forward. Close relationships between local muscle and bone have been observed in many morphological [3] and functional studies [4, 5]. However, which one, the muscle forces or gravitation-derived force, predominates the mechanical loading of the bones in the lower extremities is still under debate [6, 7]. Currently, it has not been fully understood how muscle forces act on bone and contribute to bone loading or bone deformation.

As the most direct approach towards the mechanical loading of the tibia, the traditional strain gauge methods has been mostly relied on to assess the *in vivo* bone deformation in humans [8, 9]. The intrinsic shortcomings of strain gauge methods, *e.g.* bonding-bending problems and less informative issues, have been discussed in Chapter 2 [10]. In order to overcome the drawbacks of the strain gauge methods, an optical segment tracking (OST) system has been proposed for bone deformation measurements in Chapter 3 [11]. The concept of the OST approach is straightforward, namely bone deformation could be derived from the relative movement of the markers affixed to certain parts of a given bone. Of note, a particular optimized configuration of the optical system has to be adopted to achieve sufficient recording resolution, accuracy and precision of the marker's movement in 3D volume. A possible application of the OST approach in human tibia deformation recording has been proposed in Chapter 3. Specifically, if few retro-reflective marker clusters with three non-collinear markers on each cluster are anchored into the anterior-medial aspect of tibia by bone screws, tibia deformation, *e.g.* bending and torsion angles, can be derived.

However, the practical feasibility of the OST approach has not been assessed before. The purpose of the study presented in this chapter was to further validate the OST approach for tibia deformation measurements in a cadaver model. More specifically, the cadaveric tibia was loaded by simulated muscle forces with a custom-made Lower Extremity Loading Device (LELD). The influence of the simulated muscle forces on tibia deformations of the cadaveric tibia were thus investigated with the OST approach.

Materials and methods

Cadaveric Specimens

Six fresh frozen human cadaveric lower extremities, including the intact lower leg and truncated thigh, were used in this study. They were from three donors, namely a 67 year-old man, a 92 year-old woman and a 94 year-old woman. The specimens were obtained by transection at the thigh approximately 20 cm above the knee joint. The knee joint, tibia, ankle joint and the foot were kept intact. The specimens were defrosted for 24 hours prior to the measurements.

The specimens were prepared by carefully removing the soft tissue above the malleolus and isolating the following muscles or muscle groups, including quadriceps (Qua), biceps femoris (BF), semimembranosus/tendinosus (Semi), gastrocnemius medialis(GM), gastrocnemius lateralis (GL), soleus (So), tibialis anterior (TA), tibialis posterior (TP). The quadriceps muscle were dissected from the distal tendon and detached from the patella. A rope linked to one of the pneumatic actuators from LELD was connected with patella by custom-made connector to allow the application of simulated muscle force. The details concerning to the LELD was explained in the following section. The proximal tendon of BF and Semi (semimembranosus and semitendinosus in combination), the distal tendon of Soleus, TA, TP were cut and enmeshed, respectively, with the steel wire network of the finger sleeves (Dr. Paul Koch GmbH, Frickenhausen, Germany) which normally are used in the hand traction system during the wrist and hand surgery to position the hand. These finger sleeves were connected to the

pneumatic actuators in the LELD to allow the application of the simulated muscle forces. Since the insertions of the gastrocnemius medialis and lateralis on femur are much localized and it was difficult to fully separate these two muscles, the gastrocnemius medialis and lateralis were dissected from the proximal tendon. Instead of their tendon insertion into femur, two bone screws ($\varnothing 4.5$ mm, 30 mm length, Marquardt Medizintechnik GmbH, Germany) were inserted into the proximal insertions in femur and connected to the pneumatic actuators from LELD with rope to allow the application of the simulated muscle forces.

Lower Extremity Loading Device (LELD)

The Lower Extremity Loading Device (LELD, Fig. 1A) was developed to fix the cadaveric specimens and apply the simulated muscle force to the cadaveric tibia by activating the pneumatic actuators. More specifically, the LELD consisted of two vertical steel beams which were fixed on the base plate to support the upper aluminum plate, lower aluminum plate anchored with pneumatic actuators (Fig. 1A). The height of the upper plate was adjustable and able to slide along the vertical beams upward or downward to suit different specimens. One of the pneumatic actuators (ADN-50-60-I-P-A, theoretical force 1178 N at 6 bar, maximum pressure 10 bar, Festo, Esslingen, Germany) fixed on the upper plate was to connect the patella and could simulate quadriceps muscle contractions. Five other pneumatic actuators (ADN-40-60-I-P-A, theoretical force 754 N at 6 bar, maximum pressure 10 bar, Festo, Esslingen, Germany) were used to simulate the contractions of biceps femoris, semimembranosus/tendinosus, gastrocnemius medialis, gastrocnemius lateralis and soleus, respectively. On the bottom aluminum plate of the LELD, two more pneumatic actuators (ADN-40-60-I-P-A, theoretical force 754 N at 6 bar, maximum pressure 10 bar, Festo, Esslingen, Germany) were used to simulate tibialis anterior and tibialis posterior contraction, respectively. The ropes between the finger sleeves and the actuators allowed the stretch force transmission to individual muscles to simulate physiological muscle forces.

In general, the gastrocnemius muscles and soleus muscle together contribute force to Achilles tendon, through calcaneus and the ankle joint, and finally to distal tibia. On the other side, an opposing force with same amplitude was applied onto the distal femur and proximal tibia through the origins of these two muscles.

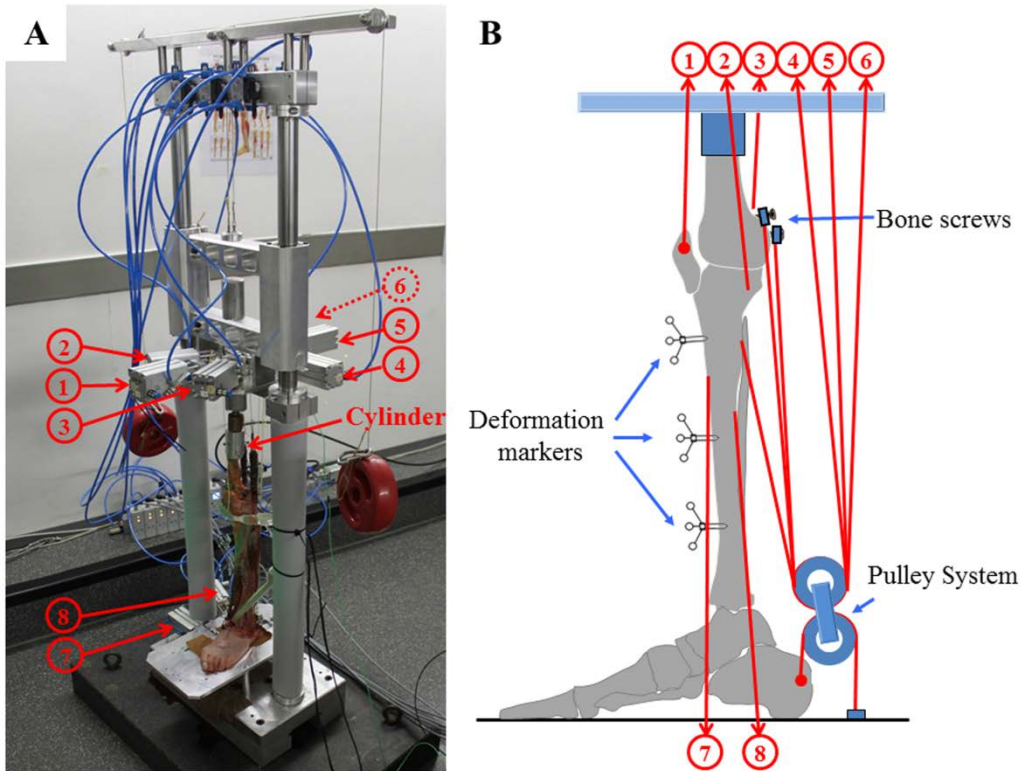


Fig. 1. Illustrations of the LEED and loading configuration to the tibia. 1-8 refers to the different pneumatic actuators linked to different muscles. 1: quadriceps, 2: semimembranosus/tendinosus (Semi), 3: biceps femoris (BF), 4: gastrocnemius medialis (GM), 5: soleus (So), 6: gastrocnemius lateralis (GL), 7: tibialis anterior (TA), 8: tibialis posterior (TP). A: a cadaveric specimen fixed on the LEED. B: the loading configuration and the pulley system. The red lines represent the muscles or connecting ropes.

Considering this fact, and in order to simulate the loading condition on the tibia as close to physiological conditions as possible, a custom-made pulley system (Fig. 1B) was invented. In the design of this pulley system, the ropes from gastrocnemius and soleus muscles were looped over the pulley which was affixed to the calcaneus, redirected and connected to the upper pneumatic actuators to allow the application of forces on the gastrocnemius muscle, soleus muscle and calcaneus simultaneously (Fig. 1B). The dissected femur of the specimens were

mounted in an aluminum cylinder, which was a part of the upper aluminum plate, (Fig. 1A) with bone cement (Polymethyl Methacrylate, PMMA) and centered in the mounting cylinder by centering screws. Prior to the measurements, neutral vertical position (0° knee joint and 90° ankle joint) of the leg were defined by adjusting the femur mounting cylinder and ensured the plantar surface of the foot on the bottom aluminum plate. The long axis of the leg was oriented visually aligning to be vertical.

The muscles loading pattern

The output stretching forces of pneumatic actuators were controlled manually by adjusting knob or automatically by a custom-programmed Labview routine (National Instrument, NI, USA).

Prior to running the loading protocol, the possible maximum forces for different muscles were tested by manually controlling the individual pneumatic actuator. It was thus possible to calculate the expected applied muscle forces in the loading protocol according to the ratio of physiological muscles cross section area reported in previous publications [12, 13]. For the upper leg, Semi and BF were always loaded and released simultaneously and their forces were set at 30% and 30% of quadriceps muscle force [12, 13]. For the lower leg, the maximum forces of TP and TA were set at 25%, 10% of triceps surea force, respectively. The maximum forces of GM and GL were set at 35% and 15% of the soleus muscle force [14]. Each muscle was preloaded with 20 N prior to all loading protocols to keep the actuator-muscle connection tight.

The loading patterns were summarized in Table 1. Three groups of muscle loading patterns were included in this study. The first group of loading pattern was to simulate 7 individual muscle contractions. The second group of loading patterns was to simulate the muscle co-contractions. The third group of loading patterns was to simulate the muscle activities during the stance phase of gait cycle, including from heel contact to opposite toe-off (G1, 0-10% of the gait cycle), from opposite toe-off to neutral body position (G2, 10-20% of the gait cycle), from neutral body position to opposite heel contact (G3, 30-50% of the gait cycle) and

from opposite heel contact to toe-off (G4, 50-60% of the gait cycle), respectively. Under each loading condition, tibia deformation were recorded when the muscles were loaded from baseline, *i.e.* 20 N, increasing until reaching the plateau, *i.e.* the maximum force, for 5 seconds.

Table 1 Loading pattern of muscle or muscle groups

	Qua	Hamst	So	GM	GL	TA	TP
Individual muscle	Qua	x					
	Hamst		x				
	So			x			
	GM				x		
	GL					x	
	TA					x	
Co-contraction	TP						x
	P1			x	x		
	P2		x	x	x		
	P3		x	x	x	x	x
Simulated gait	P4	x	x	x	x		x
	G1	x	x	x	x	x	
	G2	x	x	x	x	x	x
	G3		x	x	x		x
	G4				x	x	

'x' indicated that the muscles were active. Qua: Quadriceps muscle, Hamst: hamstrings, So: soleus muscle, GM: gastrocnemius medialis muscle, GL: gastrocnemius lateralis muscle, TA: tibialis anterior muscle, TP: tibialis posterior muscle. P1, P2, P3 and P4 referred to the loading pattern in which muscle co-contractions were simulated. G1, G2, G3 and G4 referred to the muscle activities during 0-10%, 10-20%, 30-50% and 50-60% of gait cycle (stance phase), respectively.

Optical segment tracking for tibia deformation recording

The OST approach was based on motion capturing and its concept has been described in the previous Chapter [11]. Briefly, three deformation marker clusters with three non-collinear retro-reflective markers ($\varnothing 5$ mm, Géodésie Maintenance Services, Nort Sur Erdre, France) on each cluster were affixed into the antero-medial aspect of tibia cortex by bone screws (Cannulated screws, $\varnothing 3$ mm, 24/6 mm, Stryker Leibinger GmbH & Co. KG, Germany). The sites for inserting bone screws were approximately 10 cm below the tibia plateau, mid-site of the tibia diaphysis and approximately 10 cm above the tibia medial malleolus, respectively. The bone screws were inserted into tibia visually perpendicular to the bone

surface and penetrated into tibia approximately 3 mm to remain the bone screws in the cortical tibia.

Using the Vicon MX motion capture system with five Vicon F40 cameras (Vicon Motion System Ltd., LA, USA), the trajectories of retro-reflective markers were captured during different loading protocols. The umbrella distribution of the cameras, manual calibration, close camera distance (<90 cm), and small markers were used according to the recommendations from Chapter 3 [11].

Determination of the Shank Anatomical Coordinate System (SACS)

The coordinates of the anatomical landmarks of the shank within the global coordinate system were positioned by extra markers prior to the tibia deformation measurements. The SACS was thus determined from the coordinates of the distal apex of the lateral, medial malleolus, the prominence of the tibial tuberosity and the head of fibula [15]. The trajectories of all markers for tibia deformation and determination of the SACS were captured at 200 Hz.

Data Analysis

Marker trajectories of the proximal and distal marker clusters over 2 seconds after the simulated muscle forces reaching the plateau were used to compute the tibia deformation. A Matlab routine (The MathWorks, Inc. Version 7.9.0 R2009b) was custom-written to process the raw trajectory data of all the markers.

Tibia deformation was computed from the relative movement of the proximal and distal tibia-affixed markers, representing as the antero-posterior, medio-lateral bending angle and internal-external torsion angle of proximal tibia with respect to the distal tibia. Briefly, the coordinates of tibia-affixed markers in SACS were determined firstly by coordinate transformation [16, 17]. The relative movement between proximal and distal marker clusters was then computed and expressed as the relative movement in 6 degree of freedom in the SACS, *i.e.* three Cardan/Euler rotation angles and three translations along the different axis of the SACS. The most representative results, *i.e.* bending and torsion angles, were reported as of tibia deformation. Each loading protocol was repeated three times to assess the repeatability of the measurements. Results were presented as mean

and standard deviation (mean \pm S.D.). The tibia deformation angles were plotted using Graphpad Prism statistical software (version 5.00, GraphPad software, Inc., La Jolla, CA).

Results

Muscle forces

Compared with the normal physiological situation, the forces achievable with the cadaveric muscles were rather low. The maximum muscle forces which we were able to apply to the specimens ranged from 68 N to 505 N for all the muscles/tendons in all of the specimens. Beyond these values, the tissue started to noticeably disintegrate. These values were clearly not comparable to the *in vivo* situations, for instance, the soleus muscle force can reach up to \sim 2500 N during the maximum tetanic contractions [18]. The achieved maximum muscle forces were summarized in Table 2. For some specimens, muscles were ruptured after few times repeated stretching.

Table 2 The force level for different muscles during the loading protocol.

Specimens	Achieved maximum force level (N)						
	Qua	Hamst	So	GM	GL	TA	TP
A	505	152	308	108	46	46	116
B	340	102	214	75	32	32	80
C	198	59	164	58	24	24	62
D	491	147	307	107	46	46	115
E	439	132	174	60	26	26	65
F	248	74	137	48	21	21	51

Tibia deformation

In keeping with the low levels of muscle forces that were achievable, the tibia bending and torsion angles were rather low. However, there was still some notable information which may provide evidence about the OST approach itself.

Tibia deformation under the relatively large muscle forces: When loading the quadriceps muscle with forces ranging between 198 N to 505 N, the proximal tibia bent to the posterior aspect with respect to the distal tibia by $0.12^\circ \pm 0.01^\circ$ - $0.25^\circ \pm 0.00^\circ$ for all specimens (Fig. 2C), and bending also occurred towards the

lateral aspect by $0.06^\circ \pm 0.01^\circ$ - $0.21^\circ \pm 0.04^\circ$ in five specimens (Fig. 2A). Tibia deformation in five specimens, except specimen C, followed the same pattern across different loading conditions. Besides, relatively large tibia bending angles were measured in ‘P4’, ‘G1’ and ‘G2’ loading protocol as well. The amplitude ranged between $0.09^\circ \pm 0.00^\circ$ and $0.26^\circ \pm 0.01^\circ$ for the lateral bending (Fig. 2A) and from $0.01^\circ \pm 0.00^\circ$ to $0.17^\circ \pm 0.01^\circ$ for the posterior bending (Fig. 2C), respectively.

Anterior bending angles: In contrast with the posterior bending detected under the other loading conditions, anterior bending angle were measured from $0.03 \pm 0.00^\circ$ to $0.10 \pm 0.00^\circ$ when hamstrings, namely BF and Semi, was loaded (Fig. 2C).

Torsion angles: Compared with the lateral and posterior bending angle, the torsion angle was relatively small. However, a similar torsion pattern can still be observed with different loading patterns. For instance, external torsion of the proximal tibia was indicated in 4 of all specimens, ranging from $0.02 \pm 0.00^\circ$ to $0.08 \pm 0.02^\circ$ and from $0.04 \pm 0.02^\circ$ to $0.11 \pm 0.00^\circ$ when ‘So’ and ‘P2’ loading protocol was applied, respectively (Fig. 2B).

Repeatability of the deformation recording: the variance between the repeated measurements remained in a very low level. The standard deviation of the mean deformation angles ranged between 0° and 0.04° for lateral bending angles, internal rotation angles and posterior bending angles, respectively (Fig. 2).

The tibia deformations, mainly the lateral bending angles, posterior bending angles and internal torsion angles of all specimens in all loading conditions were summarized in Fig. 2.

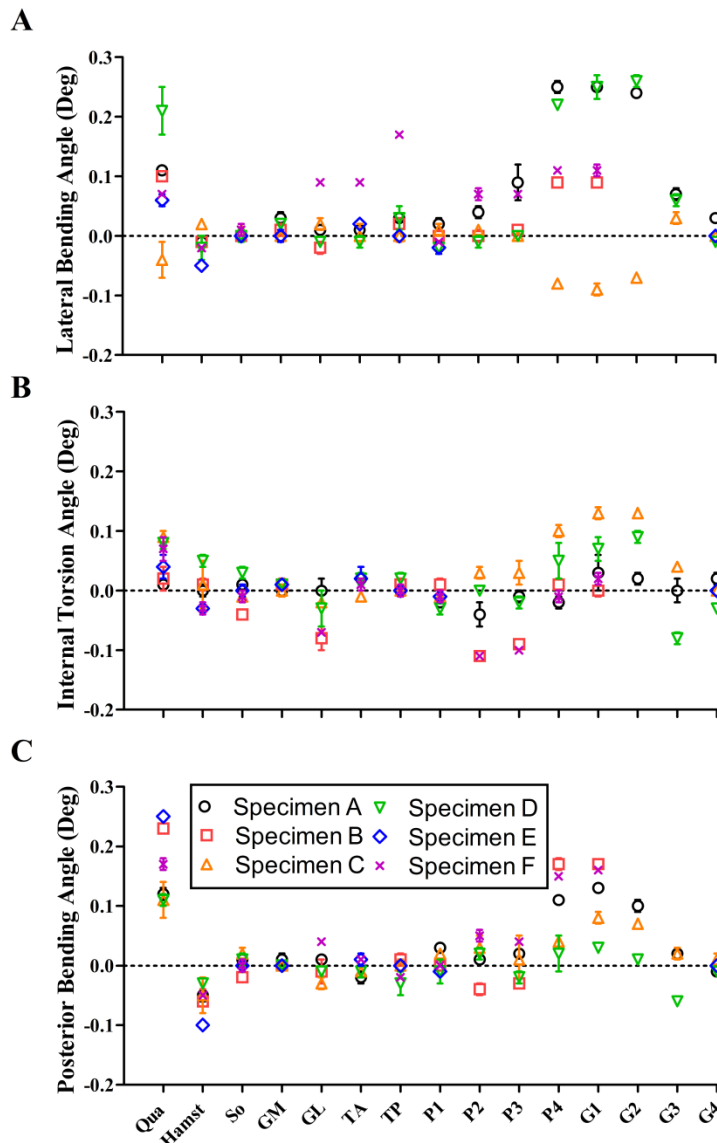


Fig. 2 Tibia deformation angles, including lateral bending angle (A), internal torsion angle (B) and posterior bending angle (C), under different loading conditions with the simulated muscle forces. Qua: Quadriceps muscle, Hamst: hamstrings, BF: biceps femoris, Semi: semimembranosus/tendinosus, So: soleus muscle, GM: gastrocnemius medialis muscle, GL: gastrocnemius lateralis muscle, TA: tibialis anterior muscle, TP: tibialis posterior muscle. P1, P2, P3 and P4 referred to the loading pattern in which muscle co-contractions were simulated. G1, G2, G3 and G4 referred to the muscle activities during 0-10%, 10-20%, 30-50% and 50-60% of gait cycle (stance phase), respectively.

Discussion and Conclusions

The presented study mainly assessed tibia deformation in a cadaveric model using a novel optical segment tracking (OST) approach. The force simulation of the

major muscles in human cadaver lower extremities were achieved by a loading device, so called Lower Extremity Loading Device (LELD). Results suggested that tibia deformation angles can be yield using the OST approach. The deformation angles varied under different loading patterns. Relatively large tibia deformation angles were observed while quadriceps muscle and the co-contraction of few muscle groups were simulated, with the maximum posterior bending angle ranging between 0.17° and 0.25° , and the maximum lateral bending angle of 0.21° - 0.26° . Most importantly, the variation between the repeated measurements remained on a very low level, with the standard deviation ranging between 0° and 0.04° (Fig. 2). It therefore seems that the OST approach can assess whole-bone deformation with high accuracy and reproducibility.

Simulated muscle forces

Simulation of the physiological muscle forces *ex vivo* is a well-known difficulty in this type of the cadaveric model studies. Given the tissue degradation *post mortem*, mostly by freezing, and the reduced mechanical properties of the tissue *ante mortem* based on the donor's age and medical record, the low levels of muscle simulation forces were no great surprise in this study. Many studies used tendon as a mediator to transmit expected large force to the segment in the cadaver models [19, 20], but this is impossible when dealing muscle origins *e.g.* in the soleus muscle of this study. Even though the finger sleeves were adopted in this study to grasp the muscle belly instead of the tendons, which has been shown to enhance transmit ability of forces, simulated muscle forces were still disappointingly small during the present experiments. The muscle quality in the presented study is apparently the restriction factor of increasing the simulated loading. As one of the consequences, comparing with the physiological conditions, only much lower muscle forces can be loaded to the specimens in this study. This might be one of the reasons of tibia deformation angles being small.

Muscle forces induced tibia deformation

Instructive results were, however, achieved in relation to muscle-bone interaction effects. For most of the loading patterns, posterior bending of the proximal tibia

with respect to the distal tibia was observed. This seems to be reasonable because anatomically the plantar flexors are located at the posterior aspect of the tibia. Even though the lever arm may be small, a considerable posterior moment can still be induced by the contraction of the plantar flexors. Another finding was that the tibia deformation pattern and magnitude are modulated by the different muscles.

However, one of the main limitations of this study was that both simulated muscle forces and mechanical properties of the tibia vary from specimen to specimen, thus inflating the inter-specimen variation in tibia deformation enormously. Because of this, the presented tibia deformation amplitude in this chapter was interesting in qualitative terms, but failed to provide true quantitative estimates of the tibia deformation induced by muscular forces.

Nevertheless, and most importantly, we can learn from this study that the OST approach is practically feasible and thus applicable in bone biomechanics measurements. In consideration of method's present resolution, accuracy and precision and the good reproducibility noted in this chapter, it is suggested that the OST approach has the capability of picking up even minute deformations of the tibia, which has been the main objective of the study in this chapter. We therefore speculate that the OST method will also be able to also pick up muscle-induced bone deformation *in vivo*.

Conclusions

To conclude, the results demonstrated that the pattern and magnitude of tibia deformation can be modulated by the contraction of simulated muscle forces. We therefore conclude that the OST method has the potential to be applied *in vivo* and pick up muscle-induced tibia deformation.

Acknowledgments

We would like to thank Hans-Martin Küsel-Feldker and Thomas Förster in the Institute of Biomechanics and Orthopaedics, German Sport University Cologne

for designing and manufacturing the Lower Extremity Loading Device (LELD) and marker clusters adopted in this study. Special thanks to Sufyan Ali for his great technical support in controlling the LELD during the simulation of muscle forces and during data collection. Peng-Fei Yang acknowledges his scholarship by the China Scholarship Council (CSC No.: 2009629013).

Funding

This research received no specific grant from any funding agency in the public, commercial, or not-for-profit sectors.

Declaration of Conflicting Interests

The Authors declare that there is no conflict of interest.

References

1. Frost HM (1990) Skeletal structural adaptations to mechanical usage (SATMU):
 2. Redefining Wolff's law: the remodeling problem. *Anat Rec* 226: 414-422.
2. Frost HM (1990) Skeletal structural adaptations to mechanical usage (SATMU):
 1. Redefining Wolff's law: the bone modeling problem. *Anat Rec* 226: 403-413.
3. Rittweger J, Beller G, Ehrig J, Jung C, Koch U, et al. (2000) Bone-muscle strength indices for the human lower leg. *Bone* 27: 319-326.
4. Manske SL, Boyd SK, Zernicke RF (2010) Muscle and bone follow similar temporal patterns of recovery from muscle-induced disuse due to botulinum toxin injection. *Bone* 46: 24-31.
5. Rittweger J, Felsenberg D (2009) Recovery of muscle atrophy and bone loss from 90 days bed rest: results from a one-year follow-up. *Bone* 44: 214-224.
6. Judex S, Carlson KJ (2009) Is Bone's Response to Mechanical Signals Dominated by Gravitational Loading? *Med Sci Sports Exer* 41: 2037-2043.
7. Robling AG (2009) Is Bone's Response to Mechanical Signals Dominated by Muscle Forces? *Med Sci Sports Exer* 41: 2044-2049.
8. Burr DB, Milgrom C, Fyhrie D, Forwood M, Nyska M, et al. (1996) In vivo measurement of human tibial strains during vigorous activity. *Bone* 18: 405-410.
9. Milgrom C, Finestone A, Simkin A, Ekenman I, Mendelson S, et al. (2000) In-

- vivo strain measurements to evaluate the strengthening potential of exercises on the tibial bone. *J Bone Joint Surg Br* 82: 591-594.
10. Yang PF, Bruggemann GP, Rittweger J (2011) What do we currently know from in vivo bone strain measurements in humans? *J Musculoskelet Neuronal Interact* 11: 8-20.
 11. Yang PF, Sanno M, Bruggemann GP, Rittweger J (2012) Evaluation of the performance of a motion capture system for small displacement recording and a discussion for its application potential in bone deformation in vivo measurements. *Proc Inst Mech Eng H* 226: 838-847.
 12. Friederich JA, Brand RA (1990) Muscle fiber architecture in the human lower limb. *J Biomech* 23: 91-95.
 13. Wickiewicz TL, Roy RR, Powell PL, Edgerton VR (1983) Muscle architecture of the human lower limb. *Clin Orthop Relat Res*: 275-283.
 14. Albracht K, Arampatzis A, Baltzopoulos V (2008) Assessment of muscle volume and physiological cross-sectional area of the human triceps surae muscle in vivo. *J Biomech* 41: 2211-2218.
 15. Grood ES, Suntay WJ (1983) A Joint Coordinate System for the Clinical Description of 3-Dimensional Motions - Application to the Knee. *J Biomech Eng-T ASME* 105: 136-144.
 16. Lafortune MA, Cavanagh PR, Sommer HJ, 3rd, Kalenak A (1992) Three-dimensional kinematics of the human knee during walking. *J Biomech* 25: 347-357.
 17. Söderkvist I, Wedin P-Å (1993) Determining the movements of the skeleton using well-configured markers. *J Biomech* 26: 1473-1477.
 18. Maganaris CN, Baltzopoulos V, Ball D, Sargeant AJ (2001) In vivo specific tension of human skeletal muscle. *J Appl Physiol* 90: 865-872.
 19. Sharkey NA, Hamel AJ (1998) A dynamic cadaver model of the stance phase of gait: performance characteristics and kinetic validation. *Clin Biomech (Bristol, Avon)* 13: 420-433.
 20. Wunschel M, Leichtle U, Obloh C, Wulker N, Muller O (2011) The effect of different quadriceps loading patterns on tibiofemoral joint kinematics and patellofemoral contact pressure during simulated partial weight-bearing knee flexion. *Knee Surg Sports Traumatol Arthrosc* 19: 1099-1106.

CHAPTER 5

***In vivo* application of the OST approach for bone deformation
recording in humans: a reliability study**

In vivo application of an optical segment tracking (OST) approach for bone deformation regimes recording in humans: a reliability study

Peng-Fei Yang, Maximilian Sanno, Bergita Ganse, Timmo Koy, Gert-Peter Brüggemann, Lars Peter Müller, Jörn Rittweger

Manuscript under submission

Abstract

It is well accepted that bone deformation plays a crucial role in bone maintenance and transformation. However, technical possibilities are currently limited to provide *in vivo* data. This paper demonstrates a novel optical segment tracking (OST) approach for amelioration. The relative movement between the retro-reflective marker clusters affixed to tibia cortex by bone screws was tracked using a motion capture system, and expressed as tibia deformation. Stable affixment of bone screws to the bone was tested by assessing the resonance frequency of the screw-marker structure prior to and after the intense exercises and the relative marker position in the static trials between hopping and jumping, respectively. Tibia deformation was recorded during squatting exercises to demonstrate the reliability of the OST approach. Results indicated that the resonance frequency remained unchanged prior to and after all exercises, at approximate 260 Hz and 380 Hz. The changes of Cardan/Euler angle between marker clusters after each cycle of hopping and jumping were rather low, maximally 0.06°. The repetition variability of the normalized tibia deformation angles during squatting remained relatively small (0.07°/m-0.97°/m). Most importantly, all surgical and testing procedures were well tolerated. To conclude, the retro-reflective markers were firmly implanted in the tibia cortex by bone screws through the planned activities.

The *in vivo* tibia deformation results during squats indicated high reliability of the OST approach. Together with the surprisingly good toleration by the test subjects, these experiences therefore nourish the hope that the OST method will enable to be a functional assessment of bone on a broader basis than in the past.

Keywords: Tibia bone deformation; Optical approach; *In vivo*; Motion capture system; Locomotive activities

Introduction

The adaptation of bone tissue to the mechanical environment has been widely demonstrated in numerous studies [1, 2] and bone deformation, or a signal derived from it is mostly regarded as the effective agent. This view was based on *in vivo* bone deformation measurements in animals and humans by several pioneers [3-7]. However, technical limitations such as debonding, the difficulty of assessing torsional and bending deformation, as well as ethical and medical reservations [8] have prevented ample data acquisition of the *in vivo* bone deformation [8-10].

In the view of the current evidence, a concept of new optical segment tracking (OST) approach for *in vivo* tibia deformation recording has been proposed in our previous publication [11]. The idea was to affix clusters with sets of three retro-reflective markers to different sites of the human bone, and to track the trajectories of these clusters with a motion capture system during different biomechanical paradigm tasks. Bone deformation can then be assessed as the relative movement between the marker clusters. Rather than calibrating the OST approach with an alternate technique, *e.g.* strain gauges, the resolution, accuracy, and repeatability of the OST approach would thus totally rely on the performance of the adopted optical system. Mock-testing with the optical system has demonstrated that a resolution of $<20\text{ }\mu\text{m}$ or $100\text{ }\mu\epsilon$ ($100\text{ }\mu\epsilon$ was computed based on the assumption of markers distance as 20 cm and the detection limit as $20\text{ }\mu\text{m}$) can be achieved with high accuracy and precision within a volume of $400\times300\times300\text{ mm}^3$ [11], and *ex vivo* testing has demonstrated further validated the OST approach (unpublished results). Briefly, three marker clusters had been affixed to human cadaveric tibia specimens by bone screws. Utilizing the proposed optical method, tibia deformation had been assessed under simulated muscle contractions and axial loading. Repeatable deformation results, *i.e.* variance between the repeated measurements was maximally 0.04° , demonstrated the possibility to apply the OST approach in the *in vivo* study. Several benefits can be expected from the OST approach. Firstly, compared to the invasiveness of

the traditional strain gauge methods, the OST approach needs smaller incisions, no further bone surface preparations or less drilled holes into bone. Secondly, the accessible of segment deformation regimes from the OST approach, rather than local strains from strain gauges, will further our understanding in terms of segment loading pattern, which is highly clinical relevant, *e.g.* to explain clinical syndromes like stress fracture from the perspective of experienced loading. By contrast, this information cannot be derived from the strain gauge approach. Thirdly and more importantly, a considerable advantage of the OST approach is that the quality of the recorded data could be evaluated by assessing the stability of the fixation of clusters. With surgeon's extensive experience and the interference fit between small pre-drilled holes (0.21 mm) and bone screws with thread diameter of 3 mm, the mechanical stability of the bone screws in tibia cortex can be expected. However, whether or not the OST approach is practically feasible in humans still remains to be determined. With the suggested sufficient accuracy, precision, and the resolution of the adopted optical system in our previous studies [11], this applies firstly to the general toleration by the test subjects, secondly to the problems of stable affixment and resonance of bone screws in tibia, and thirdly to the results reliability when applied in a human experiment. The purpose of this paper is to solve those problems by evaluating the stability of bone screws in tibia through several exercises. Furthermore, the *in vivo* recording reliability was demonstrated with the tibia deformation results during squatting exercise.

Materials and Methods

Five healthy male subjects (26-50 years old, weight: 78.9 ± 7.1 kg, height: 181.4 ± 4.8 cm, tibia length: 379 ± 13 mm) volunteered to participate in this study. They were free of any muscle or joint injury and without any orthopedic surgery in the lower extremity within twelve months prior to the study. This study had been approved by the relevant Ethics Committees, and informed consent was given before inclusion into the study. The operations and the *in vivo* exercise battery

were performed at the Department of Orthopedic and Trauma Surgery of the University Hospital of Cologne.

Surgical Technique

On the right shank of each subject, surgical implantation and explantation of the bone screws was performed under local anesthesia by injecting Xylocain 1% and Carbostesin 0.5% into the skin and the periosteum. Prior to that, Ibuprofen (600 mg) and Cefuroxime (1500 mg) had been administered. Transverse MRI (Magnetic Resonance Imaging, 1.5 T, Philips, Best, The Netherlands) images of the shank had been obtained to measure the thickness of tibia cortex. To avoid the bone screws penetrating into the bone cavity, only the sites where the tibia cortex is thicker than 4 mm were considered to implant bone screws. Eventually, the sites for implantation of bone screw into tibia were selected at approximately 10 cm below the tibia plateau, mid-site of the tibia diaphysis and approximately 10 cm above the tibia medial malleolus, respectively.

Surgical incisions of approximately 1 cm length were made (Fig. 1A), and holes were drilled 2-3 mm into the tibia cortex with a 2.1 mm diameter drill (Stryker Leibinger GmbH & Co. KG, Germany) into which the bone screws (Asnis Micro cannulated titanium screws, Ø3 mm, total length: 24 mm, thread length: 6 mm, Stryker Leibinger GmbH & Co. KG, Germany) were implanted. The bending stiffness (flexural stiffness, the product of elastic modulus and area moment of inertia) of the bone screw shaft is 0.41 Nm^2 .

Bone screw removal after the testing took place in the same operation theatre, between 6 and 8 hours later. Bone screw positions were documented by peripheral quantitative computed tomography (pQCT) with a XCT3000 (Stratec Medizintechnik, Pforzheim, Germany) after screw removal (Fig. 1D).

OST Approach

Onto the bone screws, a total of three marker clusters, with a set of three non-collinear retro-reflective markers (Ø5 mm, Géodésie Maintenance Services, Nort Sur Erdre, France) on each cluster were mounted (Fig. 1C). The total weight of the marker cluster was minimized as much as possible to 5.6 gram during the

manufacturing. The distance between bone surface and the plane determined by the three markers in the cluster was typically 26.6 mm. A Vicon MX optical motion capture system with eight Vicon F40 cameras (Vicon Motion System Ltd., LA, USA) was used to capture the trajectories of the marker clusters at 300 Hz (Fig. 1B). In order to obtain optimal accuracy and precision, the optical system was configured as previously proposed [11].

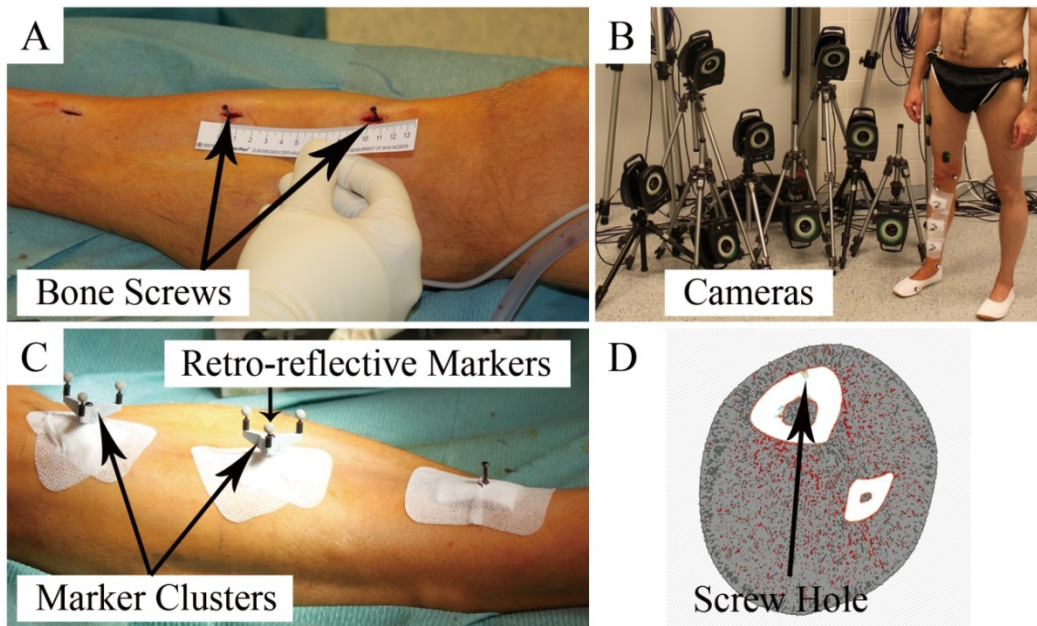


Fig. 1. Illustration of the surgical technique and the OST approach in this study. A: bone screw implantation into the tibia cortex; B: the motion capture system with 8 high resolution cameras to track the retro-reflective markers; C: marker clusters were fixed on the top of the bone screws; D: the pQCT image of the cross section area of the shank. The black arrow indicates the screw hole after the bone screw being removed.

Stability of bone screws: resonance frequency

As the representative of all test subjects, resonance frequency of the screw-marker structure from two subjects was assessed prior to and after the exercises, including approximately 10 minutes walking, 10 minutes running, 30 cycles of double legs hopping, 30 cycles single leg hopping, 3 times drop jump and 3 times countermovement jump. Because the proximal tibia generally has more trabecular bone distribution than mid-shaft and distal tibia, the proximal bone screws is most likely to be loose than the distal one, meaning the resonance frequency of the proximal screw-cluster structures is very likely to be lower or close to the distal

ones. Hence, the excitation of the proximal marker clusters was conducted by flipping with a finger of the same lab staff while the test subjects were in the sitting position and their shank was free of any loading, with simultaneous motion capturing at 1000 Hz. From the marker trajectories, the frequency spectrum was extracted with custom-written routine in MATLAB (The MathWorks, Inc. Version 7.9.0 R2009b).

Frequency component of ground reaction forces (GRF)

In order to assess whether the ground reaction forces could possibly contribute to the resonance vibration of the screw-cluster structure, thus leading a dramatic increase of the vibration amplitude, the frequency components of the GRF during the intense task, *i.e.* double legs hopping, are evaluated as well. GRF during the task were recorded at 1000 Hz by a force plate (AMTI OR6-5, Watertown, MA, USA).

Stability of bone screws: relative movement between the tibia-affixed markers

If the bone screws were firmly affixed into tibia through the exercises, the relative position between the tibia-affixed marker clusters was supposed to be fixed before and after the exercises. To evaluate the relative position between the marker clusters, between the repetitions of most intense exercises, *i.e.* hopping and jumping, the trajectories of the tibia-affixed markers were captured at 300 Hz for 1-2 seconds while the subjects were in the sitting position and the shank was free of any loading (these were the static recording trials ideally without any bone deformation). To label the orientation of the shank in 3D, general retro-reflective markers (Ø16 mm, Vicon Motion System Ltd., LA, USA) were attached on the skin at the position of shank anatomical landmarks, namely the tip of medial and lateral malleolus, tip of tibia tuberosity and the head of fibula, as indicated in Fig.2A (black spots). Simultaneously with tibia-affixed markers, the coordinates of skin-attached markers were recorded for further generating Shank Anatomical Coordinate System (SACS) [12]. More specifically, the origin of the SACS was located at the midpoint of the line between the tip of medial and lateral malleolus.

A quasi-coronal plane was determined by the head of fibula, lateral malleolus and SACS origin. A quasi-sagittal plane which was orthogonal to the quasi-coronal plane, and contained SACS origin and the tip of tibia tuberosity was determined. The third plane, *i.e.* quasi-transverse plane, was perpendicular to the quasi-coronal and quasi-sagittal plane. Y axis was the intersection between the quasi-coronal and quasi-sagittal plane with positive direction upwards. Z axis was in the quasi-coronal plane and perpendicular to the Y axis with positive direction pointing right. X axis was perpendicular to the Y and Z axis with positive direction pointing anterior.

Tibia deformation reliability: results during squatting exercise

To further demonstrate the reliability of the OST approach for *in vivo* tibia deformation measurements, tibia-affixed markers trajectories were captured at 300 Hz during squatting. All test subjects were requested to perform squats with body weight, 20 kg extra weight and 40 kg extra weight, respectively. All squats were performed with the same rhythm of 3 seconds knee bending to maximum knee flexion angles at approximately 90° and 3 seconds from knee bending returning to standing position. At least three repetitions were performed at each weight condition.

Data analysis

Raw trajectory data of the markers was further processed with custom-written routine in MATLAB (The MathWorks, Inc. Version 7.9.0 R2009b).

Resonance frequency analysis and frequency component of GRF: Marker trajectories after the flipping impact were Fourier-transformed, and the frequency spectrum was computed. The modal frequency, *i.e.* the frequency with greatest amplitude was taken as the resonance frequency of the screw-marker cluster complex. The frequency spectrum of the GRF during hopping was calculated after Fourier transformation. The result graphs were generated with Graphpad Prism statistical software (version 5.00, GraphPad software, Inc., La Jolla, CA).

Determination of SACS and assess the relative movement between tibia-affixed markers before and after the exercises: For each subject, one frame from the static

recording trial was utilized for determining an initial Cartesian SACS from the skin-attached tibia landmarks. In the SACS, X, Y, and Z axis indicated the anterior-posterior, proximal-distal, and medial-lateral direction, respectively [12]. The coordinates of the tibia-affixed markers from the marker clusters in the determined SACS were then calculated by coordinate transformation [13, 14]. The relative position between every two marker clusters in SACS were then calculated and expressed as mean \pm standard deviation (SD) of three Cardan/Euler angle and three translations along the axis of SACS, respectively (Fig. 2A).

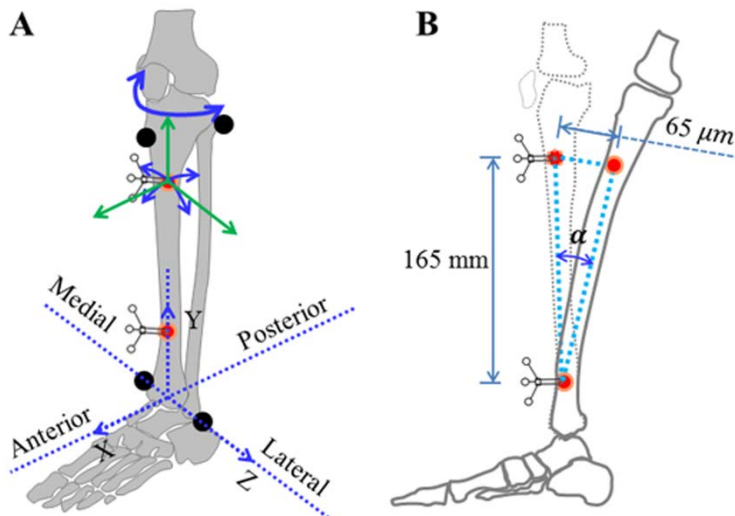


Fig. 2. Sketch of the relative position between proximal and distal marker clusters. A: the movement of proximal marker clusters with respect to the distal one, including three Cardan/Euler angles (solid blue arrow) and three translations (solid green arrow). Dashed arrows: Shank Anatomical Coordinate System (SACS); Black spots: the locations of the skin attached markers to determine the SACS. B: posterior translation with $65 \mu\text{m}$ of the proximal marker cluster with respect to the distal one. α was the posterior bending angle.

Assessment of tibia deformation during squatting: The coordinates of the tibia-affixed markers were subjected to coordinate transformation and were transformed from the global coordinate system to the SACS. The relative movement between the screw-inserted bone sites, which were determined by the proximal and distal marker clusters, was then derived by the second coordinate transformation in SACS. During squatting, the relative movement between two bone sites in SACS was expressed as mean \pm standard deviation (SD) of three Cardan/Euler angles. Antero-posterior (AP) bending angle, medio-lateral (ML)

bending angle, and inter-external torsion angle were then derived from Cardan/Euler angle and reported as tibia deformation angles. In this paper, the relative movement of the proximal tibia-markers in relation to distal tibia-markers was presented. Thus, AP bending, ML bending, and inter-external torsion indicated the bending and torsion of the proximal tibia with respect to the distal tibia in this paper. Peak to peak (p2p) deformation angles during the squat cycles were then derived. The actual distance between the bone sites where bone screws were installed in SACS were derived from the trajectories of the markers. Considering the variance in tibia length and marker cluster distance between subjects, the p2p tibia deformation angles were normalized by dividing the distance between the marker clusters for each subject. The tibia deformation finally was expressed as Degree/meter.

Statistics

Statistical analyses were performed using R statistic software (version 2.15.1, R Development Core Team, 2012). In order to assess the stability of the marker clusters, for each test subject, the homogeneity of the variances of the relative position (three Cardan/Euler angle and three translations along the axis of SACS) were tested with the Fligner-Killeen's test. Furthermore, a linear mixed-effects model (the exercise as the fixed factor, the subject as the random factor) was employed to examine the effects of exercises on the changes of the relative position between every two marker clusters in SACS. Furthermore, for squatting, a one-way ANOVA linear model was employed to examine the main effects of test subject, different bearing weight on the tibia deformation angles, respectively. Statistical significance was accepted at $p \leq 0.05$.

Results

The pain rating results (form 0 to 10 indicating no pain to intolerable pain) suggested that only one subject reported 1 (a little bit pressure) during a passive loading test on tibia and all the other subjects reported 0 through all exercises. Overall, no pain or other issues was reported by the subjects through the

experiments. At the time of bone screws extraction, all of the bone screws were still firmly inserted into the tibia. No loosening has been observed.

Resonance frequency of screw-marker structure

As demonstrated in the frequency spectrum diagram, the resonance frequencies of the structure in two subjects were approximately 259 Hz, 381 Hz (Fig.3A) and 262 Hz, 382 Hz (Fig.3B), respectively. The resonance frequency of the screw-marker structure did not obviously change after the exercises comparing that prior to the exercises (Fig. 3).

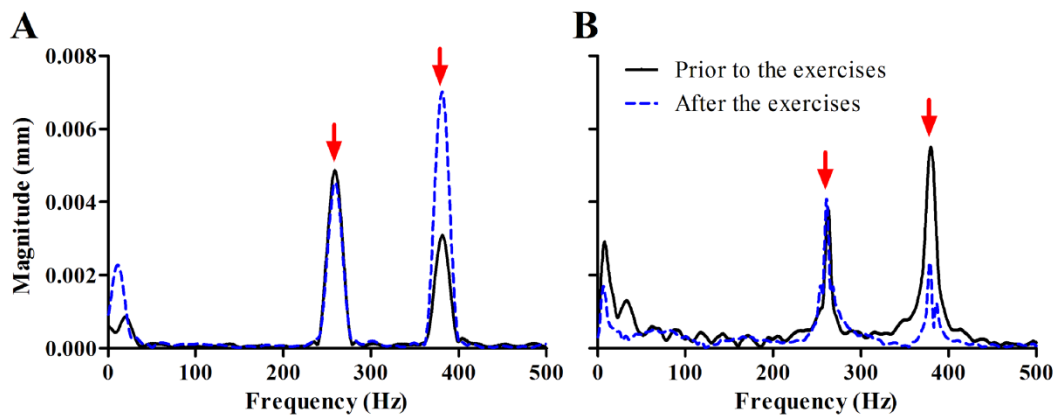


Fig. 3. Frequency spectrum of the marker trajectories after the structure of bone screw and marker cluster being flipped by a finger. A and B indicated the results from subject D and E, respectively. Solid black line: Frequency spectrum of the markers recorded prior to all of the exercises; Dashed blue line: Frequency spectrum of the markers recorded after the exercises. Red arrows: the resonance frequencies of the screw-marker structure were approximately 260 Hz and 380 Hz, respectively.

The relative position of the tibia-affixed markers

For all test subjects, no significant effects of different exercises on the homogeneity of the variances of the relative position between every two marker clusters were found ($p = 0.09$). Similarly, from the mixed-effects model, the Cardan/Euler angles around x ($p = 0.81$), y ($p = 0.73$), z axis ($p = 0.46$) and the translations along x ($p = 0.09$), y ($p = 0.50$), z axis ($p = 0.14$) were comparable before and after the exercises (minimum $p = 0.09$).

Because the relative position between marker clusters was different among the test subjects, the mean and SD of the relative position between clusters before and

after the hopping and jumping tasks from one of the subjects was summarized in Table 1. After hopping and jumping, the largest change of the Cardan/Euler angle between marker clusters was from $0.19^\circ \pm 0.02^\circ$ to $0.22^\circ \pm 0.02^\circ$ (the distal marker cluster with respect to the middle one, Cardan/Euler angle along Z axis of SACS). The largest change in translation was found from -1.210 ± 0.058 to -1.143 ± 0.045 mm in x axis of SACS between proximal and middle marker clusters. Among the repetitions of the same task, the largest variation (SD) of the Cardan/Euler angle and translation were 0.06° and $65 \mu\text{m}$, respectively.

Table 1 Relative position between pairs of marker clusters in SACS

Marker Clusters	Tasks	Cardan/Euler angle (Degree)			Translations (mm)		
		x axis	y axis	z axis	x axis	y axis	z axis
Prox. vs. Distal	Hopping	0.07±0.01	-0.01±0.02	-0.09±0.01	12.688±0.065	207.462±0.010	-0.300±0.031
	Jumping	0.09±0.02	-0.01±0.01	-0.10±0.01	12.649±0.043	207.473±0.012	-0.285±0.028
Prox. vs. Mid.	Hopping	-0.04±0.02	-0.04±0.02	0.11±0.02	1.210±0.058	107.712±0.005	0.515±0.035
	Jumping	-0.04±0.03	-0.03±0.06	0.12±0.02	1.143±0.045	107.716±0.006	0.488±0.018
Distal vs. Mid.	Hopping	-0.11±0.02	-0.03±0.01	0.19±0.02	-10.774±0.050	-99.793±0.010	1.221±0.030
	Jumping	-0.13±0.02	-0.05±0.03	0.22±0.02	-10.718±0.035	-99.805±0.020	1.250±0.024

For all of the repeated static trials between hopping and jumping, the mean and standard deviation of the relative position between marker clusters were determined. Prox. vs. Distal: the position of proximal marker cluster with respect to the distal marker cluster in the SACS; Prox. vs. Mid.: the position of proximal marker cluster with respect to the middle marker cluster in the SACS; Distal vs. Mid.: the position of distal marker cluster with respect to the middle marker cluster in the SACS. SACS: shank anatomical coordinate system.

Frequency spectrum of GRF during hopping

During double legs hopping, most of the frequency component of GRF distributed below 20 Hz. No further high frequency distribution was observed. The largest amplitude in the frequency spectrum was found at approximately 2 Hz (Fig. 4).

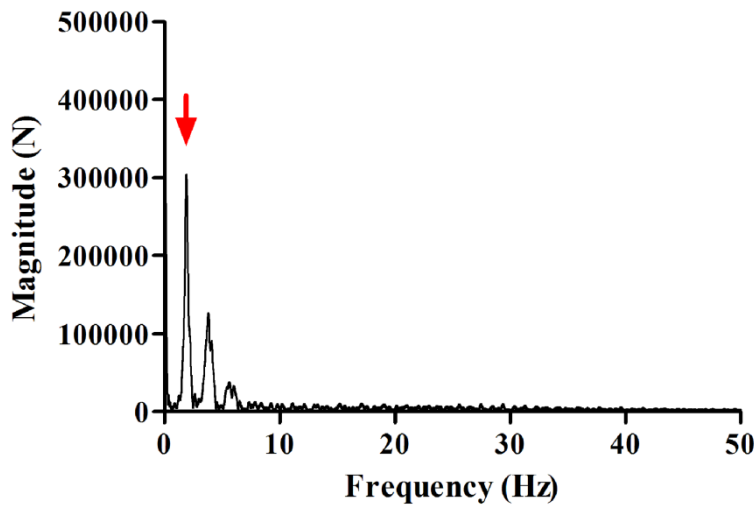


Fig. 4. Frequency spectrum of the ground reaction force (GRF) during double legs hopping.

No high amplitude was found beyond 20 Hz. Red arrow: the largest amplitude of the spectrum was at approximately 2 Hz.

Normalized tibia deformation angles during squatting exercise

During squats, the proximal tibia bent to posterior aspect, lateral aspect and twisted to the external aspect with respect to the distal tibia. Significant main effects of subject were found on the AP bending angle ($p < 0.001$), torsion angle ($p < 0.001$) and ML bending angle ($p < 0.001$). Therefore, the deformation results are presented on the basis of the individual test subject (Fig. 5).

The actual distance between bone screws in SACS varied between subjects, namely being 197 mm, 165 mm, 185 mm, 180 mm and 207 mm for subject A to E, respectively. The normalized AP bending angle increased with the squat weight for all test subjects (subjects A: between $3.81^\circ/m \pm 0.18^\circ/m$ and $5.78^\circ/m \pm 0.28^\circ/m$, subject B: $3.09^\circ/m \pm 0.14^\circ/m$ and $5.68^\circ/m \pm 0.43^\circ/m$, subject C: $3.01^\circ/m \pm 0.46^\circ/m$ and $3.87^\circ/m \pm 0.33^\circ/m$, subject D: $3.33^\circ/m \pm 0.38^\circ/m$ and $4.53^\circ/m \pm 0.35^\circ/m$, subject E: $4.84^\circ/m \pm 0.18^\circ/m$ and $7.00^\circ/m \pm 0.07^\circ/m$, $p < 0.001$). Normalized torsion angle during squats with 40 kg extra weight (external torsion angle: between $2.60^\circ/m \pm$

$0.49^\circ/\text{m}$ and $4.61^\circ/\text{m} \pm 0.63^\circ/\text{m}$, $p = 0.008$) was larger than body weight (external torsion angle: between $1.64^\circ/\text{m} \pm 0.13^\circ/\text{m}$ and $4.61^\circ/\text{m} \pm 0.63^\circ/\text{m}$) and 20 kg (external torsion angle: between $2.05^\circ/\text{m} \pm 0.57^\circ/\text{m}$ and $3.84^\circ/\text{m} \pm 0.75^\circ/\text{m}$). Similarly, the larger normalized ML bending angle was found during squats with 40 kg weight (lateral bending angle: between $2.80^\circ/\text{m} \pm 0.22^\circ/\text{m}$ and $3.87^\circ/\text{m} \pm 0.47^\circ/\text{m}$, $p < 0.001$) than body weight (lateral bending angle: between $2.16^\circ/\text{m} \pm 0.16^\circ/\text{m}$ and $3.10^\circ/\text{m} \pm 0.58^\circ/\text{m}$) and 20 kg weight (lateral bending angle: between $2.42^\circ/\text{m} \pm 0.30^\circ/\text{m}$ and $3.08^\circ/\text{m} \pm 0.38^\circ/\text{m}$). The standard deviation for AP (between $0.07^\circ/\text{m}$ and $0.46^\circ/\text{m}$), ML bending angle (between $0.13^\circ/\text{m}$ and $0.69^\circ/\text{m}$) and torsion angle (between $0.13^\circ/\text{m}$ and $0.97^\circ/\text{m}$) remained small during the repetitions of squats.

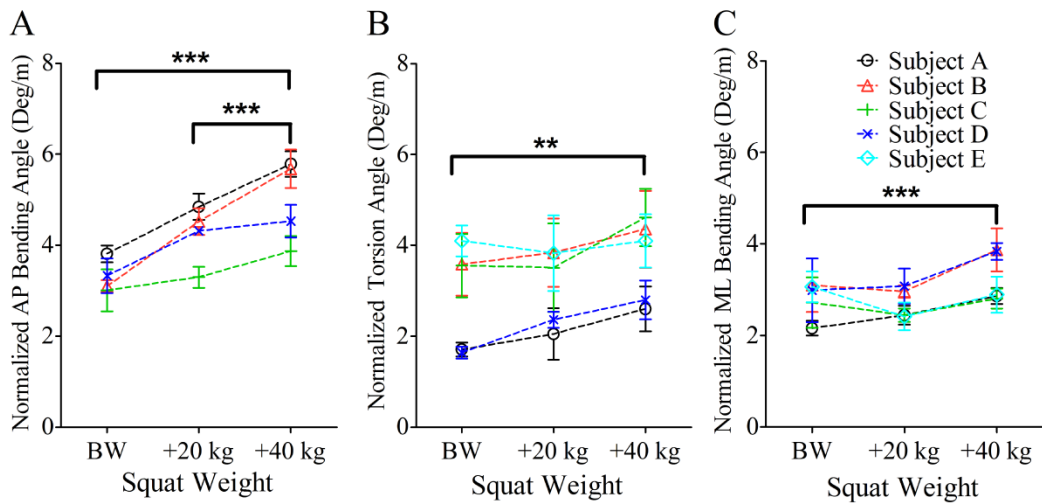


Fig. 5. Normalized tibia deformation angles during squats with different weight. A: normalized tibia AP bending angles; B: normalized tibia torsion angle; C: normalized tibia ML bending angle. **: $p < 0.01$; ***: $p < 0.001$.

Discussion and Conclusions

To summarize, a novel optical segment tracking (OST) approach for *in vivo* bone deformation recording was applied in an *in vivo* study in humans for the first time. In this paper, the feasibility of the OST approach was demonstrated in terms of general toleration, marker cluster stability and resonance frequency, and deformation reliability during repeated squats cycles. Results suggested that the resonance frequency was relatively high and remained unchanged before and after the exercises,

implying that bone screws were firmly implanted into the tibia cortex across the intense exercises. Furthermore, the influence of the intense exercises on the relative positions of the tibia-affixed markers remained in a low level, even though the sample size was limited in the presented study (minimum $p = 0.09$ for five subjects). Of note, the variation of the Cardan/Euler angles and translations between the marker clusters were relatively small, typically in the range 0.01° - 0.06° and 6 - $65\ \mu\text{m}$, respectively. The variability of the recorded tibia deformation angles (standard deviation) between the repetitions of squats remained relatively small, typically in the range 0.02° - 0.18° .

Stability of bone screws in tibia cortex: resonance frequency

Results in this paper suggested that the resonance frequency of the screw-marker structure remained unchanged at approximately 260 Hz and 380 Hz for two subjects across all of the exercises, meaning that the loosening of the bone screws did not occur due to the high intensive activities. On the other hand, the resonance frequencies of \sim 260 Hz and \sim 380 Hz were relatively high and very close to the sampling rate of bone deformation (300 Hz, Fig. 3). Considering that the resonance frequency of tibia is approximately 110 Hz [15, 16] and the frequency component of GRF during hopping is less than 20 Hz (Fig. 4), as the common sense, the potential contribution of the GRF and tibia vibration to the resonance vibration of the screw-cluster structure can be avoided. The similar resonance frequency of the screw-cluster structure should be achieved using the same procedure to install bone screws in tibia cortex, which was also confirmed by comparable resonance frequency results from the two tested subjects, *i.e.* \sim 260 Hz and \sim 380 Hz. However, the limited number of the subjects (two out of five) in the resonance frequency assessments may attenuate the power to conclude that the bone screws were firmly installed in the tibia cortex for the other subjects as well, which is needed to be clarified in the future studies. Given the results demonstrated above, the fixation of the bone screws in tibia cortex would fulfill the requirement of bone deformation recording.

Stability of bone screws: relative movement between the tibia-affixed markers

Further evidence in support of the stability of the bone screws in tibia cortex was provided by the constancy of the relative positions between the tibia-affixed markers

prior to and after the high intensive activities. Of note, a fair amount of position discrepancy between marker clusters initially exists due to their different locations in the determined SACS. So evaluation of variance of Cardan/Euler angle and translations, rather than their mean value, make more sense to help us understand the relative movement between marker clusters. Results suggested that the changes of mean Cardan/Euler angle between marker clusters after different tasks, *i.e.* hopping and jumping, were maximally 0.03° (Table 1). Furthermore, the largest variance of Cardan/Euler angle between marker clusters are 0.06°, indicating that any angle change between marker clusters (tibia bending angle) above 0.06° would be capable to be detected. The SD of the translations between marker clusters ranged from 6-65 μm (Table 1). Of note, most of the SD value above 30 μm distributed in x axis of the SACS, *i.e.* anterior-posterior direction. As presented above, the actual distance between screws varied between subjects. The maximum possible recording error of the deformation angle induced by the variance of the anterior-posterior translation could be assumed by taking the maximum variance of the translation (65 μm) and the minimum distance between the bone screws (165 mm) as follows.

$$\alpha = \sin^{-1}(65 \text{ } \mu\text{m}/165 \text{ } \text{mm}) \approx 0.02^\circ$$

The calculated results indicated that even the variance of 65 μm in translation was still acceptable for tibia deformation recording. Moreover, since unpublished data from this study suggested that tibia deformation in response to muscle contractions was much larger than the reported variance level, it had to be considered that the ‘resting’ variation may still be contaminated by involuntary minor muscle contractions. These results implied that the complex of bone screw and marker cluster was firmly inserted into the tibia cortex across all of the exercises, which provided the preliminary, but crucial requirement for the *in vivo* application of the OST approach. Based on above evidence, it can be concluded that the slight changes of the relative position between the markers were not induced by screw loosening, but might mainly contributed by the recording noise of the optical system and potential minute muscle contractions.

As a matter of fact, the system noise always accompanies with the data recording and

cannot be totally avoided [17]. As demonstrated by previous studies, the performance of the optical motion capture system can be influenced by many factors, such as cameras set-up, marker quality and surrounding environment conditions [11, 18-20]. So, many efforts have been invested to diminish the noise level and improve the performance of the adopted optical system in this study, such as optimizing the camera number and positions with respect to the markers and improving the marker quality. Eventually, the relative movement of the markers (tibia deformation) during each trial of exercise was calculated by taking the static relative position of the markers as the references. By doing so, the influence of these minute relative movements of the markers on the ‘true’ tibia deformation would be minimized.

Tibia deformation during squats with different weight

Another interesting finding was that considerable amount of antero-posterior, medio-lateral bending angle, and torsion angle occurred during squats. The deformation angles during 40 kg squats were larger than body weight and 20 kg squats. Apart from the deformation angles observed during the squats, the primary goal to perform the squats exercise was to demonstrate the reliability of the OST approach in *in vivo* tibia deformation recording. Given that the principle and the output of the OST approach is completely different with the traditional strain gauge technique, the necessities of comparing the deformation results between these two approaches is rather weak, as long as the resolution, accuracy, and repeatability of the OST approach is sufficient during the recording of minor movement of markers [11].

The small variability of the tibia deformation angle (between 0.02° and 0.18°) between the repetitions of squats indicated the high repeatability of the OST approach during tibia deformation measurements.

Limitations

As indicated above, although the OST approach has the capability of contributing new knowledge to the *in vivo* tibia deformation, some open questions have been still left. Firstly, the invasiveness, even less than the strain gauge approaches, might still be one of the obstacles to expand the OST approach to the other research field. To our knowledge, non-invasive methods for directly measuring *in vivo* bone deformation in

humans are currently not available. Recently, a notable and very promising modeling approach showed its potential to compute bone strains of different bones integrating with the kinematics and anatomical information [21, 22]. However, as the other bone strain assessing approaches [23, 24], the validation of the model needs the results from *in vivo* experiments as the reference. Considering that bone strains from strain gauges are mostly from local sites of bone and are not able to represent the other sites of bone, the bone deformation results from the OST approach would be another ideal candidate to validate the modeling calculations. Secondly, as with strain gauge approaches, the sites or bone in humans to apply the OST approach are limited, because most of the bone surface is covered with muscles. This is a common issue for all the current available in-site measuring techniques, which will be highly appreciated with the solutions from the further studies. Thirdly, the OST approach could not provide local strain levels directly, but only presenting the segment tibia deformations. However, one could also regard this as strength of the OST approach. It is very possible that the segment deformation of tibia, rather than the local strain from a spot of tibia surface, can provide more insights into the biomechanical loading pattern of the entire tibia. For instance, it does not necessarily mean that the whole bone is under compression, even if the compression strain is recorded from the strain gauges on one spot of tibia surface. It can also mean that the measured aspect of tibia is under compression, whilst the opposite aspect of tibia is under tension, *i.e.* the whole tibia is experiencing bending. Knowing the bone segment loading pattern would definitely further our understanding on some clinical syndromes, *e.g.* tibia fatigue fracture of the runners. Even more important, integrating the presented deformation regimes with a Finite Element model (FEM) of bone would be very promising to derive strain distribution across the bone shaft in the future studies. Fourthly, the sampling rate of the optical system in the OST approach is limited at 300 Hz due to the high requirement of the system resolution and the certain amount of capture volume. The resonance vibration, if there was, of the screw-cluster structure (resonance frequency were approximately 260 and 380 Hz) during the intense dynamic exercises, *e.g.* hopping, may not be able to be captured, thus leading to the

aliasing issue, although it was unlikely to happen during squatting. Technically, the occurrence of the resonant vibration can be possibly excluded by analyzing the frequency spectrum of the raw signal and the contribution of the aliasing frequencies to the raw signal. Certainly, the ideal solution to avoid the aliasing issue is to sample the signal with higher sampling rate, which would rely on the future development of the advanced optical system. Fifthly, the sample size of the test subjects in the presented study was limited to five, which may be less powerful during the interpretation of the statistic results in this study, *e.g.* the influences of the intense exercises on the relative positions of the tibia-affixed markers. The larger sample size of the test subjects would be appreciated in the future studies.

To summarize, to which extent the OST approach can be applied in wide range is still to be determined because of the limitations of the OST approach. However, prior to designing a study that utilizes OST, it is paramount to totally understand what can be achieved and what cannot with the approach. Thus, further expanding the application of the OST approach would be objectives-oriented.

Conclusions and future applications

Taking together these results, we conclude that the OST approach is feasible and well tolerated, that screw affixment is stable, that measurements of bone deformation are unlikely to be affected by resonance problems and that the *in vivo* tibia deformation recording is reliable. In addition, considering that the approach offers good, and with future camera development even better spatial resolution [11], that it avoids the ‘bonding & bending’ problems of the more traditional strain gauge approach, and that it also is less invasive than the latter, it is very perceivable than the new OST approach lends itself to a much more ample application wherever insights into bone function are desired. This may cover quite a large field of application, ranging from biomechanical studies into specific exercises quite as much into clinical studies on fractures or osteoporotic patients.

Acknowledgments

We would like to thank Hans-Martin Küsel-Feldker and Jürgen Geiermann at the Institute of Biomechanics and Orthopaedics, German Sport University Cologne, Germany, for fine manufacturing the marker clusters. Thanks also to Andreas Kriechbaumer, Peter Gauger, and Jakob Kümmel for their kind help during the data collection. Peng-Fei Yang acknowledges Helmholtz Space Life Sciences Research School (SpaceLife) and his scholarship by the China Scholarship Council (CSC No.: 2009629013).

References

1. Frost HM (1994) Wolff's Law and bone's structural adaptations to mechanical usage: an overview for clinicians. *Angle Orthod* 64: 175-188.
2. Turner CH (1998) Three rules for bone adaptation to mechanical stimuli. *Bone* 23: 399-407.
3. Burr DB, Milgrom C, Fyhrie D, Forwood M, Nyska M, et al. (1996) In vivo measurement of human tibial strains during vigorous activity. *Bone* 18: 405-410.
4. Foldhazi Z, Arndt A, Milgrom C, Finestone A, Ekenman I (2005) Exercise-induced strain and strain rate in the distal radius. *J Bone Joint Surg Br* 87: 261-266.
5. Lanyon LE, Hampson WG, Goodship AE, Shah JS (1975) Bone deformation recorded in vivo from strain gauges attached to the human tibial shaft. *Acta Orthop Scand* 46: 256-268.
6. Milgrom C, Finestone A, Levi Y, Simkin A, Ekenman I, et al. (2000) Do high impact exercises produce higher tibial strains than running? *Br J Sports Med* 34: 195-199.
7. Milgrom C, Radeva-Petrova DR, Finestone A, Nyska M, Mendelson S, et al. (2007) The effect of muscle fatigue on in vivo tibial strains. *J Biomech* 40: 845-850.
8. Yang PF, Bruggemann GP, Rittweger J (2011) What do we currently know from in vivo bone strain measurements in humans? *J Musculoskelet Neuronat Interact* 11: 8-20.
9. Al Nazer R, Lanovaz J, Kawalilak C, Johnston JD, Kontulainen S (2012) Direct in vivo strain measurements in human bone—A systematic literature review. *J Biomech* 45: 27-40.
10. Mendelson S, Milgrom C, Finestone A, Lewis J, Ronen M, et al. (1998) Effect of cane use on tibial strain and strain rates. *Am J Phys Med Rehabil* 77: 333-338.

11. Yang PF, Sanno M, Bruggemann GP, Rittweger J (2012) Evaluation of the performance of a motion capture system for small displacement recording and a discussion for its application potential in bone deformation *in vivo* measurements. *Proc Inst Mech Eng H* 226: 838-847.
12. Grood ES, Suntay WJ (1983) A joint coordinate system for the clinical description of three-dimensional motions: application to the knee. *J Biomech Eng* 105: 136-144.
13. Lafontaine MA, Cavanagh PR, Sommer HJ, 3rd, Kalenak A (1992) Three-dimensional kinematics of the human knee during walking. *J Biomech* 25: 347-357.
14. Söderkvist I, Wedin P-Å (1993) Determining the movements of the skeleton using well-configured markers. *J Biomech* 26: 1473-1477.
15. Collier RJ, Donarski RJ (1987) Non-invasive method of measuring resonant frequency of a human tibia *in vivo* part 1. *J Biomed Eng* 9: 321-328.
16. Collier RJ, Donarski RJ (1987) Non-invasive method of measuring the resonant frequency of a human tibia *in vivo* part 2. *J Biomed Eng* 9: 329-331.
17. Gopfert B, Krol Z, Freslier M, Krieg A (2011) 3D video-based deformation measurement of the pelvis bone under dynamic cyclic loading. *BioMed Eng OnLine* 10: 60.
18. Liu H, Holt C, Evans S (2007) Accuracy and repeatability of an optical motion analysis system for measuring small deformations of biological tissues. *J Biomech* 40: 210-214.
19. Schmidt J, Berg DR, Ploeg H-L (2009) Precision, repeatability and accuracy of Optotrak optical motion tracking systems. *International J Exp Comp Biomech* 1: 114-127.
20. Windolf M, Gotzen N, Morlock M (2008) Systematic accuracy and precision analysis of video motion capturing systems--exemplified on the Vicon-460 system. *J Biomech* 41: 2776-2780.
21. Al Nazer R, Kłodowski A, Rantalainen T, Heinonen A, Sievanen H, et al. (2011) A full body musculoskeletal model based on flexible multibody simulation approach utilised in bone strain analysis during human locomotion. *Comput Methods Biomed Engin* 14: 573-579.
22. Al Nazer R, Rantalainen T, Heinonen A, Sievanen H, Mikkola A (2008) Flexible multibody simulation approach in the analysis of tibial strain during walking. *J Biomech* 41: 1036-1043.
23. Grecula MJ, Morris RP, Laughlin JC, Buford WL, Jr., Patterson RM (2000) Femoral surface strain in intact composite femurs: a custom computer analysis of the photoelastic coating technique. *IEEE Trans Biomed Eng* 47: 926-933.
24. Yang L, Zhang P, Liu S, Samala PR, Su M, et al. (2007) Measurement of Strain Distributions in Mouse Femora with 3D-Digital Speckle Pattern Interferometry. *Opt Lasers Eng* 45: 843-851.

CHAPTER 6

**Bending and torsion predominate the *in vivo* human tibia
deformation regimes during walking and running**

Bending and torsion predominate the *in vivo* human tibia deformation regimes during walking and running

Peng-Fei Yang, Maximilian Sanno, Bergita Ganse, Timmo Koy, Gert-Peter Brüggemann, Lars Peter Müller, Jörn Rittweger

Manuscript under submission

Abstract

Bone modeling and remodeling is related to bone mechanical strains. Currently, our understanding on bone strains mainly comes from the traditional strain gauge approaches. Due to the technical limitations, information concerning the bone deformation regimes, *e.g.* bending and torsion, remains unknown in humans. Taking tibia as the object of our study, we hypothesised that bending and torsion do occur within the deformation regimes of the human tibia. Utilizing a novel optical approach, the regimes of the *in vivo* tibia deformation in humans were investigated during walking and running. Results suggest that the proximal tibia primarily bends to the posterior aspect (bending angle: 0.15°-1.30°), medial aspect (bending angle: 0.38°-0.90°) and twisted to the external aspect (torsion angle: 0.67°-1.66°) with respect to distal tibia during the stance phase of overground walking between 2.5 and 6.1 km/h. Peak posterior bending and peak torsion occurred during the first and second half stance phase, respectively. The peak to peak (p2p) antero-posterior (AP) bending angles increased linearly with the vertical ground reaction force and speed, respectively. Similarly, p2p torsion angles increased with the vertical free moment for four test subjects and speed for three test subjects, respectively, but p2p medio-lateral (ML) bending angles did not. On the treadmill, p2p AP bending angles increased with the walking and running speed, but p2p torsion angles and p2p ML bending angles remained

constant during walking. P2p AP bending angle during treadmill running was speed-dependant and larger than that during walking. In contrast, p2p tibia torsion angle was smaller during treadmill running than during walking. To conclude, bending and torsion deformation of substantial magnitude was observed in the human tibia during walking and running, with systematic distribution of peak amplitude during the first and second stance phase, respectively.

Keywords: Tibia deformation; Optical approach; *In vivo*; Bending; Torsion; Walking

Introduction

Mechanically controlled bone modeling and remodeling has a major influence on bone metabolism. As proposed by Harold Frost [1] and recently substantiated by new evidence [2], mechanical strains dominate the bone responses to its mechanical environment. Recent animal study has shown that the from low to high strain level, typically from $\sim 300 \mu\epsilon$ to $\sim 5000 \mu\epsilon$, is essentially linear with the bone response, *i.e.* from disuse to new bone formation [2]. The few human studies conducted so far have suggested that the peak principal strains in human tibia during regular locomotive activities range between $1300 \mu\epsilon$ and $3200 \mu\epsilon$ [3, 4].

However, our present understanding of *in vivo* bone strains stems from studies that have used surgically implanted strain gauges. Several shortcomings with this approach have been well highlighted lately [5, 6]. Thus, strain gauges can only measure where they are attached, and are hardly feasible to be attached on two opposite sides of a human bone, in particular for human tibia, without affecting the regular muscle functions. They thus fail to provide the overall distribution and the type of the human tibia strains, *i.e.* deformation regimes such as bending or torsion. To understand which deformations occur during physical activity in humans would be important, as it has been demonstrated that bone formation responds differently to different deformation regimes [7]. However, the overall *in vivo* bone deformation during daily activities remains unknown.

Whether bending characterizes the long bone loading is still under debate. A school of thought in the literature proposes that the bending moment should be minimized by the muscular contractions to keep the bone material, especially in the long bones in the body, away from the bending stress accumulation and fracture risk [8-11]. However, an opposite opinion based on the observation of bone curvature speculated that bending should be enhanced by the muscle contractions and the off-axis orientation of the bone to the center of body mass [12]. Using paired strains gauges from opposite surfaces of bone, bending moments have been approximated in mammals or avian species in cases where

limb motion is mainly in a parasagittal plane. Of note, substantial bending has been observed during the different activities [13-17], and in these activities, up to 75-95% of the mid-shaft surface strain was due to bending. However, one can apply paired gauges only where opposing sides of the bone are free of muscles insertion, and such anatomical situations are not available in human long bones. Given that virtually all human long bones offer areas of attachment for muscles, it is likely that the role of bending is becoming even more important, as muscle contractions will induce additional moments. Considering the anatomy of the human tibia, most muscle groups in the human shank insert into the posterior aspect of tibia or fibula (Fig. 2A). Although these muscles work against poor lever arms, they still generate very large flexion moments [18, 19].

In addition to bending, torsion is mostly neglected in scientific discussions, even though it was found to dominate the mechanical loading on the femur and tibiotarsus of the emu during running and gait [20]. Of note, torsion seems to be the main determinant of the design of long bones in birds [20-24]. To date, there is no salient evidence to suggest a strong role for torsional strains in the design of human long bones. However, one would intuitively assume that torsion is the driving loading regime to maintain the almost circular cross-sectional geometry of long hollow bones [25], as it is capable to produce similar bone strain all along the circumference in different sites of the long bone. Results from an *in vivo* knee joint loading study indicated that the tibia-femur contact torsion moment was relatively small, with the peak value ranging from 0.53 %BWM (normalized by body weight times meter) to 1.1 %BWM [26]. However, considering the low capability of bone to resist torsional loading, we hypothesise that the human tibia may experience considerable torsional deformation during walking and running.

Therefore, the goal of the present study was to use a novel optical segment tracking (OST) approach to investigate, for the first time, the regimes of the *in vivo* tibia deformation, including tibia antero-posterior (AP), medio-lateral bending angles (ML) and torsion angles, during most common locomotive activities for humans on the ground, *e.g.* walking and running. Furthermore, the

relationship between the movement speed, ground reaction force, moment and tibia deformation was assessed.

Material and Methods

Five healthy male subjects (26-50 years old) were recruited to participate in this study. They were free of any muscle or joint injury and had not undergone orthopedic surgery in the lower extremities within twelve months prior to the study. Written and oral explanation of the purposes, benefits and risks of the study procedures were given to the subjects at least 3 days before they signed the consent forms. This study had been approved by the two relevant Ethics Committees, namely the ethical committee of the North-Rhine Medical Board in Düsseldorf and the ethical committee of the Faculty of Medicine in the University of Cologne. The operations and experiments were performed at the Department of Orthopedic and Trauma Surgery of the University Hospital of Cologne.

OST approach for tibia deformation measurements

A novel OST approach for tibia deformation recording that has recently been developed by our labs [27] has been adopted in this study. Briefly, three mono-cortical bone screws were partially implanted into the anterior-medial aspect of tibia cortex (Fig. 1B). Onto each bone screw, a marker cluster was mounted with a set of three non-collinear retro-reflective markers ($\varnothing 5$ mm, Géodésie Maintenance Services, Nort Sur Erdre, France, Fig. 1C). The trajectories of the marker clusters were captured at 300 Hz by a Vicon MX optical motion capture system with eight Vicon F40 cameras (Vicon Motion System Ltd., LA, USA) (Fig. 1A). In order to optimize resolution, accuracy and precision, the optical system used in this study included even more cameras than the previous validation study. The optical system was configured in line with our recent recommendations [27]. Recommendations from that study were followed, *i.e.* locating the cameras in the exact position as the mock-up tests, setting the appropriate capture volume and the optimal distance between cameras and the tibia-affixed markers. It can therefore be taken as granted that the performance of the camera system was as good as

or even better than in the mock-up study, meaning a resolution of better than 20 μm within the capture volume of $400 \times 300 \times 300 \text{ mm}^3$ with high accuracy, namely a maximal absolute error of 1.8 μm during displacements by 20 μm and repeatability of 2.5 μm . An in detail error analysis has also been performed in order to estimate absolute distance recording errors as a function of bending angle errors (see Discussion). Prior to the *in vivo* experiments, an *ex vivo* study on measuring tibia deformation under artificial loading in six cadaveric specimens has shown the fair repeatability and the feasibility of the OST approach (Yang *et al.*, in preparation). Briefly, the variance between the repeated tibia deformation measurements using the OST approach was assessed, whilst the cadaveric tibia was loaded by simulated muscle forces with a custom-made static loading device. Results suggested that the standard deviation of the mean bending and torsion deformation angles remained at a low level, from 0° to 0.04° for different loading conditions, indicating its potential to be applied *in vivo*. During the *in vivo* study, the stability of the bone screws in the tibia cortex was assessed by testing the resonance frequency of the screw-cluster structure and the relative position between the marker clusters prior to and after the planned exercises. Prior to and after the exercises, the resonance frequency remained constant, between $\sim 260 \text{ Hz}$ and $\sim 380 \text{ Hz}$, and the small drift between the marker clusters during the course of the experimentation, which was maximally 0.06° , indicated that the implantation of the bone screws was extremely stable [28]. The good toleration to the OST approach by the subjects also indicated its applicability for the *in vivo* measurements [29].

In order to identify the tibia anatomical landmarks, general retro-reflective markers ($\varnothing 16 \text{ mm}$, Vicon Motion System Ltd., LA, USA) were attached on the skin over the medial and lateral malleolus, the tibia tuberosity and over the head of fibula. Prior to each trial of the activities, the trajectories of skin-attached markers were recorded simultaneously with tibia-affixed markers for 1-2 seconds while the shank was in a static position and free of any loading, namely static trial,

for further generating Shank Anatomical Coordinate System (SACS). Tibia deformation was expressed as the relative movement between the tibia-affixed marker clusters in SACS.

Surgical technique

Surgical implantation and explantation of the bone screws was performed under local anesthesia by injecting Xylocain 1% and Carbostesin 0.5% into the skin and the periosteum of the right shank of each subject. Prior to the operation, Ibuprofen (600 mg) and Cefuroxime (1500 mg) had been administered to reduce pain perception and the risk of infection. The thickness of tibia cortex had been determined from transverse MRI (Magnetic Resonance Imaging, 1.5 T, Philips, Best, The Netherlands) images of the shank. To prevent intrusion into the bone marrow, the sites for screw implantation were selected so that the thickness of tibia cortex was thicker than 4 mm. Thus, screws were implanted at approximately 10 cm below the tibia plateau, in the middle of the tibia diaphysis and at approximately 10 cm above the tibia medial malleolus.

Surgical incisions of approximately 1 cm length were made into the skin. A drill guide and a 2.1 mm diameter drill (Stryker Leibinger GmbH & Co. KG, Germany) were used to drill three holes into the tibia cortex to a depth of 2.5 mm. Bone screws (Asnis Micro cannulated titanium screws, Ø3 mm, 24/6 mm, Stryker Leibinger GmbH & Co. KG, Germany) were implanted with a dedicated screw driver. At the end of the experiment, *i.e.* between 6 and 8 hours later, bone screws were removed.

Investigated locomotive activities

All of the subjects wore gymnastic shoes during the experiments. Members of staff were familiarized with the experimental procedure once a week during 6 months preceding the study, and study subjects underwent preparatory training during at least one day prior to the real experiments in order to be fully acquainted with the protocol. Testing included the most common locomotive activities during daily life: (1) walking on a walkway with force plate embedded at self-selected slow, free and fast speed, respectively (Fig. 1A); (2) walking at 2.5, 3.5, 4.5 and

5.5 km/h on a treadmill (Schiller MTM-1500 med, h/p/cosmos sports & medical GmbH, Germany); (3) running at 5.5 and 9 km/h on a treadmill (Two test subjects participated the running test at 9 km/h). At least three repetitions have been performed at each speed of walking on the walkway, and a minimum of sixteen complete walking or running cycles were recorded on the treadmill, respectively.

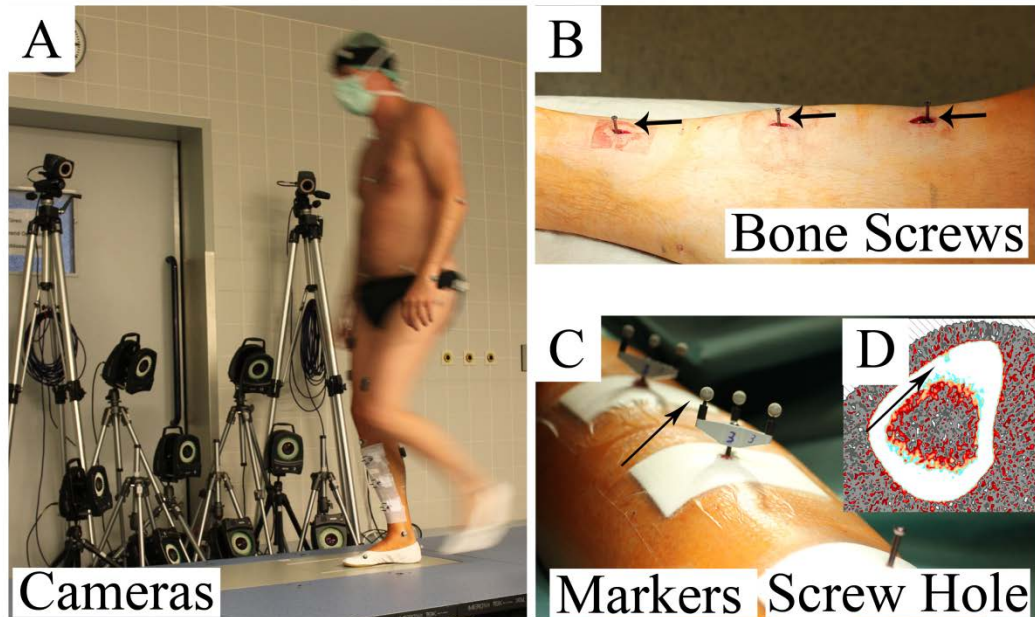


Fig.1. Illustration of the surgical details and the application of the OST approach in this study. A) The optical motion capture system with 8 high resolution cameras to track the retro-reflective markers affixed into tibia cortex, as well as two of the ten cameras for full body motion capturing; B) Implanted bone screws into the tibia cortex; C) Marker clusters were affixed to the endings of the bone screws; D) Cross-sectional pQCT image. The black arrow indicates the hole left behind after removal of the bone screw.

Assessment of speed and ground reaction forces during walking

A second, independent motion capturing system with ten Bonita cameras (Vicon Motion System Ltd., LA, USA) was installed for the assessment of whole-body movement. Two general retro-reflective markers (Ø16 mm, Vicon Motion System Ltd., LA, USA) were attached on the skin of left and right posterior superior iliac spine (PSIS). The trajectories of these two markers were sampled at 100 Hz for all subjects. Ground reaction forces during walking on the walkway were recorded at 1000 Hz with a force plate system (AMTI OR6-5, Watertown, MA, USA). The two motion capturing systems were synchronized by an external trigger.

Peripheral quantitative computed tomography (pQCT) imaging

Horizontal pQCT scans of the tibia on the sites of screw implantation were obtained one to three days after screw removal with a XCT3000 (Stratec Medizintechnik, Pforzheim, Germany) to document the screw holes and geometry of the tibia cross section area for further calculations (Fig. 1D).

Data analysis

Raw marker trajectory data and ground reaction forces were further processed with custom-written MATLAB routines (The MathWorks, Inc. Version 7.9.0 R2009b). The raw marker trajectory data for tibia deformation recording was filtered using a 10 points moving average filter. Ground reaction force data were low-pass filtered using a 2nd order, zero lag Butterworth filter with cut-off frequency at 15 Hz.

Determination of SACS, tibia bending and torsion angles: For each subject, a randomly selected frame from the static trial was utilized for determining an initial Cartesian SACS from the skin-attached tibia landmarks. In the SACS, X, Y and Z axis indicate the anterior-posterior, proximal-distal and medial-lateral direction, respectively [30]. The coordinates of the marker clusters implanted into the tibia were then subjected to coordinate transformation [31, 32] to yield tibia deformation within the SACS. The relative position between each two sets of marker clusters in SACS was then calculated and expressed as mean \pm standard deviation (SD) of three Cardan/Euler angle and three translations along the axis of SACS, respectively. Because the anterior-medial aspect of the tibia is free of muscle insertions, the effect of bone tissue inhomogeneity on anterior-medial tibia surface deformations was assumed to be negligible. AP bending angle, ML bending angle and inter-external torsion angle derived from Cardan/Euler angle were reported as tibia deformation. In the following, the relative movement of the proximal tibia-markers will be presented in relation to distal tibia-markers. Thus, AP bending (Fig. 2B), ML bending and internal-external torsion (Fig. 2C) always indicate the bending and torsion of the proximal tibia with respect to the distal tibia (Fig. 2).

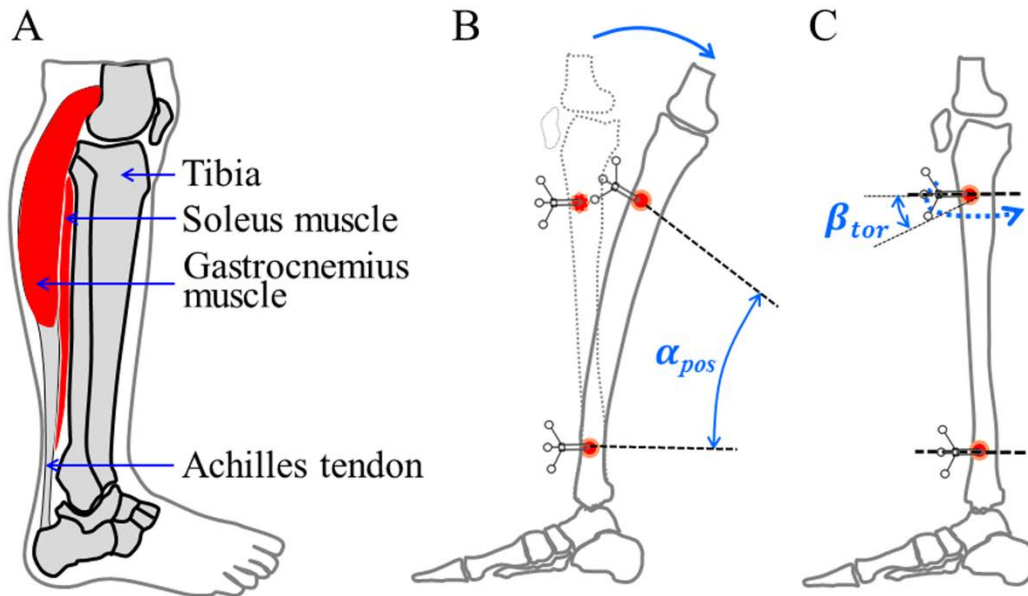


Fig. 2. The anatomy of the human shank and the tibia posterior bending angle and torsion angle. A: anatomy of human shank. B: the demonstration of the posterior bending of the proximal tibia. α_{pos} indicates the posterior bending angle. C: proximal tibia torsion deformation. β_{tor} indicates the internal torsion angle whilst the tibia is twisted.

Calculation of the ground reaction force: Vertical ground reaction force (VGRF) during walking was derived from the filtered ground reaction force. In general, there were two noticeable peaks for the VGRF during walking. These two peak values of VGRF were identified and used for further analysis. Vertical Free moment (VFM) is the torque which acts about the vertical axis through the center of pressure of the ground reaction force. By subtracting the AP moment and the ML moment from the total transverse ground reaction moment, VFM about the vertical axis through the center of pressure of the force plate was determined. The details on the moment calculation can be referred to the ‘Instruction Manual’ of the AMTI Company [33]. VGRF was normalized to body weight (N). VFM was normalized to the product of body weight (N) and foot length (m).

Calculation of walking speed on the walkway: During walking trials on the walkway, the coordinates of the mid-point of two PSIS markers in global transverse plane were extracted from the filtered total trajectories data. The average walking speed of the subjects was determined as the moving distance of

the mid-point of two PSIS markers divided by time over the stance phase of the right leg on the force plate.

Statistics

Statistical analyses were performed using R statistic software (version 2.15.1, R Development Core Team, 2012). Least-squares linear regression was performed to determine the correlation between the tibia deformation angles and the moving speed, VGRF or VFM for individual subject, respectively. The 95% confidence interval for the slope was calculated. Furthermore, a one-way ANOVA linear model was employed to examine the main effects of test subject, moving speed and the type of activities on the tibia deformation angles, respectively. Within-subject effect due to moving speed was assessed with the error analyses in an ANOVA linear model. Statistical significance was accepted at $p \leq 0.05$.

Results

All subjects have performed the planned walking and running without reporting pain or any other complaints. The bone screws were firmly inserted into the tibia until the end the experiments.

Walking on the walkway with force plate embedded

A typical example of the tibia deformation angle during a stance phase of gait cycle is presented in Fig. 3. As the overground walking speed was not strictly controlled and computed after the experiments, the results in Fig. 4-6 provide all data on an individual basis. During the stance phase, there were generally posterior bending, external torsion and medial bending of the proximal tibia with respect to the distal tibia, with posterior bending being most pronounced during the first half, and torsion being predominant during the second half stance phase.

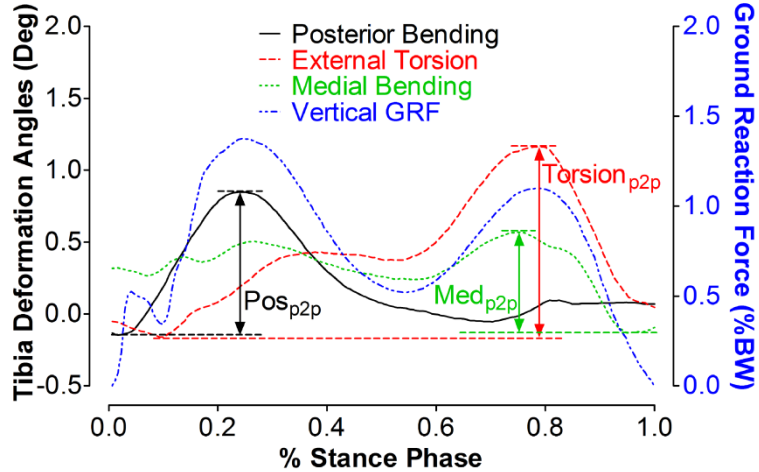


Fig. 3. Illustration of tibia deformation example during the stance phase of a gait cycle with force plate recording. Solid black line: AP bending angle of the proximal tibia with respect to the distal tibia. Dashed red line: torsion angle. Dotted green line: ML bending angle. Dash-dot blue line: vertical ground reaction force. Pos_{p2p} and Med_{p2p} refers to the peak to peak AP and ML bending angle of the proximal tibia, respectively. $\text{Torsion}_{\text{p2p}}$ refers to the peak to peak torsion angle.

Tibia deformation versus walking speed: Statistical analysis yielded main effects of the test subject on the deformation angles ($p = 0.02$ and $r^2 = 0.57$ for tibia AP bending, $p < 0.001$ and $r^2 = 0.09$ for tibia torsion, $p < 0.001$ and $r^2 = 0.03$ for tibia ML bending). There were no significant within-subjects effects due to walking speed ($p = 0.36$ for tibia AP bending, $p = 0.07$ for tibia torsion, $p = 0.1$ for tibia ML bending). Therefore, the correlation analysis between deformation angles and walking speed was done separately for the individual test subjects (Fig. 4). For all test subjects, p2p AP bending angle linearly increased with the walking speed. P2p AP bending angles changed from 0.15° to 1.30° at the speed of 2.5-6.1 km/h. The slope of the regression line was ranged from 0.17 to 0.32 with r-squared value from 0.70 to 0.96 (Fig. 4A). Significant correlations between p2p tibia torsion angles and the speed were found in three of five test subjects. P2p tibia torsion angle changed from 0.67° to 1.66° at the speed of 2.5-6.1 km/h (Fig. 4B). By contrast, p2p ML bending angles were rather small, within 0.38° - 0.90° , and were mostly un-related to walking speed, except for test subject B (Fig. 4C). The linear regression results were summarized in Table 1.

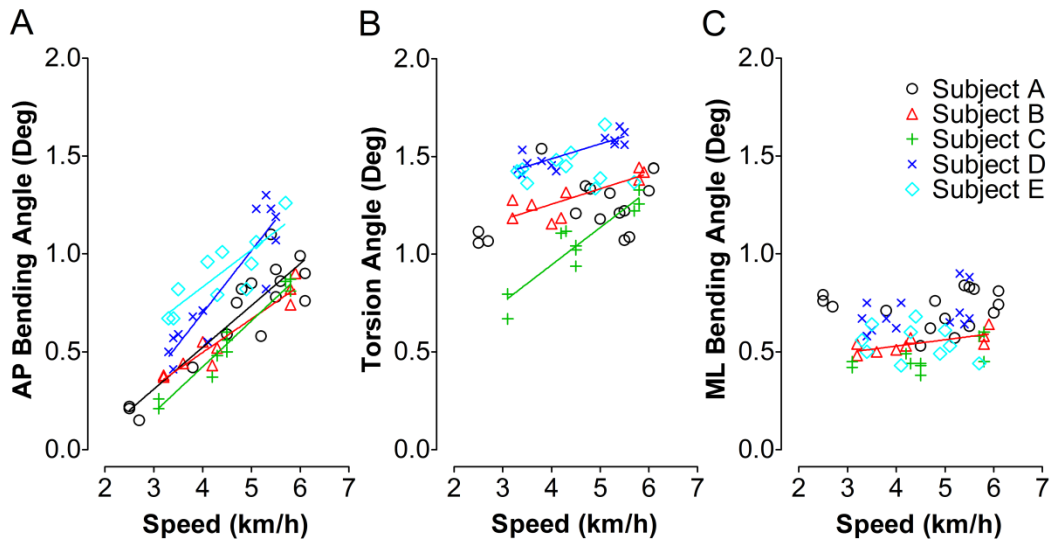


Fig. 4. Illustration of individual tibia deformation data during walking on the walkway in relation to walking speed. The AP bending (A), torsion (B) and ML bending angle (C) indicated the extent of AP bending, external torsion and ML bending of the proximal tibia with respect to the distal tibia. The regression lines were given only when correlation between deformation angle and speed was significant. It can be appreciated from these data that a high correlation exists between overground speed and bone deformation. This is despite the fact that locomotor patterns will contain elements that will not scale linearly with speed, which may underline the validity of the bone deformation measurements.

Table 1 Least-squares linear regression statistics for tibia bending angles versus walking speed. The linear model used is: $y_1 = b_1x_1 + a_1$ (y_1 indicates the tibia bending angles, x_1 indicates walking speed, 95% Confident interval)

Subject	Deformation angles	b_1 (degree*h/km)	a_1 (degree)	r^2	p value	N
A	AP Bending	0.21***	-0.33	0.82	< 0.001	16
	Torsion	0.05	1.02	0.16	0.12	
	ML Bending	7.57e-4	0.72	9.90e-05	0.97	
B	AP Bending	0.17***	-0.19	0.92	< 0.001	9
	Torsion	0.08**	0.94	0.68	0.006	
	ML Bending	0.03*	0.40	0.56	0.02	
C	AP Bending	0.23***	-0.52	0.96	< 0.001	10
	Torsion	0.19***	0.18	0.85	< 0.001	
	ML Bending	0.04	0.28	0.36	0.07	
D	AP Bending	0.32***	-0.58	0.82	< 0.001	13
	Torsion	0.08***	1.19	0.71	< 0.001	
	ML Bending	0.05	0.49	0.19	0.14	
E	AP Bending	0.19**	0.07	0.70	0.0027	10
	Torsion	0.01	1.39	0.01	0.80	
	ML Bending	-0.03	0.67	0.07	0.46	

*: $p < 0.05$, **: $p < 0.01$, ***: $p < 0.001$

Tibia deformation versus ground reaction force: Regression analysis suggested that tibia p2p AP bending angle increased linearly ($p < 0.001$) in relation to the peak VGRF during the first half stance phase, with the slope of the regression line ranging between 1.99 degree*h/km and 2.56 degree*h/km (r^2 : 0.77-0.97, Fig. 5A). By contrast, there was no such relationship between p2p torsion angle and peak VGRF during the second half stance phase, except for subject C ($p < 0.001$, $r^2 = 0.94$, Fig. 5B). Not VGRF, but VFM was correlated with p2p torsion angles four test subjects, except subject A ($p = 0.056$, $r^2 = 0.22$, Fig. 5C). The linear regression results are summarized in Table 2.

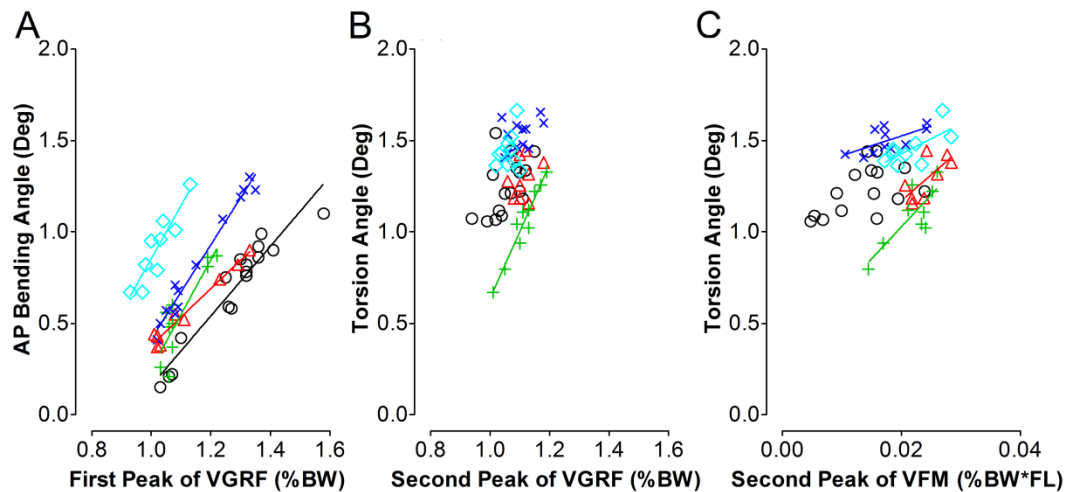


Fig. 5. The relationship between the tibia deformation angles and the VGRF or VFM during walking. A: AP bending angles v.s. VGRF during the first half stance phase of gait. B and C: Torsion angles v.s. VGRF and VFM during the second half stance phase of gait cycle. The regression lines are displayed only where correlations were significant. VGRF: vertical ground reaction force, VFM: vertical free moment:

Table 2 Least-squares linear regression statistics for tibia deformation angles *v.s.* VGRF and VFM. The linear model used is: $y_3 = b_3 x_3 + a_3$ (y_3 indicates the tibia deformation angles, x_3 indicates VGRF or VFM, 95% Confident interval)

Subject	Deformation angles	b_3 (degree*h/km)	a_3 (degree)	r^2	p value	N
A	AP Bending <i>v.s.</i> VGRF	1.91***	-1.75	0.91	< 0.001	16
	Torsion <i>v.s.</i> VGRF	1.34	-0.17	0.24	0.054	
	Torsion <i>v.s.</i> VFM	11.97	1.07	0.25	0.056	
B	AP Bending <i>v.s.</i> VGRF	1.56***	-1.18	0.97	< 0.001	9
	Torsion <i>v.s.</i> VGRF	1.02	0.16	0.11	0.38	
	Torsion <i>v.s.</i> VFM	28.43*	0.60	0.51	0.046	
C	AP Bending <i>v.s.</i> VGRF	2.99***	-2.74	0.77	< 0.001	10
	Torsion <i>v.s.</i> VGRF	3.67***	-3.03	0.94	< 0.001	
	Torsion <i>v.s.</i> VFM	34.91**	0.33	0.66	0.008	
D	AP Bending <i>v.s.</i> VGRF	2.57***	-2.16	0.97	< 0.001	13
	Torsion <i>v.s.</i> VGRF	0.85	0.59	0.21	0.11	
	Torsion <i>v.s.</i> VFM	10.71**	1.31	0.42	0.003	
E	AP Bending <i>v.s.</i> VGRF	2.90***	-2.04	0.84	< 0.001	10
	Torsion <i>v.s.</i> VGRF	1.05	0.33	0.08	0.43	
	Torsion <i>v.s.</i> VFM	16.52*	1.10	0.47	0.04	

VGRF: vertical ground reaction force, VFM: vertical free moment, *: $p < 0.05$, **: $p < 0.01$, ***: $p < 0.001$

Walking and running on a treadmill

During treadmill walking, significant main effects of the test subjects on the AP bending ($p < 0.001$, $r^2 = 0.89$), torsion ($p < 0.001$, $r^2 = 0.85$) and ML bending angle ($p = 0.0046$, $r^2 = 0.62$) were found. Within-subjects effects due to walking speed was not found ($p = 0.24$ for AP bending, $p = 0.37$ for torsion, $p = 0.16$ for ML bending). Therefore, the deformation results are presented on basis of the individual test subject (Fig. 6). The AP bending angle increased with the walking speed (posterior bending angles: from $0.23^\circ \pm 0.03^\circ$ to $0.90^\circ \pm 0.22^\circ$, $p < 0.001$) and running speed (posterior bending angles: from $1.07^\circ \pm 0.11^\circ$ to $2.15^\circ \pm 0.27^\circ$, $p < 0.001$), and, for the same speed, running induced larger AP bending angle than walking (Fig. 6A, $p < 0.001$). No main effects of speed were found on tibia torsion during treadmill walking (torsion angles: from $0.86^\circ \pm 0.10^\circ$ to $1.85^\circ \pm 0.15^\circ$, $p = 0.067$). Interestingly, for four test subjects, tibia torsion during running

was lower than that during walking (Fig. 6B, $p = 0.048$). During the exercises on the treadmill, ML bending occurred on somewhat low levels when compared to bending deformation, and was almost constant across speeds. One exception is that a larger ML bending angle was generated during running at 9 km/h than during running at 5.5 km/h and walking at different speed (Fig. 6C, $p < 0.001$). Tibia torsion of two test subjects responded differently to the running speed. The tibia torsion angle significantly increased for test subject D ($p < 0.001$), but decreased in subject E (Fig. 6B, $p = 0.0013$). The variation across the exercises was assessed by the standard deviation of the deformation angles (Table 3).

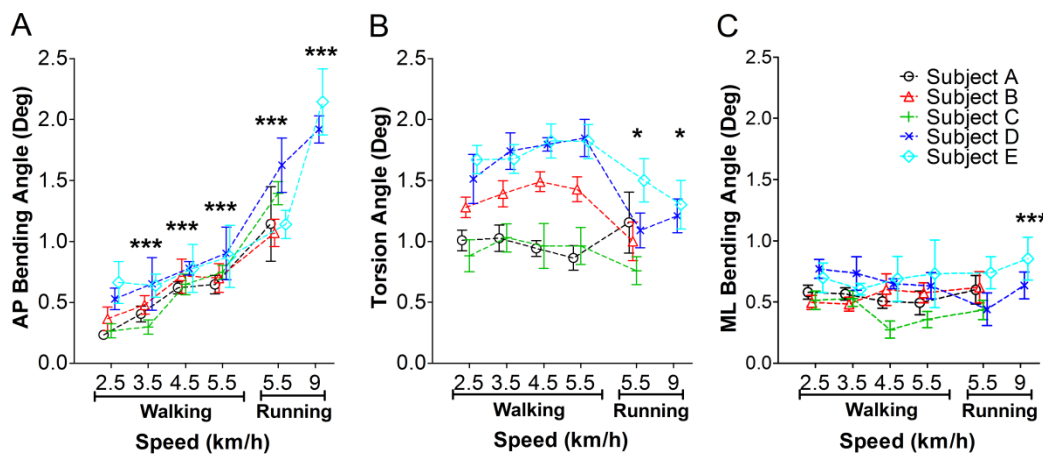


Fig. 6. Tibia deformation angles during walking and running on a treadmill at different speed. A: tibia AP bending angles at different speed of walking and running. B: tibia torsion angle. C: tibia ML bending angle. *: $p < 0.05$; ***: $p < 0.001$.

Table 3 The variation across the walking and running cycles were assessed with the standard deviation (SD) of the deformation angles.

Subject	Exercises	Cycles	SD (Deformation Angles, Degree)		
			AP Bending	Torsion	ML Bending
A	walking	5-19	0.03-0.07	0.08-0.10	0.06-0.12
	running	22	0.31	0.25	0.12
B	walking	22-15	0.10-0.20	0.08-0.13	0.06-0.13
	running	41	0.11	0.16	0.13
C	walking	23-48	0.06-0.08	0.13-0.19	0.06-0.08
	running	30	0.09	0.11	0.08
D	walking	6-39	0.09-0.22	0.05-0.20	0.08-0.14
	running	39-53	0.11-0.22	0.14	0.11-0.13
E	walking	16-39	0.09-0.25	0.12-0.17	0.05-0.25
	running	18-28	0.12-0.27	0.18-0.20	0.13-0.18

Discussion

In this paper, utilizing a novel optical segment tracking (OST) approach, the regimes of the *in vivo* tibia deformation in humans, *e.g.* bending angles, torsion angles of the proximal tibia with respect to the distal tibia, during walking and running were investigated and reported for the first time. Furthermore, the effects of the walking speed and running speed, VGRF and VFM on the bone deformation angles were further evaluated. In addition to the expected result that tibia deformation would generally increase with locomotion speed and with ground reaction forces, this study has yielded a number of novel and less obvious findings. Firstly, and most importantly, bone deformation, almost like a finger-print, contains highly specific personal information. In other words, there were very close relationships found between *e.g.* ground reaction force and tibia deformation within each test subject, but the exact nature of these relationships varied between people. Secondly, the anterior-posterior bending and torsion were the prevailing deformation regimes, whilst medio-lateral bending was much less important. Thirdly, the different tibia deformation regimes did not scale uniformly with locomotion speed or ground reaction force. Each locomotor activity was rather characterized by a variable amount of bending and torsional deformation. Fourth, on the basis of many studies on the bone deformation amplitude in the past, this study provides evidence to revisit the potential importance of deformation regimes and its features during the exercises, *e.g.* walking.

Analysis of recording errors

As with any new method, an assessment of limits for interpretation arising from recording errors is vitally important. We see four major sources of error.

Firstly, the accuracy and the repeatability of the adopted optical system for recording minute marker movement in the targeted 3D volume have to be considered. As outlined above, the accuracy (absolute error) and the repeatability were very favorable within the volume of $400 \times 300 \times 300 \text{ mm}^3$, namely maximum $1.8 \mu\text{m}$ and $2.5 \mu\text{m}$, respectively, to assess displacements by $20 \mu\text{m}$. That error

can be translated in terms of angular deviation (α_{error} in Fig. 7A) with the equations given as follows. The maximum between-marker distance within a marker cluster amounts to 25 mm, and we have to consider accuracy errors at both ends of the marker cluster. Thus, the total alignment error amounts to $2^{1/2} * 1.8 = 2.55 \mu\text{m}$, and the error for estimates of α_{error} is $180^\circ - 2 * \arccos(2.55 \mu\text{m} / 25 \text{ mm}) = 0.012^\circ$ (the calculations of arccos was based on angles, Fig. 7A), α_{error} value that is smaller than reported results by two orders of magnitude.

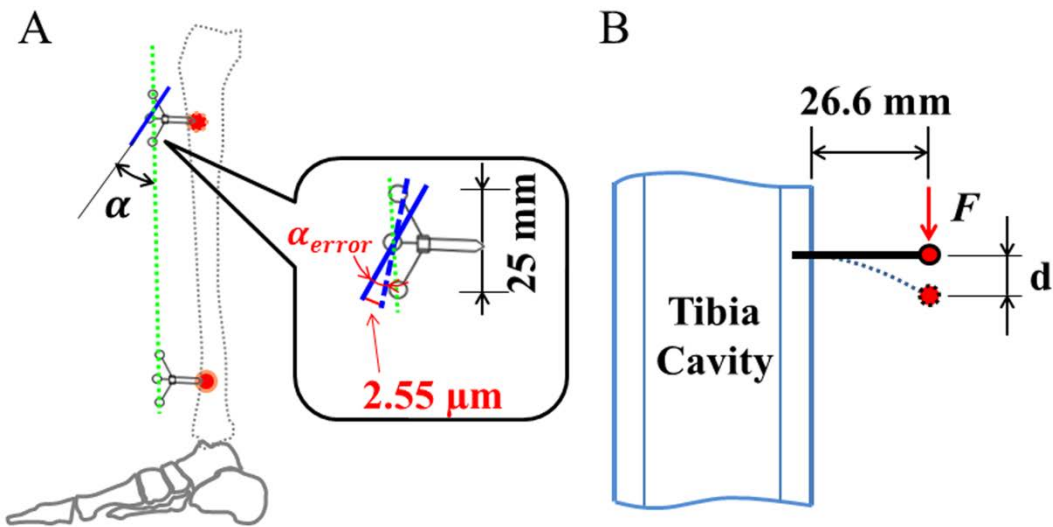


Fig. 7. The recording error analysis of the OST approach. A: the deformation angle deviation α_{error} assumed from the absolute error of $2^{1/2} * 1.8 = 2.55 \mu\text{m}$ for both ends of the markers in the marker cluster. Bold black line referred to the plane determined by three markers in the marker cluster. 25 mm indicated the maximum distance between the markers in one marker cluster. α refers to the angle between the marker clusters. B: the potential marker displacement (d) due to the vibration induced by the acceleration force (F) of the screw/cluster structure. The bold black line refers to the bone screw. The red spot indicates the position of the plane determined by the markers in this cluster. 26.6 mm indicated the distance between the plane determined by three markers in one marker cluster and the bone surface.

Secondly, there is an undeterminable source of error associated with longitudinal variation as per the biological experiment itself. Our experience from the aforementioned *ex vivo* study suggests a reproducibility of approximately 0.04° . This value includes both measurement and experimental-longitudinal variation and is approximately twice as large as the measurement error only, but still substantially smaller than reported results.

Thirdly, we have to consider that the bone screws could have loosened, *e.g.* due to the impact during the locomotor activities. However, the screws were deemed as stable upon removal after exercises had been performed, and both surgeons involved in this study had performed hundreds of materials removals in their surgical practice. Moreover, the constant resonance frequency of the screw-cluster structure and the non-systematic and negligible drift between the marker clusters suggested firm fixation of the bone screws in tibia cortex.

Fourthly, it is possible, in theory, that the marker cluster resonated during locomotor activities and thus produced artificial displacement. However, the vibration amplitude of the screw-cluster structure during the locomotor activities can be assessed with the known characteristics of the marker clusters and following equations, as illustrated in Fig. 7B. The weight of the marker cluster is 5.6 gram, and the most intense exercise, *i.e.* hopping, yielded acceleration of 3.5 times gravity, thus causing a force F of 0.19 N. The distance between the bone surface and the plane determined by three markers in the cluster is 26.6 mm (L), and the bending stiffness (flexural stiffness, *i.e.* the product of elastic modulus and area moment of inertia) of the bone screw shaft is 0.41 Nm² (elastic modulus of the screw material: $E = 110$ GPa, inner and outer diameters of 1.5 and 3 mm, respectively, and thus area moment of inertia $I = 3.73$ mm⁴). Thus potential vibration amplitude of the markers induced by the acceleration of the marker cluster is maximally [34]

$$d = F \times L^3 / (3 \times E \times I) = 2.93 \mu\text{m}$$

Thus, results suggested that the amplitude of any vibration of the screw/cluster structure will relatively small, being certainly smaller than resolution of the optical system, and probably negligible in comparison to reported results.

Main findings on tibia deformation during walking on the walkway

Results from this study showed that the proximal tibia mainly twisted to the external aspect and bent to the posterior aspect, as well as to some extent to the medial aspect with respect to the distal tibia during the stance phase of walking

and running. Previously, the tibia contact force and moment have been investigated with an instrumented knee implant [19, 26]. Those results also suggested that the occurrence of posterior bending moments during the stance phase, medial bending moment during the stance phase and external torsion moment during the second half of stance phase were found during level walking. In line with this, bending and torsion moments have been predicted to occur during walking in a musculoskeletal model calculation [18]. However, the results in our study disagree with previous reports of tibia bending assessed during running by inverse dynamics analysis, in which anterior, rather than posterior tibia bending moments were postulated during the stance phase of running [35]. The inconsistencies may relate to the inherent limitations of the inverse dynamics analysis approach, *e.g.* only joint reaction forces, but not the realistic load on tibia can be calculated from the inverse model. In this context, the present results may provide further, indirect evidence to the view that the largest skeletal forces arise from muscle contractions, rather than from mass acceleration [36].

Another important finding is the non-uniform scaling of deformation regimes. As exemplified in Fig. 3, there were generally two noticeable peaks, one in antero-posterior bending that coincided with heel-strike, and one in torsion that coincided with toe lift-off. This was confirmed by statistical analyses, which suggested that the peak to peak antero-posterior bending angles were linearly correlated with the first peak of the vertical ground reaction force, while peak to peak torsion angle was unrelated to the second peak of the VGRF, but with the peak VFM during the second half of stance phase. Considering the fact that the mechanical load on tibia shaft is generally from body weight and muscle contractions and the plantar flexors are primary active during the second half of stance phase during gait, therefore, it is therefore tempting to assume that the body weight primarily induces the posterior bending of the tibia, while torsion is mainly produced by the plantar flexors contraction. Certainly, further analysis regarding to the relationship between the deformation angles and body weight or muscle activities is needed to draw a firm conclusion.

Effects of walking speed on tibia deformation

During walking on the walkway, tibia antero-posterior bending increased linearly with walking speed, which is congruent with previous bone strain results of numerous of animals, *e.g.* dog tibia, dog radius, horse tibia, horse radius and goat tibia [17, 37]. Similarly, for three test subjects, the torsion angles, not the medio-lateral bending angles, slightly and linearly increased with walking speed. The medio-lateral bending angles remained rather constant with speed. As in overground walking, during treadmill walking, antero-posterior bending increased with speed. Interestingly, for three test subjects, tibia torsion angles increased linearly with walking speed during overground walking, but remained constant during treadmill walking, indicating that the tibia load might be different for these two cases. It has been shown that larger compression and tension strains were generated during the overground running than during the treadmill running [38]. It becomes furthermore evident that the VGRF during the mid- and late-stance phase of treadmill walking differs from overground walking [39], which might be able to explain the deformation difference found in this study.

Relationship between tibia deformation and ground reaction force or moment

The results from this study revealed a strong relationship between the VFM and the tibia torsion deformation for four of the test subjects. It is of interest in this context that VFM seems to be closely related to the loading history of the tibia, and that it is predictive of tibia stress fractures [40]. For VGRF, conversely, the results show that tibia deformation or load could not be totally predicted.

Tibia deformation during running on the treadmill

In general, running is a more demanding exercise than walking. The muscles in the lower extremities are generally more active during running than in walking. Results from this study suggested that the antero-posterior bending angle during running is significantly larger than that during walking, even at the same speed of locomotion (Fig. 6). Despite the limited number of subjects ($n = 2$) participating in the jogging trials at 9 km/h, antero-posterior and medio-lateral bending were still significantly larger than at 5.5 km/h. Conversely, tibia torsion was profoundly

decreased during jogging at 9 km/h, even below levels observed during walking. Previous strain gauges measurements generally found principal tibia strains to be higher during running than during walking. However, no measurements in bending and torsion were made in these studies [3, 41].

Taken all of the above together, results of the present study indicate that not only the amplitude, but even more so the deformation regime within the tibia load differs between running and walking. It has been well accepted that stress fractures in the anterior tibia shaft are common among long distance runners [42]. Our experiment suggests that such stress fractures may be related to the high tension in the anterior tibia, whilst the posterior tibia was under even larger compression. Likewise, an inverse dynamics analysis study on runners indicated that the superposition of the joint reaction force and muscle force magnified the tibia posterior compression and attenuated the tibia shear force [43]. This might be one of the reasons why torsion angles from our measurements were lower during running than during walking.

Limitations

As indicated above, although new knowledge on human tibia deformation was contributed, the OST approach leaves some open questions. Firstly, unlike the strain gauge approaches, the local strain information from one or few spots of tibia surface is missing. A more detailed analysis of the present data will be required to determine the true strain values. Such a high-fidelity estimation or calculation should rely on an inversely-driven Finite Element Model (FEM), with anatomical tibia data – an approach that is by no means trivial. Secondly, the capture volume of the optical system is limited ($400 \times 300 \times 300 \text{ mm}^3$ in this case) in order to maintain acceptable accuracy and repeatability during the deformation recording, meaning that tibia-affixed markers have to be in this volume during the recording trials of the exercises. As a consequence, the types of exercises which can be performed, *e.g.* continuous recording of long term walking (Even for single gait cycle, the full swing phase is not always available due to the restriction of the capture volume) or running over ground, are limited. To summarize, it remains

uncertain in how far the OST approach will be applied widely in future studies, due to its invasiveness. Understanding what can and what cannot be expected from the OST approach will guide the design of future studies, which firstly need to focus on improvement of the OST approach to then further expand its application when justifiable.

Conclusions

In summary, taking together the tibia deformation results from this first application of the proposed OST approach in humans *in vivo*, we conclude that human tibia experiences a considerable amount of bending and torsion deformation during walking and running. The maximum p2p antero-posterior bending, torsion and medio-lateral bending angles reached up to 1.30°, 1.66° and 0.90° during walking, respectively. The tibia antero-posterior bending angles and torsion angles increased linearly with the walking speed and VGRF or VFM. More interestingly, a more or less fixed phase-relationship exists between different types of deformation during the stance phase of walking. Running generates larger antero-posterior bending angles, but smaller torsion angles than walking. These new findings on tibia deformation regimes during walking and running are therefore bound to change our understanding of long bone deformation in humans and provide more insights into the mechanical load distribution rather than mechanical load amplitude alone.

Funding

This research received no specific grant from any funding agency in the public, commercial, or not-for-profit sectors.

Acknowledgments

Great thanks to Peter Gauger, Wolfram Sies, Andreas Kriechbaumer and Jakob Kümmel for their kind help during data collection. We also would like to thank Hans-Martin Küsel-Feldker and Jürgen Geiermannat of the Institute of

Biomechanics and Orthopaedics, German Sport University Cologne, Germany, for fine manufacturing the marker clusters. Peng-Fei Yang acknowledges Helmholtz Space Life Sciences Research School (SpaceLife) and his scholarship by the China Scholarship Council (CSC No.: 2009629013). Last but not least we are very grateful to our test subjects - without their selfless contribution, this work would not have been possible.

References

1. Frost HM (1987) Bone “mass” and the “mechanostat”: A proposal. *Anat Rec* 219: 1-9.
2. Sugiyama T, Meakin LB, Browne WJ, Galea GL, Price JS, et al. (2012) Bones' adaptive response to mechanical loading is essentially linear between the low strains associated with disuse and the high strains associated with the lamellar/woven bone transition. *J Bone Miner Res* 27: 1784-1793.
3. Burr DB, Milgrom C, Fyhrie D, Forwood M, Nyska M, et al. (1996) In vivo measurement of human tibial strains during vigorous activity. *Bone* 18: 405-410.
4. Milgrom C, Finestone A, Simkin A, Ekenman I, Mendelson S, et al. (2000) In-vivo strain measurements to evaluate the strengthening potential of exercises on the tibial bone. *J Bone Joint Surg Br* 82: 591-594.
5. Al Nazer R, Lanovaz J, Kawalilak C, Johnston JD, Kontulainen S (2012) Direct in vivo strain measurements in human bone-a systematic literature review. *J Biomech* 45: 27-40.
6. Yang PF, Bruggemann GP, Rittweger J (2011) What do we currently know from in vivo bone strain measurements in humans? *Journal of Musculoskeletal & Neuronal Interactions* 11: 8-20.
7. Rubin C, Gross T, Qin YX, Fritton S, Guilak F, et al. (1996) Differentiation of the bone-tissue remodeling response to axial and torsional loading in the turkey ulna. *J Bone Joint Surg Am* 78: 1523-1533.
8. Sverdlova NS, Witzel U (2010) Principles of determination and verification of muscle forces in the human musculoskeletal system: Muscle forces to minimise bending stress. *J Biomech* 43: 387-396.
9. Munih M, Kralj A (1997) Modelling muscle activity in standing with considerations for bone safety. *J Biomech* 30: 49-56.
10. Munih M, Kralj A, Bajd T (1992) Bending Moments in Lower-Extremity Bones for 2 Standing Postures. *J Biomed Eng* 14: 293-302.
11. Pauwels F (1965) *Gesammelte Abhandlungen zur funktionellen Anatomie des Be wegungsapparates*. Berlin Heidelberg New York: Springer.
12. Bertram JEA, Biewener AA (1988) Bone curvature: Sacrificing strength for load predictability? *J Theor Biol* 131: 75-92.

13. Biewener AA (1991) Musculoskeletal design in relation to body size. *J Biomech* 24 Suppl 1: 19-29.
14. Biewener AA, Thomason JJ, Lanyon LE (1988) Mechanics of locomotion and jumping in the horse (*Equus*): in vivo stress in the tibia and metatarsus. *J Zool* 214: 547-565.
15. Rubin CT, Lanyon LE (1984) Dynamic strain similarity in vertebrates; an alternative to allometric limb bone scaling. *J Theor Biol* 107: 321-327.
16. Biewener AA, Thomason J, Goodship A, Lanyon LE (1983) Bone Stress in the Horse Forelimb during Locomotion at Different Gaits - a Comparison of 2 Experimental Methods. *J Biomech* 16: 565-576.
17. Rubin CT, Lanyon LE (1982) Limb Mechanics as a Function of Speed and Gait - a Study of Functional Strains in the Radius and Tibia of Horse and Dog. *J Exp Biol* 101: 187-211.
18. Wehner T, Claes L, Simon U (2009) Internal loads in the human tibia during gait. *Clin Biomech* (Bristol, Avon) 24: 299-302.
19. Heinlein B, Kutzner I, Graichen F, Bender A, Rohlmann A, et al. (2009) ESB Clinical Biomechanics Award 2008: Complete data of total knee replacement loading for level walking and stair climbing measured in vivo with a follow-up of 6-10 months. *Clin Biomech* (Bristol, Avon) 24: 315-326.
20. Main RP, Biewener AA (2007) Skeletal strain patterns and growth in the emu hindlimb during ontogeny. *J Exp Biol* 210: 2676-2690.
21. De Margerie E, Sanchez S, Cubo J, Castanet J (2005) Torsional resistance as a principal component of the structural design of long bones: Comparative multivariate evidence in birds. *Anat Rec* 282A: 49-66.
22. Carrano MT, Biewener AA (1999) Experimental alteration of limb posture in the chicken (*Gallus gallus*) and its bearing on the use of birds as analogs for dinosaur locomotion. *J Morphol* 240: 237-249.
23. Judex S, Gross TS, Zernicke RF (1997) Strain gradients correlate with sites of exercise-induced bone-forming surfaces in the adult skeleton. *J Bone Miner Res* 12: 1737-1745.
24. Swartz SM, Bennett MB, Carrier DR (1992) Wing bone stresses in free flying bats and the evolution of skeletal design for flight. *Nature* 359: 726-729.
25. Feldman S, Capozza RF, Mortarino PA, Reina PS, Ferretti JL, et al. (2012) Site and sex effects on tibia structure in distance runners and untrained people. *Med Sci Sports Exerc* 44: 1580-1588.
26. Kutzner I, Heinlein B, Graichen F, Bender A, Rohlmann A, et al. (2010) Loading of the knee joint during activities of daily living measured in vivo in five subjects. *J Biomech* 43: 2164-2173.
27. Yang PF, Sanno M, Bruggemann GP, Rittweger J (2012) Evaluation of the performance of a motion capture system for small displacement recording and a discussion for its application potential in bone deformation in vivo measurements. *Proc Inst Mech Eng H* 226: 838-847.
28. Yang PF, Sanno M, Ganse B, Koy T, Bruggemann GP, et al. (Unpublished)

- results) In vivo application of a novel optical approach for bone deformation recording in humans: a reliability study.
- 29. Ganse B, Yang PF, Bruggemann GP, Rittweger J, Mueller LP, et al. (Unpublished results) An optical approach for in-vivo assessment of human bone deformation using bone screws - surgical experience.
 - 30. Grood ES, Suntay WJ (1983) A joint coordinate system for the clinical description of three-dimensional motions: application to the knee. *J Biomech Eng* 105: 136-144.
 - 31. Soderkvist I, Wedin PA (1993) Determining the movements of the skeleton using well-configured markers. *J Biomech* 26: 1473-1477.
 - 32. Lafortune MA, Cavanagh PR, Sommer HJ, 3rd, Kalenak A (1992) Three-dimensional kinematics of the human knee during walking. *J Biomech* 25: 347-357.
 - 33. AMTI (2004) AMTI biomechanics platform instruction manual. http://ganeshauoregonedu/images/c/c7/Force_Platform_Manual_20pdf Version 2.0.
 - 34. Gere JM, Goodno BJ (2012) Mechanics of Materials CL Engineering. 1152 p.
 - 35. Haris Phuah A, Schache AG, Crossley KM, Wrigley TV, Creaby MW (2010) Sagittal plane bending moments acting on the lower leg during running. *Gait Posture* 31: 218-222.
 - 36. Rittweger J (2007) Physiological targets of artificial gravity: adaptive processes in bone. In: Clement G, Buckley A, editors. *Artificial Gravity*. Berlin: Springer. pp. 191-231.
 - 37. Biewener AA, Taylor CR (1986) Bone strain: a determinant of gait and speed? *J Exp Biol* 123: 383-400.
 - 38. Milgrom C, Finestone A, Segev S, Olin C, Arndt T, et al. (2003) Are overground or treadmill runners more likely to sustain tibial stress fracture? *Br J Sports Med* 37: 160-163.
 - 39. White SC, Yack HJ, Tucker CA, Lin HY (1998) Comparison of vertical ground reaction forces during overground and treadmill walking. *Med Sci Sports Exerc* 30: 1537-1542.
 - 40. Milner CE, Davis IS, Hamill J (2006) Free moment as a predictor of tibial stress fracture in distance runners. *J Biomech* 39: 2819-2825.
 - 41. Milgrom C, Finestone A, Levi Y, Simkin A, Ekenman I, et al. (2000) Do high impact exercises produce higher tibial strains than running? *Br J Sports Med* 34: 195-199.
 - 42. Brubaker CE, James SL (1974) Injuries to runners. *J Sports Med* 2: 189-198.
 - 43. Sasimontonkul S, Bay BK, Pavol MJ (2007) Bone contact forces on the distal tibia during the stance phase of running. *J Biomech* 40: 3503-3509.

CHAPTER 7

**On the relationship between the *in vivo* tibia torsional deformation
in humans and muscle contractions**

The *in vivo* tibia torsional deformation in humans is related to local muscle contractions

Peng-Fei Yang, Andreas Kriechbaumer, Kirsten Albracht, Maximilian Sanno, Bergita Ganse, Timmo Koy, Gert-Peter Brüggemann, Lars Peter Müller, Jörn Rittweger

Manuscript under submission

Abstract

As stated by the mechanostat theory, bone adapts to the experienced bone strains. The largest load on bone is primarily caused by muscle forces, rather than reaction forces. However, uncertainty remains about 1) the consistence of bone deformation regimes, 2) which type of bone deformation is essential to maintain bone structure, and 3) most importantly, what is the role of muscle forces in bone deformation. In this study, utilizing an optical segment tracking technique, the regimes of the *in vivo* tibia deformation in humans were investigated during walking, forefoot and full foot stair ascent, forefoot and rearfoot running, and isometric voluntary plantar flexion. Results suggested that the proximal tibia primarily bent to the posterior aspect, medial aspect and twisted to the external aspect with respect to the distal tibia during the stance phase of walking, running and stair ascent. Peak posterior bending and peak torsion occurred during the first half (21%-22%) and second half (72%-76%) of the stance phase of walking, respectively. Two noticeable peaks of torsion with forefoot contact (38% and 82% of stance phase), but only one peak of torsion with full foot contact (78% of stance phase) were found during stair ascent. The peak-to-peak torsion angle was larger with forefoot contact than full foot contact during both stair ascent ($0.68^\circ \pm 0.02^\circ - 1.08^\circ \pm 0.06^\circ$ vs. $0.90^\circ \pm 0.09^\circ - 1.39^\circ \pm 0.26^\circ$) and running ($1.70^\circ \pm 0.04^\circ$

- $1.79^\circ \pm 0.01^\circ$ vs. $1.15^\circ \pm 0.09^\circ$ - $1.40^\circ \pm 0.14^\circ$). The tibia deformation regimes were characterized more by torsion ($0.62^\circ \pm 0.16^\circ$ - $1.35^\circ \pm 0.07^\circ$) than bending ($0.18^\circ \pm 0.04^\circ$ - $0.52^\circ \pm 0.07^\circ$) during maximum volunteer plantar flexion. To conclude, bending and torsion predominated the tibia deformation regimes during the investigated activities. It thus is speculated that the unexpectedly large torsional deformation might be another candidate, besides the compression and tension, to drive the long bone adaptation. Together with the well-understood related muscle activities during the investigated activities, it seems that tibia torsion deformation is closely related to the local muscle contractions.

Keywords: Muscle contractions; Tibia deformation; Torsion; Optical approach;

In vivo

Introduction

Across different species, *e.g.* tetrapods, avian and humans, the limb long bones are designed to withstand weight and provide the resistance to support the experienced load, bowing to the constraint to minimize the amount of material used. The experienced mechanical loading is one of the dominant influences on bone adaptions to build appropriate architecture. Locomotive activities provoke the long bones to experience various types of loading and lead to very informative bone strains, *e.g.* different strain amplitude, strain rate and frequency [1, 2]. It seems also evident that bone formation is closely related to these strains [3, 4]. Of note, the hollow cylindrical geometry of the limb long bones is perfectly designed to resist bending and torsion, but does not improve the pure axial loading resistance over that of a solid beam. Given the fact that bone hollow morphology has adapted to the experienced mechanical environment, it is therefore reasonable to deduce that torsion, rather than bending, seems to be the primary driving factor to maintain the nearly cylindrical geometry of the long bones [5], as it is capable to produce near uniform strains across the bone shaft. In line with this view, recent *in silico* experiments underline the crucial role of torsion for mechano-adaptation of long bones [6].

However, in contrast to the amount of attention that compression and tension strains have received in literature, the occurrence of torsional strain in the long bone deformation regimes has mostly been neglected. Of note, substantial torsion was observed in the limb bones of lizard and crocodilian, due to the large rotating motion of their femur and tibia during the locomotive activities [7]. It was a surprise, though, when substantial torsion was also found in the femur [8] and tibiotarsus [9] of chicken and the femur and tibiotarsus of emu during overground locomotive activities [10]. It thus seems that torsion is prevalent in the avian limb bones, and even a crucial feature for the design of the wing bones of the flying vertebrates [11]. Likewise, the ratio between torsion moments of femur diaphysis and the ultimate torsional strength remained constant throughout the growing

period of rats [12], indicating that the torsion might be the factor that the femur actually adapts to the growth. To date, the deformation regimes of the long bones, *e.g.* bending and torsion, in another bipedal species, humans, remain utterly unknown. Taking the available evidence together, we hypothesise that torsion is crucially involved in the deformation regimes in human long bones as observed in animals.

Apart from our relative ignorance about the long bone deformation regimes in humans, it is also still unresolved where and how the loads on long bones emerge, especially in the lower extremities [13]. It has been long accepted that muscle contractions, rather than the body weight, contribute the largest voluntary force on the bone, even in the so called ‘weight bearing’ bones [14]. Indeed, evidence also showed the close relationship between muscles and related bones [15] during development [16], growth [17] and in the general populations [18]. Therefore, one can be lead to conceive that bone adapts to the largest strains, and that these are caused by muscle contractions. However, finite element analysis on human femur suggested that muscular contractions would compensate the bending and shear stress accumulation on the bone and prevent the potential fracture [19]. This seems to be confirmed by an *in vivo* tibia strain measurement, in which the authors conceived that larger amplitude of compression and tension strains on the antero-medial aspect of tibia could be generated after muscle fatigue [20]. Therefore, the existing ambiguity about the role of muscle contractions for bone loading warrants more advanced *in vivo* studies.

Accordingly, utilizing the optical segment tracking (OST) approach, the purpose of the present study was to investigate the regimes of the *in vivo* tibia deformation, *e.g.* tibia antero-posterior (AP) bending angle, medio-lateral (ML) bending angle, torsion angle, during walking, forefoot and full foot stair ascent, forefoot and rearfoot running, and isometric plantar flexion. The character of the muscular contractions in tibia deformation regimes was examined by analyzing the phase constitution of the tibia deformation regimes, assessing phase relationship between peak muscle activities and peak tibia deformation, comparing the tibia

deformation between forefoot and full foot stair ascent, forefoot and rearfoot running, respectively.

Materials and Methods

Subjects

Five healthy male participants (26-50 years old) were recruited in this study. They were free of any muscle or joint injury and without any orthopedic surgery in lower extremities at least twelve months prior to the study. Ethical approvals were obtained from both the ethical committee of the North-Rhine Medical Board in Düsseldorf and the ethical committee of the Faculty of Medicine in the University of Cologne. Prior to study participation, written and oral explanation of the purposes, benefits and risk of this study were given to the subjects. All subjects provided written informed consent. The operation and the experiments were performed at the Department of Orthopedic and Trauma Surgery of the University Hospital of Cologne as previously described [21, 22].

The OST approach for tibia deformation recording

Dynamic trials for tibia deformation recording: The OST approach has been recently developed and validated by our lab and was adopted to record tibia deformation in this study [23]. Briefly, three bone screws were partially implanted into the anterior-medial aspect of cortical tibia. A marker cluster, with a set of three non-collinear retro-reflective markers ($\varnothing 5$ mm, Géodésie Maintenance Services, Nort Sur Erdre, France), was then mounted onto the bone screw (Fig. 1A). A specifically configured Vicon MX optical motion capture system with eight Vicon F40 cameras (Vicon Motion System Ltd., LA, USA) was used to capture the trajectories of the markers at 300 Hz (Fig. 1B) with optimized resolution, accuracy and precision [23].

Static trials for reference coordinate system determination: In order to obtain the location of tibia-affixed markers with respect to the anatomical structure of the shank, generic retro-reflective markers ($\varnothing 16$ mm, Vicon Motion System Ltd., LA, USA) were attached with tape on the skin at the position of shank anatomical

landmarks, namely the tip of medial and lateral malleolus, tip of tibia tuberosity and the head of fibula. Prior to each trial of the activities, the trajectories of skin-attached markers and tibia-affixed markers were simultaneously capturing for 1-2 seconds while the shank was in a static position and free of any loading. This is done to further generate the Shank Anatomical Coordinate System (SACS) and calculate the location of tibia-affixed markers in the SACS.

Surgical technique

From the transverse MRI (Magnetic Resonance Imaging, 1.5 T, Philips, Best, The Netherlands) images of the shank, the thickness of tibia cortex was determined. Three sites where the anterior-medial tibia cortex was thicker than 4 mm were selected to implant bone screws, namely at approximately 10 cm below the tibia plateau, mid-site of the tibia diaphysis and approximately 10 cm above the tibia medial malleolus, respectively. Prior to the operation, Ibuprofen (600 mg) and Cefuroxime (1500 mg) were administered for analgesia and to reduce the risk of infection. Screws were inserted under local anesthesia injected to the skin and periosteum with Xylocain 1% and Carbostesin 0.5%. Surgical skin incisions of approximately 1 cm length were made at the previously selected sites. Three holes with a depth of 2.5 mm were drilled into the tibia cortex perpendicular to bone surface by a specific drill guide and a 2.1 mm diameter drill (Stryker Leibinger GmbH & Co. KG, Germany). Bone screws (Asnis Micro cannulated titanium screws, Ø3 mm, 24/6 mm, Stryker Leibinger GmbH & Co. KG, Germany) were implanted with special screw driver. Bone screws were removed at the end of the experiment, typically, between 6 and 8 hours later.

All procedures were well tolerated by the subjects during the whole study. No exercise abnormalities were observed and the bone screws were still firmly implanted at termination of the experiments [22, 24].

Investigated locomotive activities

All subjects wore gymnastic shoes during the experiments. To familiarize themselves with the experimental procedures and the investigated activities, each subject participated in at least two training sessions prior to the *in vivo*

experiments. Tibia deformation was investigated during the following locomotor activities: (1) overground walking on a walkway at self-selected slow, free and fast speed, respectively; (2) walking at 2.5, 3.5, 4.5 and 5.5 km/h on a treadmill; (3) stair ascent with forefoot contact (Fig. 1C) and full foot contact at self-selected comfort speed; (4) Two subjects participated in the running test at 5.5 and 9 km/h with forefoot and rearfoot on a treadmill; (5) isometric voluntary plantar flexion (Fig. 1E). At least three repetitions were performed at each speed of walking on the walkway, stairs ascent and isometric voluntary plantar flexion, and a minimum of sixteen complete walking or running cycles were recorded on the treadmill, respectively.

Whole-body kinematography and ground reaction force recording

Another independent motion capture system (Vicon Motion System Ltd., LA, USA) was used during ground reaction force recording. Ground reaction forces were recorded at 1000 Hz during walking on the walkway and stairs ascent with a force plate system (AMTI OR6-5, Watertown, MA, USA).

Assessment of muscles electromyography (EMG)

Surface electromyography (EMG) of soleus, gastrocnemius medialis (GM), tibialis anterior (TA) and vastus medialis (VM) muscles was recorded using Trigno wireless EMG system (Delsys Inc. Boston, USA). The skin above the selected muscle group was cleaned and shaved. The surface electrodes were then attached above the belly of the targeted muscles with the long axis of electrodes parallel to muscle fibers. EMG signals were recorded telemetrically and sampled at 4000 Hz.

Implementation of isometric contractions

Isometric plantar flexion (Fig. 1E) and dorsiflexion (Fig. 1D) were conducted using a custom-made dynamometer (Fig. 1E). Briefly, two bi-axis force sensors (Tension and Compression Load Cell, Models 8531-2000, Burster praezisionsmesstechnik GmbH & co kg, Gernsbach, Germany) were anchored underneath the walkway and beside an embedded force plate oppositely (Fig. 1E). Few centimeters above the force plate, a box-shaped aluminum frame (Fig. 1D)

was connected to the force sensors to allow the forces transmission from the frame to the force sensors.

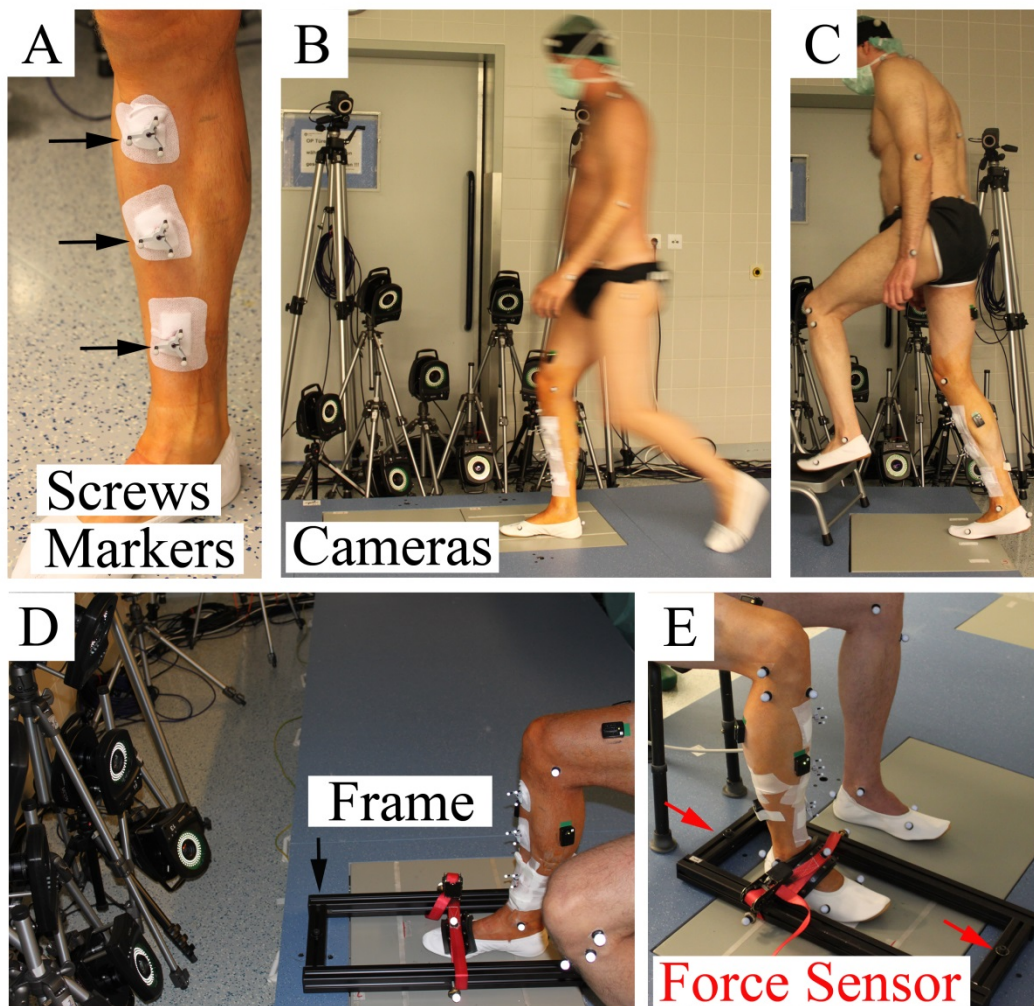


Fig.1. Illustration of the application of the OST approach during different locomotor activities. A: The retro-reflective markers affixed to the tibia cortex with bone screws. The black arrows indicate the three marker clusters. B: The motion capture system with 8 cameras to track the tibia-affixed markers. C: Tibia deformation recording during forefoot stair ascent. D and E: Dorsiflexion and plantar flexion with custom-made dynamometer. The black arrow in D indicates the aluminum frame which was connected to the force sensor underneath the walkway. The red arrows in E indicate the locations of two force sensors underneath the walkway.

Prior to the isometric contraction trials, the subjects were asked to sit on a stool with knee angle of approximate 90° and put their foot within the box-shaped frame and on the force plate. A rigid nylon belt across the aluminum frame was then used to press against the instep side of the subjects' foot while the belt was tightened. The vertical reaction force on the belt was recorded by the force sensors

when the subjects performed isometric plantar or dorsiflexion contractions in the sitting position. The ground reaction forces during isometric contractions were documented by the underneath force plate as a reference.

The signals from the bi-axial force sensors were amplified by an amplifier (In-Line amplifier, Model 9235; Burster praezisionsmesstechnik GmbH & Co Kg, Gernsbach, Germany) and recorded using a PowerLab data acquisition system (PowerLab 8/30, ADInstruments Pty Ltd., Bella Vista NSW, Australia) at 1000 Hz. The two motion capturing systems, EMG system and dynamometer were synchronized by a trigger from the EMG system.

Data analysis

Raw marker trajectory data, ground reaction forces and EMG were further processed with custom-written routines in MATLAB (The MathWorks, Inc. Version 7.9.0 R2009b). The marker trajectory data for tibia deformation recording was filtered using a low pass moving average filter with a span of 10. The results graphs were generated using Graphpad Prism statistical software (version 5.00, GraphPad software, Inc., La Jolla, CA).

Determination of SACS and tibia deformation angles in SACS: Three axes of the SACS, namely X, Y and Z, indicated the antero-posterior (AP) aspects, the long axis of the shank and the medio-lateral (ML) aspects, respectively. A randomly selected frame of coordinate data of the skin-attached landmarks from the static trial was used to determine a Cartesian SACS [25]. From the same frame of the static trial, the relative positions of tibia-affixed markers in the SACS while tibia was free of loading were derived by matrix transformation [26, 27]. Together with the relative movement between the marker-clusters calculated during dynamic trials, *i.e.* three Cardan/Euler rotation angles and translations, the tibia deformation was finally obtained by transforming these relative moments to the SACS. By doing so, the tibia AP bending angles, torsion angles and ML bending angles were then expressed as the Cardan/Eular rotation angles around the Z, Y and X axis in SACS, respectively.

In this paper, the relative movement of the marker-cluster in the proximal tibia in relation to the one in the distal tibia is presented as the tibia deformation. Accordingly, AP bending, torsion and ML bending indicate the bending and torsion angles of the proximal tibia with respect to the distal tibia. Peak to peak (p2p) deformation angles during each of the gait cycle, running cycle, stance phase of stair ascent and isometric contraction were reported. Moreover, considering the specific focus of the presented paper, the phase information of the different deformation regimes during walking was reported in this paper. More specifically, the occurrence time of the peak tibia deformation in terms of the percentage of stance phase was computed.

Ground reaction force and dynamometer force analysis: The ground reaction force data during overground walking and stair ascent were low-pass filtered at 15 Hz using a 2nd order, zero lag Butterworth filter. The force signal from the force sensors was smoothed using a low pass moving average filter with the span of 100. The peak force during the maximum volunteer plantar flexion and dorsiflexion for each subject was identified for further analysis. Vertical ground reaction force (VGRF) was normalized to body mass.

EMG analysis: The raw EMG signal was notch-filtered at 60 Hz, band pass filtered with the pass frequency of 20-500 Hz and then rectified. By using a 2nd order, zero lag Butterworth filter with low pass frequency at 10 Hz, the linear envelope of the EMG signal was obtained. In addition, the maximal EMG of soleus, GM and TA for each subject were determined while the maximum force was produced during the isometric contraction. The amplitudes of soleus, GM and TA EMG during the exercises were normalized to the maximal EMG. During general squats, the amplitude of the VM muscle was normalized to the peak EMG.

Phase analysis between peak EMG and peak tibia deformation: The time delay (unit: milliseconds) between the soleus, GM activities and the peak tibia torsion deformation was further calculated, identified as the time delay between the peaks in the EMG envelope and in the torsion angle within the stance phase, to assess their potential phase relationship and expressed as mean \pm standard deviation.

Statistics

Statistical analyses were performed using R statistic software (version 2.15.1, R Development Core Team, 2012). A one-way ANOVA linear model was employed to assess the main effects of the subject, the type of foot contact during stair ascent and running and the force generation levels of isometric contraction on the tibia deformation angles. A second one-way ANOVA linear model was employed to assess the effects of the subject, walking speed on the time delay between muscle activities and tibia torsion deformation. $P < 0.05$ was considered to be significant.

Results

Tibia deformation during overground walking and treadmill walking

During overground walking, the proximal tibia primarily bent to the posterior aspect and medial aspect, while it twisted to the external aspect during the stance phase of the gait cycle. As illustrated in Fig. 2 A1, the major posterior bending angles were found during the first half stance phase ($22\% \pm 6\%$ of the stance phase), but the major external torsion angles occurred during the second half stance phase ($76\% \pm 3\%$ of the stance phase). Meanwhile, the noticeable peaks of EMG linear envelopes from soleus and GM were found at $64\% \pm 8\%$ and $61\% \pm 10\%$ of the stance phase, respectively (Fig. 2 B1 and C1). The peaks of EMG linear envelop from TA and VM particularly distributed in the initial stance phase of gait cycle (Fig. 2 D1). The time delay between soleus muscle activities and tibia torsion angles was inversely linear related to walking speed (Fig. 3A, $p = 0.04$, $r^2 = 0.32$), but not dependent from the subject (minimum $p = 0.13$). For all subjects, peak EMG of soleus occurred 80 ± 49 ms ahead of peak tibia torsion angle during overground walking. By contrast, no significant effect of walking speed on the time delay between GM activities and tibia torsion deformation was found (Fig. 3B, $p = 0.63$, $r^2 = 0.15$). The time delay between GM muscle activities and tibia torsion angles was also not dependent on the subject (minimum $p = 0.20$).

For all subjects, peak EMG of GM occurred 90 ± 42 ms ahead of peak tibia torsion angle during overground walking.

Likewise, during walking on the treadmill, the peak of the posterior bending angles and external torsion angles were found at $21\% \pm 4\%$ and $72\% \pm 6\%$ of the stance phase for most of walking trials, respectively (Fig. 2 A2). An exception was that the noticeable peak of the posterior bending angles from subject C occurred during the second half stance phase of gait ($76\% \pm 4\%$ of stance phase) at both 2.5 and 3.5 km/h. The peaks of EMG linear envelope from soleus muscle and GM were found at $58\% \pm 12\%$ and $54\% \pm 11\%$ of the stance phase, respectively (Fig. 2 B2 and C2).

A significant effect of walking speed ($p < 0.001$, $r^2 = 0.35$) and subject (maximum $p = 0.012$) on the time delay between soleus muscle activities and tibia torsion angles was found (Fig. 4A). However, walking speed did not affect the time delay between GM activities and tibia torsion deformation was found (Fig. 4B, $p = 0.57$, $r^2 = 0.19$). Except in subject B ($p = 0.018$), there was no significant effect of the subject (minimum $p = 0.11$) on the time delay between GM muscle activities and tibia torsion angles.

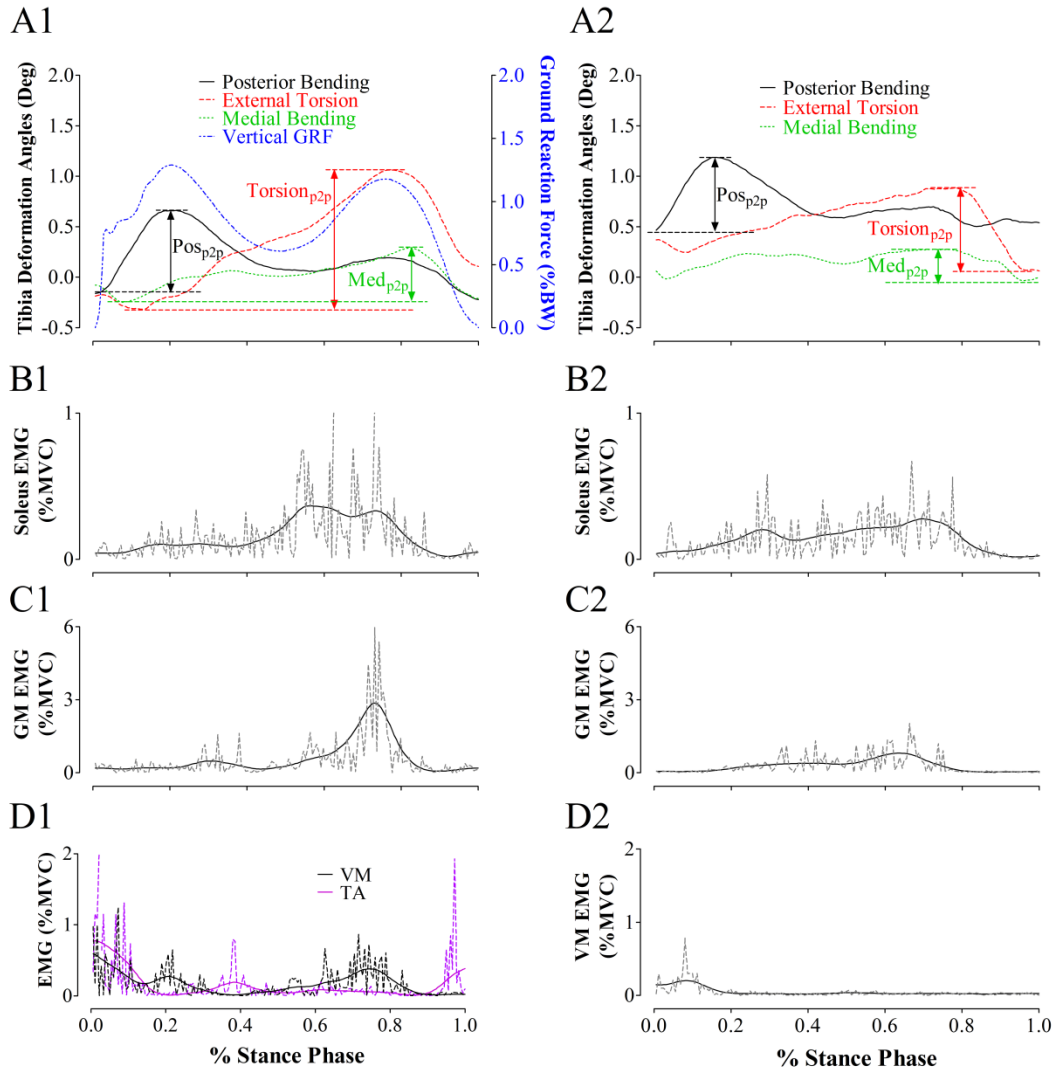


Fig. 2. Illustration of tibia deformation angles, muscle EMG and VGRF during stance phase of overground gait cycle (a trial from test subject B) and treadmill gait cycle (a trial from test subject C). A1-D1: the illustration of tibia deformation angles, VGRF and EMG of soleus muscle (B1), GM (C1), TA and VM (D1) during the stance phase of the overground gait cycle. A2-D2: the illustration of tibia deformation angles and EMG of soleus muscle (B2), GM (C2) and VM (D2) during the stance phase of the treadmill gait cycle. In graph A1 and A2, solid black line: AP bending angle, red dash line: torsion angle, dotted line: ML bending angle, dotted dash line: vertical ground reaction force. $Torsion_{p2p}$: the p2p torsion angle, Pos_{p2p} : the p2p AP bending angle, Med_{p2p} : the p2p ML bending angle. In graph B1-D1 and B2-D2, the gray dash line: the rectified raw EMG signal of the muscles, the solid black line: the muscle EMG linear envelope. GM: gastrocnemius muscle, TA: tibialis anterior, VM: vastus medialis.

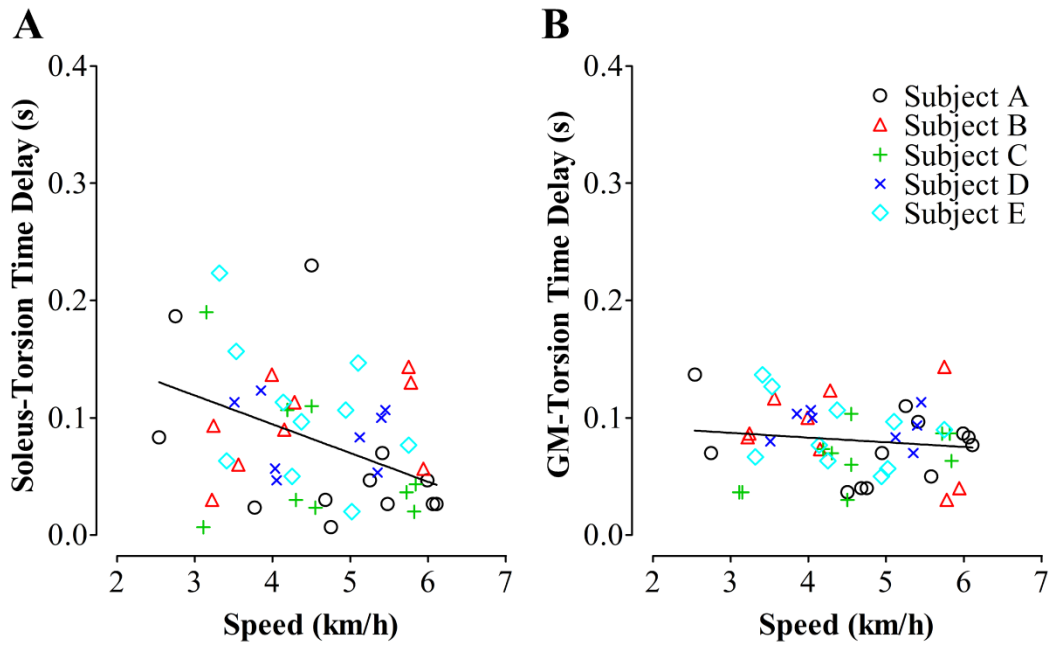


Fig. 3. Time delay between muscle EMG and tibia torsion angles during overground walking. A and B referred to the time delay between soleus EMG, GM EMG and tibia torsion angle. GM: gastrocnemius muscle. As the effects of subject on the time delay was not significant, the regression line of the results from all subjects was plotted.

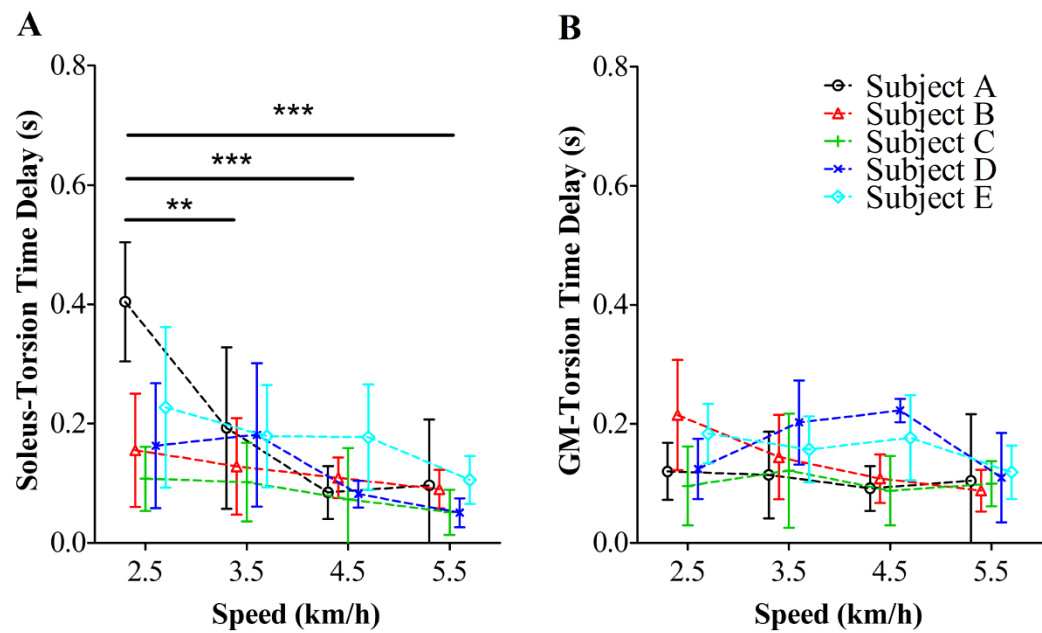


Fig. 4. The time delay between muscle activities and tibia torsion angles during treadmill walking. A: time delay between soleus muscle EMG and tibia torsion angle. B: time delay between GM muscle EMG and tibia torsion angle. GM: gastrocnemius muscle. **: $p < 0.01$, ***: $p < 0.001$

Tibia deformation during stairs ascent

Stairs ascent with full foot contact: Similar to the tibia deformation regimes during walking, the proximal tibia primarily bent to the posterior aspect (p2p AP bending angle: between $0.90^\circ \pm 0.07^\circ$ and $1.48^\circ \pm 0.10^\circ$) and twisted to the external aspect (p2p torsion angle: between $0.68^\circ \pm 0.02^\circ$ and $1.08^\circ \pm 0.06^\circ$) during full foot stair ascent. By contrast, the p2p ML bending angle was rather small, with the angle value ranging between $0.17^\circ \pm 0.05^\circ$ and $0.77^\circ \pm 0.15^\circ$. The proximal tibia tended to bend medially at the initial and mid- stance phase, but laterally at push off stance phase. The most noticeable peaks in the posterior bending angle and external torsion angle occurred at $29\% \pm 3\%$ and $78\% \pm 9\%$ of the stance phase. During the second of stance phase, another second peak posterior bending angle with relatively small amplitude was found at $84\% \pm 4\%$ (Fig. 5 A1). The peaks of EMG linear envelopes from soleus muscle and GM were found at $75\% \pm 15\%$ and $80\% \pm 3\%$ of the stance phase (Fig. 5 B1 and C1). The peak of EMG linear envelopes from TA and VM generally distributed in the initial stance phase (Fig. 5 D1 and E1).

Stair ascent with forefoot contact: The tibia bent to its posterior aspect (p2p AP bending angle: $0.74^\circ \pm 0.24^\circ - 1.75^\circ \pm 0.08^\circ$) and twisted to the external aspect (p2p torsion angle: $0.90^\circ \pm 0.09^\circ - 1.39^\circ \pm 0.26^\circ$) during forefoot stair ascent. The ML bending angle remained relatively small (p2p ML bending angle: $0.22^\circ \pm 0.11^\circ - 0.74^\circ \pm 0.03^\circ$). The major noticeable peak and another relatively small peak of posterior bending angle were found at $28\% \pm 4\%$ and $86\% \pm 6\%$ of the stance phase, respectively. Most interestingly, two noticeable peaks of external torsion angle with near equal amplitude were found in the first ($38\% \pm 9\%$) and second half ($82\% \pm 2\%$) of the stance phase (Fig. 5 A2).

Compared with the muscle activities during full foot stair ascent, two apparent active activity bursts of soleus muscle ($32\% \pm 11\%$ and $80\% \pm 7\%$ of stance phase) and GM ($36\% \pm 10\%$ and $80\% \pm 5\%$ of stance phase) were distinguished from EMG results during the stance phase, respectively. The TA and VM EMG pattern remained only active during the initial stance phase (Fig. 5 B2-E2).

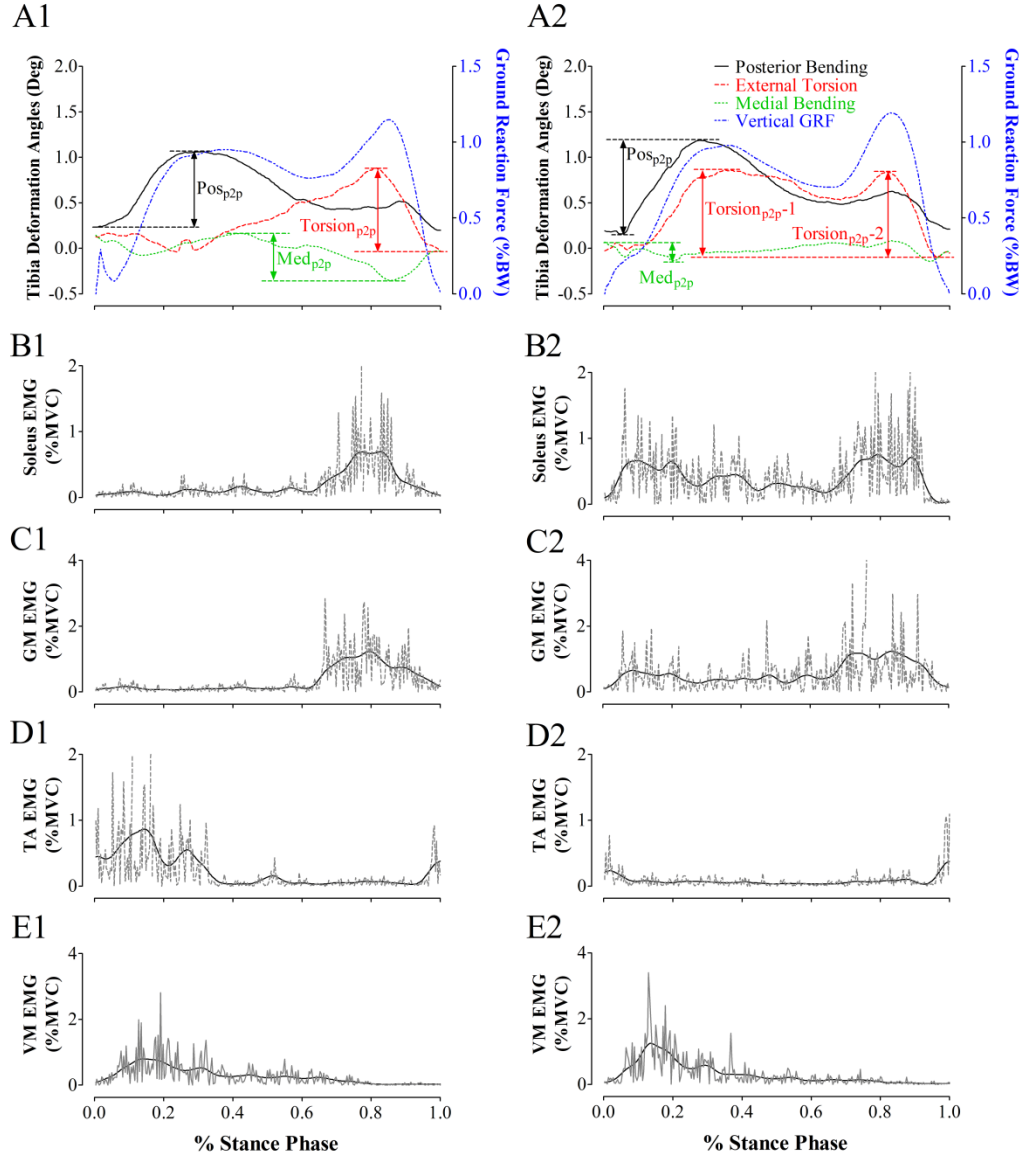


Fig. 5. Illustration of tibia deformation angles, VGRF and the EMG of soleus, GM, VM muscles from test subjects C during the stance phase of full foot (A1-E1) and forefoot (A2-E2) stair ascent. In A1 and A2, solid black line: AP bending angle, red dash line: torsion angle, dotted line: ML bending angle, dotted dash line: VGRF. $Torsion_{p2p}$: the p2p torsion angle, Pos_{p2p} : the p2p AP bending angle, Med_{p2p} : the p2p ML bending angle. $Torsion_{p2p}-1$: the peak torsion angle during the first half stance phase, $Torsion_{p2p}-2$: the peak torsion angle during the second half stance phase. In graph B1-E1 and B2-D2, the gray dash line: the rectified raw EMG signal of the muscles, the solid black line: the EMG linear envelope of the muscles.

Four subjects have participated in the stair ascent tests. Statistical analysis suggested that there was significant main effect of the test subject on the deformation angles (first peak of AP bending angle: $p < 0.001$, first peak of

torsion angle: $p = 0.0014$, first peak of ML bending angle: $p < 0.001$; second peak of AP bending angle: $p < 0.001$, second peak of torsion angle: $p < 0.001$, second peak of ML bending angle: $p = 0.0014$). Therefore, the deformation angles are presented here on basis of the individual subjects (Fig. 6).

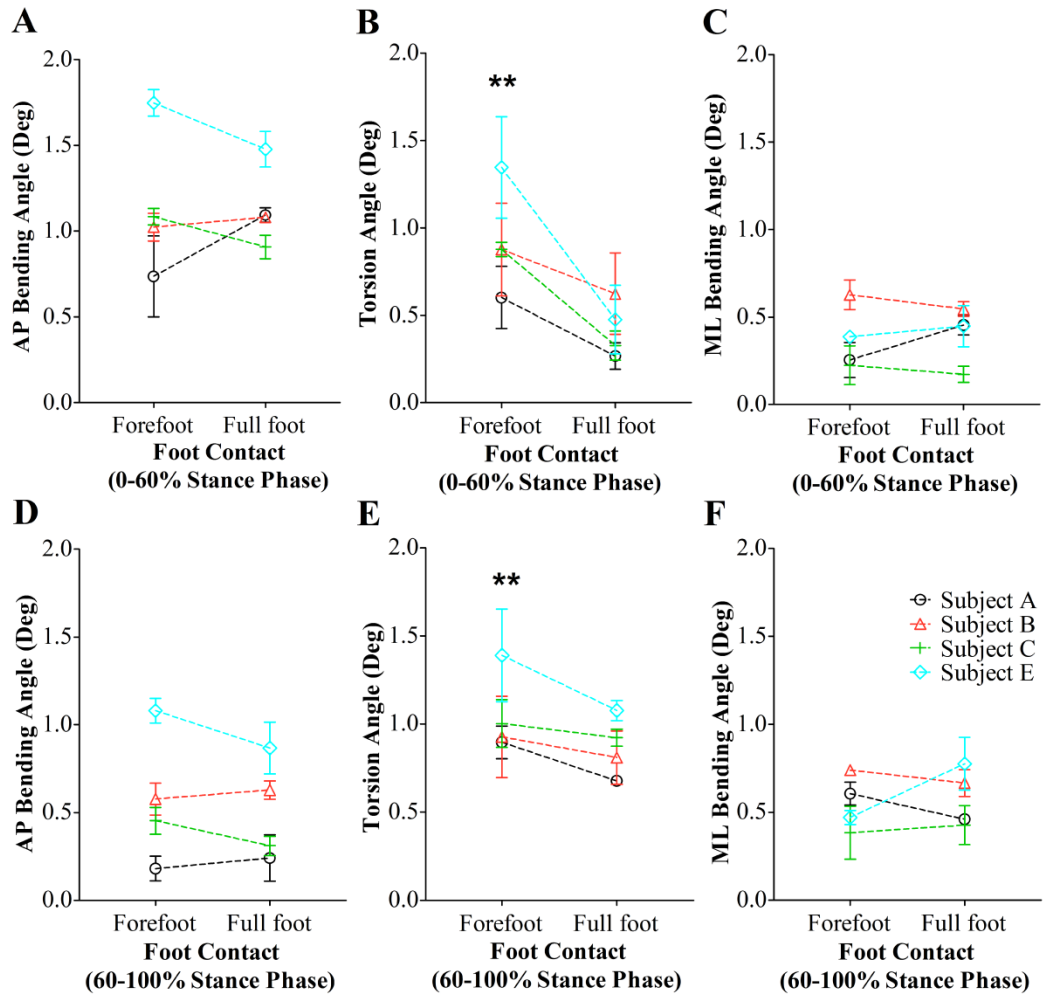


Fig. 6. Tibia deformation angles during the stance phase of forefoot and full foot stair ascent. A and D: the p2p AP bending angle. B and E: the p2p torsion angle. C and F: the p2p ML bending angle. A-C and D-E referred to the tibia deformation angles during the first half (0-60%) stance phase and the second half (60%-100%) stance phase, respectively. **: $p < 0.01$.

The AP bending angle and the ML bending angle varied between the test subjects during forefoot and full foot stair ascent. The torsion angle during forefoot stair ascent was larger than that during the full foot stair ascent, both during the first half stance phase (Fig. 6B, forefoot: between $0.60^\circ \pm 0.18^\circ$ and $1.35^\circ \pm 0.29^\circ$, full foot: between $0.27^\circ \pm 0.08^\circ$ and $0.62^\circ \pm 0.23^\circ$, $p = 0.009$) and during the second

half stance phase (Fig. 6E, forefoot: between $0.90^\circ \pm 0.09^\circ$ and $1.39^\circ \pm 0.26^\circ$, full foot: between $0.68^\circ \pm 0.02^\circ$ and $1.08^\circ \pm 0.06^\circ$, $p = 0.002$).

Tibia deformation during running with forefoot and rearfoot

The illustration of the tibia deformation angles during forefoot and rearfoot running are shown in Fig. 7. Comparable to walking, the tibia primarily bends to the posterior and medial aspect and twisted to the external aspect during the stance phase of running. Soleus and GM were more active during forefoot running than rearfoot running (Fig. 7 B1, B2, C1 and C2).

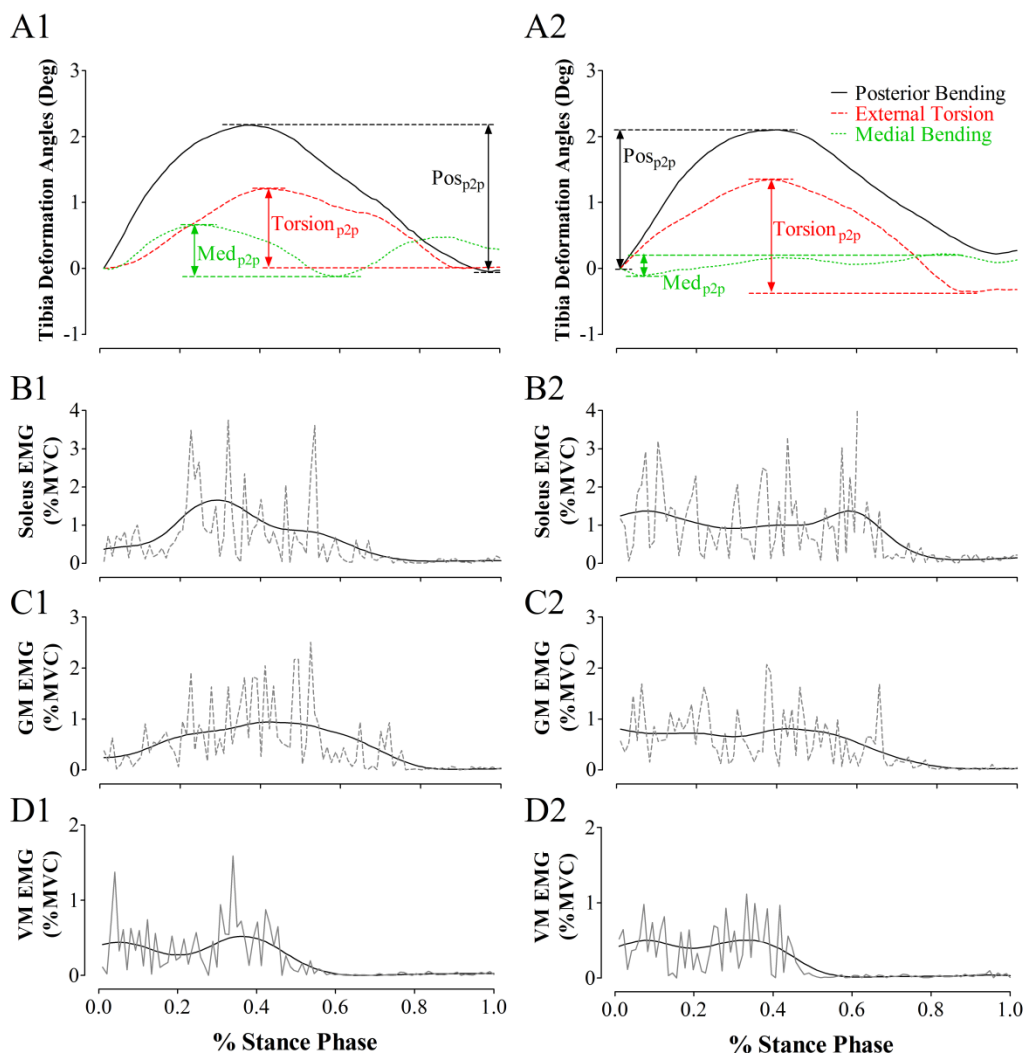


Fig. 7. Illustration of tibia deformation angles and the EMG of soleus, GM, VM muscles during one trial of rearfoot (A1-D1) and forefoot (A2-D2) running cycle from subject E at 9 km/h. In A1 and A2, solid black line: AP bending angle, red dash line: torsion angle, dotted line: ML bending angle. Torsion_{p2p}: p2p torsion angle, Pos_{p2p}: p2p AP bending angle, Med_{p2p}: p2p ML bending angle. In graph B1-D1 and B2-D2, gray dash line: the rectified raw muscles EMG signal. Solid black line: muscle EMG linear envelope.

Statistical analysis suggests significant main effects of forefoot vs. rearfoot running on the p2p AP bending ($p < 0.001$), p2p ML bending ($p < 0.001$) and p2p torsion ($p < 0.001$) angles. Nevertheless, at both 5.5 km/h and 9 km/h speed, tibia AP and ML bending angle during the forefoot and rearfoot running responded differently between two test subjects.

Individual data are presented due to the main effects of the test subject on tibia AP bending angle ($p < 0.001$), torsion angle ($p = 0.02$) and ML bending angle ($p < 0.001$). For Subject D and E, the torsion angle during forefoot running was 55.7% ($1.79^\circ \pm 0.01^\circ$ v.s. $1.15^\circ \pm 0.09^\circ$) and 21.2% ($1.70^\circ \pm 0.04^\circ$ v.s. $1.40^\circ \pm 0.14^\circ$) larger than rearfoot running, respectively (Fig. 8).

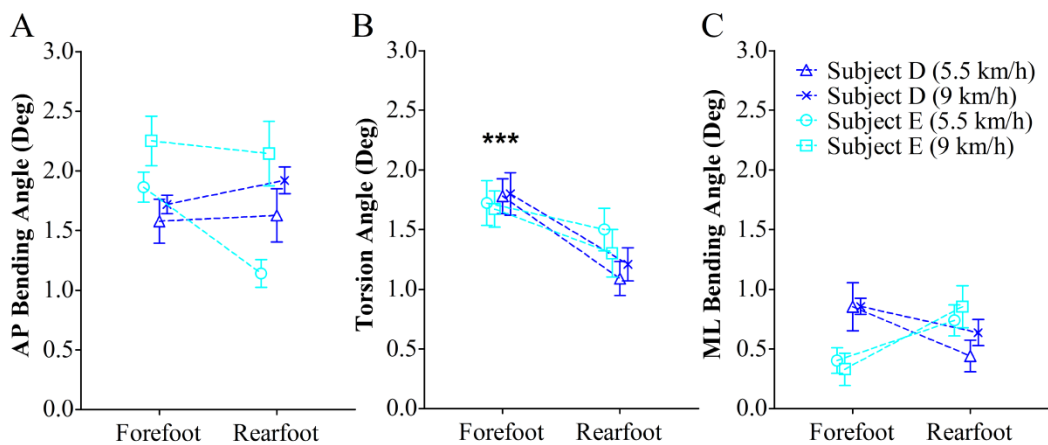


Fig. 8. Tibia deformation angles during forefoot and rearfoot running at 5.5 km/h and 9 km/h from test subjects D and E. A: p2p AP bending angle, B: torsion angle, C: p2p ML bending angle. ***: $p < 0.001$.

Tibia deformation during isometric voluntary plantar flexion

Contrasting with the deformation regimes during walking, stair ascent and running, anterior and lateral bending were found, both during 50% (AP bending angle: between $-0.11^\circ \pm 0.03^\circ$ and $-0.21^\circ \pm 0.03^\circ$, ML bending angle: between $-0.10^\circ \pm 0.02^\circ$ and $-0.29^\circ \pm 0.03^\circ$) and 100% (AP bending angle: between $-0.18^\circ \pm 0.04^\circ$ and $-0.38^\circ \pm 0.03^\circ$, ML bending angle: between $-0.22^\circ \pm 0.06^\circ$ and $-0.52^\circ \pm 0.07^\circ$) maximum isometric plantar flexion. Of note, both bending angles remained on a low level and were in opposite direction compared to locomotion activities. By contrast, torsion did occur with more noticeable magnitude and was external,

as during locomotion, during the 50% (torsion angle: $0.35^\circ \pm 0.00^\circ - 0.74^\circ \pm 0.12^\circ$) and 100% (torsion angle: $0.62^\circ \pm 0.16^\circ - 1.35^\circ \pm 0.07^\circ$) maximum isometric voluntary contraction (Fig. 9).

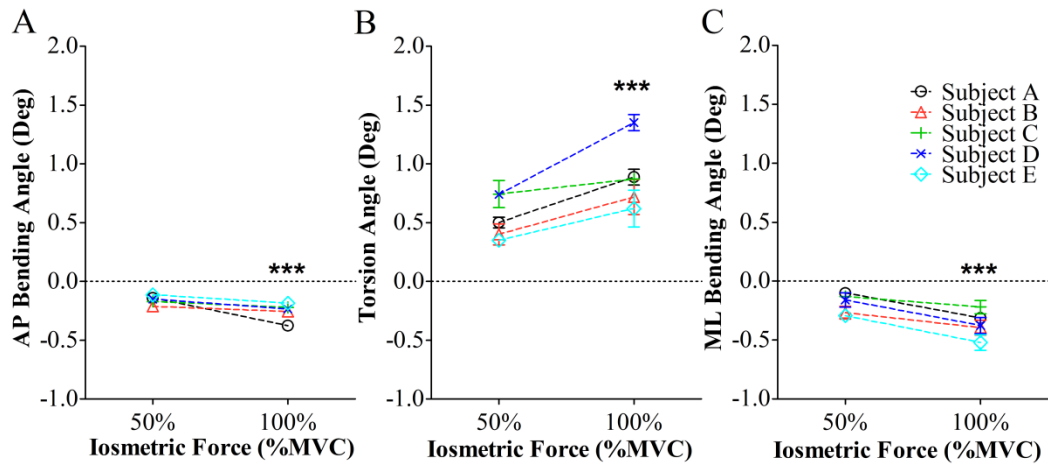


Fig. 9. Tibia deformation angles during 50% and 100% maximum volunteer isometric plantar flexion. A: p2p AP bending angle (negative value indicated the anterior bending). B: torsion angle. C: p2p ML bending angle (negative value indicated the lateral bending).

***: $p < 0.001$.

Discussion

In this paper, the regimes of the *in vivo* tibia deformation and the timing of different deformation regimes in humans have been investigated by an optical segment tracking (OST) approach. Utilizing this novel established OST approach, the bending angles and torsion angles of the proximal tibia in relation to distal tibia in humans were reported for the first time. Most importantly, the character of the muscular contractions in tibia deformation regimes was further assessed by comparing different locomotive activities. Several new findings in the present study were highly relevant to our understanding of ‘muscle–bone interactions’. Firstly, as the most surprising finding, local muscular contractions, *i.e.* from the calf muscle, were closely related to the tibia torsion deformation in the sense of phase relationship during walking. Secondly, as expected, torsion and bending were involved in the total regimes of the tibia deformation during investigated locomotor activities.

Findings from the constitution analysis of tibia deformation during walking

The kinematics, kinetics and muscles activities of the human lower extremities during gait have been extensively investigated in the past and well documented in the textbooks [28]. During the early stance phase of gait, co-contractions of knee extensors and flexors occur until the mid-stance phase to stabilize the knee joint and absorb the shock of the ground impact force from heel strike. From the initial heel contact until the mid-stance phase, the center of mass stays posterior to the tibia, thus resulting in a flexion moment in the knee joint together with the force generated by quadriceps muscles acting on the proximal tibia (Fig. 10A). This flexion moment acting on the tibia may explain the present findings on the posterior bending of the proximal tibia during the first half stance phase. In the mid-stance phase, the whole body mass is supported by the leading leg. The tibia is near vertically oriented and aligns with the center of mass (Fig. 10B). A relatively smaller moment is generated on the proximal tibia at this stage [29, 30]. Through the mid-stance phase, the plantar flexors are acting to stabilize the ankle joint and generate large push off force to provide the propulsion of the body (Fig. 10C). Another large posterior bending moment on the proximal tibia was normally detected with an implanted tibial tray during this stage [29, 31]. Of note, noticeable external torsion, but not posterior bending of the tibia was found during the second half stance phase in the present study. Considering that the knee load observed in previous studies mainly focused on the moment acting on tibia plateau [29, 31], it seems unlikely to reflect the true loading pattern across the tibia shaft. One of the reasons is that the origin of the most powerful muscle of the lower leg, the soleus muscle, inserts in the middle third posterior margin of the tibia. Across the tibia shaft, the posterior bending moment acting on the proximal tibia might be compensated by the moments generated by the soleus muscle contractions. Furthermore, the moments generated by the other plantar flexors, except gastrocnemius, may be another contribution to the attenuation of posterior moment of the tibia during the second half stance phase.

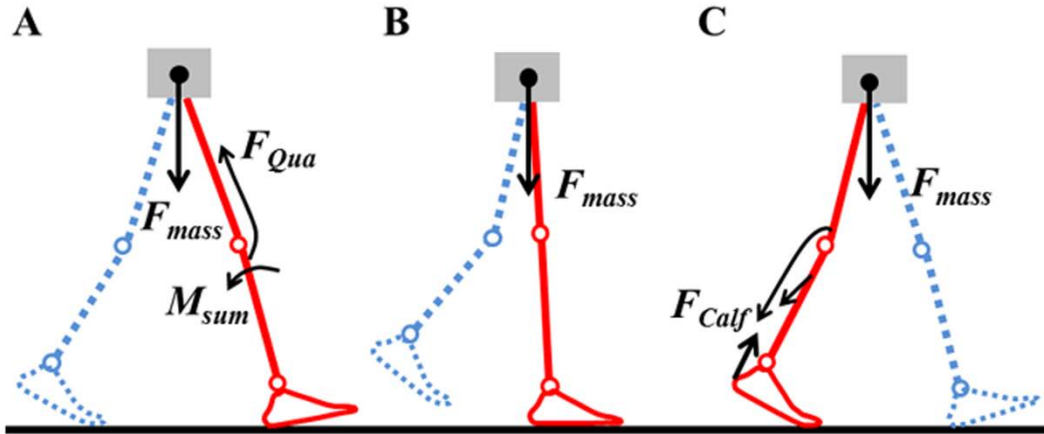


Fig. 10. Illustration of primary forces and moments acting on tibia during the initial (A), mid- (B) and push off (C) stance phase. F_{mass} : the force induced by gravity. F_{Qua} : the force generated by the quadriceps contraction. M_{sum} : the moment generated by both the body weight and the quadriceps contraction. F_{calf} : the force generated by the calf muscle contractions.

Interestingly, the results in the present study clearly showed that the external torsion dominated the deformation regimes of the tibia in the second half stance phase of the gait cycle. One could reasonably speculate that the torsion of the tibia might be produced following the related muscle contractions, *e.g.* primarily gastrocnemius muscle and soleus muscle and the other plantar flexors. As exemplified in Fig. 2, 3 and 4, they were indeed very close timing, but with visible short delay, between the peak tibia torsion angle and the EMG linear envelop peaks of gastrocnemius and soleus muscles. Considering the fact that the force generated by the muscles is transmitted through the aponeurosis and the tendons to bone, the delay between the active state of the muscles and the development of the force has been well known as electromechanical delay [32]. In the present study, the time delay between the peak torsion angle and the peak soleus, gastrocnemius muscle EMG envelope during overground and treadmill walking was assessed. The presented time delay between muscle activities and the tibia torsion deformation was within the expected order of magnitude, albeit slightly longer than the delay (55.5 ms) reported during the concentric contractions of elbow flexors [32], in which electromechanical delay generally indicates the delay between the onset of muscles EMG and the onset of the related

force. However, it should be pointed out that the estimated delay in the present study was congruent with the previous study in which the delay (80 ± 20 ms) between the peak muscle force and apparent peak of EMG from human biceps and triceps [33]. Of note, the presented results indicate that the time delay between soleus activities and the tibia torsion deformation is inversely dependent on the walking speed during overground and treadmill walking. This finding indicates indicating that the time delay, possibly via alterations in electromechanical delay, may depend on the movement speed [34], even though similar relationship was not found in gastrocnemius muscle. More importantly, the reasonable delay between the soleus muscle activities and tibia torsion deformation provides convincing evidence that soleus, perhaps with the other plantar flexors as well, participates in the generation of tibia torsion deformation angle during the second half stance phase of gait.

Evidence from comparisons between forefoot and full foot stair ascent

Stair ascent is a more demanding task than level walking, as larger force or moment to lift the body upwards is needed [35, 36]. Although the forefoot contact is observed on regular basis during the stair ascent, the different foot placement, *i.e.* forefoot contact and full foot contact, represents the active level of the related muscle, mainly the plantar flexors, during the stair ascent. Typically, higher plantar flexion moments are required to keep the heel lifted during the initial stance phase of forefoot stair ascent [36], which also can be confirmed on the soleus and gastrocnemius muscles EMG during the forefoot stair ascent in the present study. On this basis, beside the peak torsion angle during the second half stance phase (at $82\% \pm 2\%$ of gait cycle), another noticeable peak of the torsion angle also was found in the first half of stance phase (at $38\% \pm 9\%$ of gait cycle) during the forefoot stair ascent. Compared to the single peak torsion angle during full foot stair ascent (at $78\% \pm 9\%$ of gait cycle), it can be speculated that muscle contractions truly contributed to the tibia torsion deformation during the first half stance phase of forefoot stair ascent.

Additionally, further evidence from the present statistics results suggests that

larger torsion angle, at both the first half stance phase (0-60% of stance phase) and the second half stance phase (60-100% of stance phase) during forefoot stair ascent, was produced than full foot stair ascent. By contrast, the antero-posterior and medio-lateral bending angle remained unchanged between two different types of foot contact. These results once more supported speculations concerning the relevance of muscle contractions and tibia torsion deformation.

Evidence from comparisons between forefoot and rearfoot running

Previous evidence indicated that runners were able to quickly adapt to the forefoot running from the rearfoot running, as similar kinematics and kinetic patterns of the motion have been found between two types of running [37]. However, plantar flexion force output [38], ankle joint power [39] and ankle joint compliance [40] were increased during forefoot running compared to rearfoot running. This finding suggests that large forces from the plantar flexors are transferred to the tibia during forefoot running. Correspondingly, the present results suggested more active soleus and gastrocnemius muscle activities during the forefoot running. However, it seems that there was no apparent difference on the tibia deformation regimes between both types of running. Of note, for all subjects involved in the running tests, larger torsion was generated during the forefoot running than rearfoot running. Clearly, it can be deduced that greater torsion was contributed by the more active plantar flexors contractions during forefoot running. However, the power to draw a firm conclusion on the speculations in the running tests was limited by the subject number in the present study, and by the lack of precise mechanical information on the tarsus. More evidence to support the mentioned conception is expected from the future studies with a greater number of test subjects and expanded set-up.

Evidence from isometric contractions

Certainly, to assess the contribution of muscle contractions to tibia deformation, loading the tibia only with the related muscle groups would be ideal, although this is rather difficult to achieve such purposes. In the present study, a custom-made dynamometer was adopted to perform 100% and 50% maximum isometric plantar

flexion in absence of axial loading on the tibia from the body weight. The goal of insulating the muscle contractions on the tibia load to the greatest possible extent from the body weight was thus achieved. With the knee angle of 90°, soleus muscle dominates the force generation rather than the gastrocnemius muscle. The present results indicate that anterior bending of the proximal tibia is caused by the passive force pointing anteriorly from the knee joint (F_{pas} , Fig. 11). Most notably, it seems apparent that torsion prevails in the tibia deformation regimes more than the antero-posterior and medio-lateral bending during the 100% and 50% maximum voluntary plantar flexion.

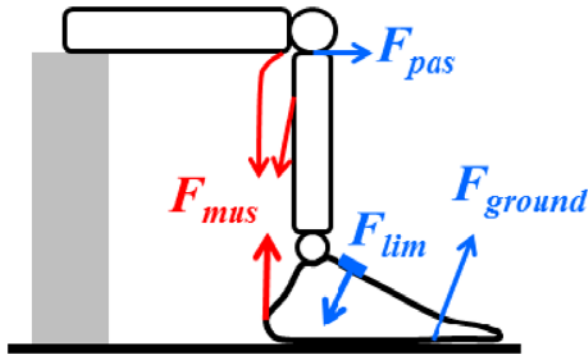


Fig. 11. Illustration of primary forces acting on the lower leg during the voluntary isometric plantar flexion measured with a custom-made dynamometer. F_{pas} : the passive force acting on the proximal tibia generated by the voluntary muscle contractions. F_{lim} : the limitation force from the dynamometer to avoid the movement of the foot during the isometric plantar flexion. F_{ground} : the ground reaction force produced during the plantar flexion. F_{mus} : the force generated by the plantar flexors contractions.

It has been known from tibiofemoral kinematics studies that the tibia segment rotated internally with respect to femur during most of the common exercises. Thus, the external angular momentum acting on the proximal tibia induced by the motion of the adjacent segments of the tibia could also induce external torsion of the proximal tibia, leading the external torsional deformation of tibia shaft. In the presented study, the angular momentum acting on the proximal tibia solely from the adjacent segments was supposed to be similar between forefoot and rear foot running and between forefoot and full foot stair ascent. The contribution of this angular momentum on the tibia torsional deformation can thus be excluded by

comparing the tibia deformation during these exercises. The excessive ACL elongation induced by the excessive internal tibia rotation (motion) might be one of the mechanisms of non-contact anterior cruciate ligament (ACL) injuries [41-43]. Associated with internal tibia rotation (motion), the resistance force or moment from muscle contractions and passive ligament tension force on the knee joint is very likely to cause tibia torsion deformation. Interestingly, previous evidence indicated that the soleus muscle acted as an ACL agonist [44], suggesting that contractions of the soleus muscle may assist to attenuate the internal tibia rotation (motion) by providing an external torque on the proximal tibia and, simultaneously, twisting the tibia externally (tibia external torsion deformation).

Clinically, the results of the present study may help to improve treatment strategies of tibia fractures, not only regarding the stability of osteosynthesis, but also concerning the deformation occurring in bone during different activities. Knowing the deformation patterns caused by different exercises, partial weight-bearing and indications for exercises in physiotherapy could be personalized regarding the deformation caused for the individual type of fracture to decrease the likelihood of malunion. As the present results suggest that tibia torsion is larger in forefoot than in full foot stair ascend and running, it should be considered to limit partial weight-bearing to the full foot in the treatment of tibia fractures.

In summary, the coincidence between the presented results and the previous tibiofemoral kinematics studies again suggests a close relationship between the tibia torsion deformation and the related muscle activities. If this holds true, then it might possible to lead us to develop muscles training protocols to prevent potential ACL injuries or improve treatment strategies in operative fracture treatment as well as physiotherapy.

Conclusions

Taking the *in vivo* tibia deformation results from the investigated activities together, we conclude that considerable amounts of bending and torsion were

involved in the tibia deformation regimes during walking, running, stair ascent and isometric plantar flexion. Posterior bending and torsion were primarily found at 21% - 22% and 72% - 76% of stance phase during overground and treadmill walking. Notably, two noticeable peaks of torsion during forefoot stair ascent (38% and 82% of stance phase) and only one noticeable peak of torsion during full foot stair ascent (78% of stance phase) occurred during stair ascent. Tibia torsion deformation angle with forefoot was larger than with full foot during stair ascent and running. Moreover, the tibia torsion rather than antero-posterior and medio-lateral bending prevailed in the tibia deformation regimes during isometric plantar flexion. In summary, it is reasonable to conclude that muscle contractions are closely related to tibia torsion deformation in humans during locomotor activities. These new findings therefore tend to update our understanding of *in vivo* long bone deformation regimes and may provide new insights to the mysteries of muscle bone interactions.

Funding

Peng-Fei Yang acknowledges Helmholtz Space Life Sciences Research School (SpaceLife) and his scholarship by the China Scholarship Council (CSC No.: 2009629013). This research itself received no specific grant from any funding agency in the public, commercial, or not-for-profit sectors.

Acknowledgments

Great thanks to Peter Gauger, Wolfram Sies and Jakob Kümmel for their kind help during the data collection. Special thanks to Tobias Weber for exchange of ideas to develop the dynamometer of the isometric contractions. We also would like to thank Hans-Martin Küsel-Feldker and Jürgen Geiermannat of the Institute of Biomechanics and Orthopaedics, German Sport University Cologne, Germany, for manufacturing the marker clusters. Great thanks to the subjects participated in this study, which could hardly be well performed without their support and efforts.

Conflict of interest statement

The Authors declare that there is no conflict of interest.

References

1. Turner CH, Owan I, Takano Y (1995) Mechanotransduction in bone: role of strain rate. *Am J Physiol* 269: E438-442.
2. Warden SJ, Turner CH (2004) Mechanotransduction in the cortical bone is most efficient at loading frequencies of 5-10 Hz. *Bone* 34: 261-270.
3. Gross TS, Edwards JL, McLeod KJ, Rubin CT (1997) Strain gradients correlate with sites of periosteal bone formation. *J Bone Miner Res* 12: 982-988.
4. Sugiyama T, Meakin LB, Browne WJ, Galea GL, Price JS, et al. (2012) Bones' adaptive response to mechanical loading is essentially linear between the low strains associated with disuse and the high strains associated with the lamellar/woven bone transition. *J Bone Miner Res* 27: 1784-1793.
5. De Margerie E, Sanchez S, Cubo J, Castanet J (2005) Torsional resistance as a principal component of the structural design of long bones: Comparative multivariate evidence in birds. *Anat Rec* 282A: 49-66.
6. Mittag U, Kriechbaumer A, Rittweger J (Unpublished results) Form follows function: A computational simulation exercise on bone shape forming and conservation. *Anat Rec*.
7. Blob RW, Biewener AA (1999) In vivo locomotor strain in the hindlimb bones of alligator mississippiensis and iguana iguana: implications for the evolution of limb bone safety factor and non-sprawling limb posture. *J Exp Biol* 202 (Pt 9): 1023-1046.
8. Carrano MT, Biewener AA (1999) Experimental alteration of limb posture in the chicken (*Gallus gallus*) and its bearing on the use of birds as analogs for dinosaur locomotion. *J Morphol* 240: 237-249.
9. Judex S, Gross TS, Zernicke RF (1997) Strain gradients correlate with sites of exercise-induced bone-forming surfaces in the adult skeleton. *J Bone Miner Res* 12: 1737-1745.
10. Main RP, Biewener AA (2007) Skeletal strain patterns and growth in the emu hindlimb during ontogeny. *J Exp Biol* 210: 2676-2690.
11. Swartz SM, Bennett MB, Carrier DR (1992) Wing bone stresses in free flying bats and the evolution of skeletal design for flight. *Nature* 359: 726-729.
12. Keller TS, Spengler DM (1989) Regulation of bone stress and strain in the immature and mature rat femur. *J Biomech* 22: 1115-1127.
13. Kohrt WM, Barry DW, Schwartz RS (2009) Muscle forces or gravity: what predominates mechanical loading on bone? *Med Sci Sports Exerc* 41: 2050-2055.
14. Frost HM (2001) From Wolff's law to the Utah paradigm: insights about bone physiology and its clinical applications. *Anat Rec* 262: 398-419.

15. Rittweger J (2008) Ten years muscle-bone hypothesis: what have we learned so far?--almost a festschrift. *J Musculoskelet Neuronal Interact* 8: 174-178.
16. Sharir A, Stern T, Rot C, Shahar R, Zelzer E (2011) Muscle force regulates bone shaping for optimal load-bearing capacity during embryogenesis. *Development* 138: 3247-3259.
17. Zanchetta JR, Plotkin H, Filgueira MLA (1995) Bone Mass in Children - Normative Values for the 2-20-Year-Old Population. *Bone* 16: S393-S399.
18. Rittweger J, Beller G, Ehrig J, Jung C, Koch U, et al. (2000) Bone-muscle strength indices for the human lower leg. *Bone* 27: 319-326.
19. Duda GN, Heller M, Albinger J, Schulz O, Schneider E, et al. (1998) Influence of muscle forces on femoral strain distribution. *J Biomech* 31: 841-846.
20. Milgrom C, Radeva-Petrova DR, Finestone A, Nyska M, Mendelson S, et al. (2007) The effect of muscle fatigue on in vivo tibial strains. *J Biomech* 40: 845-850.
21. Yang PF, Sanno M, Ganse B, Koy T, Bruggemann GP, et al. (Unpublished results) In vivo application of a novel optical approach for bone deformation recording in humans: a reliability study.
22. Ganse B, Yang PF, Bruggemann GP, Rittweger J, Mueller LP, et al. (Unpublished results) An optical approach for in-vivo assessment of human bone deformation using bone screws - surgical experience.
23. Yang PF, Sanno M, Bruggemann GP, Rittweger J (2012) Evaluation of the performance of a motion capture system for small displacement recording and a discussion for its application potential in bone deformation in vivo measurements. *Proc Inst Mech Eng H* 226: 838-847.
24. Yang PF, Sanno M, Ganse B, Koy T, Bruggemann GP, et al. (Unpublished results) In vivo application of a novel optical approach for bone deformation recording in humans: a reliability study.
25. Grood ES, Suntay WJ (1983) A joint coordinate system for the clinical description of three-dimensional motions: application to the knee. *J Biomech Eng* 105: 136-144.
26. Lafortune MA, Cavanagh PR, Sommer HJ, 3rd, Kalenak A (1992) Three-dimensional kinematics of the human knee during walking. *J Biomech* 25: 347-357.
27. Soderkvist I, Wedin PA (1993) Determining the movements of the skeleton using well-configured markers. *J Biomech* 26: 1473-1477.
28. Uustal H, Baerga E (2004) Gait Analysis. In: Cuccurullo S, editor. *Physical Medicine and Rehabilitation Board Review*. New York: Demos Medical Publishing. pp. 409-415.
29. Kutzner I, Heinlein B, Graichen F, Bender A, Rohlmann A, et al. (2010) Loading of the knee joint during activities of daily living measured in vivo in five subjects. *J Biomech* 43: 2164-2173.
30. Wehner T, Claes L, Simon U (2009) Internal loads in the human tibia during gait. *Clin Biomech (Bristol, Avon)* 24: 299-302.
31. Heinlein B, Kutzner I, Graichen F, Bender A, Rohlmann A, et al. (2009) ESB

- Clinical Biomechanics Award 2008: Complete data of total knee replacement loading for level walking and stair climbing measured in vivo with a follow-up of 6-10 months. *Clin Biomech (Bristol, Avon)* 24: 315-326.
32. Cavanagh PR, Komi PV (1979) Electromechanical delay in human skeletal muscle under concentric and eccentric contractions. *Eur J Appl Physiol Occup Physiol* 42: 159-163.
 33. Inman VT, Ralston HJ, De C.M. Saunders JB, Bertram Feinstein MB, Wright Jr EW (1952) Relation of human electromyogram to muscular tension. *Electroencephalogr Clin Neurophysiol* 4: 187-194.
 34. Norman RW, Komi PV (1979) Electromechanical delay in skeletal muscle under normal movement conditions. *Acta Physiol Scand* 106: 241-248.
 35. Costigan PA, Deluzio KJ, Wyss UP (2002) Knee and hip kinetics during normal stair climbing. *Gait Posture* 16: 31-37.
 36. Riener R, Rabuffetti M, Frigo C (2002) Stair ascent and descent at different inclinations. *Gait Posture* 15: 32-44.
 37. McClay IS, Williams DS, 3rd (1998) Lower extremity mechanics in a converted forefoot strike pattern in runners. North American Congress on Biomechanics. University of Waterloo, Waterloo, Ontario, Canada.
 38. Perl DP, Daoud AI, Lieberman DE (2012) Effects of footwear and strike type on running economy. *Med Sci Sports Exerc* 44: 1335-1343.
 39. Williams DS, 3rd, Green DH, Wurzinger B (2012) Changes in lower extremity movement and power absorption during forefoot striking and barefoot running. *Int J Sports Phys Ther* 7: 525-532.
 40. Lieberman DE, Venkadesan M, Werbel WA, Daoud AI, D'Andrea S, et al. (2010) Foot strike patterns and collision forces in habitually barefoot versus shod runners. *Nature* 463: 531-535.
 41. Bellchamber TL, van den Bogert AJ (2000) Contributions of proximal and distal moments to axial tibial rotation during walking and running. *J Biomech* 33: 1397-1403.
 42. Clement DB, Taunton JE, Smart GW, Mcnicol KL (1981) A Survey of Overuse Running Injuries. *Med Sci Sports Exer* 13: 83-83.
 43. Markolf KL, Burchfield DI, Shapiro MM, Shepard ME, Finerman GAM, et al. (1995) Combined knee loading states that generate high anterior cruciate ligament forces. *J Orthop Res* 13: 930-935.
 44. Elias JJ, Faust AF, Chu YH, Chao EY, Cosgarea AJ (2003) The soleus muscle acts as an agonist for the anterior cruciate ligament - An in vitro experimental study. *Am J Sports Med* 31: 241-246.

CHAPTER 8

General discussion and conclusions

General discussion

The main purposes of this thesis are to understand the character of local muscle activities in the *in vivo* bone deformation in humans during different locomotive activities, including walking, running, stair-case negotiation, isometric muscle contraction, and so on. By choosing one of the long bones in humans, namely tibia, as the object, firstly, tibia deformation during different locomotor activities was determined using a novel optical segment tracking (OST) approach based on a motion capture system. Of note, prior to performing the *in vivo* experiments in humans, the OST approach was devised, in order to address important aspects of *in vivo* bone deformation that had been identified as lacking in a review of the existing literature. The OST approach was then established in mock-up tests and in an *ex vivo* study with cadaveric specimens. Next, the typical deformation regimes in the tibia were identified in an *in vivo* study, and finally, their relation to locomotion activities and with local muscle contractions were studied, using electromyography (EMG).

In this chapter, the main findings will be revisited, discussed and summarized, and conclusions shall be drawn from them.

1. Methodological considerations for in vivo bone deformation measurements

Before embarking on the envisioned *in vivo* experiments, we had realized that certain methodological issues should be fundamentally re-considered when recording the tibia deformation *in vivo*, as several open questions still have not been addressed due to the shortcomings of the traditional strain gauge approaches [1, 2], and we wished to gain more profound insights into the matter. The details about the shortcomings of the traditional strain gauge approaches were described in Chapter 2 of this thesis. Briefly, the strain gauge approaches were perceived as unsuitable for our purposes, because it is highly invasive, unable to quantify the bonding quality of the strain gauges or staples in bone, incapable of directly obtaining the bending and torsion bone deformation in humans without disturbing the regular muscle function, and lacking of the segment deformation regimes.

Aiming at resolving these problems and to further our understanding of the *in vivo* bone loading patterns, this thesis presented a less invasive, more informative OST approach based on a commercial motion capture system and demonstrated its first application in an *ex vivo* and *in vivo* study, for which we propose the term ‘optical segment tracking (OST)’.

Instead of measuring the shortening or elongation of the bone surface covered by the strain gauges, the OST approach focusses on capturing the relative movement between markers affixed in the tibia cortex. Thus, the tibia deformation were derived from the relative movement of the markers and expressed in three-dimensional coordinates. The principle of the OST approach for tibia deformation measurements is quite straightforward. As a matter of fact, similar techniques have been applied in many biomechanics studies in the past decades, *e.g.* assessing three-dimensional kinematics of the tibiofemoral joint [3, 4], patellofemoral joint [5] and the relative movement between the foot bones [6] using intracortical pins and the reflective marker clusters. The relative movement between the relevant bones can be expressed simply with three bending angles around the axes and three translations along the axes in a well-defined joint coordinate system [7]. However, the required accuracy of the measurements in these biomechanics studies is generally low. In addition, bone pins can potentially be bent by the muscles, because of the long length of the bone pins and its interference with the muscles, particularly for the bone pins affixed in the femur. As one of the consequences, it is difficult to minimize the recording error.

The contribution of the present thesis to these methodological issues is the substantial improvement of its resolution, accuracy and repeatability by a dedicated configuration of the optical system, by the novel construction of the marker clusters, careful choice of the bone screws and the anatomical sites for screw installation. Of note, by focusing the optical cameras on a relatively small capture volume of $400 \times 300 \times 300 \text{ mm}^3$, improving the quality of the reflective markers and limiting the marker-camera distance, the OST approach is able to achieve a resolution of $20 \mu\text{m}$ with high accuracy (absolute error for $20 \mu\text{m}$ ’s

movement is 1.2-1.8 μm) and precision (standard deviation of the repeated measurements for 20 μm 's movement is 1.5-2.5 μm) [8].

Furthermore, the concept of the OST approach was validated with a cadaveric model. Despite the fact that large variation of tibia deformation was observed – which was probably due to the different loading conditions and mechanical properties of the different cadaveric specimens – well repeatable results across the repeated measurements did demonstrate the feasibility of the OST approach in such measurements.

Eventually, the reliability of the OST approach for the *in vivo* applications was assessed during the *in vivo* experiments in humans. In particular, the stability of the screw-cluster structure across high intense exercises, *i.e.* hopping and jumping, and the repeatability of the tibia deformation recording during squatting exercise were evaluated. Results suggested that the resonance frequency of the screw-cluster structure remain unchanged at approximately 260 Hz and 380 Hz prior to and after more than 30 hopping cycles and 6 times jump cycles. The changes of the relative position between the marker cluster after these intense exercises was low, maximally 0.06°. The variability of the tibia deformation angles, including antero-posterior bending angle, medio-lateral bending angle and internal-external torsion angle, between the repeated squatting exercise remained relatively small, between 0.02° and 0.18°. More significantly, the high correlation (coefficient of determination in the linear regression is maximally 0.96) between the speed and tibia deformation during overground walking eliminated all remaining doubts about any unreliability of the OST approach.

Apart from the noticeable technical reliability of the OST approach discussed above, the subject compliance was another crucial issue which must be considered carefully. Before the *in vivo* experiments, pain by the installation of the bone screws into the tibia cortex was deemed as the most important difficulty. However, no subject complained about pain, neither during nor after the experiments. The operations and the experiments were conducted in an operation theater to reduce the potential infection risk, even though the risk was minimized by leaving the

bone cavity closed during the screw installation. There were some difficulties in the very first experiment, in which bleeding called for interruption of the experimental protocol. Accordingly, a different bandaging technique was used in the subsequent experiments to prevent bleeding from penetrating, and it was also possible to reduce the amount of bleeding itself by injecting a smaller dose of local anesthetic than in the first experiment. With these precautions, all experiments could be carried out without any difficulty or inconvenience for the subjects.

Taking these results together, we have convinced ourselves that the OST approach has remarkably good reliability, and that it was surprisingly well tolerated by the subjects during the *in vivo* experiments. It is convicive, therefore, to conclude that the OST approach is capable of being applied in such studies and will lend itself to greater application areas of bone physiology, from biomechanics studies to the clinical studies on the bone fracture and osteoporosis patients.

2. *Tibia deformation during human locomotion activities*

The major discussion about the findings of tibia deformation during walking and running was well documented in Chapter 6 and 7. As mentioned, the tibia deformation were expressed as the bending angles and torsion angles in this thesis due to the unique features of the OST approach.

Considering that walking is one of our most common physical activities, mechanical loading caused by walking ought to be a major component of daily loading for the lower extremities. Hence, this thesis firstly focused on the understanding of tibia deformation regimes during walking. It was found that bending, especially posterior bending, and external torsion of the proximal tibia characterized the tibia deformation regimes. Besides, there was a specific phase relationship between the peak bending and torsion components during the stance phase of the gait cycle. More specifically, the peak posterior bending and the external torsion primarily occurred during the first half stance phase (~22% of the stance phase) and the second half stance phase (~76% of the stance phase), respectively, which coincide with the timing of the well-known second vertical

ground reaction force peak and the free moment peak during the stance phase of walking. In line with this finding, peak posterior bending moment and external torsion moment on the proximal tibia with the similar phase features were observed by an instrumented knee implant during the level walking [9], indicating that the moment or force from the tibiofemoral joint may be a source of tibia load during walking.

Likewise, congruous tibia deformation regimes were found during full foot stair ascent. The difference is that the antero-posterior bending angle amplitude during the full foot stair ascent seems to be larger than walking at most of the investigated speed. This can be explained by the different kinematic and muscle activities. As indicated in Chapter 7, during the first stance phase of stair ascent, the quadriceps muscle group remains active to stabilize the knee joint, meaning that the quadriceps muscle may greatly contribute to the posterior bending moment to the proximal tibia through patella tendon, but this does not occur during walking.

Tibia deformation regimes during running were clearly different from walking and stair ascent. The unavailability of the ground reaction force during running leads to some difficulties in understanding the responses of tibia deformation to ground reaction forces. However, the single peak antero-posterior bending and torsion angle did coincide with the well-known single major peak of the vertical ground force. Larger antero-posterior bending angles during running than during walking and stair ascent were found in the present study. This is not surprising, given that running is more demanding than the walking and stair ascent. These findings were also supported by previous bone strain studies with strain gauge approaches [10, 11].

In the respect of the unavailability of the tibia strain results across tibia shaft, the tibia deformation regimes presented in this thesis seem to be more suitable as a surrogate to further our understanding of tibia internal loading pattern during the different locomotive activities. The dominating posterior bending results of tibia shaft during all investigated exercises in this thesis suggested that the anterior and

posterior tibia cortex are primarily under tension and compression, respectively, meaning human tibia is mostly experiencing the bending in one direction. The congruent findings in the long bones of the animal legs, *e.g.* horse radius, were documented previously [12-14]. Given the fact that bones adapt to the loading patterns they are subjected to, the results from this thesis may give new insights that explain the triangular geometry of the tibia cross section area. On the other hand, the slight anterior curvature of human tibia would amplify the posterior bending of tibia when it is under any longitudinal loading [15]. The evidence from this thesis quantitatively supports the previous explanation about how the long bone curvatures can help to avoid the development of microfracture, namely it is better for bones to be loaded in one mode rather than a mixed pattern [16].

To summarize the findings in *in vivo* tibia deformation angles and to make comparisons among the subjects, different activities and different deformation regimes, an overview of tibia deformation was presented in Fig. 1. Owing to the rather low amplitude of the medio-lateral bending angle (when compared to other types of deformation), the antero-posterior bending angle and torsion angle during the investigated activities were presented in Fig. 1. The summarized results intuitively suggested that the running, particularly the full foot running, has the potential to induce largest torsion and antero-posterior bending deformation. By contrast, the gait at 5.5 km/h induced relatively small amount of the antero-posterior bending angles. Certainly, according to the presented results in Chapter 6, gait at lower speed would generate even smaller amounts of tibia deformation. As stated by the ‘mechanostat’ theory, bones adapt to the maximum forces experienced during a long process. Although the ‘mechanostat’ may not provide the comprehensive, quantitative models, it can still guide our reasoning in an intuitive way to explain the mechanical adaptation of bone. In this sense, the presented results in this study can provide some insights on the recommended daily exercises to benefit the bones. If the ‘mechanostat’ theory holds true, *i.e.* the bones adapt to the largest load it experienced, the presented results suggest that forefoot running should be one of the most important exercises which will build

the most resistant bones, despite the fact that the importance of different bone deformation regimes on bone adaptation still remains largely unexplored.

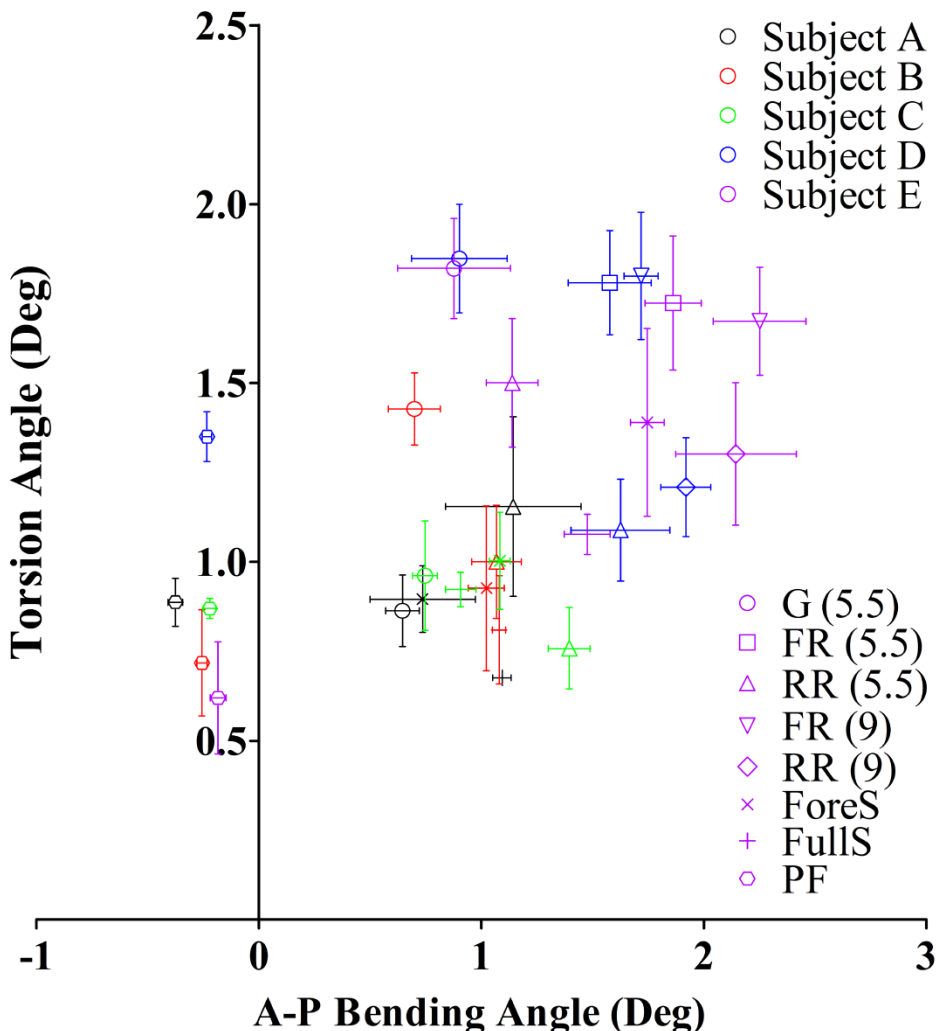


Fig. 1. Tibia antero-posterior bending angle *versus* torsion angle during different locomotive activities. G (5.5): gait at 5.5 km/h. RR (5.5): rear foot running at 5.5 km/h. RR (9): rear foot running at 9 km/h. FR (5.5): forefoot running at 5.5 km/h. FR (9): forefoot running at 9 km/h. ForeS: forefoot stair ascent. FullS: full foot stair ascent. PF: maximum volunteer plantar flexion.

3. How do local muscles contribute to tibia deformation?

Finally, and to respond to the question raised in Chapter 1 about the contribution of the muscle forces on the tibia deformation, the relationship between the muscle activities, mainly the calf muscles, and the tibia deformation angles was investigated by the comparisons between different functional exercises. The major discussions on the related findings were documented in Chapter 7.

The great challenge to assess *in vivo* muscle forces leads to the difficulties of quantitatively understanding the contribution of muscle activities to the *in vivo* tibia loading or deformation. In this thesis, muscle surface EMG was employed as an indirect indication of the muscle forces, even though there are still enormous disputes about whether muscle EMG could completely represent muscle force [17]. More importantly, the characters of the muscle activities on tibia deformation were studied primarily by comparing the tibia deformation regimes between the low and high intensity of the calf muscle contractions, namely full foot stair ascent *v.s.* forefoot stair ascent and rearfoot running *v.s.* forefoot running. Quite unexpectedly, not all of the tibia deformation regimes were associated with the calf muscle activities. The antero-posterior bending angles did not respond to the state of calf muscle activities during stair ascent and running. In contrast, the torsion amplitude and pattern were significantly changed by the muscle activities during both exercises. It is more obvious that tibia torsion pattern is different due to the muscle activities. Of note, the association between muscle activities and tibia torsion deformation presented in this thesis rely on their phase or timing relationship. Quantitative relationship has to be dealt with in the future studies as a direct continuation of the present work. Beyond that, the phase or timing of the tibia deformation angles during walking was thoroughly studied. Once again, the close timing between the peak torsion angle and peak EMG indicated the potential relationship between the calf muscle activities and the tibia torsion deformation. On the other hand, the other muscle groups of human body may produce considerable angular momentum on the investigated shank when they generate force to move the body to walk, but great cancelation of the angular momentum between the adjacent segments *i.e.* between foot and shank, or between shank and the thigh, may eventually yield low level of angular momentum acting on tibia [18]. Moreover, the soleus muscle is actually contributing to the whole body angular momentum to move the body forward during the late stance phase [19]. This leads us to accept more confidently that local muscles greatly contribute to the tibia torsion deformation. Future studies may focus on the computation of the

angular momentum induced by the dynamic movement of the human body, thus finally isolating the contributions of the calf muscle activities and angular momentum induced by the other muscles to the tibia deformation.

Another interesting observation relates to the tibia deformation regimes during the isometric plantar flexion, which is conceived as a pure muscle loading acting on tibia. Results suggested that torsion predominated the tibia deformation regimes. In contrast, the bending deformation remained on a very low level, and they were in the opposite direction as during locomotion. In this respect, muscular contributions to bone loading must be movement-pattern specific. Regardless, our findings clearly indicated that the capability of the plantar flexors to generate tibia torsion deformation. Irrespective of the differences between the locomotor activities and the isometric condition, *e.g.* the way of recruiting muscles, the lever arm of the tendons, the appreciable linear relationship between the detected external forces and the tibia torsion angles still suggested the possibilities to predict the tibia deformation from the external forces, which is supported by the tibia torsion deformation results during 50% maximum volunteer contractions, *i.e.* for most of the test subjects, the amplitude of tibia torsion angles during maximum voluntary contractions is nearly two times larger than 50% maximum voluntary contractions.

To summarize, the evidence from this thesis has changed our understanding of muscle-bone interactions in more than one way. Whilst the discussion was formerly centered on strain magnitudes, it is now the kind of loading regime that is in the heart of the interest. However, whether the association between the calf muscles and tibia deformation can be generalized also to other situations, *e.g.* femur, is still remaining unclear and will require further studies. More interestingly, taking the muscle-bone findings in this thesis and the muscle-bone interaction theory together, it is proposed that torsion may be a more relevant type of tibia deformation in humans than it was thought in the past.

4. Advantages and Limitations

As demonstrated and discussed in the previous chapters, a new understanding of *in vivo* tibia deformation, specifically in relation to tibia loading, was benefited from several noteworthy advantages of the OST approach.

- Firstly, the capability of exploring the components of the tibia deformation is one of the highlights of the OST approach. Certainly, the traditional strain gauge approaches can provide the information of local principal compression, tension strain and shear strain [10, 20]. However, the local principal axial strain and shear strain can be caused by bending and the combination of torsion and bending, respectively. The evidence in this thesis also showed that the bending and torsion characterized the tibia deformation regimes during the investigated exercises. With the reference to the bone strain studies which mainly focused on strain amplitude in the past, the new findings in this thesis might lead us to revisit the importance of the deformation regimes during the exercises.
- Secondly, the deformation regimes of tibia segment, which are speculated to be more closely related to the entire tibia loading than local strains, was obtained in humans for the first time in this thesis during different locomotor activities. The tibia segment deformation regimes provide a unique reference to understand the *in vivo* tibia loading and where the tibia load is derived from. For instance, the evidence in this thesis indicated that the antero-posterior bending and torsion deformation linearly related to the vertical ground reaction force and free moment during walking, respectively. More interestingly, local muscles seem to substantially contribute to the tibia torsion deformation.

Nevertheless, the study in this thesis with the OST approach still left some open questions to be resolved or issues needed to be considered in the future studies.

- Firstly, with the OST approach, the tibia deformation must be expressed with the relative movement of the markers in three dimensions. It stands to reason

to firstly determine a 3D coordinate system. In this thesis, the coordinate system to derive the tibia deformation angles was determined based on the well-established shank segment anatomical coordinate system in biomechanics studies [7], meaning that the interpretation of the presented tibia deformation rely on the pre-determined coordinate system and should be cautious under some special situations, such as while comparing the presented results with the bone strain data from the strain gauge approaches. Beyond that, another consequence is that the strain distribution across the tibia shaft cannot be determined directly, even though it is well accepted that the bone strain level is site-specific across the sites [21].

- Secondly, during the *in vivo* experiments, the capture volume was limited to achieve the optimal resolution, accuracy and precision of the adopted optical system, meaning that tibia deformation only can be recorded whilst tibia-affixed markers remain visible to the cameras within the volume. This confined the possibility of long-term continuous deformation recording during wide range of locomotor activities.
- Thirdly, as a pilot and exploring study, only a small number of test subjects was involved in the *in vivo* experiments. This may, to some extent, limit the generalizability of the presented results to the other special populations, such as the athletes, patients with musculoskeletal disorders and so forth. Evidence suggested that muscle fatigue leads to a significant increase of the tibia strains, indicating the importance of the regular muscle activities in maintaining safe tibia strain and avoiding the potential stress fracture development [22]. Likewise, utilizing micro-finite element analyses, trabecular bone tissue strain of the proximal femur was shown to have larger magnitude and less uniformly distributed in the osteoporosis femur than the healthy one [23]. More importantly, the tibia deformation angles in this thesis also showed its variability between the individuals. So, to which extent the presented results are representative is still to be determined in the future.

5. Outlook

As noted in the previous sections, several methodological issues and scientific questions need to be considered in our future studies.

- From the perspective of methodology

The OST approach still has possibilities of improvement by further optimizing the configuration of the optical system. For instance, with the development of the cameras, the spatial resolution, accuracy and precision to track the markers can be improved. The restriction of the marker-camera distance thus can be lifted following with the capability of capturing in a relatively large volume.

Besides of improving the OST approach, development of other new methods to further our understanding on *in vivo* bone deformation should also be anticipated. Finite element modeling (FEM) is one of the attractive non-invasive methods to assess *in vivo* bone deformation which has been widely applied in this research field [24, 25]. Generally, the bone strain can be and was predicted with FEM based on the known forces on the targeted bone, no matter whether the forces is artificial loaded [25] or estimated from other ways [26]. However, the exact forces acting on bone during the locomotive activities remain unknown which may lead to great discrepancy during the computation of the bone deformation with FEM. Nevertheless, it is conceivable that future studies could yield more substantial information by integrating the *in vivo* bone deformation results with the individualized bone FEM.

- From the perspective of scientific understanding on *in vivo* bone loading

Even with the evidence from this thesis, it is still impossible to completely address the question raised in Chapter 1 about the importance of the gravity-derived forces and the muscles forces on tibia load. The gravity-derived forces are essentially different from the ground reaction forces. The nature of the former is the body weight plus the impact force while the velocity of a free fall mass turned from maximum value to zero, which does not exist independently as the muscles always remain active to avoid free fall of the segments, *e.g.* lower extremities, and attenuate the impact forces. The latter, *i.e.* ground reaction force, is the

combination of the muscle forces and the gravity-derived forces. None of the locomotor activities is able to truly distinguish the effects of the gravity-derived forces and the muscles forces on tibia load. In the investigated exercises in this thesis, although the isometric plantar flexion can, mostly, separate the gravity-derived forces and the muscle forces, it does not mean that the muscles work in the same way as during the locomotor activities. Thus, the contribution of gravity-derived forces and the muscles forces on tibia load or deformation is anticipated to be addressed with new models or the new ways of thinking in the future studies.

Nevertheless, the evidence from this thesis did suggest that the local muscles were involved in the contribution of tibia torsion loading (Chapter 7). If torsional loading is truly crucial for the hollow structure of the long bones as speculated, does it mean that bone structure can be maintained by a substitute of artificial external torsion loading, or training the local muscles? Addressing these open questions in the future may greatly help the development of the training protocol or countermeasures to maintain or recover regular bone structure and function.

Conclusions

In summary, taking together the results from this thesis, several conclusions can be drawn as follows.

- Firstly, the inherent drawbacks of the traditional strain gauge approaches truly limited our understanding on *in vivo* bone deformation regimes in humans.
- Secondly, with certain configurations, the adopted system for optical segment tracking is capable of achieving sufficient resolution, accuracy and repeatability for long bone deformation recording. More importantly, it is practically feasible and reliable to apply the OST approach in the *in vivo* tibia deformation measurements in humans.
- Thirdly, tibia deformation was characterized by considerable amount of bending and torsion deformation during walking, running, stair ascent and isometric plantar flexion. The peak to peak antero-posterior bending angles and torsion angles were linearly correlated with the walking speed and

vertical ground reaction force or vertical free moment. Running led to large bending angles, but smaller torsion angles than walking. Of note, the relationship of tibia deformation with overground speed bears highly individual-related information.

- Fourthly, despite their individual close relationships with overground locomotion speed, the mutual amplitude relationship between antero-posterior bending and torsion angles was rather weak. During the investigated exercises in this thesis, forefoot running seems to induce the largest antero-posterior bending and torsion deformation angles, which suggested that the forefoot running may serve as one of the most effective training protocols to lead bone adaptation.
- Fifthly, there was considerable variation between subjects' tibia deformation regimes that was not due to measurement noise, but reflective of true biological variation.
- Finally, a specific fixed phase relationship exists between the posterior bending angles and torsion angles, torsion angles and local muscle activities during walking. Considerable torsion angles were closely relevant to the high local muscle activities, mainly calf muscles, induced by the exercises *i.e.* forefoot stair ascent and forefoot running, than the exercises with relatively low muscle activities, *i.e.* full foot stair ascent and rearfoot running. Likewise, the torsion angles prevailed the tibia deformation regimes during the isometric plantar flexion rather than the bending angles.

Thus, several new insights in the tibia deformation regimes and the contribution of muscle activities on tibia deformation were found in this thesis. These findings are very relevant to our current understanding of tibia deformation or tibia load in humans during different locomotor activities, and they are apt to change the common view angle in this research field. Furthermore, the evidence about the close relationship between the local muscle activities and tibia torsion deformation tends to update the knowledge of muscle-bone interaction and to further promote our thinking along the lines of the mechanostat theory.

References

1. Al Nazer R, Lanovaz J, Kawalilak C, Johnston JD, Kontulainen S (2012) Direct in vivo strain measurements in human bone—A systematic literature review. *J Biomech* 45: 27-40.
2. Yang PF, Bruggemann GP, Rittweger J (2011) What do we currently know from in vivo bone strain measurements in humans? *J Musculoskelet Neuronal Interact* 11: 8-20.
3. Benoit DL, Ramsey DK, Lamontagne M, Xu LY, Wretenberg P, et al. (2006) Effect of skin movement artifact on knee kinematics during gait and cutting motions measured in vivo. *Gait & Posture* 24: 152-164.
4. Ishii Y, Terajima K, Terashima S, Koga Y (1997) Three-dimensional kinematics of the human knee with intracortical pin fixation. *Clin Orthop Relat R*: 144-150.
5. Ramsey DK, Wretenberg PF (1999) Biomechanics of the knee: methodological considerations in the in vivo kinematic analysis of the tibiofemoral and patellofemoral joint. *Clin Biomech* 14: 595-611.
6. Nester C, Jones RK, Liu A, Howard D, Lundberg A, et al. (2007) Foot kinematics during walking measured using bone and surface mounted markers. *J Biomech* 40: 3412-3423.
7. Grood ES, Suntay WJ (1983) A Joint Coordinate System for the Clinical Description of 3-Dimensional Motions - Application to the Knee. *J Biomech Eng-T ASME* 105: 136-144.
8. Yang PF, Sanno M, Bruggemann GP, Rittweger J (2012) Evaluation of the performance of a motion capture system for small displacement recording and a discussion for its application potential in bone deformation in vivo measurements. *Proc Inst Mech Eng H* 226: 838-847.
9. Kutzner I, Heinlein B, Graichen F, Bender A, Rohlmann A, et al. (2010) Loading of the knee joint during activities of daily living measured in vivo in five subjects. *J Biomech* 43: 2164-2173.
10. Burr DB, Milgrom C, Fyhrie D, Forwood M, Nyska M, et al. (1996) In vivo measurement of human tibial strains during vigorous activity. *Bone* 18: 405-410.
11. Milgrom C, Miligram M, Simkin A, Burr D, Ekenman I, et al. (2001) A home exercise program for tibial bone strengthening based on in vivo strain measurements. *Am J Phys Med Rehabil* 80: 433-438.
12. Biewener AA, Thomason J, Goodship A, Lanyon LE (1983) Bone stress in the horse forelimb during locomotion at different gaits: a comparison of two experimental methods. *J Biomech* 16: 565-576.
13. Biewener AA, Thomason J, Lanyon LE (1983) Mechanics of Locomotion and Jumping in the Forelimb of the Horse (*Equus*) - Invivo Stress Developed in the Radius and Metacarpus. *J Zool* 201: 67-82.
14. Rubin CT, Lanyon LE (1982) Limb Mechanics as a Function of Speed and Gait - a Study of Functional Strains in the Radius and Tibia of Horse and

- Dog. J Exp Biol 101: 187-211.
- 15. Bertram JEA, Biewener AA (1988) Bone Curvature - Sacrificing Strength for Load Predictability. *J Theor Biol* 131: 75-92.
 - 16. Reilly GC, Currey JD (1999) The development of microcracking and failure in bone depends on the loading mode to which it is adapted. *J Exp Biol* 202: 543-552.
 - 17. Crowninshield RD, Brand RA (1981) A Physiologically Based Criterion of Muscle Force Prediction in Locomotion. *J Biomech* 14: 793-801.
 - 18. Herr H, Popovic M (2008) Angular momentum in human walking. *J Exp Biol* 211: 467-481.
 - 19. Neptune RR, McGowan CP (2011) Muscle contributions to whole-body sagittal plane angular momentum during walking. *J Biomech* 44: 6-12.
 - 20. Gross TS, McLeod KJ, Rubin CT (1992) Characterizing bone strain distributions in vivo using three triple rosette strain gages. *J Biomech* 25: 1081-1087.
 - 21. Judex S, Gross TS, Zernicke RF (1997) Strain gradients correlate with sites of exercise-induced bone-forming surfaces in the adult skeleton. *J Bone Miner Res* 12: 1737-1745.
 - 22. Milgrom C, Radeva-Petrova DR, Finestone A, Nyska M, Mendelson S, et al. (2007) The effect of muscle fatigue on in vivo tibial strains. *J Biomech* 40: 845-850.
 - 23. Van Rietbergen B, Huiskes R, Eckstein F, Ruegsegger P (2003) Trabecular bone tissue strains in the healthy and osteoporotic human femur. *J Bone Miner Res* 18: 1781-1788.
 - 24. Duda GN, Heller M, Albinger J, Schulz O, Schneider E, et al. (1998) Influence of muscle forces on femoral strain distribution. *J Biomech* 31: 841-846.
 - 25. Zauel R, Yeni YN, Bay BK, Dong XN, Fyhrie DP (2006) Comparison of the linear finite element prediction of deformation and strain of human cancellous bone to 3D digital volume correlation measurements. *J Biomech Eng* 128: 1-6.
 - 26. Al Nazer R, Rantalainen T, Heinonen A, Sievanen H, Mikkola A (2008) Flexible multibody simulation approach in the analysis of tibial strain during walking. *J Biomech* 41: 1036-1043.

Publications

1. **Peng-Fei Yang**, Gert-Peter Brüggemann, Joern Rittweger, What do we currently know from *in vivo* bone strain measurements in humans? *J Musculoskelet Neuronal Interact*, 2011; 11(1): 8-20. **(Chapter 2)**
2. **Peng-Fei Yang**, Maximilian Sanno, Gert-Peter Brüggemann, Joern Rittweger, Evaluation of the performance of a motion capture system for small displacement recording and a discussion for its application potential in bone deformation *in vivo* Measurements. *Proceedings of the Institution of Mechanical Engineers, Part H Journal of Engineering in Medicine*, 2012; 226(11): 838-47. **(Chapter 3)**
3. **Peng-Fei Yang**, Karsten Engel, Maximilian Sanno, Jens Dargel, Kilian Wegmann, Gert-Peter Brüggemann, Jörn Rittweger. Bone deformations induced by simulated muscle forces: *ex vivo* validation of the optical segment tracking (OST) approach in human tibia, *In Preparation*. **(Chapter 4)**
4. **Peng-Fei Yang**, Maximilian Sanno, Bergita Ganse, Timmo Koy, Gert-Peter Brüggemann, Lars Peter Müller, Jörn Rittweger, *In vivo* application of a novel optical approach for bone deformation recording in humans: a reliability study, *Manuscript under submission*. **(Chapter 5)**
5. **Peng-Fei Yang**, Maximilian Sanno, Bergita Ganse, Timmo Koy, Gert-Peter Brüggemann, Lars Peter Müller, Jörn Rittweger, Bending and torsion predominate the *in vivo* human tibia deformation regimes during walking and running, *Manuscript under submission*. **(Chapter 6)**

6. **Peng-Fei Yang**, Andreas Kriechbaumer, Kirsten Albracht, Maximilian Sanno, Bergita Ganse, Timmo Koy, Gert-Peter Brüggemann, Lars Peter Müller, Jörn Rittweger, The *in vivo* tibia torsional deformation in humans is relevant to local muscle contractions, *Manuscript under submission.* (Chapter 7)

7. Bergita Ganse, **Peng-Fei Yang**, Gert-Peter Brüggemann, Lars Peter Müller, Jörn Rittweger, Timmo Koy, An optical approach for *in-vivo* assessment of human bone deformation using bone screws - surgical experience and results from a three-point bending test, *Clinical Orthopaedics and Related Research, under review.*

Acknowledgements

Coming to Germany and pursuing a Ph.D has been one of the most important decisions I have made in my first 25 years of my life. Nearly four years later, as of today, I have almost completed my doctoral journey. I must say that it has been a great privilege to spend the past few years in the Department of Space Physiology, Institute of Aerospace Medicine, German Aerospace Center and I have enjoyed my stay in Germany very much. Completion of this thesis would not be possible without the kind support and assistance from many people.

First and foremost, I would like to express my deepest appreciation to my supervisors, Prof. Jörn Rittweger and Prof. Gert-Peter Brüggemann, who support me to proceed through my doctoral work and complete the thesis with their great patience and profound knowledge. Without their guidance and supervision, this thesis would not have been possible. I want to thank Joern for his continuing encouragement during the difficult time of my doctoral journey and always leading lively academic discussion with his broad-mind to push the work forward. He has been, and will remain to be, a role-model for me in academic research. Beyond that, he made me feel like home in Germany and never tired of answering my dumb questions about German culture. These exciting experiences of my many ‘firsts’, such as my first visit in England to Stonehenge and the city of Bath, my first indoor climbing and the hiking in Zugspitze (the highest mountain in Germany), and so on, have given me a deeper understanding of Germany and left me with wonderful memories, which are the treasures of my life.

Special thanks to Maximilian Sanno, who has always made himself available to offer his kind help during the establishment of the optical approach, *ex vivo* study until the *in vivo* experiments. I have learned so much from his expertise in the optical system. The colleagues from Department of Space Physiology, Bergita

Ganse, Jochen Zange, Andreas Kriechbaumer, Tobias Weber, Michel Ducos, Peter Gauger, Wolfram Sies and Margot Molitor; the colleagues from the Institute of Biomechanics and Orthopaedics, Karsten Engel, Kirsten Albracht, Hans-Martin Küsel-Feldker and Thomas Förster; the colleagues from Department of Orthopaedic and Trauma Surgery, University Hospital of Cologne, Timmo Koy, Lars Peter Müller, Jens Dargel and Kilian Wegmann, also deserve my sincere thanks. I would like to thank Helmholtz Space Life Sciences Research School (SpaceLife) for the opportunity of doing my Ph.D in Germany. I also would like to thank Dr. Christine Hellweg and Mrs. Anna-Maria Trautmann for their kind help concerning to the SpaceLife affairs. Their friendship and selfish assistance mean a lot to me. My doctoral work would not be completed without their invaluable assistance and tremendous contribution.

I am very grateful to our test subjects and donors - without their selfless contribution, this work would not have been possible.

I would like to thank my Master supervisor Prof. Peng Shang from Northwestern Polytechnical University, Xi'an, China, for enlightening me the first glance of scientific research and continuous support during my doctoral study. I would like to thank China Scholarship Council for my scholarship (CSC No.: 2009629013).

I wish to deeply thank my grandfather, Hong-Quan Yang, who I grew up with and left me all wonderful childhood memory, but he has unfortunately passed away during my stay in Germany. I miss him so much and will always love him with all my heart. I would like to thank my parents, Zhi-Min Tian and Feng-Gang Yang, for supporting me spiritually throughout my life and being my driving force to move forward. I hope that this work can make all of them proud. I would like to thank my younger brother, Peng-Hui Yang, who is coming to Germany as well and pursuing his Ph.D later this year. It feels always wonderful to share my experience with him. I wish all the best for his future. Also, I would like to thank

all my relatives for their continuous care and support to me.

The last, but by no means least acknowledgement I have saved to my dear wife, Wei Wang, who made so much sacrifice to stay in Germany with me and unconditionally supported me in every possible way to complete this journey. Around three month ago, a newest family member, my little son, Zhuo-Yuan (Tommy) Yang, came to our small family. It is great feeling and most exciting experience to be a new-borne daddy. I am very glad to have him to share this joy with me.

Appendix

1. Curriculum Vitae
2. Original Papers

Curriculum Vitae

Peng-Fei Yang, born in Shandong, China, in October 1983. He started to study Mechanical Engineering at Shandong Jianzhu University in 2001 and graduated in July 2005 with a Bachelor Degree in Engineering. From 2005 to 2006, he worked as research assistant in the School of Life Science, Northwestern Polytechnical University, China. In September 2006, he became a master student in the Northwestern Polytechnical University and received his Master Degree in Engineering in 2009. Shortly after that, he received a Ph.D scholarship from China Scholarship Council (CSC), which allowed him to be a SpaceLife doctorate candidate of the Helmholtz Space Life Sciences Research School in the Institute of Aerospace Medicine, German Aerospace Center under the guidance of Prof. Dr. Jörn Rittweger. Meantime, he became a Ph.D student of Prof. Dr. Gert-Peter Büggemann in German Sport University Cologne.

In the past few years, he focused on the understanding of *in vivo* bone loading pattern in humans during different locomotive activities and how the muscle contractions affect the bone loading. Together with the colleagues from German Aerospace Center, German Sport University Cologne and University Hospital of Cologne, he has performed an invasive study in humans, under the supervision of Prof. Rittweger and Prof. Brüggemann, to introduce a novel optical approach for assessing bone deformation, explore the *in vivo* tibia deformation during different exercises, and eventually provide evidence to answer several open questions in muscle-bone interaction research field.



What do we currently know from *in vivo* bone strain measurements in humans?

P.F. Yang^{1,2,3}, G-P. Brüggemann², J. Rittweger¹

¹Division Space Physiology, Institute of Aerospace Medicine, German Aerospace Center, Cologne, Germany; ²Institute of Biomechanics and Orthopaedics, German Sport University Cologne, Cologne, Germany; ³Key Laboratory for Space Bioscience and Biotechnology, Faculty of Life Sciences, Institute of Special Environmental Biophysics, Northwestern Polytechnical University, Xi'an, China

Abstract

Bone strains are the most important factors for osteogenic adaptive responses. During the past decades, scientists have been trying to describe the relationship between bone strain and bone osteogenic responses quantitatively. However, only a few studies have examined bone strains under physiological condition in humans, owing to technical difficulty and ethical restrictions. The present paper reviews previous work on *in vivo* bone strain measurements in humans, and the various methodologies adopted in these measurements are discussed. Several proposals are made for future work to improve our understanding of the human musculoskeletal system. Literature suggests that strains and strain patterns vary systematically in response to different locomotive activities, foot wear, and even different venues. The principal compressive, tension and engineering shear strain, compressive strain rate and shear strain rate in the tibia during running seem to be higher than those during walking. The high impact exercises, such as zig-zag hopping and basketball rebounding induced greater principal strains and strain rates in the tibia than normal activities. Also, evidence suggests an increase of tibia strain and strain rate after muscle fatigue, which strongly supports the opinion that muscle contractions play a role on the alteration of bone strain patterns.

Keywords: Bone Strain, *In vivo*, Bending, Strain Gauge, Muscle Fatigue

Introduction

It is well accepted that bones adapt to different types of loading, e.g. by various exercises or by disuse, the former being followed by anabolic responses and the latter by bone losses. Literature suggests that specific exercises or training can improve people's bone mass and strength¹. On the other hand, disuse during space flight was shown to induce a loss of more than 2% in hip trabecular volumetric bone mineral density (vBMD) per month². Inevitably, bone deformation will be induced by dynamic loading (because the static bone loading rarely happens *in vivo*, it is not included in this discussion).

The authors have no conflict of interest.

Corresponding author: Peng Fei Yang, Division Space Physiology, Institute of Aerospace Medicine, German Aerospace Center, Linder Höhe, D-51147 Cologne, Germany
E-mail: Pengfei.Yang@dlr.de

Edited by: F. Rauch
Accepted 21 February 2011

The effects of the various factors involved in bone loading, which include strain magnitude, strain rate, and the number of loading cycles are well documented³⁻⁴. Strain magnitude (symbol: ϵ or $\mu\epsilon$) which refers to the extent of bone deformation is easy to understand. Strain rate (symbol: ϵ/s or $\mu\epsilon/s$) is the rate of strain change per unit of time, or more simply, the rapidity with which strain alterations occur. Evidence from animal studies indicates that strain rate can constitute an osteogenic stimulus independent of strain magnitude⁵⁻⁶.

It is commonly thought that both ground reaction force (so called weight-bearing) as well as forces arising from muscular contraction contribute to the loading of the leg bones. Importantly, biomechanical analyses suggest that, of the two, the larger forces are caused by muscular contractions⁷. Moreover, there are co-contractions of agonist-antagonist muscle systems in virtually all motion patterns. Therefore, mere estimations of bone deformation by assessment of external loading and inverse dynamics approach can not provide a full account of the relationship between bone strains and osteogenic bone response. Even though the importance of bone strain for bone metabolism has been realized, knowledge of *in vivo* bone strains during habitual physical activities and specific exercises is very limited.

With development of the methodology of *in vivo* bone strain measurements it has become possible to record bone deformation under physiological conditions. A number of *in vivo* animal studies provide compelling quantitative evidence for the relationship between bone strain and osteogenic response. In these studies, different methods for *in vivo* bone strain measurement have been applied.

It has to be considered, though, that *in vivo* bone strain measurements are invasive and technically challenging. Nevertheless, the first pioneering study in humans stems from 1975⁸ and the bulk of the currently available studies started from 1996 onwards. Today there are a total of approximately 40 subjects of whom *in vivo* bone strain data have been published. However, there are a couple of important questions that have still not been addressed, which is the subject of the following appraisal.

Type of bone deformation

Strain is the geometric deformation within the material. One way to measure it is by strain gauges. Strain is expressed as the ratio between the length change and original length, and it is therefore given as a dimensionless number.

According to the following equations:

$$\text{Compressive strain: } \varepsilon_{\text{compressive}} = \frac{L - L_o}{L_o} = \frac{-|\Delta L|}{L_o} \quad (1)$$

$$\text{Tensile strain: } \varepsilon_{\text{tensional}} = \frac{L - L_o}{L_o} = \frac{|\Delta L|}{L_o} \quad (2)$$

Where L_o : original length; L : current length; $|\Delta L|$: length change. According to above equations, compressive strain and tensile strain are negative and positive values, respectively.

Strain can be simply tensile or compressive (axial strain, Figure 1A). More complex strains are generated by e.g. two planes sliding over each other (shear strain, Figure 1B), by bending (bending strain, Figure 1C) or by rotation (torsion strain, Figure 1D).

Axial strain

Axial strain is, by definition, a strain in the same direction as the applied load. Both compressive strain and tensile strain are axial strains. For long bones, axial strain under physiological conditions is mostly along the long axis of the bone.

It is generally thought that compressive and tensile strains are the main component for most kinds of activities.

Shear strain

When loading a solid material, there will always be both compressive and tensile strains, with a certain angle between them. In any direction within this angle, shear strain exists along the surface of the structure.

Generally, the distortion in shear can be described as the combination of two ideal types of strain: simple shear (Figure 2A) and pure shear (Figure 2B). The sum of these two shears is equal to the so called engineering shear strain which is defined as the angle change between two lines initially perpendicular

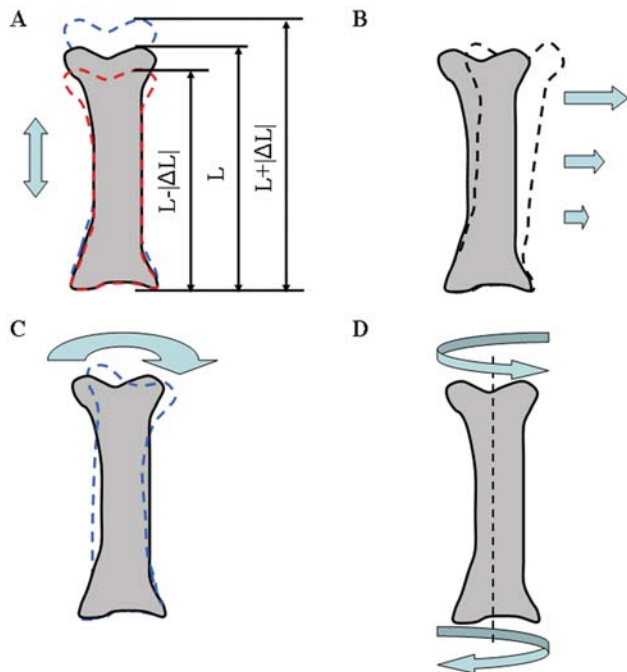


Figure 1. Different types of bone strain. **A:** axial strain; **B:** shear strain; **C:** bending strain; **D:** torsion strain.

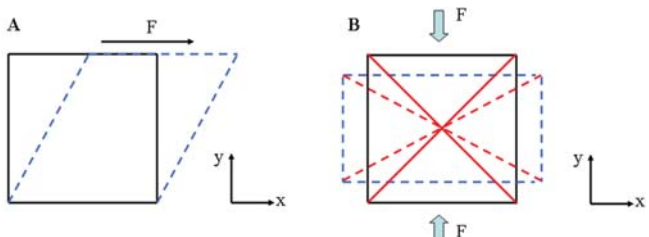


Figure 2. Shear strains. These are due to a two-dimensional geometric deformation of an infinitesimal material element (plain black line: original geometry, dashed blue line: sheared geometry). **A:** simple shear. **F:** shear force exerted on the infinitesimal material element; **B:** pure shear. There is pure shear along the diagonals of the element (plain red lines: original diagonals, dashed red lines: sheared diagonals). **F:** compression force exerted on the element.

to each other in the non-deformed or initial configuration. Because the engineering shear strain is equal to the difference between two principal strain values, it can conveniently be calculated and has frequently been reported in literature⁹⁻¹². As expected, shear strain was found during almost all activities, such as walking, running, and hopping.

Bending strain

Bone bending strain is induced by the external force or force component which is applied perpendicular to the longitudinal

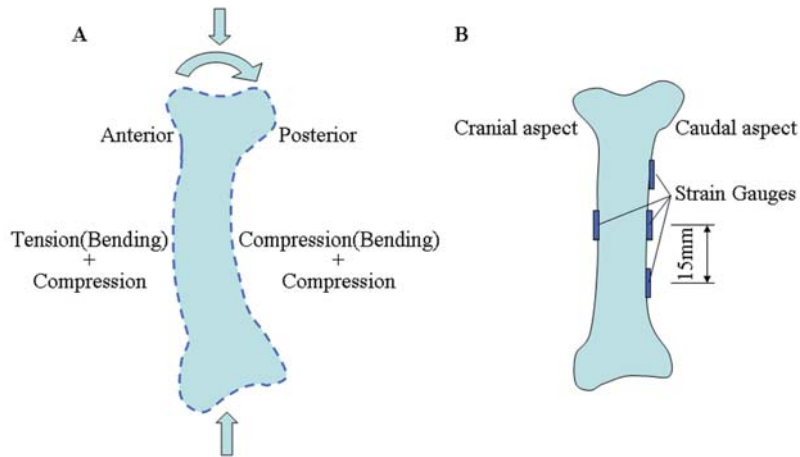


Figure 3. **A:** Bending superimposed with axial compression; **B:** As a demonstration of bending strains in previous study, strain gauges were attached on both side of the radius in goat¹⁴.

axis of the bone. The external force can be due to eccentric (off-axis) loading, and also due to axial force acting about a bone's longitudinal curvature¹³. The bending strain may cause tension in one part (e.g. anterior aspect) of the bone and compression in the opposite part (e.g. posterior aspect) of the bone (Figure 3A). Normally, the bending strain is superimposed with axial compressive strain (Figure 3A), and the question arises how bending and principle strain magnitude compare to each other.

Some evidence, however, does exist to account for the presence and magnitude of *in vivo* bending strains in the human body. For example, it has been observed during zig-zag hopping that the angle of maximum principal compression to the long axis of tibia varies considerably, much more than during walking and jogging¹². The most likely explanation for that angle change seems to be variation induced by bending moments during intense exercise, such as zig-zag hopping. However, no direct or quantitative *in vivo* bending strain data are as yet available in humans .

Torsion

Finally, there is a possibility of torsional loading on bone if the long axis of bone is twisted (Figure 1D). Assuming the long axis of the bone as 0°, the orientations of torsion strain in relation to the long bone axis will be at 45° or -45°, respectively, depending on the twisted direction of the long axis. For example, torsion of tibia is produced by the combination of ground frictional force relative to the foot and the resulting moment. Bones are generally weak in shear, and shear is typically induced by torsion or bending. In *ex vivo* testing, the fatigue strength of bovine compact bone under torsion loading is about half of the compressive fatigue strain for the same material¹⁵. According to Taylor et al.¹⁵, the largest part of shear strain arises from torsion, whilst transverse tensile stress *in vivo* is rare. Shear strain induced by torsion might therefore play an important role in bone fatigue fracture.

The methodology adopted for *in vivo* bone strain measurements

The development of appropriate bonding and recording methods made it possible to assess bone strain *in vivo* in animals and humans. Since the 1940s, scientists have started to establish and apply different methods for measuring bone strain *in vivo*¹⁶. Although several methods have been developed during the past few decades, only two of them (strain gauges and bone staples) have successfully been applied in the human body as so far. The development of these methods will be discussed in the following.

The first generation: Strain gauges method

The principle and the procedure of strain gauges measurements

As the gold standard of material strain and stress analysis, electric resistance wire strain gauges have been used in most *in vivo* bone strain measurement studies.

Their principle is based on the fact that the electrical resistance of a specially designed wire increases with increasing strain, and that it decreases with decreasing strain. When strain gauges are firmly attached on a material, they are assumed to undergo the same deformation as the material, and measurement of the electrical resistance, then allows the assessment of strain . However, a single wire strain gauge can measure strain in one direction only. In order to measure the strain with unknown directions, rosette strain gauges (Figure 4) have to be used. In that case, the principal strain and the angle between the grid of strain gauge and the principal strain can be calculated. The details about the rosette strain gauges can be referred to the technical notes from manufacturers¹⁷.

A series of original investigations and review papers in the 1970s have described how the strain gauges should be prepared and correctly used in bone strain measurements *in vivo*¹⁸⁻²⁰. Some modifications were also made for improving the bonding

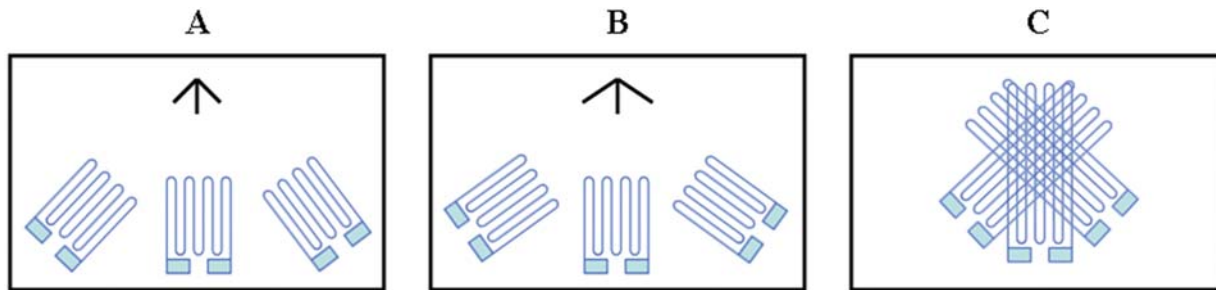


Figure 4. Basic types of rosette strain gauges: (A) 45° rectangular rosette strain gauges; (B) 60° delta rosette strain gauges; (C) Stacked construction rosette strain gauges. Three strain gages are placed together in a “rosette”-like layout with each gage oriented in a different direction. When the strain direction is unknown, the principal strains and their direction can be calculated by the signal from three strain gauges of rosette strain gauge.

quality *in vivo* at a later stage²¹. So far, most *in vivo* bone strain measurement approaches have used such strain gauges, even though some modifications have been made (refer to the discussion of bone staples methods). With rosette strain gauges bonded directly to the bone surface, Lanyon LE et al. and Burr et al. performed the first and second *in vivo* bone strain recording in humans, respectively⁸⁻⁹. The general procedure for implanting strain gauges during that study is described as following: The tissue overlying the proposed gauges site of the leg was anaesthetized first, and then a 5-10 cm long incision down to the periosteum was made. Part of the periosteum was removed and the bone surface cleaned. Next, the strain gauges were glued on the prepared bone surface with adhesive (isobutyl 2-cyanoacrylate monomer or polymethyl methacrylate). Then the wire of strain gauges were passed out of the wound and sutured to the periosteum. Importantly, the operation in that study took approximately 1 hour, but the strain gauge could stay thereafter for 3 days for data collection.

In Burr's and Milgrom's paper, degreasing of bone surface with alcohol and scoring with a bone punch are reported, as additional measures to improve strain gauge bonding^{9,22}. The strain gauge signal was recorded with a portable analog tape recorder in that study, which allowed the subjects a greater degree of mobility. No pain or discomfort was reported.

Disadvantages of strain gauges

Bonding problems: Technically, the surface for bonding strain gauges should be chemically clean (i.e. free of oil, greases, organic contaminants and soluble chemical residues), water proof and sufficiently rough. However, it is almost impossible to reach these harsh conditions by preparation *in vivo*, especially during long time recordings. In the study of Burr et al., strain gauges from one of two subjects were not firmly attached when they were checked after recording, and the data from this subject had to be abandoned⁹. Even without significant debonding, there is no way to evaluate the bonding stability *in vivo*. The bonding quality is the key point for the accuracy of foil strain gauges. Insecure bonding is likely to result in under-estimation of strain values.

Bending strain: Assessing bending strains with strain gauges is feasible only with a set of two rosette strain gauges attached on two opposing aspects of bone²³. In a study by Biewener et al.¹⁴, for example, the strain gauges were bonded on the cranial and caudal aspect of the radial and tibial diaphysis of goats (Figure 3B). Then, the ratio between the compressive strain due to bending and axial compression in three goats during gait at a constant speed (up to 5 m/s) was calculated, as 8.1 for the radius and 11.6 for the tibia. Furthermore, this ratio did not change significantly throughout the speed range. This suggests that bending is the predominant strain in bone during gait. Unfortunately, such an approach is hardly feasible for the human body, in particular for the tibia, as it is by virtue of the human anatomy quite impossible to attach a pair of strain gauges on two opposite sides of a bone, without destroying muscles. However, the axial and bending strain of bone can not be distinguished with strain gauge attached on one side of a bone only. Accordingly, there are as yet no measurements in human body to provide *in vivo* bone 3D deformation.

Temperature drift: Temperature related effects are the most common cause of error in the application of strain gauges. This is because electrical resistance is dependent on temperature. For obvious reasons, using two or more strain gauges *in vivo* in order to compensate for the effect of temperature, as one would do in an engineering scenario, is not feasible.

Calibration: For the strain gauges, the purpose of calibration is to develop an accurate relationship between the output voltage and bone strain. The calibration procedure is a cumbersome business, because of the potential affects of the implantation procedure²⁴, the linearity of strain gauges and the length of lead wire required for strain gauges (the wire cables which connect the strain gauges to the Wheatstone bridge. When the strain gauges are remote from the recording instrument, the resistance of wire cable has to be taken into account)²⁵.

The second generation: Extensometers and bone staples with strain gauges

Obviously, there is a desire to reduce the invasiveness of direct bonding of strain gauges to bone. To this effect extensome-

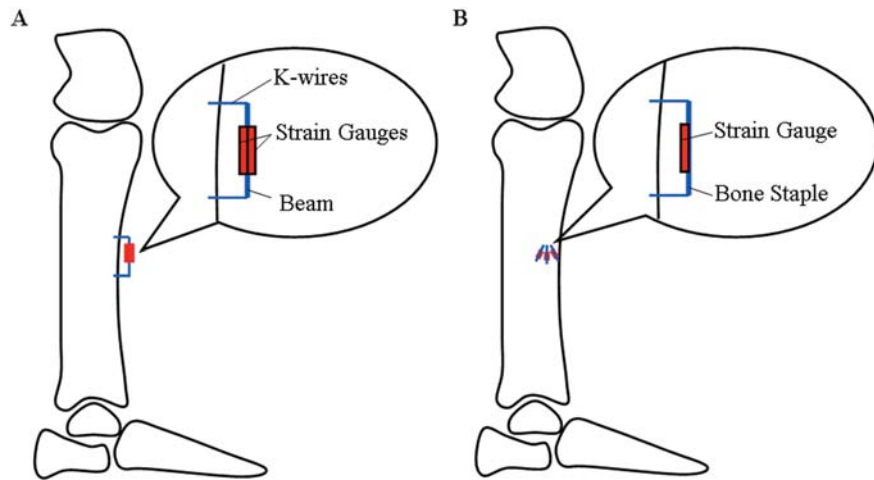


Figure 5. Diagram of extensometer and strain gauges in bone staples. The principle idea is to create a mechanically stable link between the bone and the extensometer to isolate strains in the extensometer. **A:** extensometer which was only able to record axial strain; **B:** strain gauges in 30° rosette pattern which was able to record axial and shear strain. Blue line: bone staples. The strain gauges were glued on the undersurface of the staples¹².

ters have been developed that can be externally mounted on two K-wires placed percutaneously into the bone cortex. The underlying idea is to isolate the deformation in a measurement device that is stably mounted on the bone. Before inserting the K-wires, local anesthesia is administered. Next, two K-wires are affixed into the predrilled holes to a depth of 4 mm, so that the extensometer can be mounted on the K-wires. The extensometer is composed of a bronze beam with two pairs of strain gauges bonding to the top and the bottom surface of the beam, respectively (Figure 5A). Bone strains are then transmitted to the beam's strain gauges through the K-wires. Again, strain gauges are connected to the recording device via cable connection. Unfortunately, however, this approach seems to generate artifacts induced by e.g. the heel strike, and it seems to generate smaller strain value readings than the classical strain gauge approach^{26–28}.

Based upon the same principle, commercial bone staples with instrumented strain gauges have also been used²⁹. Subsequently, Milgrom C. et al. modified this method and included three strain gauges into three bone staples in a 30° rosette pattern (Figure 5B)³⁰. Obviously, this requires additional holes in the tibia, which causes a practical problem related to increased invasiveness, as well as a theoretical problem related to possible effects of the holes upon structural rigidity of the instrumented bone. On the other hand, principal compressive and tensile strain as well as engineering shear strain can be conveniently calculated with this set up.

Compared to strain gauges glued directly onto the bone, the application of bone staples resolves the bonding problem. Moreover, this technique requires less invasive surgery for the subjects because the periosteum is mostly left intact. However, gauge failure or damage due to the surgery occurred very often¹⁰.

Results from *in vivo* bone strain measurements in humans

Results from *in vivo* bone strain measurements in humans have been summarized in Table 1.

Bone strain induced by different activities

To date, most *in vivo* bone strain measurements focus on the human tibia. Pioneering work was done by Lanyon and co-workers as early as in 1975⁸. With a rosette strain gauge attached to the anteromedial aspect of tibia midshaft, tibia strains were recorded during walking on a treadmill and on the floor. The principal strain and strain angle relative to the tibia's long axis were calculated. The strain magnitude when walking was found to be approximately -430 $\mu\epsilon$ ('-' : compression strain) during heel off to toe off, but up to 850 $\mu\epsilon$ ('+' : tensile strain) when running during toe strike to toe off. As commented by D.B. Burr et al.⁹, that work demonstrated the general possibility of such strain recording in humans.

Almost 20 years later, after the development of a portable strain measurement system, Burr et al. performed the second *in vivo* human tibia strain measurement during vigorous activity⁹. Data from this investigation indicate that the greatest principal strains and engineering shear strain during most vigorous activities (jogging, sprinting, running, zigzag running) were significantly higher than those during walking. The greatest strain was engineering shear strain which occurred during zigzag uphill and downhill running (approximately 2000 $\mu\epsilon$). For strain rate, the greatest compressive, tensile and engineering shear strain rate was recorded during sprinting on a level surface. By contrast, the strain rate during walking is much smaller than those of running (see also Table 1 and 2). Burr's study gave us the first comprehensive impression about the *in vivo* tibia strain in human during vigorous activities.

Table 1. Overview of *in vivo* bone strain (tibia, metatarsal and radius) results in humans.

Study	Type of exercises	Peak Strain ($\mu\epsilon$)			Peak Strain Rate ($\mu\epsilon/s$)		
		Com. (-)	Tension (+)	Shear (+)	Com.	Tension	Shear
Tibia							
Lanyon LE et al. 1975	Walking	30-850	30-580	-	-	-	-
Burr DB et al. 1996	Walking, Jogging, Sprinting, Zigzag running	400-1300	380-750	700-2000	7000-30000	7000-20000	13500-50000
Milgrom C et al. 1996	Walking and running with different shoes	400-1000	540-680	760-1500	2200-14000	-	-
Rolf C et al. 1997	Forward jump with forefoot and heel landing	-	-	-	-	-	-
Fyhrie DP et al. 1998	Walking before and after exhaustion	-	-	-	-	-	-
Mendelson S et al. 1998	Walking with and without cane	Axial peak to peak strain: 65-230			270-2500	-	-
Milgrom C et al. 1998	Walking and running with different shoes	-	-	-	-	-	-
Milgrom C et al. 2000	Running, Drop jump	1900-2100	900-1000	5300-7400	9600-13000	4800-7600	28500-50900
Milgrom C et al. 2000	Running, Cycling, leg press	290-1700	270-1400	630-5000	1500-1000	1300-8200	4500-38000
Milgrom C et al. 2000	Walking, Running, Basketball rebound	560-3200	700-1600	1200-9000	4300-19000	3700-7400	12500-58000
Milgrom C et al. 2001	Walking, Jogging, jump, Hopping	250-2200	500-2200	400-4100	2000-8000	2500-16000	5000-25000
Milgrom C et al. 2001	Walking with four different shoes	700-1200	460-720	1250-2600	6200-6500	2800-4000	12700-16000
Ekenman I et al. 2002	Walking and running with different shoes	Axial peak to peak strain: 1000-2400			3000-15000	4200-15600	-
Milgrom C et al. 2002	Walking, Jogging, broad jump, Vertical jump	360-700	160-1250	-	2500-8300	2100-14000	-
Milgrom C et al. 2003	Running at treadmill and on asphalt	400-2500	650-1250	-	3200-15000	3200-17000	-
Milgrom C et al. 2007	Before and after fatigue (2 km run, 30 km march)	470-720	340-610	-	3700-4700	4400-5600	-
Metatarsal							
Milgrom C et al. 2002	Walking, Jogging, Jumping	2600-2700	230-1100	-	9800-46000	3400-12000	-
Arndt A et al. 2002	Walking before and after fatigue	1500-2200	140-440	-	4200-5500	-	-
Radius							
Földházy Z et al. 2005	Arm curl, Chin up, Fall, Push up, Stirring, type writing, vacuuming carpet and wrist curl	0-6000	0-1500	-	0-85000	-	-

Table 2. Overview of *in vivo* bone strain studies in humans.

Study	N	t	Aim	Methods and site	Type of exercises	Output
Lanyon LE et al. 1975	1	3d	Tibia strain recording	Foil 45° rosette SG Anteromedial aspect of tibial midshaft	Walking on treadmill or the floor, with or without shoes, with 0, 21, 45, or 71kg weights	<p>1. Walking: The end of swing period, prior to 'heel strike', principal CS > principle TS, in line with long axis;</p> <p>2. Swing forward: strain pattern reversed;</p> <p>3. Wearing shoes (swing phase): deformation increased and decreased when foot was on the ground;</p> <p>4. Walking on a concrete floor with increasing loading: angle pattern keep constant,</p> <p>5. Between 'full foot' and 'heel off', strain increased greatly.</p> <p>6. Running without shoes: larger deformation during stance phase of running than when compared to walking.</p>
Burr DB et al. 1996	2	<1d	Tibia strain during vigorous activities	45° rosette SG Medial tibial midshaft	Walking (5 km/h) Jogging (10.15 km/h) Sprinting(13.38km/h) Walking with 17kg load Walking or running, zigzag running uphill, downhill	<p>1. Principal CS: -414 $\mu\epsilon$ (downhill walk)~1226 $\mu\epsilon$ (zigzag-run uphill)</p> <p>2. Principal TS: 381(walking + 17kg) ~743 $\mu\epsilon$ (zigzag run uphill)</p> <p>3. SS: 1583 $\mu\epsilon$ (sprinting)~871 $\mu\epsilon$(walking)</p> <p>4. Highest CSR and TSR: sprinting and downhill zigzag run and smallest when walking</p> <p>5. Highest SSR: sprinting, downhill running</p>

Table 2. (cont.)

Study	N	t	Aim	Methods and site	Type of exercises	Output
Milgrom C et al. 1996	2	<1d	Compare the tibia strain when subjects wearing different shoes	45° rosette SG Medial tibial midshaft	Walking at 3miles/h with shoes: 1. Rockport prowalker 7580 2. New balance running shoes 3. Light Israeli infantry boots 4. 2 layer sole infantry boots 5. Zohar infantry boots Running on the track (50m/11s) with the 2 nd , 3 rd and 5 th shoes	During walking 1. Zohar infantry boots had lowest principal CS and CSR; 2. New balance running shoes had lowest SS; 3. no single shoe lowered all the strain and SR; During running, zohar boot had lowest strain and SR.
Fyhrie DP et al. 1998	7(6)	<1d	Fatigue, tibia strain and age	extensometer (SG) Anteromedial tibial midshaft	5 km/h Walking before and after exhaustion exercise	1. Tibia strain depicts a increase after muscle fatigue in old people, but have no change in young people; 2. Heel strike impact is increased in young people, but decreased in old people after muscle fatigue;
Mendelson S, et al. 1998	7(6)	<1d	Tibia strain and cane usage	extensometer (SG) Anteromedial tibial midshaft	Walking without cane Walking with cane in right hand Walking with cane in left hand	1. Cane did not reduce the peak to peak tibial axial strain: 170, 169 vs. 148 $\mu\epsilon$ 2. However, cane usage reduced the max. tibial tibial CSR: 1048, 794 vs. 757 $\mu\epsilon$ s
Milgrom C et al. 1998	7(6)	<1d	Compare the shoes' effect on tibia strain	extensometer (SG) Anteromedial tibial midshaft	Walking (5 km/h), run (16.3 km/h): 1. Nike Air Max running shoes 2. Zohar sport shoes 3. Two layers' sole infantry boots	1. Walking: Zohar shoe had lowest CS, TS and CSR, TSR; 2. Running: No differences on CS, TS and SR between these shoes; 3. No difference on CS, TS and SR between walking on corridor and on treadmill
Milgrom C et al. 2000	6(4)	1d	Tibia strain during high impact exercise and running	Bone staples in rosette pattern (SG) Medial aspect of midtibial diaphysis	Running at 17 km/h Drop jump (26, 39 and 52 cm)	1. No difference in CS, TS and SS with increasing jump heights, but CSR decreased; 2. No relation between max. principal CS and jump potential energy; 3. No difference between the principal strain during running and jumping from 52 cm (up to ~5500 $\mu\epsilon$), but TSR higher during running.
Milgrom C et al. 2000	6	1d	Evaluation of potential strengthening exercise with tibia strain	Bone staples in rosette pattern (SG) Medial aspect of mid tibial diaphysis	Running on cinder track at 17 km/h; Running on treadmill at 5 km/h; Cycling at 60 c/s, power 100W; Stepmaster, aerobic mode 4, 5 min; During leg press.	1. No difference in principal TS, CS and SS between walking, leg press or stepmaster; 2. Higher strain during running than walking; 3. TSR and SSR are lower in cycling than walking; 4. Max. TSR during walking were higher than leg press, stepmaster and cycling; 5. Highest max. CS and SS during running, during walking were higher than cycling and leg press. 6. From the view of bone strain, only running is effective strengthening for tibia.
Milgrom C et al. 2000	3	1d	Assess bone strain developed during sporting activities	Bone staples in rosette pattern (SG) Medial aspect of midtibial diaphysis	Walking at 5 km/h Running at 17 km/h Performing basketball rebound	1. The principal CS, TS and SS during running were 2 to 4.5 times those of walking, but those during basketball rebounding were 2.25 to 7.41 times greater than during walking. 2. The TSR, CSR and SSR during rebounding and running were 2.16 to 4.60 times higher than during walking

Table 2. (cont.)

Study	N	t	Aim	Methods and site	Type of exercises	Output
Milgrom C et al. 2001	2	1d	Assess the bone strain induced by lower limb indoor exercise compared with those of walking	Bone staples in rosette pattern (SG) Medial aspect of midtibial diaphysis	Free walking; Jogging at 17 km/h; Vertical jump on two legs to 5 cm; Standing broad jump to 20 cm; Hopping 50 cm on right leg; Zig-zag hopping on the right leg.	Male: 1. Highest CS: jogging, hopping 50 cm and zig-zag hopping; 2. Highest TS: jogging, vertical jump on right leg to 5cm, hopping 50 cm and zig-zag hopping; 3. Highest SS: hopping 50cm and zig-zag hopping; 4. Highest SSR: jogging; 5. Highest CSR and TSR: zig-zag hopping; 6. Lowest SR and compression strain: Walking Female: 1. Highest CS and TS: zig-zag hopping; 2. Highest SS: vertical jump on right leg to 5 cm, hopping 50 cm and zig-zag hopping; 3. Highest CSR and TSR: zig-zag hopping; 4. Highest SSR: jogging, standing broad jump to 20 cm and hopping to 50 cm; 5. Lowest strain and SSR: walking
Milgrom C et al. 2001	3	1d	Test the influences of shoe sole composition on bone strain and strain rate	Bone staples in rosette pattern (SG) Medial aspect of midtibial diaphysis	Walking at 5 km/h with shoes: 1. 65 shore A polyurethane (SAP) 2. 65 SAP with heel air cell 3. 75 SAP 4. Composite of 40 and 65 SAP	CS, SS and shear SR is lower with air cells embedded shoes; Lower TS and CSR with 75 SAP shoes; Lower SS rate with air cells embedded shoes;
Ekenman I et al. 2002	9		Access the influence of running shoes and military boots with shoe orthoses on bone strain	Bone staples in rosette pattern (SG) Medial aspect of middle and distal tibial diaphysis	Walking 5 km/h before and after run; Running shoes and army boots with and without semirigid and soft orthoses; walking 5 km/h; Run 2km (13 km/h) + running shoes Run 1km +army boots;	Before running: Walking: higher peak to peak axial (p-p) strain with boots than running shoes; lower p-p strain with orthoses; soft orthoses with boot lowered the TSR and CSR; Running: p-p strain with boots was not higher than running shoes; semirigid orthoses with boots increased TSR and CSR; walking again after running; No increase in TSR and CSR compared with before running; Shoe orthoses may be warranted for fracture during mostly walking exercise, but not mostly running exercise.
Milgrom C et al. 2002	2	1d	Compare the strain in second metatarsal with the tibia and access the effect of shoe gear on these strain	Bone staples with two perpendicular SG • Medial aspect midtibial diaphysis • Dorsal surface of mid 2 nd metatarsal diaphysis	1. Walking at 5 km/h 2. Jogging at 11 km/h One subject: 50 cm broad jump Vertical jump to 10cm (one leg) Vertical jump to 10 cm (two legs)	Barefoot walking: 1. Peak axial metatarsal CS, TS, SR > those of tibia 2. Barefoot jogging: 3. Peak metatarsal CS and SR > those of tibia; 4. Peak axial CS reach 5677 $\mu\epsilon$; Wearing running shoes: 1. Metatarsal strain lower, but not tibia compression strain; 2. Tension strain increased; 3. Metatarsal CS, TS and SR > those of tibia; 4. Broad jumping, vertical jumping: strain>3000 $\mu\epsilon$;

Table 2. (cont.)

Study	N	t	Aim	Methods and site	Type of exercises	Output
Arndt A et al. 2002	8	<3h	Evaluate the effect of muscle fatigue on metatarsal strain	Bone staples with two perpendicular SG Dorsal surface of mid 2 nd metatarsal diaphysis	Walking barefoot (3 km/h) until Fatigue: Pre-fatigue without 20 kg backpack; Pre-fatigue with 20 kg backpack; Post-fatigue without 20 kg backpack; Post-fatigue with 20 kg backpack;	Pre-fatigue, no backpack: 1. Toe down was followed by peak tension (8±7%), followed by max. compression (65±15%), immediately after, compression decreased to about zero; 2. Mean peak CS: -1534±636με, TS: 346±359με; SR: 4165±1233με/s; 3. Peak compression during baseline without backpack less than other condition; 4. SR increased with backpack but not post-fatigue; Post-fatigue: 1. Peak tension decreased with backpack; 2. Time of peak CS was later for post fatigue without backpack; 3. Peak TS occurred earlier without backpack;
Milgrom C et al. 2003	3	1d	Determine the tibia strain difference during treadmill and overground running	Bone staples with one SG Medial aspect of the mid tibial diaphysis	With Nike Air Max shoes: Running at 11km/h at treadmill Free running on asphalt at 11 km/h;	Peak mean axial CS and TS, peal mean TSR and CSR were higher during running on overground than on treadmill; 1. Overground: CS: 1957 με, SR: 12876 με/s; TS: 1273 με, SR: 14160 με/s 2. Treadmill: CS: 664με, SR: 3346 με/s; TS: 860με. SR: 6645 με/s.
Földhazy Z et al. 2005	10	<2h	Evaluate the radial strain with different type of exercises	Bone staples with two perpendicular SG distal radial metaphysis	Arm curl with 7 kg Chin up; Fall, standing and kneeling; Push up on knee; Stirring; Type writing; Vacuuming carpet; Wrist curl in extension with 2 kg; Wrist curl in flexion with 2 kg;	1. Max. CS for falling and push up > for the others (except falling on knee vs. arm-curl and wrist-curl); 2. Max. TS for chin-up > for arm-curl, fall kneeling, push up, stirring and typing; 3. For push-up: there is no any tension, p-p strain around 2300 με; 4. Median value of strain rate: for falling (from standing: 45954 με/s, on kneeling: 18582 με/s) > for the other activities;
Milgrom C et al. 2007	4		Evaluate the effect of muscle fatigue on tibia strain	Bone staples in rosette pattern (SG) Medial aspect of midtibial diaphysis	Before and after fatigue: Max. right GM isokinetic torque, Tibia strain, force plate measure; Fatigue procedure: 1. 2 km run (>12 km/h) 2. 30 km march (6 km/h)	After the march: 1. The peak GM isokinetic torque was reduced by 37%, 31%, 21% and 23% respectively; 2. TS: 26% increased post run and 29% increased after march; 3. TSR: 13% increased post run and 11% increased after march 4. CS: 15% decreased post run and 24% decreased after march; 5. CSR: 9% increased post run and 17% increased after march;

N: number of the subject; t: time period of the study; SG: strain gauges; CS: compression strain; TS: tension strain; SS: shear strain; CSR: compressive strain rate; TSR: tension strain rate; SSR: shear strain rate;

Moreover, the principal compressive, tension and engineering shear strain, compressive strain rate and shear strain rate in the tibia during running on a cinder track were found to be significantly higher than those during walking, which was seen as baseline due to its minimal bone remodeling¹¹. Surprisingly, during running, the principal strains are comparable to those during high impact exercise (drop jump), and the strain rate seems to be even higher in running than during the drop jump exercises¹⁰. All of the above running data were based on running on cinder track. Much lower axial principal strains and strain rates were reported in literature during treadmill running³¹.

However, compared to running, walking, vertical jump and hopping, higher principal strains and strain rates in the tibia were found during other kinds of high impact exercises, such as zig-zag hopping¹², and even more so during basketball rebounding, where the greatest values of principal compression, tension and shear strain during rebounding were about 2 to 7 times greater than those during walking. The strain rates were approximately 2 to 5 times higher than during walking³⁰.

As mentioned in the ‘methodology’ section, three methods were adopted in the previous studies in tibia strain recording: strain gauges directly bonded onto the tibia, the extensometer method and the approach with bone staples. With the extensometer method, the range of tibial strains observed during walking was approximately one third of the strains recorded with strain gauge directly bonded to the tibia²⁶. The discrepancy between methods can arise in several ways. Firstly, the stability of the K-wire inside the tibia was not checked during the measurements. Second, there is a possibility of artefacts induced by K-wires bending during the measurements. On the other hand, the two approaches (directly bonded strain gauges and staples) yielded very similar results during walking. This suggests that the bone staple may be a quite efficient substitute for the method of direct bonding to bone surface under certain circumstances^{9,32}.

Besides the tibia, the metatarsal is another common site of study. It is of specific interest because it is a common site for fatigue fractures. Few studies have recorded the human metatarsal strain during different locomotive activities. The results indicate that peak axial metatarsal compressive and tensile strains, as well as strain rate are significantly higher than those in the tibia during treadmill walking. Moreover, high strains seem to also occur when subjects are jogging barefoot (Table 2). During jumping on one and two legs, the tensile and compressive strains exceeded 3000 $\mu\epsilon$ ³³. These data may indicate that the metatarsals have a much higher fatigue fracture incidence than the tibia because of the greater strains that they are typically exposed to.

To the best of our knowledge, there is only one *in vivo* strain recording available in the human upper extremity, namely in the distal radial metaphysis. Ten different activities, mainly with upper extremity, were studied, including arm curl, chin up, fall forward from standing and kneeling, push up, wrist curl in extension and flexion with 2 kg weight. Results indicate that the largest radius tensile strain occurs during chin up. Conversely, there was no tensile strain in the radius observed dur-

ing arm curl, fall or push up exercise. Among all those activities, falling and push up exercises resulted in the largest compressive strain, which amounted to up to -6000 $\mu\epsilon$ and -4300 $\mu\epsilon$, respectively³⁴.

External factors influencing bone strain and strain rate

As often advertised for running shoes, the soft soles or embedded air cells in shoes are supposed to absorb the impulse energy from the ground reaction force. To some extent, this point of view is supported by scientific literature. As previous studies have shown, the compression and engineering shear strains were significantly attenuated with heel air cell embedded in the shoe during walking (from ~900 to ~700 $\mu\epsilon$ and from ~1800 to ~1250 $\mu\epsilon$, respectively). Shear strain rate also was significantly reduced by the heel air cell³². Similarly, results in another study suggested that soft orthoses have potential to lower the tibia tension and compressive strain rate during walking³⁵.

Finally, one study has investigated the effects of ipsilateral and contralateral cane use upon tibia axial strains and strain rate. Interestingly, cane usage generally failed to reduce tibial strains, but decreases in strain rate were observed²⁶.

From geometric evidence, close functional relationship between muscle function and bone anabolism exists³⁶. Besides the ground reaction force, agonistic muscles also exert force on bone through tendons to realize the specific movement of human body. Accordingly, muscular contraction forces also seem to be a source of mechanical stimulation. Also, as the counterpart of agonistic muscles, antagonistic muscle can increase the loading on bone during ‘ballistic’ or ‘open-loop’ motor actions.

So far, only few data relate muscle activities to *in vivo* bone strain. Arndt et al.³⁷ reported the alteration of human second metatarsal (MTII) dorsal strain before and after M. flexor digitorum longus (FDL) fatigue. FDL contractions will induce dorsal tensile strains and reduce compressive deformation of MTII which is induced by ground reaction force and dorsiflexors during the stand phase. Part of this inference was tested in the study under discussion. Tensile strain of dorsal MTII surface was in close temporal relationship to activation of FDL. The peak activation of FDL occurred during the transition from MTII tensile strain to compressive strain during mid-stance phase. After the FDL muscle was fatigued the average peak compressive strain increased 42% and the peak tensile strain decreased 55%³⁷. It seems, therefore, that the bone strain protecting capacity of FDL was attenuated after the muscle had been fatigued. Similarly, in another study, after whole body fatigue (2 km running and 30 km march), tibia strain during walking was measured. Compared to the initial conditions, the tensile strain increased and the compressive strain decreased following the run and the march, respectively (The quantitative data is shown in Table 2). The tensile and compressive strain rates also increased after fatigue (Peak gastrocnemius torque was measured in this study to assess muscle fatigue)³⁸. Thus, muscular fatigue can be assumed to cause high bone strains and may therefore contribute to the devel-

opment of stress fracture. In the study of Fyhrie et al., the tibia strains were assessed after the fatigue exercise. Results suggested that high strain rates were induced after fatigue in younger subjects which means that bone strain rate, in addition to strain magnitude might contribute more to the stress fracture²⁸. Moreover, a study by Milgrom et al. has also reported that tibia strain is significantly enhanced by fatigue, and that higher strains are to be recorded during vigorous physical activities in a fatigued state, which again underlines a possible causative role of muscle fatigue in the development of stress fracture³⁸.

Risk evaluation (Pain and Infection)

Most *in vivo* studies have reported swelling and tenderness at the surgical site in some subjects. These complaints did generally recover well, so that subjects were able to return to their normal activities within few weeks, except for one or two exceptions who required longer recovery (less than a few months). Another problem which has to be considered seriously is the risk of infection, especially during the application of bone staples. In previous studies, bone staples were inserted into cortical bone to a depth of approximately 4 mm to avoid penetration of the cortex, thereby reducing the infection risk. Despite this, the risk is still one of the obvious problems in bone strain *in vivo* measurements.

What should be done in the future?

As discussed above, the few *in vivo* bone strain measurements that have been done in the past decade have greatly contributed to musculoskeletal science^{8-12,22,26-35,37-38}. On the other hand, these studies have given us only an incomplete impression about *in vivo* bone strain, and they were mainly limited to the tibia and metatarsal. Accordingly, there are many open questions which we can not answer.

First, there are serious limitations imposed by the current methodological approach. As mentioned above, the goal must be to improve our understanding of bone strain within the human body, and to do so in a way that is less invasive and more accurate at the same time, to ideally reveal also 3-dimensional strain information. Of interest, accurate and less invasive approaches have been proposed, although no data from human *in vivo* application are available as yet. One such approach is based upon an optical technique for non-contact, 3-dimensional deformation measurement, namely the digital image correlation (DIC). This has been employed to measure the strain distribution of animals' bone *ex vivo*. In this method, a high contrast speckle pattern (normally with painting or spraying) is applied onto the bone surface. The speckle pattern changes during loading are then optically tracked. Compared with strain gauges, this method is more informative for anisotropic materials, such as bone. Although some *in vivo* bone strain recordings have been done in animals³⁹⁻⁴⁰, further improvements are needed to avoid exposing and painting bone surface for *in vivo* bone strain measurements in human. To

overcome the limitations of invasiveness in the methods mentioned above, ultrasound wave assessment was introduced to measure bone deformation⁴¹. Again, no *in vivo* data are available as yet. Summarizing the above discussion, from the available methods so far, there are not too many choices to assess *in vivo* bone strains in the human body. With the exception of strain gauges and bone staples which have been used in previous *in vivo* studies, a few new methods are perceivable, none of which is easy to apply. However, these new methods could have the potential to give more strain information and thus may constitute a new step in the field of bone research.

Second, the strain pattern of bone *in vivo* is not clear during locomotive activities, even in tibia and metatarsal. Besides compressive and tensile strain, torsion and bending strain are very important composition of bone strain pattern as well, the latter one was even believed to be one of the key factors in bone fracture. However, with the available techniques, no reliable data can be obtained to understand bending and torsion strains.

Third, strain gauges, as frequently used in bone surface strain measurement *in vivo* and *in vitro*, do not provide global strain distribution and 3D component of strain. From literature, almost all the strain data are recorded in one or two sites of bone which can not represent that in other bone sites. In addition, the mechanical properties of cortical and trabecular bone are different, and previous data have shown that the bone periosteal and endocortical region have different responses to the non-invasive loading⁴². This implies that the strain gradient in the radial direction of long bone should not be ignored. How to measure the inner bone strain *in vivo* is still a big challenge. Future work could yield more information about strain distribution and 3D strain, which would certainly help to improve our understanding about the relationship between bone strain and bone modeling, remodeling process.

Fourth, according the theory of 'Wolff's law', bone will optimize its structure in response to the way it is loaded. Accordingly, the strain distribution might vary between subjects with different bone architecture. For example, with micro CT scanning and finite element analyses, Rietbergen and his co-workers have suggested that differences in strain magnitude and distribution may exist between osteoporotic and healthy femurs⁴³. If *in vivo* bone strain data were available from different populations with healthy and unhealthy bones, in combination with information on their bone structure, there will be more evidence to evaluate 'Wolff' law' quantitatively.

Fifth, close functional relationships between the musculature and bone were observed in many studies⁴³⁻⁴⁶. Muscle has been proposed as a primary source of mechanical stimulation for bone metabolism. If this hypothesis is true, bone strain, as an indicator of mechanical stimulation in bone, should have strong relationship with muscle activities. However, muscle activities, especially in lower leg, are also linked to ground reaction force which is also recognized as one of the sources of bone deformation. So, how much bone strain is contributed by ground reaction force and muscle activities, respectively? Some *in vivo* study suggested that more than 70% of the forces in femur during gait were resulted from muscle forces, only

less than 30% derived from body weight⁴⁷. However, there is no quantitative data available in tibia so far. Another question arising in this context is whether there are spatial and temporal relationships between muscle activities and bone strain patterns. The answer will be yes if the muscle forces do indeed play a decisive role in the loading of bone.

Conclusions

The pioneering works of Evans, Lanyon and other scientists mark the beginning of the *in vivo* bone strain research field, and extensive data have been recorded in animal studies since then. The unique data from these studies has helped to expand our understanding of the bone adaption to bone strain induced by muscle contraction and external force. However, the measurements in human body are limited by the invasiveness and complexity.

Due to the restriction of externally available specific zones of bone *in vivo*, strain measurements are limited to few locations only, for example the anteromedial aspect in the human tibia and dorsal surface in the metatarsal. According to these data, the strain magnitude in the tibia is within the range of 0-5000 $\mu\epsilon$, and in some vigorous activities, such as jumping, basketball rebounding, the tibia strain magnitude can reach approximately 9000 $\mu\epsilon$. Relative to strain magnitude, high rate strain is another potential stimuli factor to stimulate osteogenic responses. Depending on the specific kinds of exercise, bone strain rate is normally in the range of 1500-20000 $\mu\epsilon/s$ and could reach up to 58000 $\mu\epsilon/s$ during vigorous activities (Table 1).

Acknowledgements

We would like to thank Thomas Förster in the Institute of Biomechanics and Orthopaedics, German Sport University Cologne for numerous discussions about the application of strain gauges. Special thanks go to Alex Ireland for linguistic scrutiny. Pengfei Yang acknowledges his scholarship by the China Scholarship Council (CSC No.: 2009629013).

References

1. Suominen H. Muscle training for bone strength. *Aging Clin Exp Res* 2006;18(2):85-93.
2. Lang T, LeBlanc A, Evans H, Lu Y, Genant H, Yu A. Cortical and trabecular bone mineral loss from the spine and hip in long-duration spaceflight. *J Bone Miner Res* 2004;19(6):1006-12.
3. Forwood MR, Turner CH. Skeletal adaptations to mechanical usage: results from tibial loading studies in rats. *Bone* 1995;17(4 Suppl):197S-205S.
4. Duncan RL, Turner CH. Mechanotransduction and the functional response of bone to mechanical strain. *Calcif Tissue Int* 1995;57(5):344-58.
5. Mosley JR, Lanyon LE. Strain rate as a controlling influence on adaptive modeling in response to dynamic loading of the ulna in growing male rats. *Bone* 1998;23(4):313-8.
6. Turner CH, Owan I, Takano Y. Mechanotransduction in bone: role of strain rate. *Am J Physiol* 1995;269(3Pt1): E438-42.
7. Rittweger J. Physiological targets of artificial gravity: adaptive processes in bone. In: Clement G, Buckley A, editors. *Artificial Gravity*. Berlin: Springer; 2007. p. 191-231.
8. Lanyon LE, Hampson WG, Goodship AE, Shah JS. Bone deformation recorded *in vivo* from strain gauges attached to the human tibial shaft. *Acta Orthop Scand* 1975; 46(2):256-68.
9. Burr DB, Milgrom C, Fyhrie D, Forwood M, Nyska M, Finestone A, Hoshaw S, Saiag E, Simkin A. *In vivo* measurement of human tibial strains during vigorous activity. *Bone* 1996;18(5):405-10.
10. Milgrom C, Finestone A, Levi Y, Simkin A, Ekenman I, Mendelson S, Millgram M, Nyska M, Benjuya N, Burr D. Do high impact exercises produce higher tibial strains than running? *Br J Sports Med* 2000;34(3):195-9.
11. Milgrom C, Finestone A, Simkin A, Ekenman I, Mendelson S, Millgram M, Nyska M, Larsson E, Burr D. *In vivo* strain measurements to evaluate the strengthening potential of exercises on the tibial bone. *J Bone Joint Surg Br* 2000;82-B(4):591-594.
12. Milgrom C, Miligram M, Simkin A, Burr D, Ekenman I, Finestone A. A home exercise program for tibial bone strengthening based on *in vivo* strain measurements. *Am J Phys Med Rehabil* 2001;80(6):433-8.
13. Biewener AA. Musculoskeletal design in relation to body size. *J Biomech* 1991;24(Suppl.1):19-29.
14. Biewener A, Taylor C. Bone strain: a determinant of gait and speed? *J Exp Biol* 1986;123(1):383-400.
15. Taylor D, O'Reilly P, Vallet L, Lee TC. The fatigue strength of compact bone in torsion. *J Biomech* 2003; 36(8):1103-9.
16. Caler WE, Carter DR, Harris WH. Techniques for implementing an *in vivo* bone strain gage system. *Journal of biomechanics* 1981;14(7):503, 507.
17. Vishay Micro-Measurements Technical Note TN-515. Strain gage rosettes: selection, application and data reduction In: Measurements Group, Inc.; 2010.
18. Van Cochran GB. A method for direct recording of electromechanical data from skeletal bone in living animals. *J Biomech* 1974;7(6):563-5.
19. Cochran GV. Implantation of strain gages on bone *in vivo*. *J Biomech* 1972;5(1):119-23.
20. Wright TM, Hayes WC. Strain gage application on compact bone. *Journal of biomechanics* 1979;12(6):471-473, 475.
21. Hoshaw SJ, Fyhrie DP, Takano Y, Burr DB, Milgrom C. A method suitable for *in vivo* measurement of bone strain in humans. *J Biomech* 1997;30(5):521-4.
22. Milgrom C, Burr D, Fyhrie D, Forwood M, Finestone A, Nyska M, Giladi M, Liebergall M, Simkin A. The effect of shoe gear on human tibial strains recorded during dynamic loading: a pilot study. *Foot Ankle Int* 1996; 17(11):667-71.
23. Rubin C, Lanyon L. Limb mechanics as a function of speed and gait: a study of functional strains in the radius and tibia

- of horse and dog. *J Exp Biol* 1982;101(1):187-211.
24. Vishay Micro-Measurements Technical Note TN-509. Error due to transverse sensitivity in strain gages. In: Measurements Group, Inc.; 2005.
 25. Vishay Micro-Measurements Technical Note TN-514. Shunt calibration of strain gage instrumentation. In: Vishay Measurements Group, Inc.; 2007.
 26. Mendelson S, Milgrom C, Finestone A, Lewis J, Ronen M, Burr D, Fyhrie D, Hoshaw S, Simkin A, Soudry M. Effect of cane use on tibial strain and strain rates. *Am J Phys Med Rehabil* 1998;77(4):333-8.
 27. Milgrom C, Burr D, Fyhrie D, Hoshaw S, Finestone A, Nyska M, Davidson R, Mendelson S, Giladi M, Liebergall M, Lehnert B, Voloshin A, Simkin A. A comparison of the effect of shoes on human tibial axial strains recorded during dynamic loading. *Foot Ankle Int* 1998; 19(2):85-90.
 28. Fyhrie DP, Milgrom C, Hoshaw SJ, Simkin A, Dar S, Drumb D, Burr DB. Effect of fatiguing exercise on longitudinal bone strain as related to stress fracture in humans. *Ann Biomed Eng* 1998;26(4):660-5.
 29. Rolf C, Westblad P, Ekenman I, Lundberg A, Murphy N, Lamontagne M, Halvorsen K. An experimental *in vivo* method for analysis of local deformation on tibia, with simultaneous measures of ground reaction forces, lower extremity muscle activity and joint motion. *Scand J Med Sci Sports* 1997;7(3):144-51.
 30. Milgrom C, Simkin A, Eldad A, Nyska M, Finestone A. Using bone's adaptation ability to lower the incidence of stress fractures. *The American Journal of Sports Medicine* 2000;28(2):245-251.
 31. Milgrom C, Finestone A, Segev S, Olin C, Arndt T, Ekenman I. Are overground or treadmill runners more likely to sustain tibial stress fracture? *Br J Sports Med* 2003; 37(2):160-3.
 32. Milgrom C, Finestone A, Ekenman I, Simkin A, Nyska M. The effect of shoe sole composition on *in vivo* tibial strains during walking. *Foot Ankle Int* 2001;22(7):598-602.
 33. Milgrom C, Finestone A, Sharkey N, Hamel A, Mandes V, Burr D, Arndt A, Ekenman I. Metatarsal strains are sufficient to cause fatigue fracture during cyclic overloading. *Foot Ankle Int* 2002;23(3):230-5.
 34. Foldhazy Z, Arndt A, Milgrom C, Finestone A, Ekenman I. Exercise-induced strain and strain rate in the distal radius. *J Bone Joint Surg Br* 2005;87(2):261-6.
 35. Ekenman I, Milgrom C, Finestone A, Begin M, Olin C, Arndt T, Burr D. The role of biomechanical shoe orthoses in tibial stress fracture prevention. *Am J Sports Med* 2002;30(6):866-70.
 36. Fricke O, Beccard R, Semler O, Schoenau E. Analyses of muscular mass and function: the impact on bone mineral density and peak muscle mass. *Pediatr Nephrol* 2010;25(12):2393-400.
 37. Arndt A, Ekenman I, Westblad P, Lundberg A. Effects of fatigue and load variation on metatarsal deformation measured *in vivo* during barefoot walking. *Journal of biomechanics* 2002;35(5):621-628.
 38. Milgrom C, Radeva-Petrova DR, Finestone A, Nyska M, Mendelson S, Benjuya N, Simkin A, Burr D. The effect of muscle fatigue on *in vivo* tibial strains. *J Biomech* 2007;40(4):845-50.
 39. Yang L, Zhang P, Liu S, Samala PR, Su M, Yokota H. Measurement of strain distributions in mouse femora with 3D-digital speckle pattern interferometry. *Optics and Lasers in Engineering* 2007;45(8):843-851.
 40. Sztefek P, Vanleene M, Olsson R, Collinson R, Pitsillides AA, Shefelbine S. Using digital image correlation to determine bone surface strains during loading and after adaptation of the mouse tibia. *Journal of biomechanics* 2010;43(4):599-605.
 41. Matsuyama J, Ohnishi I, Sakai R, Suzuki H, Harada A, Bessho M, Matsumoto T, Nakamura K. A new method for measurement of bone deformation by echo tracking. *Med Eng Phys* 2006;28(6):588-95.
 42. LaMothe JM, Zernicke RF. The relation between loading rate, strain gradients, and bone adaptation. *J Bone Joint Surg Br* 2008;90-B(SUPP_1):78-c-.
 43. Van Rietbergen B, Huiskes R, Eckstein F, Ruegsegger P. Trabecular bone tissue strains in the healthy and osteoporotic human femur. *J Bone Miner Res* 2003; 18(10):1781-8.
 44. Manske SL, Boyd SK, Zernicke RF. Muscle and bone follow similar temporal patterns of recovery from muscle-induced disuse due to botulinum toxin injection. *Bone* 2010;46(1):24-31.
 45. Rittweger J, Felsenberg D. Recovery of muscle atrophy and bone loss from 90 days bed rest: results from a one-year follow-up. *Bone* 2009;44(2):214-24.
 46. Fricke O, Beccard R, Semler O, Schoenau E. Analyses of muscular mass and function: the impact on bone mineral density and peak muscle mass. *Pediatr Nephrol* 2010.
 47. Lu TW, Taylor SJ, O'Connor JJ, Walker PS. Influence of muscle activity on the forces in the femur: an *in vivo* study. *J Biomech* 1997;30(11-12):1101-6.

Evaluation of the performance of a motion capture system for small displacement recording and a discussion for its application potential in bone deformation *in vivo* measurements

Peng-Fei Yang^{1,2,3}, Maximilian Sanno²,
 Gert-Peter Brüggemann² and Jörn Rittweger^{1,4}

Abstract

The aim of this study is to evaluate the performance of a motion capture system and discuss the application potential of the proposed system in *in vivo* bone-segment deformation measurements. In this study, the effects of the calibration procedure, camera distance and marker size on the accuracy and precision of the motion capture system have been investigated by comparing the captured movement of the markers with reference movement. The results indicated that the system resolution is at least 20 µm in a capture volume of 400 × 300 × 300 mm³, which mostly covers the range of motion of the tibia during the stance phase of one gait cycle. Within this volume, the system accuracy and precision decreased following the increase of camera distance along the optical axis of the cameras. With the best configuration, the absolute error and precision for the range of 20 µm displacement were 1.2–1.8 µm and 1.5–2.5 µm, respectively. Small markers (Ø3–8 mm) yielded better accuracy and repeatability than the larger marker (Ø10.5 mm). We conclude that the proposed system is capable of recording minor displacements in a relative large volume.

Keywords

Motion capture system, bone strain, *in vivo*, accuracy, precision

Date received: 21 August 2011; accepted: 5 June 2012

Introduction

Bone strain is widely accepted as one of the most important factors in bone adaptation. Reliable and quantitative evidence from many studies over the past few decades suggests an inseparable relationship between bone strain and osteogenic responses.^{1–4} Nevertheless, *in vivo* bone strain measurement is still technically challenging, especially in humans. Despite the invasiveness, in previous *in vivo* bone strain studies, the inherent shortcomings of the methodologies based on strain gages *in vivo* are likely to result in the underestimation of the strain value owing to the low bonding quality.^{5–8} On the other hand, strain gages can only reflect strains in specific areas that are covered by the gages, but yield no information regarding the bone-segment deformation on a large scale. Even more importantly, it is difficult, not to say impossible, to

assess bending and torsional strains with strain gages in humans.⁵

In order to overcome the drawbacks of this traditional method, several new methods have been developed to assess bone strains, such as a non-contact

¹Institute of Aerospace Medicine, German Aerospace Center, Germany

²Institute of Biomechanics and Orthopaedics, German Sport University Cologne, Germany

³Key Laboratory for Space Bioscience and Biotechnology, Northwestern Polytechnical University, China

⁴Institute for Biomedical Research into Human Movement and Health, Manchester Metropoliation University, UK

Corresponding author:

Peng-Fei Yang, Division of Space Physiology, Institute of Aerospace Medicine, German Aerospace Center, Linder Höhe, D-51147, Cologne, Germany.
 Email: Pengfei.Yang@dlr.de

optical technique, referred to as digital image correlation (DIC),^{9–11} as well as ultrasound wave propagation.¹² However, the potential of these methods for *in vivo* application is still debatable.

Camera-based motion capture systems are nowadays widely used in biomechanics studies. The human motion can be captured by tracking markers that are attached on the skin of the human body. The data processing then involves (a) location of the markers in the two-dimensional (2D)-space of each camera, and (b) reconstruction of each marker in the real-world three-dimensional (3D)-space by convergence of the information from the set of cameras.¹³ Although the performance of the motion capture system varies with the specific system set-up,¹⁴ it is theoretically possible to achieve very high accuracy with a proper calibration procedure, choice of markers and the positioning of the cameras. Liu et al.¹⁵ evaluated the accuracy and precision of the Qualisys motion capture system (Qualisys, Inc., Gothenberg, Sweden) in the measurements of small displacements in a small field of view. Results indicated that, in a $68 \times 51 \text{ mm}^2$ field of view, the system resolution was $10 \mu\text{m}$. In the range of $20\text{--}200 \mu\text{m}$, the absolute displacement errors were from ± 2.1 to $\pm 3.0 \mu\text{m}$ for diamond markers, and from ± 2.5 to $\pm 4.25 \mu\text{m}$ when sphere markers were used. The standard deviation of the recording was $1.7\text{--}2.3 \mu\text{m}$ for diamond markers, and $1.9\text{--}3.9 \mu\text{m}$ for sphere markers, respectively.¹⁵ With the Vicon-460 motion capture system (Vicon Motion System Ltd, LA, USA), accuracy of $63 \mu\text{m}$ and precision of $15 \mu\text{m}$ can be achieved in a volume of $180 \times 180 \times 150 \text{ mm}^3$.¹⁴ Overall, the previous studies have demonstrated that, with proper parameters and set-up, commercially available motion capture systems are able to provide sufficient accuracy and precision (also called repeatability or reproducibility) to measure small movement of the markers in a relatively small 3D volume. If these markers are affixed to the bone, e.g. human tibia, theoretically, the tibia-segment deformation should be able to be measured by capturing the relative movement between the markers. By doing so, the complex measurements of different types of tibia-segment deformation essentially turn out to be the simple measurements of the markers' coordinate in a 3D volume. During the stance phase of one human gait cycle, the range of motion of the tibia is almost constant and limited within a certain 3D volume. In another words, the movement of the markers that affixed to the tibia during the stance phase of one gait cycle also stay within a certain 3D volume. As long as the markers' coordinates in this 3D volume is recorded with high accuracy and repeatability, axial, shear and torsion bone-segment deformation should be able to be calculated. However, despite the requirement of high accuracy and repeatability, the very limited volume covered in the aforementioned studies seems to impede the application of motion capture camera systems for *in vivo* bone-segment deformation measurements. To our knowledge, neither the performance of motion

capture systems in a relatively large volume, nor the potential of applying a motion capture system in bone deformation (most commonly refer to tibia) *in vivo* measurements, has been reported and discussed before.

Taking the human tibia as an example, assuming the distance between the markers affixed in the tibia as $L = 20 \text{ cm}$ and the detection limit of the optical method as $100 \mu\epsilon$ (compared with approximately $2000 \mu\epsilon$ *in vivo* tibia strain,^{6,16} the detection limit of $100 \mu\epsilon$ is acceptable), respectively, the required resolution of the optical method, ΔL , can be calculated as $\Delta L = L \times 100 \mu\epsilon = 20 \mu\text{m}$. Although this is only a rough figure, it can inform us about the required resolution of an optical method to assess the *in vivo* tibia deformation. We therefore ventured to evaluate the performance of a motion capture system on small displacement measurements ($20 \mu\text{m}$) in a relatively large volume. More specifically we are addressing, first, whether $20 \mu\text{m}$ of resolution is able to be achieved with proposed system configuration in this study was assessed; and second, the accuracy and precision during the measurement of $20 \mu\text{m}$ movement in a large volume were evaluated. In addition, the application potential of this method in bone-segment deformation *in vivo* measurements was discussed.

Materials and methods

The Vicon MX motion capture system (Vicon Motion System Ltd, LA, USA), including Vicon F40 cameras (4 Megapixel, 370fps full frame top speed), MX Gigabit controlling hardware module and Vicon Nexus 1.6.1 software, was adopted to capture the motion of the retro-reflective markers. The performance (accuracy and precision) of this system was evaluated to establish the proposed method.

As mentioned above, the markers affixed to the tibia during the stance phase of one gait cycle stays within a certain volume, which is able to be assumed by the length of tibia. Typically, the length of the tibia is approximately 400 mm . Accordingly, the volume of interest during a tibia's stance phase has dimensions of $400 \times 300 \times 300 \text{ mm}^3$. In this volume, the performance of this optical system was assessed. Assuming an inter-marker distance of 20 cm , one has to resolve marker displacement by $20 \mu\text{m}$ in order to assess strains of $100 \mu\epsilon$ – a goal that seems worthwhile to achieve. Several previous *in vivo* bone strain studies with strain gages suggested that more than $2000 \mu\epsilon$ of bone deformation can be reached during different exercises.⁵ Comparably, we believe that the detection limit of $100 \mu\epsilon$ in the proposed method would be acceptable for *in vivo* bone strains recording in humans.

Within the selected volume, the minute movement of the markers was performed by a universal milling machine (DMU 50M, DMG Vertriebs und Service GmbH, Bielefeld, Germany). The milling machine is capable of positioning its spindle in three dimensions

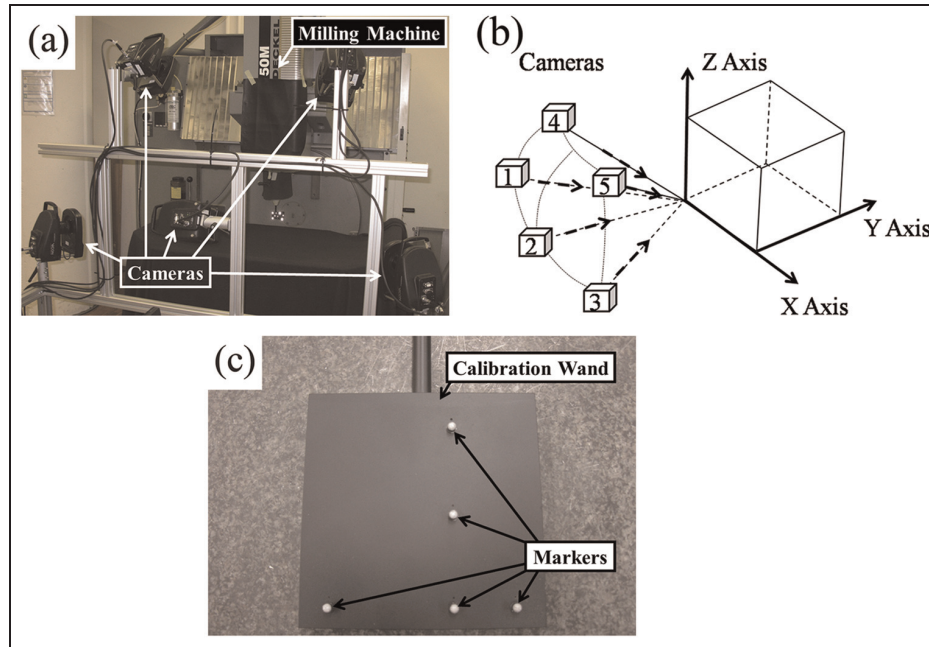


Figure 1. The configuration of optical system and calibration procedure. (a) Configuration of the cameras and the milling machine. (b) The sketch of camera distribution and the volume. Boxes 1–5 refer to different cameras; dashed arrow: optical axes of cameras; X, Y and Z axes are the three orthogonal directions along which the markers were moved. (c) Custom made calibration wand that was used in this study.

accurately (resolution in all axes: 1 µm). After being affixed on the spindle of the milling machine, the markers were moved along three orthogonal directions within the volume of $400 \times 300 \times 300$ mm³ (Figure 1).

Parameters in the optical system configuration

Cameras setup. Five Vicon F40 cameras with 16 mm focal length lenses were used in this study. Custom-made aluminum frames were used to position the cameras. The cameras were placed as close as possible to the milling machine in order to maximize the resolution of the system. The distance between the cameras and the center of the volume ranged between 100 and 120 cm.

The cameras were set up in near umbrella configuration according to the recommendations by the manufacturer.¹⁷ The optical axis and location of each camera were adjusted to involve the volume of $400 \times 300 \times 300$ mm³ into the overlap field of view. The sampling frequency of the system is set at 100 Hz.

System calibration. A custom-made calibration wand (Figure 1(c)), with Ø4 mm sphere markers, was used to calibrate the system before the measurements. In the selected volume, manual and automatic calibrations were carried out respectively to assess the effects of the calibration procedure on the performance of this optical system.

The manual calibration was performed by hand according to the manufacturers' recommendations. During the automatic full volume calibration, the calibration wand was moved (speed: 5 m/min) along the custom-programmed motion path through the entire volume.

Camera distance and axis. The sphere markers were driven to a total of 80 positions that uniformly distributed in the selected volume (Figure 2). At each position, the markers were driven for a distance of 20 µm along the positive direction of three orthogonal axes respectively and back (Figure 2, X, Y and Z axis). For the distance of 20 µm, the starting position, movement path and the final position of the markers has been recorded. Measurements were repeated three times for each specific condition. The increase of camera distance relative to camera position (Figure 2, D1: the closest distance; D2, D3 and D4: the furthest distance) mostly aligned with Y axis. Twenty positions were located at each distance.

Marker size. In order to assess the effects of marker size on the performance of the proposed optical method, sphere markers in four different sizes (diameter: Ø3 mm, Ø4 mm, Ø8 mm and Ø10.5 mm) were used in this study. The sphere markers were manufactured as copper balls coated with standard Vicon retro-reflective tape (Vicon Motion System Ltd, LA, USA). The smallest markers that are possibly manufactured with a smooth surface (Ø3 mm and Ø4 mm markers) were selected to evaluate the effects of small markers on the performance of the system. Reasonably large markers (Ø8 mm and Ø10.5 mm markers), which are suitable for future *in vivo* tibia-segment deformation measurements and have low opportunities of markers overlap, were selected as well.

Random noise. Random noise of the system induced by ambient factors has to be considered during very

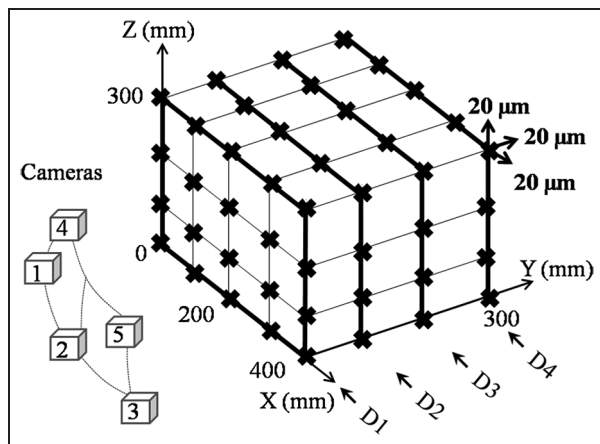


Figure 2. Demonstration of the 80 positions within the sampling volume ($400 \times 300 \times 300 \text{ mm}^3$). ‘*’ denotes the different positions. D₁, D₂, D₃ and D₄ are the different camera distance at 0, 100 mm, 200 mm and 300 mm of y axis, respectively. Bold lines: the vertical planes at different camera distances.

accurate measurements. A previous study has indicated that the resolution and system repeatability were affected by the random noise level.¹⁵ So, the markers coordinates, under static condition, was recorded to evaluate the random noise level in proposed system.

Data processing

Raw trajectory data of the markers were further processed with MATLAB (The MathWorks, Inc. Version 7.9.0 R2009b).

Coordinate transformation. The Cartesian dimensions of the milling machine could deviate from the Cartesian dimensions of the optical system. Coordinate transformation was performed to compensate such mis-alignment.

System accuracy. In order to minimize the effect of noise, marker coordinates data over 1 s (100 frames) at each position were averaged. The system accuracy describes the closeness of the recorded displacement to the reference displacement of the milling machine (20 µm). In order to assess the effects of different parameters (calibration procedure, cameras distance, marker size and axis) on the performance of the optical system, the absolute error between recorded displacement and the reference displacement of each measurement was calculated. The measurement accuracy was then expressed as the percentage error, which is given by

$$\text{Percentage error} = \frac{\text{absolute error}}{\text{reference value}} \times 100\% \quad (1)$$

System precision. The precision describes the repeatability of the recorded value with the same set-up of system. With the repetitions of the measurements at each camera distance (Figure 2: D₁, D₂, D₃ and D₄), the standard deviation (SD) of the recorded value was calculated as the system precision.

Random noise. Noise level along different axis was expressed as the root mean square (RMS) amplitude about the mean value of the data under static capturing with 100 Hz.

Statistics

Statistical analyses were performed using R statistic software (version 2.12.2, R Development Core Team, 2011) and Graphpad Prism statistical software (version 5.00, GraphPad software, Inc., La Jolla, CA). Three-way analysis of variance (ANOVA) was employed to examine the main and interaction effects of the four parameters mentioned above (calibration procedure: manual and automatic calibration; marker size: Ø3 mm, Ø4 mm, Ø8 mm and Ø10.5 mm; camera distance: D₁, D₂, D₃ and D₄; axis: X, Y and Z) on the accuracy. Data regarding the accuracy of the system are presented as mean (\pm SD) of the absolute error.

As the reflection of the system precision (the SD of the repeated measurements), the homogeneity of the variances of the recorded movement (reference movement is 20 µm) were assessed by the Fligner-Killeen’s test. Main and interaction effects of system factors on the precision were reported. Data regarding to the precision are presented as the \pm SD value. Statistical significance was accepted at $p \leq 0.05$.

Results

System accuracy

Calibration procedure. For the displacement of 20 µm, the effects of calibration procedures were assessed by the optical system over all 80 positions. Statistical analysis of the data showed no significant ($p = 0.37$) main effect of the calibration procedure on system accuracy (Figure 3). However, significant main effects of camera distance ($p < 0.001$) and axis ($p < 0.001$) were found on the system accuracy. Moreover, an interaction effect ($p < 0.001$) between camera distance and axis was indicated. A greater error in the Y axis was encountered for camera distance D₃ and D₄ than for D₁ ($p < 0.001$).

Camera distance, marker size and axis. Statistical analysis of the data showed significant ($p < 0.001$) main effects of the camera distance and axis on system accuracy, respectively. System accuracy reduced (the absolute error increased) significantly along the Y axis ($p = 0.04$). Furthermore, two-way interactions were found between camera distance and axis ($p < 0.001$), marker size and axis ($p = 0.03$), respectively. At camera distance D₃, larger absolute errors in the Y axis was associated with the usage of larger markers (Ø10.5 mm) as compared with smaller markers (Ø3 mm, Ø4 mm and Ø8 mm) ($p = 0.02$, Figure 4). For all the markers, larger absolute errors in the Y axis than the other axes were found at camera distances D₂, D₃ and D₄ ($p < 0.001$ versus $p = 0.17$ at D₁).

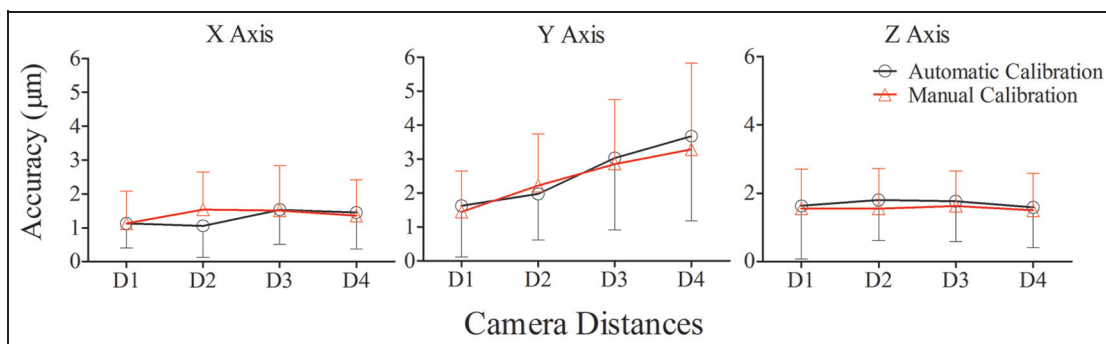


Figure 3. The system accuracy in the X, Y and Z axis with the automatic and manual calibration procedures, respectively. No significant difference on absolute error was found with two calibration procedures ($p = 0.37$). With both of the calibration procedures, the absolute error in the Yaxis increased with the increase of camera distance, especially in camera distance D3 and D4 ($p < 0.001$).

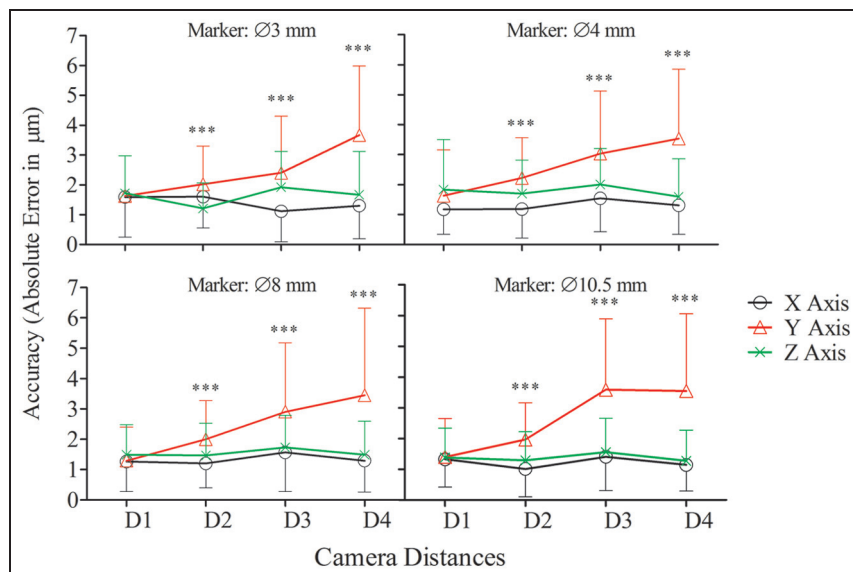


Figure 4. The effect of different parameters on the accuracy of the optical system. For all the markers, larger absolute error was induced with the increase of the camera distance in Yaxis at camera distance D2, D3 and D4 (***: $p < 0.001$). At the cameras distance D3, larger marker ($\varnothing 10.5$ mm) brought more absolute error than the other markers ($p = 0.02$).

By contrast, no significant main effect of marker size was found ($p = 0.22$). The statistical results indicated no other significant interaction effects, including three-way interactions among camera distance, marker size and axis ($p = 0.16$).

When averaged over all axes, the accuracy ranged 1.2–1.8 μm (6%–9%) at D1, 1.0–2.2 μm (5%–11%) at D2, 1.1–3.6 μm (5.5%–18%) at D3 and 1.2–3.7 μm (6%–18.5%) at D4, respectively.

System precision

Calibration procedure. Both calibration procedures yielded comparable results with regards to system precision ($p = 0.65$, Figure 5). There were, however, main effects of camera distance at D2, D3 and D4, and axis in the Y axis, demonstrating larger (worse) precision,

as compared the other distances ($p < 0.001$) and axes ($p < 0.001$).

Camera distance, marker size and axis. Main effects of the three parameters (camera distance, marker size and axis) on system precision indicated the major differences in axes ($p < 0.001$) and camera distance ($p < 0.001$), but only minor differences in marker size ($p = 0.18$, Figure 6).

All the different camera distances, except D1, were associated with a larger precision error along the Y axis ($p < 0.001$, $p = 0.96$ at D1). At camera distance D3, the marker with $\varnothing 10.5$ mm induced larger precision values than $\varnothing 3$ mm marker in the Y axis ($p = 0.02$, Figure 6). No other interactions were found among camera distance, marker size and axis. For all the axes,

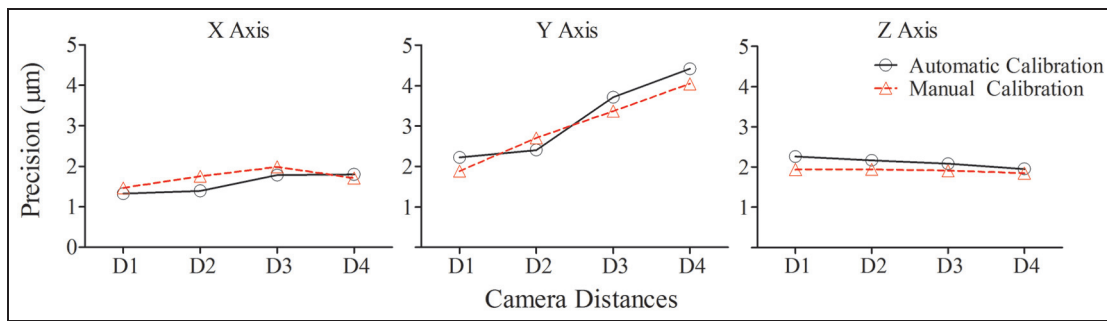


Figure 5. The precision at all 80 positions along the X, Y and Z axis with both calibration procedures. Similar to the results of absolute error, no significant difference in precision was found between the two calibration procedures ($p = 0.65$). With both the calibration procedures, the precision in the Yaxis increased with increasing camera distance ($p < 0.001$).

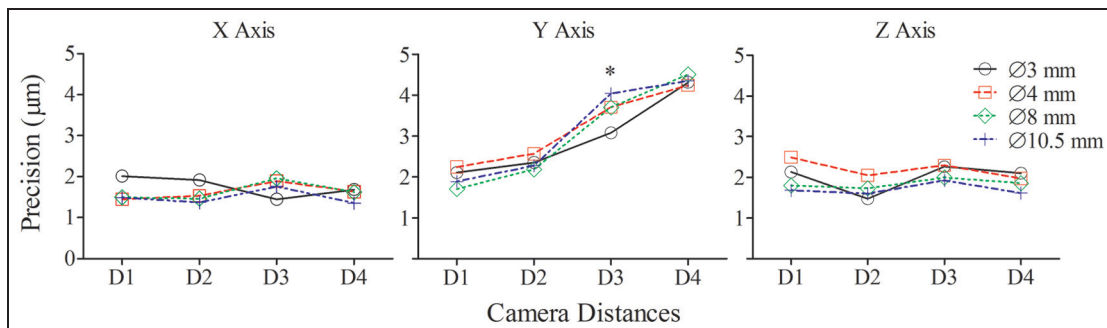


Figure 6. The effects of different camera distances, marker size and axis on the precision of the optical system. The precision value increased with the increase of the camera distance in the Yaxis. In the other axes, no effects of camera distance and marker size on the system precision were found. *: comparison of precision between 3 mm marker and 10.5 mm marker in the Yaxis at distance D3. *: $p < 0.05$.

precision ranged 1.5–2.5 μm at camera distance D1, 1.4–2.6 μm at D2, 1.4–4.0 μm at D3 and 1.4–4.5 μm at D4, respectively.

Random noise

The system random noise (RMS amplitude) was 1.9 μm , 4.0 μm and 3.0 μm in X, Y and Z axis, respectively.

Discussion and conclusions

This study assessed the performance of an optical system for measuring small amplitude movements in a relative large volume. The effects of the calibration procedure, retro-reflective marker size, camera distance and axis upon system accuracy and precision have been evaluated. From the results of this study, it seems prudent to suggest that 20 μm movements could be measured with acceptable accuracy and precision within a volume of $400 \times 300 \times 300 \text{ mm}^3$, which means the system resolution was at least 20 μm in this volume.

Large volume

Previous studies have successfully tracked the minute motion with high resolution, accuracy and precision,

but only in a relatively small volume.^{14,15,18,19} The system information and results from previous studies are summarized in Table 1. Thus, compared with most previous studies, a better resolution (at least 20 μm), better accuracy and precision have been achieved by the presented approach, despite the fact that a larger volume has been used. It is evident that this improvement in system performance is mostly attributable to the higher resolution of the cameras (4 Megapixel), even though some parameters in the system configuration will probably also have contributions. More importantly, for most of the cases, the volume evaluated in this study covers the motion of the tibia during a stance phase of gait. The results suggest that the trajectory of the markers can be recorded in this volume with high accuracy and precision. Accordingly, the tibia deformation can be calculated with the same accuracy and precision if the markers are affixed to the tibia.

Calibration procedure, camera distance and marker size

Unlike the observations in the study of Windolf et al.,¹⁴ calibration procedure did not affect the system performance in our study. Our results, therefore, imply that systematic error of this optical system, which are

Table I. Summary of the optical system information and results from previous and this study.

Studies	Optical system	Volume, field of view or camera distance	Markers	Resolution	Accuracy	Precision
Liu et al. ¹⁵	Qualisys ProReflex-MCU120 ^a	Field of view: 68.18 × 51.14 mm ²	Ø2.5 mm, sphere, retro-reflective	10 µm	1.39%–2.37%	1.9–3.9 µm
Maletsky ¹⁸	Optotrak 3020 ^b	Camera distance: 1.75 m–4 m	Active marker ^c	—	≥3%	0.29 mm
Windolf et al. ¹⁴	Vicon-460 ^d	Volume: 180 × 180 × 150 mm ³	Ø25mm, sphere, retro-reflective	—	63 ± 5 µm	15–21 µm
Schmidt et al. ¹⁹	Optotrak ^b	Camera distance: 1.5 m–4.5 m	Active marker	< 10 µm	In-plane: < 0.53%; out-of-plane: < 1.56%	0.6–29.2 µm
In this study	Vicon MX ^d	Volume: 400 × 300 × 300 mm ³ Camera distance to the center of the volume: 100–120 cm	Ø3, 4, 8, 10.5 mm, sphere, retro-reflective	≤20 µm	6%–9%	1.5–2.5 µm

^a Qualisys motion capture system (Qualisys, Inc., Gothenberg, Sweden).^b Optotrak motion capture system (Northern Digital Inc., Waterloo, Ontario).^c Infrared light-emitting diodes.^d Vicon motion capture system (Vicon Motion System Ltd, LA, USA).

mostly induced by the calibration procedure, was very low and did not go to such an extent as to affect the system accuracy. In keeping with the conclusion of the study by Maletsky et al.,¹⁸ increasing the camera distance increased the measured error and decreased the precision of the system along the main *Y* axis. In some contrast with the findings from Windolf et al.,¹⁴ greater marker size did not improve accuracy and precision over smaller markers, especially in the *Y* axis. This finding can be explained as follows: Although more pixels are available with larger markers, that does imply an improvement for marker location precision, as more artifacts during the calculation of the marker center might be introduced while the marker moves further from cameras or the surface of the markers is not perfectly smooth. The other factors, such as different camera set-up, cameras numbers, marker quality (roundness and reflective quality) and surrounding environment condition, might also affect the performance of the optical system, as has been partly demonstrated in the past.^{14,17}

Why is the error enhanced in the *Y* axis?

At 80 positions of the measured volume, accuracy and precision have been evaluated in three orthogonal directions (*X*, *Y* and *Z* axis). The results suggested that the accuracy and precision was greater in the *X* and *Z* axis than that in the *Y* axis at two greatest camera distances (D3 and D4). A similar tendency was found when different sizes of markers were used. Interestingly, similar observations have been made in the study of Liu et al.¹⁵ and Windolf et al.¹⁴ as well. The likely explanation for these effects is that the number of pixels available from each marker diminishes when the markers are remote from the cameras. A reduction in pixel number is bound to enhance the error when calculating the central points of the marker with the gray scale reconstruction and circle fitting techniques. Oppositely, movement in the *X* and *Z* axis does not affect the pixel number, and it did accordingly not induce as large error as in *Y* axis.

Is the proposed approach good enough to serve its purpose?

Owing to the irregular shape of long bones, axial deformation, shear, bending, torsion and their combination will occur on them under different loading condition. The traditional methods for measuring strains, e.g. strain gages, is not suitable for describing bone-segment deformation in three dimensions.⁵

As mentioned above, the purpose of this study was to establish an optical method and explore its application potential for *in vivo* bone-segment deformation measurements. For humans, the feasible anatomical sites for such measurements are limited. To date, most *in vivo* bone strain studies in humans have focused on the tibia. Results from these studies have shown that a

peak principal tibia strain is approximately $1200 \mu\epsilon$ under the conditions of daily normal activity,^{5,6,20} and that peak principal strains $>3000 \mu\epsilon$ can be observed during more vigorous activities.²¹ However, in these studies, bone strains were measured by traditional strain gage approaches. With these technical set-ups, strains were available over a very limited surface area, typically a few square millimeters. To our knowledge, no methods are available to record the tibia-segment deformation *in vivo* so far, owing to the invasiveness and technical issues during the measurements.⁵

Based on the rough calculations mentioned in the 'Introduction' section and the results from this study, at least $20 \mu\text{m}$ resolution, high accuracy and precision in the defined volume demonstrates that the present approach has the ability to record *in vivo* tibia deformation in humans.

Moreover, as indicated in a recent review article about *in vivo* bone strain measurements,⁵ no information is available in humans regarding the possible bending and torsion deformation *in vivo*. During the past decades, intracortical pins or screws with marker clusters were used in numerous studies to measure 3D kinematics of the tibiofemoral²² and the patellofemoral joint,²³ as well as the foot bones.²⁴ The relative bone motion in six degrees of freedom (three rotations and three translations) can be clearly described, most commonly, in the anatomical coordinate systems.²⁵ For example, based on the Cardan–Eular angle, the flexion–extension, abduction–adduction, internal–external knee rotation and the translation can be calculated in the knee joint.

During kinematics studies, the bone segments were usually considered to be rigid, thus totally neglecting any bone deformation. However, the methodology to describe the flexion–extension, abduction–adduction,

internal–external rotation and the translation can still be adopted to refer to the bending, torsion and axial deformation of bone. So, the following set-up (Figure 7) is recommended to be used in tibia-segment deformation recording *in vivo*. Few bone pins or screws with retro-reflective marker clusters (three marker clusters with non-collinear markers on each cluster in Figure 7) could be inserted into the anterior–medial aspect of proximal, mid-shaft and distal tibia. The optical system and configuration proposed in this study then could be adopted to capture the coordinates of the markers during one step of the different locomotive activities, such as gait. Whatever the type of bone deformation is, axial, shear or torsion, all of them are able to be expressed by the relative movement between marker clusters and calculated based on the coordinates data of the markers.

Recommendation for the application of the proposed method in bone-segment deformation *in vivo* measurements

According to the results from this study and the proposed set-up of the markers in human tibia in Figure 7, close camera positioning (camera distance: D1, $< 90 \text{ cm}$) and reducing marker size ($\varnothing 3\text{--}\varnothing 8 \text{ mm}$) seems to be the best choice to improve the performance of this optical system and realize *in vivo* tibia-segment deformation recording with high accuracy and precision. Furthermore, the movement of the markers in the direction of cameras distance should be avoided, as much as the subjects can, during different exercises.

Concerning the detailed technically issues of applying the proposed method in tibia-segment deformation *in vivo* measurements, the pain induced by the screw insertion should be minimized by using thin bone screws. The invasiveness inflicted upon the subjects will be reduced with bone pins, as the periosteum will almost not be severed. In addition, a skin incision with appropriate length at the site of the bone screw insertions should be made to avoid the contact between soft tissues with bone screws during the exercises.

Comparison between the proposed method and the existing method

As the gold standard for measuring mechanical strain in engineering applications, strain gage methods have been often used in *in vivo* bone strain measurements in the past. However, the credibility of the strain gage approach is under debate owing to the uncontrollable of the bonding quality on the bone surface. This means that the so call 'gold standard' method might not suit *in vivo* bone strain measurements perfectly because of the potential poor bonding quality. Comparatively, the proposed method overcomes several drawbacks of the traditional strain gages method. First, it will provide the tibia-segment deformation information that has

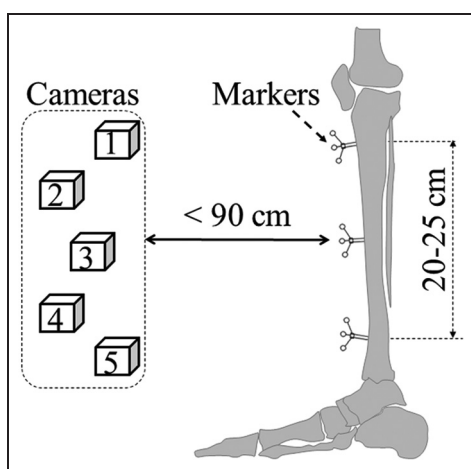


Figure 7. The recommended configuration for *in vivo* tibia deformation recording in humans. First, the marker clusters (at least three markers in one cluster) with small markers ($\varnothing 3\text{--}\varnothing 8 \text{ mm}$) and close camera distance ($< 90 \text{ cm}$) should be used. In addition, the movement of the tibia along the optical axis of camera lens (Yaxis in this study) should be minimized as little as possible.

never been observed *in vivo* before. Integrating with anatomical coordinate system or more advanced method, such as finite element model, 3D *in vivo* tibia strain distribution will then be able to be calculated. Second, it will make it possible to explore to which extent bending and torsion are occurring in the human tibia. As mentioned above, on top of the previously mentioned novel possibilities by our proposed method, the strain detection limit of this new approach is acceptable for the *in vivo* bone-segment deformation recording. Based on different principals with the proposed method, several other optical methods, such as DIC^{9–11} and machine vision photogrammetry (DISMAP),²⁶ have been explored to measure bone strains as well. Unquestionably, these methods have the ability of obtaining high-resolution strain distribution on certain areas of bone surface. However, so far, it is apparently difficult for these optical methods to measure the *in vivo* bone strains owing to its specific requirement of bone surface preparation and exposure to the cameras. This will probably be the main limitation for the application of the above two optical methods in the future of bone strain *in vivo* measurements.

Conclusion

To conclude, the performance of the proposed method, based on a motion capture system, is capable of recording the displacement of 20 µm with high accuracy and precision in a relative large volume of 400 × 300 × 300 mm³. Therefore, the results suggest that the proposed method has sufficient application potential in tibia-segment deformation *in vivo* measurements in the future.

Funding

This research received no specific grant from any funding agency in the public, commercial, or not-for-profit sectors.

Acknowledgments

We would like to thank Hans-Martin Küsel-Feldker and Thomas Förster at the Institute of Biomechanics and Orthopaedics, German Sport University Cologne, Germany, for operating the milling machine and numerous discussions about the ideas in this study. Thanks also to Michel Ducos for the discussion regarding to statistics. Peng-Fei Yang acknowledges his scholarship by the China Scholarship Council (CSC No.: 2009629013).

Conflict of interest

The Authors declare that there is no conflict of interest.

References

- 1 Duncan RL and Turner CH. Mechanotransduction and the functional response of bone to mechanical strain. *Calciif Tissue Int* 1995; 57(5): 344–358.
- 2 Forwood MR and Turner CH. Skeletal adaptations to mechanical usage: results from tibial loading studies in rats. *Bone* 1995; 17(4 Suppl); 197S–205S.
- 3 Turner CH, Owan I and Takano Y. Mechanotransduction in bone: role of strain rate. *Am J Physiol* 1995; 269(3 Pt 1): E438–442.
- 4 Mosley JR and Lanyon LE. Strain rate as a controlling influence on adaptive modeling in response to dynamic loading of the ulna in growing male rats. *Bone* 1998; 23(4): 313–318.
- 5 Yang PF, Bruggemann GP and Rittweger J. What do we currently know from *in vivo* bone strain measurements in humans? *J Musculoskelet Neuronal Interact* 2011; 11(1): 8–20.
- 6 Burr DB, Milgrom C, Fyhrie D, et al. *In vivo* measurement of human tibial strains during vigorous activity. *Bone* 1996; 18(5): 405–410.
- 7 Ekenman I, Halvorsen K, Westblad P, et al. The reliability and validity of an instrumented staple system for *in vivo* measurement of local bone deformation. An *in vitro* study. *Scand J Med Sci Sports* 1998; 8(3): 172–176.
- 8 Milgrom C, Finestone A, Hamel A, et al. A comparison of bone strain measurements at anatomically relevant sites using surface gauges versus strain gauged bone staples. *J Biomech* 2004; 37(6): 947–952.
- 9 Yang L, Zhang P, Liu S, et al. Measurement of strain distributions in mouse femora with 3D-digital speckle pattern interferometry. *Opt Lasers Eng* 2007; 45(8): 843–851.
- 10 Sztefek P, Vanleene M, Olsson R, et al. Using digital image correlation to determine bone surface strains during loading and after adaptation of the mouse tibia. *J Biomech* 2010; 43(4): 599–605.
- 11 Zauel R, Yeni YN, Bay BK, et al. Comparison of the linear finite element prediction of deformation and strain of human cancellous bone to 3D digital volume correlation measurements. *J Biomech Eng* 2006; 128(1): 1–6.
- 12 Matsuyama J, Ohnishi I, Sakai R, et al. A new method for measurement of bone deformation by echo tracking. *Med Engng Phys* 2006; 28(6): 588–595.
- 13 Abdel-Aziz YI and Karara HM. Direct linear transformation from comparator coordinates into object space coordinates in close range photogrammetry. In: *Proceedings of the symposium on close-range photogrammetry*, Falls Church, VA: American Society of Photogrammetry, 1971.
- 14 Windolf M, Gotzen N and Morlock M. Systematic accuracy and precision analysis of video motion capturing systems—exemplified on the Vicon-460 system. *J Biomech* 2008; 41(12): 2776–2780.
- 15 Liu H, Holt C and Evans S. Accuracy and repeatability of an optical motion analysis system for measuring small deformations of biological tissues. *J Biomech* 2007; 40(1): 210–214.
- 16 Milgrom C, Finestone A, Levi Y, et al. Do high impact exercises produce higher tibial strains than running? *Br J Sports Med* 2000; 34(3): 195–199.
- 17 Nigg BM and Herzog W (eds). *Biomechanics of the musculo-skeletal system*. West Sussex: Wiley and Sons Ltd, 2007.
- 18 Maletsky LP, Sun J and Morton NA. Accuracy of an optical active-marker system to track the relative motion of rigid bodies. *J Biomech* 2007; 40(3): 682–685.
- 19 Schmidt J, Berg DR and Ploeg H-L. Precision, repeatability and accuracy of Optotrak optical motion tracking systems. *Int J Exper Compl Biomech* 2009; 1: 114–127.

- 20 Milgrom C, Miligram M, Simkin A, et al. A home exercise program for tibial bone strengthening based on *in vivo* strain measurements. *Am J Phys Med Rehabil* 2001; 80(6): 433–438.
- 21 Milgrom C, Simkin A, Eldad A, et al. Using bone's adaptation ability to lower the incidence of stress fractures. *Am J Sports Med* 2000; 28(2): 245–251.
- 22 Ramsey DK, Wretenberg PF, Benoit DL, et al. Methodological concerns using intra-cortical pins to measure tibiofemoral kinematics. *Knee Surg, Sports Traumatol, Arthrosc* 2003; 11(5): 344–349.
- 23 Ramsey DK and Wretenberg PF. Biomechanics of the knee: methodological considerations in the *in vivo* kinematic analysis of the tibiofemoral and patellofemoral joint. *Clin Biomech (Bristol, Avon)* 1999; 14(9): 595–611.
- 24 Nester C, Jones RK, Liu A, et al. Foot kinematics during walking measured using bone and surface mounted markers. *J Biomech* 2007; 40(15): 3412–3423.
- 25 Grood ES and Suntay WJ. A joint coordinate system for the clinical description of three-dimensional motions: application to the knee. *J Biomech Eng* 1983; 105(2): 136–144.
- 26 Kim DG, Brunski IB and Nicolella DP. Microstrain fields for cortical bone in uniaxial tension: optical analysis method. *Proc IMechE, Part H: J Engineering in Medicine* 2005; 219(2): 119–128.